Systematics of capture and fusion dynamics in heavy-ion collisions

Bing Wang[a], Kai Wen[b,1], Wei-Juan Zhao[a], En-Guang Zhao[b,c], Shan-Gui Zhou[b,d,c,e,*]

[a] *Department of Physics, Zhengzhou University, Zhengzhou 450001, China*
[b] *CAS Key Laboratory of Frontiers in Theoretical Physics, Institute of Theoretical Physics, Chinese Academy of Sciences, Beijing 100190, China*
[c] *Center of Theoretical Nuclear Physics, National Laboratory of Heavy Ion Accelerator, Lanzhou 730000, China*
[d] *School of Physics, University of Chinese Academy of Sciences, Beijing 100049, China*
[e] *Synergetic Innovation Center for Quantum Effects and Application, Hunan Normal University, Changsha, 410081, China*

Abstract

We perform a systematic study of capture excitation functions by using an empirical coupled-channel model. In this model, a barrier distribution is used to take effectively into account the effects of couplings between the relative motion and intrinsic degrees of freedom. The shape of the barrier distribution is of an asymmetric Gaussian form. The effect of neutron transfer channels is also included in the barrier distribution. Based on the interaction potential between the projectile and the target, empirical formulas are proposed to determine the parameters of the barrier distribution. Theoretical estimates for barrier distributions and calculated capture cross sections together with experimental cross sections of 220 reaction systems with $182 \leqslant Z_{\rm P}Z_{\rm T} \leqslant 1640$ are tabulated. The results show that our empirical formulas work quite well in the energy region around the Coulomb barrier. This model can provide prediction of capture cross sections for the synthesis of superheavy nuclei as well as valuable information on capture and fusion dynamics.

*Corresponding author.
Email address: sgzhou@itp.ac.cn (Shan-Gui Zhou)
[1] Present address: Faculty of Pure and Applied Sciences, University of Tsukuba, Tsukuba 305-8571, Japan

Contents

1. Introduction

In recent decades, the study of capture and fusion dynamics in heavy-ion collisions has been a subject of intense experimental and theoretical interests because the heavy-ion fusion not only is of central importance for nucleosynthesis but also can reveal rich interplay between nuclear structure and reaction dynamics [1–8]. Experimentally, the capture cross sections cannot be measured directly. If the fast fission is neglected, the capture cross sections are measured as a sum of the fusion and quasifission (QF) cross sections,

$$\sigma_{\rm capture} = \sigma_{\rm fusion} + \sigma_{\rm QF}. \tag{1}$$

After two nuclei fuse, the newly formed excited compound nucleus cools down through emitting particles or fission. Consequently, the fusion cross section is the summation of the evaporation residual (EvR) and fusion-fission (FuF) cross sections,

$$\sigma_{\rm fusion} = \sigma_{\rm EvR} + \sigma_{\rm FuF}. \tag{2}$$

For light and medium-heavy systems, each capture event leads to the formation of a compound nucleus. Meanwhile, the fission is forbidden owing to the high fission barrier of the compound nucleus. In this case, $\sigma_{\rm capture} \simeq \sigma_{\rm fusion} \simeq \sigma_{\rm EvR}$, thus the measured fusion excitation functions can be used to study the capture and fusion processes simultaneously. For heavy systems, especially for more symmetric ones or those leading to superheavy compound nuclei, the QF process comes in and competes with the fusion process [9–24]. In some reactions, only a small number of the capture events go to fusion, hence the fusion cross section is only part of the capture cross section. In this case, it is necessary to clearly distinguish the capture and fusion processes [25–27]. The whole process of the synthesis of superheavy nuclei can be divided into three stages: i) the capture process in which the projectile is captured by the target and then a composite system is formed; ii) the process of the formation of a compound nucleus, which competes against the quasifission; iii) the survival process in which the excited compound nucleus cools down through emitting neutrons or fission. Therefore, it's very important to examine carefully these three steps in the study of the synthesis mechanism of superheavy nuclei. In this work, we will only focus on the capture process.

Theoretically, the capture process is often treated as a barrier penetration problem, i.e., the system overcomes or penetrates through the potential barrier between the two interacting nuclei, then the projectile is captured by the target, forming a composite system. The single barrier penetration models (SBPM) have been applied to describe successfully the capture (fusion) excitation functions for light reaction systems. However, for medium-heavy and heavy systems, a significant enhancement of sub-barrier fusion cross sections was observed in comparison to predictions of SBPM [28]. The enhancement can be explained by the strong coupling between the relative motion and intrinsic degrees of freedom (the vibration of nuclear surfaces, the rotation of deformed nuclei, etc.) and the coupling to the nucleon transfer channels [29–31]. To account for these couplings, a more quantal approach, the coupled-channel (CC) model, has been developed [32–34]. The CC model is very successful in describing fusion excitation functions near the Coulomb barrier [35]. However, for heavy systems, it is necessary to take into account a large number of channels which is not easy to realize in the CC model. Moreover, the structure information of the interacting nuclei are needed as inputs. Therefore, full CC calculations become intractable in many cases including many fusion reactions leading to superheavy nuclei. In the eigenchannel framework, the couplings to other channels split the original single barrier into a set of discrete barriers

[3, 34]. These barriers distribute around the original single barrier, each of them has a certain weight representing the probability of encountering the corresponding barrier. Therefore, the probability of fusion substantially changes owing to the barrier distribution as compared with that from the SBPM. Those barriers lower than the original single barrier are responsible for the enhancement of the sub-barrier fusion cross section in comparison to the predictions of SBPM. Based on the concept of the barrier distribution, several empirical CC approaches have been developed [25, 27, 36–39]. Different shapes of the barrier distribution were assumed in these empirical CC approaches [25, 36–38] and different methods were proposed to determine the parameters of the barrier distributions [25, 36–38, 40, 41]. In Refs. [36, 37], an asymmetric Gaussian shape was assumed for the barrier distribution and dynamical deformations of the projectile and target were introduced to explain the enhancement of fusion cross sections at sub-barrier energies. In Ref. [38], the authors proposed that the weighting function of the barrier is the superposition of two Gaussian functions. Actually, these empirical CC approaches provide an alternative to the full CC calculations, especially in the cases where the full CC calculations become intractable. The main shortcoming of empirical CC approaches is the choice of the distribution function of barriers which are responsible for couplings of relative motion to intrinsic degrees of freedom. In most of the empirical CC approaches, the barrier distribution has only one maximum, while the experimental barrier distributions extracted from the capture excitation functions, i.e., $d^2(E\sigma_{\rm capture})/dE^2$ [42, 43], usually exhibit more complicated structure. Note that besides the SBPM and the full and empirical CC approaches, several microscopic dynamics models, such as the time-dependent Hartree-Fock (TDHF) theory [44, 45] and the quantum molecular dynamics (QMD) model [46–49], have been also used to explore the fusion dynamics [50–65]. In recent years, Sargsyan *et al.* developed a quantum diffusion approach [66–68] for describing the capture process, which is based on the quantum master equation for the reduced density matrix. In the quantum diffusion approach, fluctuation and dissipation effects in collisions of heavy ions are taken into account to model the couplings to various channels. For addressing both dissipation and decoherence effects on the capture (fusion) process, a coupled-channel density-matrix approach based on the Lindblad equation has been developed [69, 70]. It was shown that the influence of decoherence on capture (fusion) and inelastic scattering, which is caused by the irreversible dissipation of flux or probability to the environment, is strong. Moreover, energy-shifting formulas for reaction and capture probabilities have been proposed for simplifying (or avoiding impracticable) coupled-channel calculations [71]. Based on reaction theory, a useful method were suggested for extracting capture cross sections from observed quasi-elastic backscattering excitation functions [72–74].

In the last forty years, a large number of fusion excitation functions, mostly for light and medium-heavy systems, have been measured. This provides us a possibility to make a systematic study on the capture and fusion dynamics. In the present work, we collect and compile the measured capture (fusion) excitation functions. We perform a systematic study of these capture excitation functions by using an empirical coupled-channel (ECC) model in which the coupled-channel effects are treated effectively by introducing a barrier distribution. The shape of the barrier distribution is chosen to be an asymmetric Gaussian form [36, 37]. Therefore, the barrier distribution is determined by three parameters, i.e., the left width, the right width, and the central value. The coupling effects of the neutron transfer channels are also considered in the barrier distribution. The purpose of this systematic study is to find an empirical way to determine the parameters of barrier distribution in the ECC model. We will show that this ECC model can give a reasonably adequate and systematic description of the capture cross sections. Note that this model has been used to study the CC effects in fusion reactions ^{32}S + ^{94,96}Zr and ^{40}Ca + ^{94,96}Zr [75] and extended to describe the complete fusion cross sections for

the reactions involving weakly bound nuclei at above-barrier energies [76].

The paper is organized as follows. In Section 2, the ECC model, the interaction potential between the two interacting nuclei, and the empirical formulas determining the parameters of the barrier distribution are introduced. The results and discussions of studying the capture excitation functions are shown in Section 3 where the effect of the neutron transfer are also investigated. A summary is given in Section 4. In the appendix, the calculated results are shown in Graphs 1–19. The parameters used in the calculations are tabulated in Table 1. The collected data are compiled in Table 2 where the calculated capture cross sections are also included.

2. The empirical coupled-channel model

First we give a sketch of our empirical coupled-channel model. In this model, as what is done in several other similar approaches, the capture cross sections are calculated in the framework of quantum tunneling through the potential barrier between the two interacting nuclei. The nuclear potential is taken to be the deformed Woods-Saxon form and the axially quadrupole shapes of the two nuclei are considered. The barrier distribution of an asymmetric Gaussian form is used to take effectively into account the effects of couplings between the relative motion and intrinsic degrees of freedom. Empirical formulas are proposed for the parameters of the barrier distribution according to the static and dynamical deformations of the two colliding nuclei. In our model, the coupling effects of the positive Q-value neutron transfer (PQNT) channels are also considered by modifying the barrier distribution. We give the details of the empirical coupled-channel model in the following Subsections.

2.1. The capture cross section

The capture cross section at a given center-of-mass energy $E_{\rm c.m.}$ can be written as the sum of the cross section for each partial wave J,

$$\sigma_{\rm capture}(E_{\rm c.m.}) = \frac{\pi\hbar^2}{2\mu E_{\rm c.m.}} \sum_{J}^{J_{\rm max}} (2J+1) T(E_{\rm c.m.}, J), \tag{3}$$

where μ denotes the reduced mass of the reaction system and $T(E_{\rm c.m.}, J)$ denotes the penetration probability. A "pocket" in the interaction potential may appear due to the competition between the long-range repulsive Coulomb interaction and the short-range attractive nuclear force. The "pocket" becomes shallower with the increase of angular momentum J because the contribution of the centrifugal potential becomes stronger. $J_{\rm max}$ is the critical angular momentum: For the partial wave with angular momentum larger than $J_{\rm max}$, the "pocket" of the interaction potential disappears [77, 78]. The interaction potential around the Coulomb barrier can be approximated by an "inverted" parabola. The analytical expression for the penetration probability is given by the well-known Hill-Wheeler formula [79]

$$T_{\rm HW}(E_{\rm c.m.}, J) = \left\{1 + \exp\left[\frac{2\pi}{\hbar\omega(J)}\left(\frac{\hbar^2 J(J+1)}{2\mu R_{\rm B}^2(J)} + B - E_{\rm c.m.}\right)\right]\right\}^{-1}, \tag{4}$$

where $R_{\rm B}(J)$ and $\hbar\omega(J)$ are the position of the barrier and the curvature for the Jth partial wave, respectively. $\hbar\omega(J)$ is calculated as

$$\hbar\omega(J) = \sqrt{-\frac{\hbar^2}{\mu}\frac{\partial^2}{\partial R^2}V(R,J)\Big|_{R=R_{\rm B}(J)}}. \tag{5}$$

Note that for deep sub-barrier penetration, Eq. (4) is not valid because of the long tail of the Coulomb potential. In Ref. [80] a new barrier penetration formula was proposed for potential barriers containing a long-range Coulomb

interaction, this formula is especially appropriate for the barrier penetration with penetration energy much lower than the Coulomb barrier. An enhancement in the fusion cross section by several orders of magnitude was observed at sub-barrier energies compared with the predictions of SBPM. This enhancement can be attributed to the coupling between the relative motion of the two nuclei and other degrees of freedom and couplings to PQNT channels. These couplings lead to a distribution of barriers rather than a single barrier. Therefore, a barrier distribution $f(B)$ is introduced to take into account the coupled-channel effects in an empirical way. Then, the penetration probability is calculated as

$$T(E_{\rm c.m.}, J) = \int f(B) T_{\rm HW}(E_{\rm c.m.}, J, B) {\rm d}B. \tag{6}$$

In the present work, the barrier distribution is taken to be an asymmetric Gaussian function

$$f(B) = \begin{cases} \frac{1}{N} \exp\left[-\left(\frac{B-B_{\rm m}}{\Delta_1} \right)^2 \right], & B < B_{\rm m}, \\ \frac{1}{N} \exp\left[-\left(\frac{B-B_{\rm m}}{\Delta_2} \right)^2 \right], & B > B_{\rm m}. \end{cases} \tag{7}$$

$f(B)$ satisfies the normalization condition $\int f(B) dB = 1$. $N = \sqrt{\pi}(\Delta_1 + \Delta_2)/2$ is a normalization coefficient. The left width Δ_1, the right width Δ_2, and the central value $B_{\rm m}$ of the barrier distribution will be discussed in Subsections 2.3 and 2.4.

Note that up to now, there is not a proof or mathematical derivation of Eq. (6) and Eq. (7) based on the coupled Schrödinger equations. In the present work, we will use these simple expressions and investigate its validity and usefulness by comparing theoretical results with available data.

2.2. The interaction potential

The interaction potential is one of the key quantities in the calculation of the penetration probability. In the present work the effective interaction potential of the two nuclei consists of the long-range Coulomb repulsive potential, the attractive short-range nuclear potential and the centrifugal potential,

$$V(R, J, \beta_{\rm P}^0, \beta_{\rm T}^0, \theta_{\rm P}, \theta_{\rm T}) = V_{\rm C}(R, \beta_{\rm P}^0, \beta_{\rm T}^0, \theta_{\rm P}, \theta_{\rm T}) + V_{\rm N}(R, \beta_{\rm P}^0, \beta_{\rm T}^0, \theta_{\rm P}, \theta_{\rm T}) + \frac{\hbar^2 J(J+1)}{2\mu R^2}. \tag{8}$$

Here R is the distance between the centroids of the two interaction nuclei and β_i^0's ($i = {\rm P}, {\rm T}$) are the ground state quadrupole deformations of the projectile and target nuclei. θ_i's ($i = {\rm P}, {\rm T}$) denote the angles measured between the symmetry axes of deformed nuclei and the collision axis, as shown in Fig. 1.

For the nuclear part of the potential between two deformed nuclei, we use the three-parameter Woods-Saxon potential [81] which is widely used in the description of the heavy-ion collisions,

$$V_{\rm N}(R, \beta_{\rm P}^0, \beta_{\rm T}^0, \theta_{\rm P}, \theta_{\rm T}) = \frac{-V_0}{1 + \exp\left[(R - R_{\rm P} - R_{\rm T})/a\right]}, \tag{9}$$

with

$$\begin{aligned} R_{\rm P} &= R_{0{\rm P}}[1 + (5/4\pi)^{1/2} \beta_{\rm P}^0 P_2(\cos\theta_{\rm P})], \\ R_{\rm T} &= R_{0{\rm T}}[1 + (5/4\pi)^{1/2} \beta_{\rm T}^0 P_2(\cos\theta_{\rm T})], \\ R_{0i} &= r_0 A_i^{1/3}, \quad i = {\rm P}, {\rm T}, \end{aligned} \tag{10}$$

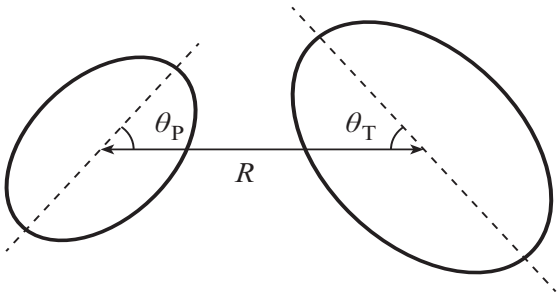

Fig. 1: Relative position of deformed projectile and target nuclei. R is the relative distance between the two nuclei. $\theta_{\rm P}$ ($\theta_{\rm T}$) denotes the angle between the symmetry axis of the deformed projectile (target) and the collision axis.

where V_0 and a denote the depth and the diffuseness parameters of the potential, respectively. r_0 is the radius parameter. The Coulomb interaction between two deformed nuclei is given as [81]

$$V_{\rm C}(R,\beta^0_{\rm P},\beta^0_{\rm T},\theta_{\rm P},\theta_{\rm T}) = \frac{Z_1Z_2e^2}{R} + \left(\frac{9}{20\pi}\right)^{\frac{1}{2}}\left(\frac{Z_1Z_2e^2}{R^3}\right)\sum_{i={\rm P,T}} R^2_{0i}\beta^0_i P_2(\cos\theta_i) + \left(\frac{3}{7\pi}\right)\left(\frac{Z_1Z_2e^2}{R^3}\right)\sum_{i={\rm P,T}} R^2_{0i}[\beta^0_i P_2(\cos\theta_i)]^2, \tag{11}$$

where $P_2(\cos\theta_i)$ is the Legendre polynomial.

The depth V_0, the radius parameter r_0, and the diffuseness parameter a are chosen as,

$$\begin{aligned} V_0 &= 80 \text{ MeV}, \\ r_0 &= 1.16 \text{ fm}, \\ a &= \left\{1.17\left[1+0.53\left(A_{\rm P}^{-1/3}+A_{\rm T}^{-1/3}\right)\right]\right\}^{-1} \text{ fm}. \end{aligned} \tag{12}$$

2.3. The parameters of the barrier distribution

Based on Eqs. (4-8), we fit the parameters of the barrier distribution to the experimental values and get the optimal parameter sets in Subsection 2.3.1. Furthermore, we also propose empirical formulas to calculate the parameters of the barrier distribution in Subsection 2.3.2.

2.3.1. Barrier distribution parameters from fitting

For the reactions with measured capture excitation functions, we can get the three parameters of the barrier distributions by fitting the data. From these fitted parameters, one may learn some systematics of the parameters of the barrier distributions. The three parameters of the barrier distribution are fitted by using the Levenberg-Marquardt method [82]. In the present work, we use a χ^2 merit function to determine the best-fit parameters by searching the minimum of χ^2, the χ^2 merit function is

$$\chi^2 = \sum_{i=1}^{N}\left[\frac{\sigma_{\rm th}(E_i)-\sigma_{\rm exp}(E_i)}{\delta\sigma_{\rm exp}(E_i)}\right]^2. \tag{13}$$

For all the reaction systems, the error of the cross section $\delta\sigma_{\rm exp}$ is assumed to be 3% of the corresponding measured cross section $\sigma_{\rm exp}$. The fitted results for the three parameters are listed in Table 1.

2.3.2. Barrier distribution parameters from empirical formulas

From fitting, one can only obtain the parameters of the barrier distributions for those reactions with measured capture excitation functions available. To also make predictions, we propose empirical formulas to calculate the parameters of the barrier distribution. In the ECC model, the barrier distribution is related to couplings to rotational states and low-lying collective vibrational states. Nuclear rotational states are related to static deformations, the vibrational modes are connected to the change of nuclear shape. Furthermore, when the two nuclei come close enough to each other, both nuclei are distorted owing to the attractive nuclear force and the repulsive Coulomb force, thus dynamical deformations develop [21]. Therefore, the barrier distribution parameters for a reaction system can be determined by the shapes of the projectile and target and the development of dynamical deformations. In the present work, we focus on a two-dimensional PES and examine the interaction potential of the two nuclei. The interaction potential of a reaction system is given as

$$V(R,\beta_{\rm P},\beta_{\rm T},\theta_{\rm P},\theta_{\rm T}) = V_{\rm C}(R,\beta_{\rm P},\beta_{\rm T},\theta_{\rm P},\theta_{\rm T}) + V_{\rm N}(R,\beta_{\rm P},\beta_{\rm T},\theta_{\rm P},\theta_{\rm T}) + \frac{1}{2}\sum_{i={\rm P,T}} C_i\Big(\beta_i-\beta_i^0\Big)^2, \tag{14}$$

where β_i's ($i={\rm P,T}$) denote quadrupole deformations of the projectile and the target. β_i^0's are the ground state quadrupole deformations. The total deformation of the reaction system is defined as $\beta=\beta_{\rm P}+\beta_{\rm T}$ and the dynamical deformations are defined as $\delta\beta_i=\beta_i-\beta_i^0$. In the present work, we assume a tip-tip orientation between the two deformed nuclei, i.e., $\theta_i=0^\circ$ (90°) if the nucleus is prolate (oblate). In order to reduce the number of parameters, we assume that the dynamical deformation energies of the two nuclei are proportional to their mass number: $C_{\rm P}\delta\beta_{\rm P}^2/C_{\rm T}\delta\beta_{\rm T}^2=A_{\rm P}/A_{\rm T}$ [21]. Thus only one parameter $\delta\beta=\delta\beta_{\rm P}+\delta\beta_{\rm T}$ is introduced. C_i's ($i={\rm P,T}$) are the stiffness parameters of the nuclear surface, which can be calculated with the liquid drop model [83]

$$C_i=(\lambda-1)\left[(\lambda+2)R_{0i}^2\sigma-\frac{3}{2\pi}\frac{Z_i^2e^2}{R_{0i}(2\lambda+1)}\right], \tag{15}$$

where R_{0i} is the radius of the nucleus. Here, we only take into account the quadrupole deformation ($\lambda=2$). σ is the coefficient of surface tension which satisfies $4\pi R_{0i}^2\sigma=a_sA_i^{2/3}$ and $a_s=18.32$ MeV is the surface energy parameter [83].

Figure 2 shows the PES of the reaction system ^{48}Ca+^{208}Pb. One can find that the Coulomb barrier changes with the total deformation. The ridge of the PES, i.e., the Coulomb barrier as a function of the total deformation of the system, is shown in Fig. 3. Note that both of the two nuclei are doubly magic and spherical in their ground states, but the total dynamical deformation of the system is 0.81 at the saddle point. This large dynamical deformation develops due to the combined effect of the attractive nuclear force and the repulsive Coulomb force. As one can see, with β increasing for the prolate configuration, the Coulomb barrier first decreases and then increases. A minimum appears in the curve which is the saddle point of the PES. Two characteristic configurations $V_{\rm B}^{\rm Sp}$ and $V_{\rm B}^{\rm S}$ in the PES are also shown in Fig. 3. $V_{\rm B}^{\rm Sp}$ denotes the Coulomb barrier of the configuration with two spherical nuclei. $V_{\rm B}^{\rm S}$ denotes the Coulomb barrier at the saddle point.

For ^{48}Ca + ^{208}Pb, $V_{\rm B}^{\rm Sp}$ is 180.2 MeV and $V_{\rm B}^{\rm S}$ is 163.6 MeV. The difference of the Coulomb barriers at these two configurations is 16.6 MeV. It is quite large, similar as the deformation energy at the saddle point which is 12.44 MeV. The barriers can distribute in a wide range due to the development of the dynamical deformation, leading to large widths of the barrier distribution. In the present work, we assume that the central value $B_{\rm m}$ of the barrier distribution is between $V_{\rm B}^{\rm Sp}$ and $V_{\rm B}^{\rm S}$. These two characteristic configurations are used to calculate $B_{\rm m}$. The widths of the barrier distributions are related to the deformation energy at the saddle point. Finally the parameters of the barrier distribution

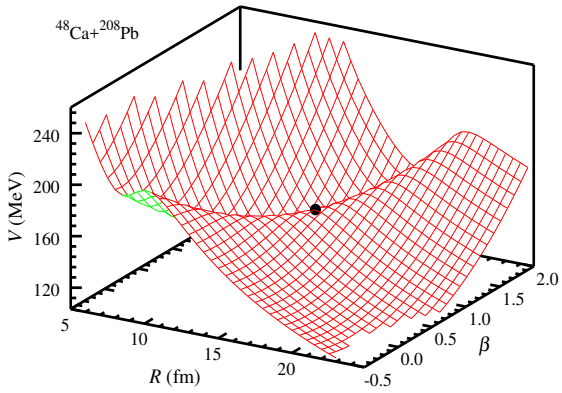

Fig. 2: Potential energy surface calculated with Eq. (14) for the reaction system $^{48}\mathrm{Ca} + {}^{208}\mathrm{Pb}$. The black dot denotes the saddle point.

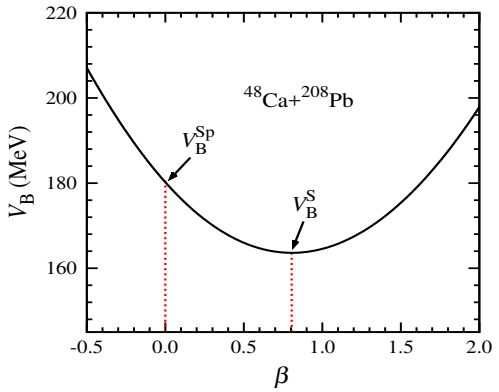

Fig. 3: Coulomb barrier for the reaction system $^{48}\mathrm{Ca} + {}^{208}\mathrm{Pb}$ as a function of the total deformation, i.e., the potential energy at the ridge of the potential energy surface (see Fig. 2). $V_{\mathrm{B}}^{\mathrm{Sp}}$ is the Coulomb barrier of the two spherical nuclei ($\beta_{\mathrm{P}} = 0$ and $\beta_{\mathrm{T}} = 0$). $V_{\mathrm{B}}^{\mathrm{S}}$ is the Coulomb barrier at the saddle point.

are chosen as follows

$$B_{\mathrm{m}} = aV_{\mathrm{B}}^{\mathrm{Sp}} + (1-a)V_{\mathrm{B}}^{\mathrm{S}}, \tag{16}$$

$$\Delta_1 = bE_{\mathrm{D}}, \tag{17}$$

$$\Delta_2 = cE_{\mathrm{D}}, \tag{18}$$

with

$$E_{\mathrm{D}} = \frac{1}{2}\sum_{i=\mathrm{P,T}} C_i \left(\beta_i^{\mathrm{S}}\right)^2. \tag{19}$$

Here E_{D} is the deformation energy of the reaction system at the saddle point. β_i^{S}'s are the deformation parameters of the projectile and the target at the saddle-point configuration. For systems in which both of the two nuclei are spherical, we found that the ECC model with the following set of the parameters $a, b,$ and c can give a good description of the

data,

$$\begin{aligned} a &= \begin{cases} 0.26, & Z_{\rm P}Z_{\rm T} < 1150, \\ 0.5, & Z_{\rm P}Z_{\rm T} \geq 1150, \end{cases} \\ b &= 0.32, \\ c &= 0.93. \end{aligned} \tag{20}$$

For deformed systems, the ECC model with a more asymmetric shape of the barrier distribution works better,

$$\begin{aligned} a &= \begin{cases} 0.23, & Z_{\rm P}Z_{\rm T} < 1150, \\ 0.37, & Z_{\rm P}Z_{\rm T} \geq 1150, \end{cases} \\ b &= 0.12, \\ c &= 1.12. \end{aligned} \tag{21}$$

2.4. The positive Q-value neutron transfer channels

A large enhancement of sub-barrier fusion cross sections have been experimentally observed in many reaction systems with positive Q-value neutron transfer channels [84–90]. Many efforts have been made to study the effect of the neutron transfer [84, 91–101]. Until now the role of the PQNT effect is still not very clear. Different viewpoints are proposed to understand the role of the PQNT effect. In Refs. [91–93], the authors suggested that the PQNT channels can provide a gain in the kinetic energy, and thus fusion is favored. In Ref. [94], it was proposed that a neutron flow between the projectile and the target nuclei before fusion could promote neck formation which provides a force strong enough to overcome the Coulomb force. Sargsyan *et al.* suggested that the deformations of the interacting nuclei change owing to the PQNT [99–101]. Thus, the influence of the PQNT channels on fusion is accompanied by the change of the nuclear deformations. In the present work, the effect of the coupling to the PQNT channels is simulated by broadening the barrier distribution. Furthermore, only one neutron pair transfer channel is considered in the present model. When the Q value for one neutron pair transfer is positive, the widths of the barrier distribution are calculated as

$$\begin{aligned} \Delta_1 &\rightarrow gQ(2n) + \Delta_1, \\ \Delta_2 &\rightarrow gQ(2n) + \Delta_2, \end{aligned} \tag{22}$$

where g is a dimensionless constant, $Q(2n)$ is the Q value for one neutron pair transfer, and Δ_1 and Δ_2 are calculated with Eqs. (16-21). For all reactions with positive Q value for one neutron pair transfer channel, g is taken as 0.32. For one neutron pair transfer from target to projectile, $Q(2n)$ is given as

$$Q(2n) = M(Z_{\rm P}, A_{\rm P}) + M(Z_{\rm T}, A_{\rm T}) - M(Z_{\rm P}, A_{\rm P}+2) - M(Z_{\rm T}, A_{\rm T}-2),$$

and for one neutron pair transfer from projectile to target, $Q(2n)$ is given as

$$Q(2n) = M(Z_{\rm P}, A_{\rm P}) + M(Z_{\rm T}, A_{\rm T}) - M(Z_{\rm P}, A_{\rm P}-2) - M(Z_{\rm T}, A_{\rm T}+2). \tag{23}$$

Nuclear masses are taken from Refs. [102, 103].

3. Results and Discussions

We have collected 220 sets of capture excitation functions for reactions with $182 \leqslant Z_P Z_T \leqslant 1640$. Among these 220 reaction systems, there are 89 with positive Q value for one neutron pair transfer channel. In the present work, the nuclear deformation parameters are taken from Ref. [104]. We assume that the involved nuclei are prolate except for ^{12}C ($\beta^0 = -0.32$ from the multi-dimensionally constrained relativistic mean field model [105–107]), ^{27}Al, and ^{28}Si. In order to achieve a better agreement with the experiment, the ground state quadrupole deformation parameters of ^{194,198}Pt are taken from Ref. [108] and for ^{35}Cl, $\beta^0 = 0.1$ is used. For each reaction system, the quadrupole deformation parameters of the projectile and the target nuclei, the position and curvature of the barrier between the two nuclei, the fitted (c.f. Subsection 2.3.1) and calculated (c.f. Subsection 2.3.2) results for the three parameters of the barrier distribution, and the Q value for one neutron pair transfer are tabulated in Table 1. In this Section, we first introduce the collection of the data. Then we define an average deviation to represent the agreement between the data and fitted (or calculated) values of the cross sections. In the last two Subsections, we show the comparison between the calculated capture cross sections and the experimental values for these 220 reactions and discuss in detail several typical examples. For convenience, we call the cross sections from our ECC model with fitted parameters "fitted" cross sections and those with parameters determined by Eqs. (16-21) "calculated" cross sections.

3.1. Collection of the capture excitation functions

220 sets of capture excitation functions are collected in the present work. There are more reaction systems for which the capture cross sections have been measured and some can be found in the NRV website [109]. Since we focus on the capture and fusion dynamics around the Coulomb barrier, only the reaction systems for which capture excitation functions are measured in this energy region are considered in this work. Note that reaction systems with weakly bound nuclei involved are also excluded, because the coupling to the breakup channel is very complicated, especially in the sub-barrier region [110–123]. Actually, in Ref. [76], we extended our ECC model by including the breakup effect which is described by a prompt-breakup probability function. For the reactions induced by ^{9}Be, the extended ECC model together with the measured prompt-breakup probabilities can give a good description of the complete fusion cross sections at above-barrier energies [76].

Among these 220 reactions, there are 71 reactions for which the values of the cross sections are not given in the corresponding references, but the measured cross sections are shown in graphs. So we extract the data from the authors' graphs for these reaction systems. For part of these 71 reactions, the graphs are obtained from scanned PDF files. To test the reliability of our procedure for extracting the data from the authors' graphs, we take two reactions, ^{18}O+^{74}Ge and ^{17}O+^{144}Sm for which the data are given both in authors' tables and in authors' graphs [95, 124], as examples. Note that, the PDF file for Ref. [124] was a scanned one and that for Ref. [95] has a better quality. We compare the extracted and tabulated values of fusion cross sections in Table A. The tabulated experimental values are listed in columns 2–5. Columns 6 and 7 show the fusion cross sections extracted from the authors' graphs. The last column shows the relative deviations $\Delta\sigma/\sigma_F^{\rm Exp.}$ between them. The deviation $\Delta\sigma$ is defined as $\Delta\sigma = \sigma_F^{\rm Exp.} - \sigma_F^{\rm Ext.}$. For ^{18}O+^{74}Ge, the relative deviations are mostly within 1%. For ^{17}O+^{144}Sm, the relative deviations are around 2% and the largest one is 3.57%. This means that our procedure of extracting the data from the authors' graphs is reliable.

Table A

Two reactions ^{18}O+^{74}Ge and ^{17}O+^{144}Sm used to test our procedure for extracting the data from the authors' graphs in Refs. [95, 124]. The two reactions and the corresponding references are tabulated in the first column. The experimental values of the capture (fusion) cross sections taken from the authors' tables are listed in columns 2–5 (the incident energies $E^{\rm Exp.}$ in the center-of-mass frame for the former and in the laboratory frame for the latter, the fusion cross section $\sigma_{\rm F}^{\rm Exp.}$ and the errors of the cross section $\delta\sigma_{\rm F}^{\rm Exp.}$). The experimental values of the capture (fusion) cross sections extracted from the authors' graphs are listed in columns 6 and 7 (the incident energies $E^{\rm Ext.}$ and the fusion cross section $\sigma_{\rm F}^{\rm Ext.}$). The last column shows relative deviations between the tabulated values of the cross sections and those extracted from the authors' graphs ($\Delta\sigma = \sigma_{\rm F}^{\rm Exp.} - \sigma_{\rm F}^{\rm Ext.}$).

Reaction	$E_{\rm c.m.}^{\rm Exp.}$ (MeV)	$E_{\rm lab}^{\rm Exp.}$ (MeV)	$\sigma_{\rm F}^{\rm Exp.}$ (mb)	$\delta\sigma_{\rm F}^{\rm Exp.}$ (mb)	$E^{\rm Ext.}$ (MeV)	$\sigma_{\rm F}^{\rm Ext.}$ (mb)	$\Delta\sigma/\sigma_{\rm F}^{\rm Exp.}$ (%)
^{18}O+^{74}Ge [95]	30.2		0.14	0.01	30.27	0.14	0.00
	30.5		0.25	0.01	30.50	0.25	0.00
	31.0		0.89	0.03	31.01	0.90	−1.12
	31.5		1.84	0.05	31.52	1.85	−0.54
	32.0		4.56	0.08	32.03	4.55	0.22
	32.5		10.0	0.1	32.50	10.02	−0.20
	33.0		16.7	0.2	33.01	16.71	−0.06
	33.5		31.5	0.3	33.49	31.54	−0.13
	34.0		46.9	0.4	34.00	47.17	−0.56
	34.5		63.1	0.6	34.51	63.32	−0.35
	35.0		82.6	0.8	35.02	83.67	−1.30
	35.5		99.4	0.9	35.53	100.76	−1.37
	36.0		136.5	1.2	36.00	135.23	0.93
	36.5		156.7	1.3	36.54	157.88	−0.75
	37.0		190.1	1.6	37.02	190.12	−0.01
	37.5		211.9	2.0	37.56	211.89	0.005
	38.0		254.8	1.8	38.04	255.17	−0.15
	38.9		292.5	2.7	38.99	293.33	−0.28
	39.9		371.3	2.3	39.97	370.04	0.34
	40.9		409.9	3.3	40.96	412.41	−0.61
	41.9		497.9	3.7	41.97	496.63	0.26
	43.0		545.6	4.4	42.99	553.50	−1.45
	44.0		593.4	4.8	43.98	598.06	−0.79
	46.0		686.5	7.4	45.99	687.51	−0.15
	46.9		731.6	7.6	46.96	731.44	0.02
	49.0		847.9	7.9	49.00	853.96	−0.71
^{17}O+^{144}Sm [124]		60.88	0.07	0.05	60.87	0.07	0.00
		61.38	0.11	0.07	61.31	0.11	0.00
		61.88	0.19	0.09	61.78	0.19	0.00
		62.38	0.40	0.09	62.36	0.40	0.00
		62.88	0.81	0.23	62.84	0.82	−1.23
		63.38	1.2	0.2	63.31	1.18	1.67
		63.88	2.4	0.2	63.79	2.45	−2.08
		64.88	5.7	0.3	64.79	5.75	−0.88
		65.88	13.9	0.5	65.79	14.08	−1.29
		66.88	30.8	0.6	66.79	31.56	−2.47
		67.88	57.2	0.7	67.79	58.46	−2.20
		68.88	90.5	0.9	68.79	93.52	−3.34
		70.01	137	1	69.90	141.06	−2.96
		70.88	171	1	70.74	173.24	−1.31
		71.88	209	1	71.75	215.91	−3.31
		72.88	253	2	72.75	261.31	−3.28
		73.88	296	2	73.80	302.63	−2.24
		74.88	345	2	74.75	350.48	−1.59
		75.88	383	2	75.75	394.15	−2.91
		76.88	428	2	76.81	443.27	−3.57
		77.88	463	3	77.75	477.03	−3.03
		78.88	508	3	78.76	520.95	−2.55
		79.88	548	3	79.81	560.63	−2.30
		89.88	852	4	89.82	870.82	−2.21
		99.88	1072	7	99.84	1101.37	−2.74

3.2. Average deviation of the fitted and calculated cross sections from experimental values

To show quantitatively the agreement between the fitted (or calculated) from measured capture excitation functions, we introduce an average deviation $\mathcal{D}$,

$$\mathcal{D} = \frac{1}{n}\sum_{i=1}^{n}\left\{\log\left[\frac{\sigma_{\rm th}(E_i)}{\sigma_{\rm exp}(E_i)}\right]\right\}^2. \tag{24}$$

Here n denotes the number of energy points for each set of experimental capture excitation function. $\sigma_{\rm th}(E_i)$ and $\sigma_{\rm exp}(E_i)$ are the fitted (or calculated) capture cross section and the experimental value, respectively.

Figure 4 shows the average deviations of the fitted [Fig. 4(a)] and calculated [Fig. 4(b)] cross sections from experimental values for these 220 reaction systems. From Fig. 4(a), one can see that most of the capture excitation functions can be well reproduced by the ECC model with the fitted barrier distribution parameters. For several reaction systems, the data in the deep sub-barrier region are also used in the fitting procedure. In some of these cases, we find that the fitted results can not reproduce the data in the deep sub-barrier region, e.g., ^{16}O+^{204,208}Pb. However, it works quite well in the energy region around the Coulomb barrier. Figure 4(b) shows that our ECC model with the barrier distribution calculated by Eqs. (16-22) can also describe well most of the capture excitation functions; the average deviations for most reaction systems are quite small. There are some reaction systems for which the deviations of the calculated results from the experiments are noticeable; further discussions about typical examples of these systems will be given in the following two Subsections.

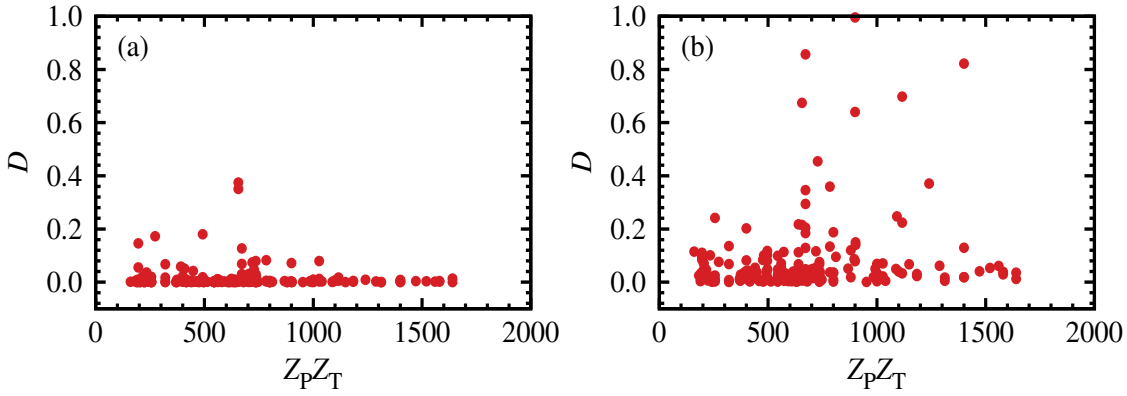

Fig. 4: The average deviation $\mathcal{D}$ of the fitted (a) and calculated (b) cross sections from the data for a total of 220 reaction systems as a function of $Z_{\rm P}Z_{\rm T}$.

3.3. Reaction systems with negative Q value for one neutron pair transfer

Graphs 1–11 show the calculated capture cross sections of 131 reaction systems for which the Q values for one neutron pair transfer are negative. In these reactions, the neutron pair transfer channel is closed. The Q values for one neutron pair transfer, i.e., $Q(2n)$s are listed in Table 1. The data are represented by solid squares or circles and the corresponding references are listed in Table 2. The arrow indicates the central value of the barrier distribution, i.e., $B_{\rm m}$ in Eq. (16). The solid line denotes the calculated cross sections. In these reactions, the vibrational and rotational couplings are responsible for the enhancement of cross sections in the sub-barrier region as compared with predictions of SBPM. From Graphs 1–11, it can be seen that the calculated capture excitation functions of most of these 131 reaction systems are

in good agreement with the measured capture excitation functions. As mentioned in Subsection 3.1, we focus on the capture and fusion dynamics around the Coulomb barrier and collect capture excitation functions measured in this energy region. Generally, for reactions with negative Q value for one neutron pair transfer channel, the present model can describe the capture excitation functions very well at energies around the Coulomb barrier. For some reactions, the deviation of the calculated results from the experiment is noticeable. Next we discuss some typical examples among these 131 reactions in detail.

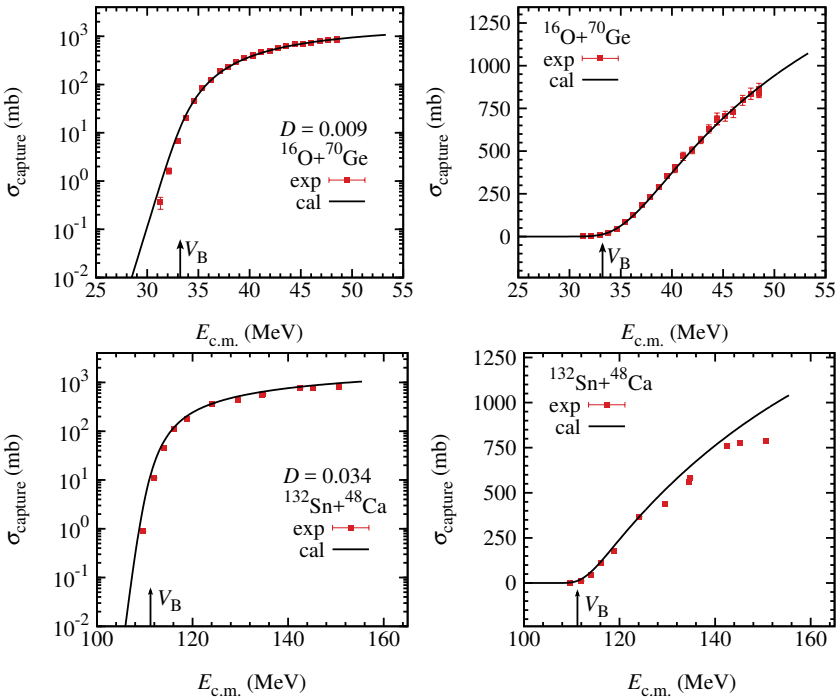

Fig. 5: The experimental and calculated capture excitation functions for ^{16}O+^{70}Ge and ^{132}Sn+^{48}Ca. The results are shown in logarithmic scale (the left panel) and linear scale (the right panel). The solid line denotes the calculated cross sections. The arrow indicates the central value of the barrier distribution $B_{\rm m}$ given in Eq. (16). The solid squares show the experimental values which are given in Table 2. $\mathcal{D}$ denotes the average deviation of the calculated cross sections from the experimental values.

3.3.1. Typical examples

For the reactions for which the calculated capture excitation functions are in good agreement with the measured ones, we select a light system ^{16}O + ^{70}Ge with $Z_{\rm P}Z_{\rm T} = 256$ and a heavy system ^{132}Sn + ^{48}Ca with $Z_{\rm P}Z_{\rm T} = 1000$ as examples. In the reaction ^{16}O + ^{70}Ge the target ^{70}Ge is deformed with the quadrupole deformation parameter $\beta = 0.241$ (see Table 1). For the reaction ^{132}Sn + ^{48}Ca, both the projectile and the target are doubly magic nuclei and their quadrupole deformation parameters are zero (see Table 1). Therefore, ^{16}O + ^{70}Ge is a deformed reaction system and ^{132}Sn + ^{48}Ca is a spherical reaction system. In Fig. 5, the comparison of the calculated capture cross sections with the experimental values for ^{16}O + ^{70}Ge and ^{132}Sn + ^{48}Ca reactions is shown. The solid line denotes the calculated cross sections. The solid squares are the experimental values which are listed in Table 2. The arrow indicates the central value of the barrier distribution $B_{\rm m}$ given in Eq. (16). For both reactions, we can see that the calculated capture cross sections are in good

agreement with the data. For ^{132}Sn + ^{48}Ca, in the well above-barrier region, the calculated cross sections overestimate the experimental values. This may be attributed to the fact that only the EvR cross sections are measured and the FuF cross sections is not taken into account at high energies (See Table 2). The average deviations $\mathcal{D}$ defined in Eq. (24) for ^{16}O + ^{70}Ge and ^{132}Sn + ^{48}Ca are 0.009 and 0.034, respectively.

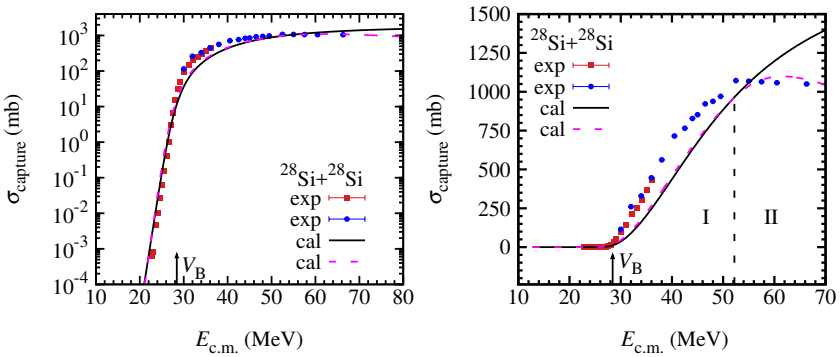

Fig. 6: Same as Fig. 5 but for ^{28}Si+^{28}Si and the dash line denotes the calculated results obtained by adjusting the parameters V_0 and r_0 of the nuclear potential.

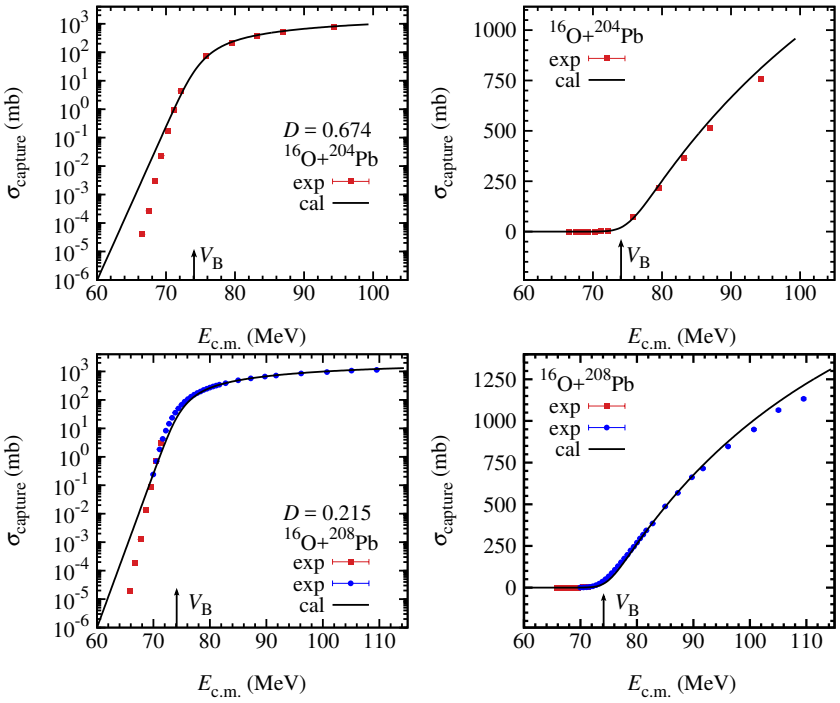

Fig. 7: Same as Fig. 5 but for ^{16}O+^{204,208}Pb.

3.3.2. Entrance channel effect and fusion hindrance in the deep sub-barrier region

A fusion excitation function can be divided into three distinct regimes which are referred to as regions I, II and III [125, 126]. In low energy region (region I), the fusion cross section increases with the energy increasing. In region II, the fusion cross section saturates, whereas in region III the fusion cross section regularly diminishes. The behavior of fusion

excitation function in region II can be explained by the entrance channel effect because the fusion cross section is limited by the disappearance of the "pocket" in the interaction potential. In the present work, this entrance channel effect is taken into account by making a cut-off at a critical angular momentum $J_{\max}$ as seen in Eq. (3). $J_{\max}$ is dependent on the behavior of the potential inside the barrier radius which is sensitive to the parameters of the nuclear potential. The "pocket" becomes shallower with the depth of the nuclear potential decreasing [77]. To describe the behavior of the capture and fusion excitation function in region II, it is needed to adjust the parameters of the nuclear potential. In the present work, the parameters of the nuclear potential are fixed as Eq. (12). Hence, for some reactions, the predictions in region II do not agree with the data well. For example, the results for ^{28}Si+^{28}Si reaction are shown in Fig. 6. The data show that the cross section saturates at energies above 1.7 times of the Coulomb barrier, while the result of our model denoted by the solid line shows that the cross section still increases in this region; actually the calculated cross section reaches saturation at a large energy which is beyond the scale of Fig. 6. By adjusting the parameters V_0 and r_0 of the nuclear potential to be 25 MeV and 1.3 fm, the results of our model represented by the dash line can reproduce the behavior of the capture (fusion) excitation function in region II. This implies that the depth of the nuclear potential might be smaller than that given in Eq. (12) for light reaction systems.

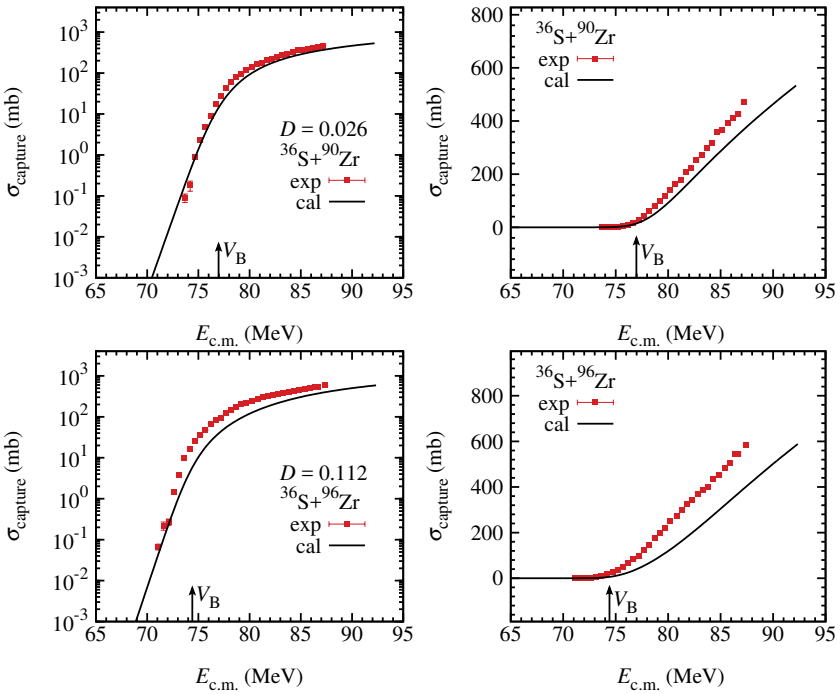

Fig. 8: Same as Fig. 5 but for ^{36}S+^{90,96}Zr.

The comparison between the calculated capture cross sections and the experimental values for ^{16}O+^{204,208}Pb reaction systems is shown in Fig. 7. One can find that the theoretical predictions overestimate the capture cross sections at sub-barrier energies below a certain energy. As mentioned in Section 2, Eq. (4) has a shortcoming and is not valid for deep sub-barrier penetration because of the long tail of the Coulomb potential. We notice that the new barrier penetration formula proposed in Ref. [80] is more proper for deep sub-barrier penetration. The implementation of this barrier penetration formula in the ECC model is in progress. In addition, this shortcoming can also be avoided in the

quantal CC model. However, the standard CC calculations overestimate the cross sections in the very deep sub-barrier region and are unable to explain the steep falloff in fusion cross sections. Different mechanisms are proposed to explain this hindrance phenomenon [69, 70, 127–131]. In the very deep sub-barrier region, the fusion mechanism is different from that at energies around the Coulomb barrier. In the present work, we focus on the capture and fusion dynamics around the Coulomb barrier and the hindrance phenomenon is beyond the scope of this work.

3.3.3. Further discussions

For the reactions with noticeable deviations of the calculated results from the experimental values, we select the ^{36}S+^{90,96}Zr as examples. The comparison of the calculated capture cross sections with the experimental values for ^{36}S+^{90,96}Zr reactions is shown in Fig. 8. The deviations of the calculated cross sections from experimental values are quite large, especially at energies above the Coulomb barrier, the predictions underestimate the cross sections. The average deviation $\mathcal{D}$ defined in Eq. (24) for ^{36}S+^{90}Zr is 0.026, which is much smaller than that of ^{36}S+^{96}Zr. The reason is that the agreement between the calculated results and the data in the sub-barrier region for ^{36}S+^{90}Zr is better than that for ^{36}S+^{96}Zr. In the present work, we use the logarithm of the ratio of the calculated cross section to the corresponding experimental value in the definition of the average deviation $\mathcal{D}$ [see Eq. (24)]. The capture cross section grows exponentially with energy in the sub-barrier region while linearly with energy at energies above the barrier. Therefore, the average deviation $\mathcal{D}$ is more sensitive to the agreement between the calculated capture cross sections and the data in the sub-barrier region than that at energies above the Coulomb barrier.

3.4. Reaction systems with positive Q value for one neutron pair transfer

Among the 220 reaction systems we have collected, there are 89 reaction systems with positive Q value for one neutron pair transfer channel. The comparison between the calculated and measured capture excitation functions for these 89 reaction systems is illustrated in Graphs 12–19. The solid line denotes the results with the effect of the one neutron pair transfer taken into account. The dotted line denotes the results with the effect of the neutron transfer neglected. The arrow indicates the central value of the barrier distribution $B_{\rm m}$ given in Eq. (16). The data are represented by solid squares or circles and the corresponding references are listed in Table 2. The Q values for one neutron pair transfer, i.e., $Q(2n)$s are also given in Table 1. From Graphs 12–19, it can be seen that the calculated capture cross sections of most of the 89 reaction systems are in good agreement with the experimental values. Generally, for the reactions with positive Q value for one neutron pair transfer, the present model can describe the capture excitation functions quite well. Next, we first give some general discussions on the influence of the neutron transfer on capture cross sections. Then we discuss the reactions for which the deviation of the calculated results from the experiment is noticeable in detail by taking some typical examples.

3.4.1. Reaction systems with negligible effects of PQNT couplings

In the present model, the coupling to the PQNT channels is simulated by broadening the barrier distribution given in Eq. (22). Therefore, the effects of PQNT couplings is related to the changes of the widths of the barrier distribution, especially the change of the left width Δ_1. If $gQ(2n)$ is large, but the ratio of $gQ(2n)$ to Δ_1 is small, i.e., the change of the left width Δ_1 is quite small, then the influence of one neutron pair transfer on capture and fusion cross sections can be ignored. In addition, for the reactions with small positive $Q(2n)$s (smaller than 1 MeV, see Table 1), the changes of

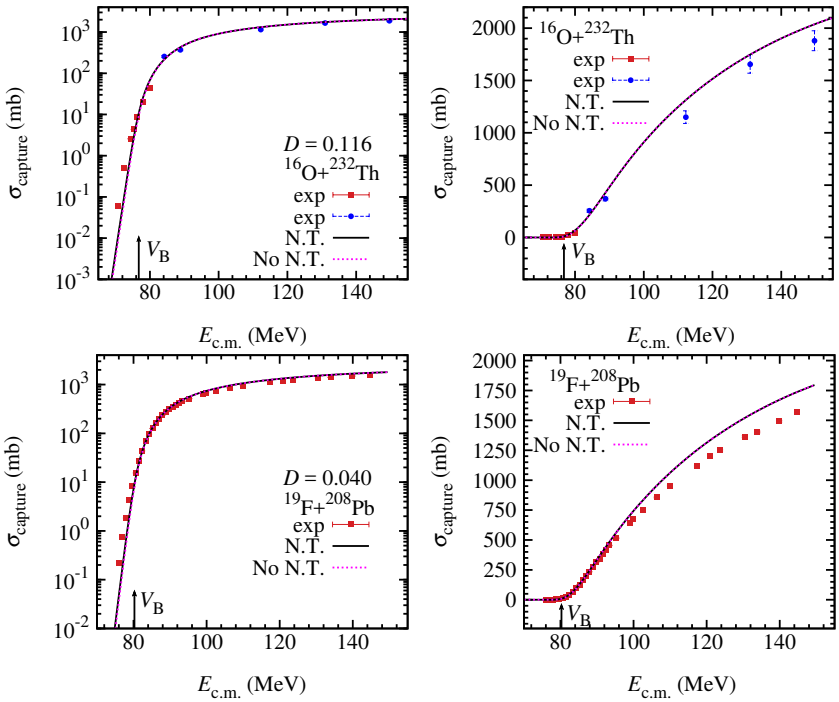

Fig. 9: The experimental and calculated capture excitation functions for ^{16}O+^{232}Th and ^{19}F+^{208}Pb. The results are shown in logarithmic scale (the left panel) and linear scale (the right panel). The solid line denotes the calculated cross section with the effect of one neutron pair transfer taken into account. The dotted line denotes the calculated cross section with the effect of neutron transfer neglected. The arrow indicates the central value of the barrier distribution $B_{\rm m}$ given in Eq. (16). The solid squares and circles show the experimental values which are given in Table 2. $\mathcal{D}$ denotes the average deviation of the calculated cross sections with the effect of one neutron pair transfer taken into account from the experimental values.

the widths of the barrier distributions are also small, the influence of one neutron pair transfer on capture and fusion cross sections can also be ignored. For example, the calculated capture cross section and the experimental values of the ^{16}O+^{232}Th and ^{19}F+^{208}Pb reactions are shown in Fig. 9. The $Q(2n)$s for the ^{16}O+^{232}Th and ^{19}F+^{208}Pb reactions are 0.63 MeV and 0.60 MeV, respectively. The solid line denotes the results with the effect of one neutron pair transfer taken into account, the dotted line denotes the results with this effect neglected. One can find that the solid line is very close to the dotted one, both the results with and without taking into account the effect of one neutron pair transfer show good agreement with the data. In other reaction systems with small positive $Q(2n)$s, the influence of one neutron pair transfer on capture and fusion cross sections can also be ignored.

3.4.2. Reaction systems with large positive $Q(2n)$: Effects of PQNT couplings

In reaction systems with large positive $Q(2n)$s, the distributions with the neutron transfer couplings taken into account become much broader as compared with those with the effect of neutron transfer neglected. Therefore, the calculated cross sections with this effect considered are much larger than those with this effect neglected in the sub-barrier region. Meanwhile, the change of the slope of the capture excitation function in the sub-barrier energy region owing to the coupling to one neutron pair transfer channel with a large positive Q value is significant. We take the

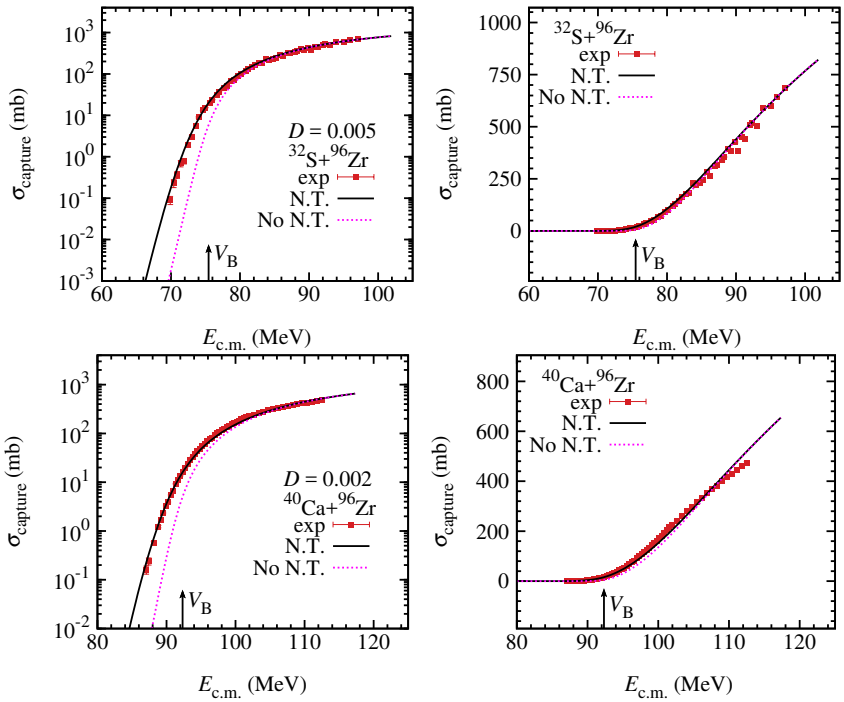

Fig. 10: Same as Fig. 9 but for ^{32}S+^{96}Zr and ^{40}Ca+^{96}Zr.

reaction systems of ^{32}S+^{96}Zr and ^{40}Ca+^{96}Zr as examples. The $Q(2n)$s for ^{32}S+^{96}Zr and ^{40}Ca+^{96}Zr reactions are 5.74 MeV and 5.53 MeV, respectively. After taking into account the coupling to PQNT channels, the changes of the widths of the barrier distributions given in Eq. (22) are about 1.8 MeV for these two reactions. The calculated capture cross sections and the experimental values of these two reactions are shown in Fig. 10. The solid line denotes the results with the effect of one neutron pair transfer taken into account. The dotted line denotes the results with the effect of the neutron transfer neglected. One can find that the measured capture cross sections show a large enhancement as compared with the results without considering the coupling effects of PQNT channels (the dotted line) in the sub-barrier region. While after taking this effect into account, the calculated values are in good agreement with the data. In the region above the Coulomb barrier, the difference between the solid line and the dotted line becomes smaller and smaller as the energy increase. Therefore the couplings to PQNT channels mainly affect the capture cross sections in the sub-barrier region.

3.4.3. Further discussions

Figure 11 shows the results for ^{32}S+^{94}Zr and ^{40}Ca+^{94}Zr. It can be seen that with the effect of one neutron pair transfer taken into account, the results from our calculations underestimate the data in the sub-barrier region. For the four reactions ^{32}S+^{94,96}Zr and ^{40}Ca+^{94,96}Zr, the $Q(2n)$s are 5.10 MeV, 5.74 MeV, 4.89 MeV, and 5.53 MeV, respectively. On one hand, in the framework of the present model, one may conclude that the influences of one neutron pair transfer on capture are similar for these four reactions because of similar $Q(2n)$s. On the other hand, only the data for ^{32}S+^{96}Zr and ^{40}Ca+^{96}Zr are well reproduced by taking into account the effect of neutron transfer (see Fig. 10). These findings drive us to investigate in detail the influence of various coupling channels on the capture cross section. To this end, we first reduce the data to eliminate the geometrical factors and static effects of the potential. Several reduction

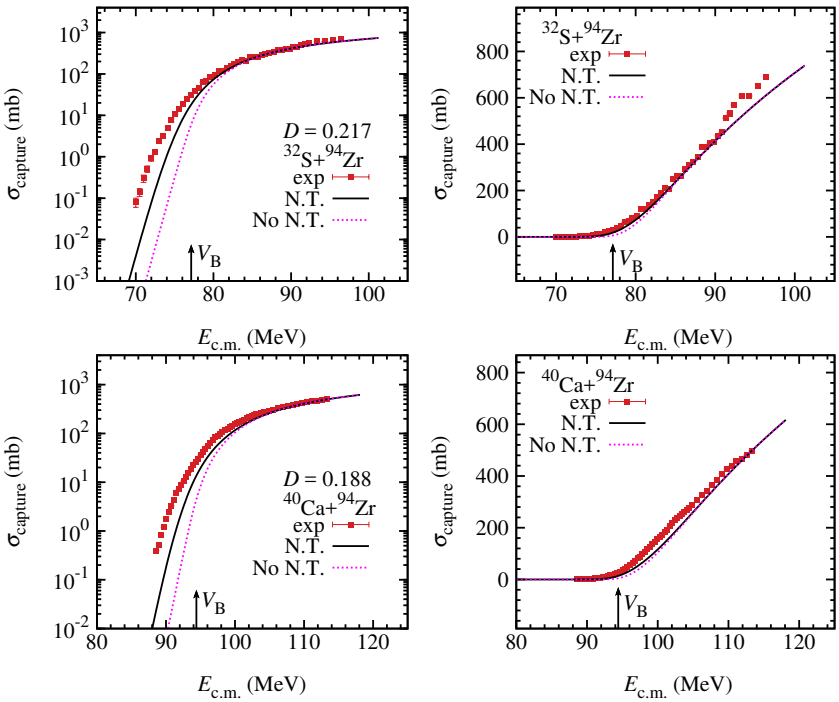

Fig. 11: Same as Fig. 9 but for ^{32}S+^{94}Zr and ^{40}Ca+^{94}Zr.

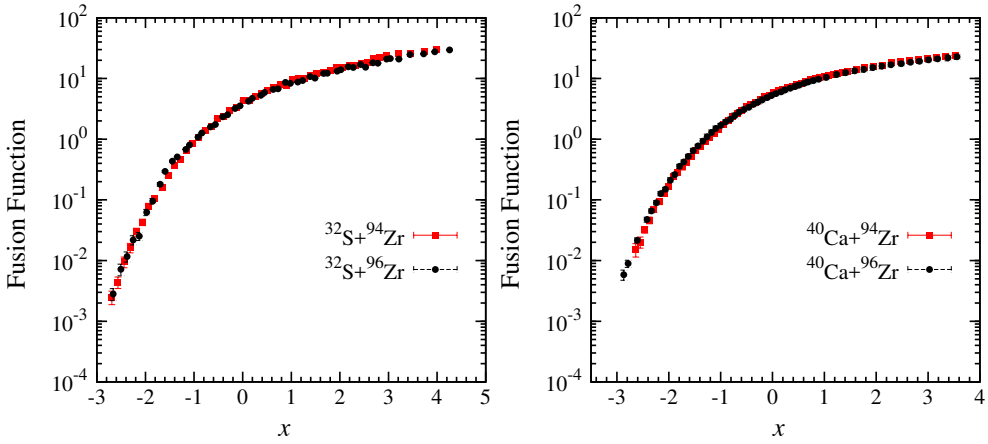

Fig. 12: The reduced capture excitation functions of the reactions ^{32}S+^{94,96}Zr and ^{40}Ca+^{94,96}Zr.

methods [132–138] can be used. In the present work, the fusion function method [135, 136] is adopted to reduce the capture excitation functions [139–141]. The barrier parameters R_B, V_B, and $\hbar\omega$ are obtained from the double folding and parameter-free São Paulo potential (SPP) [142–144]. The reduced capture excitation functions of the reactions ^{32}S+^{94,96}Zr and ^{40}Ca+^{94,96}Zr are shown in Fig. 12. One can find that the behaviors of the reduced capture excitation functions of ^{32}S+^{94}Zr and ^{32}S+^{96}Zr are very similar. The situation is the same for the reactions ^{40}Ca+^{94,96}Zr. This means that the effects of the couplings (to the inelastic excitations and the neutron transfer channel) in ^{32}S+^{94}Zr are similar to that in ^{32}S+^{96}Zr. The same conclusion can be drawn for the reactions ^{40}Ca+^{94,96}Zr. In the present work, the static quadrupole deformation parameters of $\beta^0 = 0.062$ and $\beta^0 = 0.217$ are used for ^{94}Zr and ^{96}Zr, respectively [104]. The underestimate of the data for the reactions ^{32}S+^{94}Zr and ^{40}Ca+^{94}Zr might come from the smaller deformation

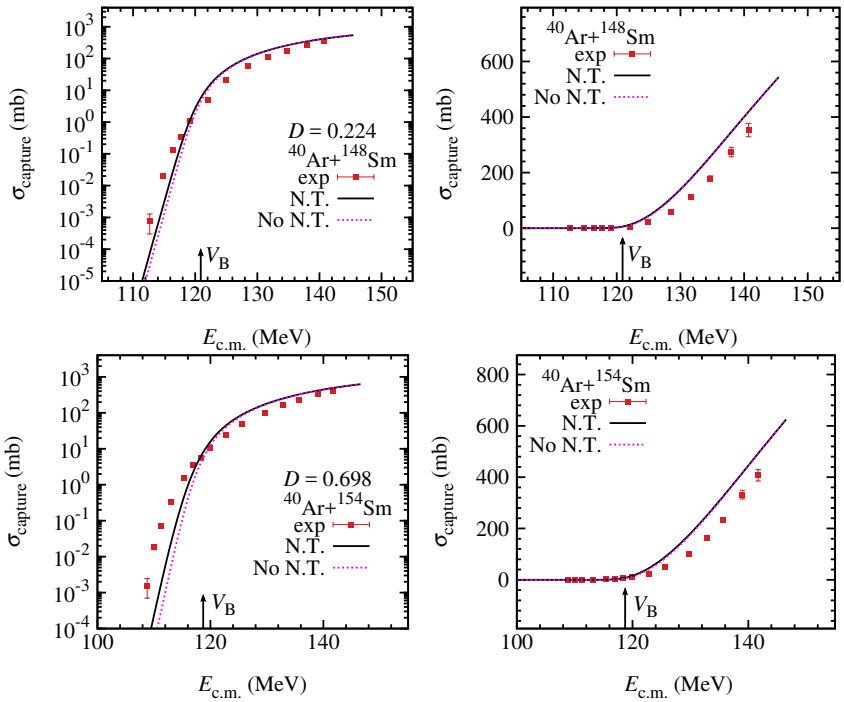

Fig. 13: Same as Fig. 9 but for ^{40}Ar+^{148,154}Sm.

parameter for ^{94}Zr used in our calculations. Further study has been done with our ECC model to elucidate which of these two effects (the coupling to the PQNT channel or the structure of ^{94}Zr) is responsible for the underestimate of the capture cross section of the reactions ^{32}S+^{94}Zr and ^{40}Ca+^{94}Zr [75]. In addition, in Ref. [145], the QCC model with a semiclassical consideration of neutron rearrangement has been used to study these reactions and it was pointed out that the sub-barrier fusion enhancements owing to neutron rearrangement and excitation of the collective vibrational and/or rotational states are not additive. Esbensen *et al.* suggested that the couplings to positive Q-value proton transfer channels are also important to explain the fusion data for the reaction ^{40}Ca+^{96}Zr [146].

In Fig. 13, the comparison of the calculated capture cross sections to the experimental values for ^{40}Ar+^{148,154}Sm reactions is illustrated. The $Q(2n)$s for these two reactions are 1.04 MeV and 1.69 MeV, respectively. One can find that the results with the effect of neutron transfer taken into account overestimate the data at energies above the Coulomb barrier and underestimate the data in the sub-barrier region. This indicates that the widths of the barrier distributions are not appropriate. From the fitted results of the parameters of the barrier distribution listed in Table 1, one can find that much broader barrier distributions than those given in Subsection 2.3.2 are needed to describe the capture excitation functions for these two reactions.

4. Summary

In this work, we use an empirical coupled-channel (ECC) model to systematically study the capture and fusion excitation functions. In this model, a barrier distribution of asymmetric Gaussian form is used to take into account the effects of couplings between the relative motion and intrinsic degrees of freedom, as well as the effect of neutron transfer channels. Based on the interaction potential between the projectile and the target, empirical formulas are proposed to

calculate the parameters for the barrier distribution. We collect and compile 220 sets of capture excitation functions for reaction systems with $182 \leqslant Z_{\rm P}Z_{\rm T} \leqslant 1640$ and for 89 of them, the Q values for one neutron pair transfer channel are positive. We tabulate the parameters of barrier distributions, the calculated capture cross sections, and the experimental cross sections of these 220 reaction systems. The results show that for most of the reactions, this empirical coupled-channel model can describe the capture (fusion) cross sections very well in the energy region around the Coulomb barrier. We expect that this model will provide prediction of capture cross sections for the synthesis of superheavy nuclei as well as useful information on capture and fusion dynamics.

Acknowledgments

Helpful discussions with G. G. Adamian, P. R. S. Gomes, Alexander Karpov, Cheng-Jian Lin, Ning Wang, Huan-Qiao Zhang, Zhen-Hua Zhang, and Jie Zhao are gratefully acknowledged. We also thank P. R. S. Gomes and Huan-Qiao Zhang for a careful reading of this manuscript. This work has been partly supported by the National Key Basic Research Program of China (Grant No. 2013CB834400), the National Natural Science Foundation of China (Grants No. 11121403, No. 11175252, No. 11120101005, No. 11275248, No. 11475115, and No. 11525524), and the Knowledge Innovation Project of the Chinese Academy of Sciences (Grant No. KJCX2-EW-N01). The computational results presented in this work have been obtained on the High-performance Computing Cluster of SKLTP/ITP-CAS and the ScGrid of the Supercomputing Center, Computer Network Information Center of the Chinese Academy of Sciences. We also point out the usefulness of the NRV website [109] which is particularly helpful in the initial stage of this work.

References

[1] P. Fröbrich. Fusion and capture of heavy ions above the barrier: Analysis of experimental data with the surface friction model. *Phys. Rep.*, 116:337–400, 1984.

[2] A. B. Balantekin and N. Takigawa. Quantum tunneling in nuclear fusion. *Rev. Mod. Phys.*, 70:77–100, 1998.

[3] M. Dasgupta, D. J. Hinde, N. Rowley, and A. M. Stefanini. Measuring barriers to fusion. *Annu. Rev. Nucl. Part. Sci.*, 48:401–461, 1998.

[4] L. F. Canto, P. R. S. Gomes, R. Donangelo, and M. S. Hussein. Fusion and breakup of weakly bound nuclei. *Phys. Rep.*, 424:1–111, 2006.

[5] A. Diaz-Torres, L. R. Gasques, and M. Wiescher. Effects of nuclear molecular configurations on the astrophysical S-factor for ^{16}O+^{16}O. *Phys. Lett. B*, 652:255–258, 2007.

[6] HuanQiao Zhang, ChengJian Lin, HuiMing Jia, ChunLei Zhang, GaoLong Zhang, Feng Yang, ZuHua Liu, Guang-Peng An, ZhenDong Wu, XinXing Xu, and Fei Jia. Heavy ion reactions around the Coulomb barrier. *Sci. China G*, 54(s1):6, 2011.

[7] B. B. Back, H. Esbensen, C. L. Jiang, and K. E. Rehm. Recent developments in heavy-ion fusion reactions. *Rev. Mod. Phys.*, 86:317–360, 2014.

[8] L. F. Canto, P. R. S. Gomes, R. Donangelo, J. Lubian, and M. S. Hussein. Recent developments in fusion and direct reactions with weakly bound nuclei. *Phys. Rep.*, 596:1–86, 2015.

[9] N. V. Antonenko, E. A. Cherepanov, A. K. Nasirov, V. P. Permjakov, and V. V. Volkov. Competition between complete fusion and quasi-fission in reactions between massive nuclei. The fusion barrier. *Phys. Lett. B*, 319:425–430, 1993.

[10] G. G. Adamian, N. V. Antonenko, and W. Scheid. Model of competition between fusion and quasifission in reactions with heavy nuclei. *Nucl. Phys. A*, 618:176–198, 1997.

[11] G. G. Adamian, N. V. Antonenko, W. Scheid, and V. V. Volkov. Fusion cross sections for superheavy nuclei in the dinuclear system concept. *Nucl. Phys. A*, 633:409–420, 1998.

[12] G. G. Adamian, N. V. Antonenko, and Y. M. Tchuvil'Sky. Effect of structural forbiddenness in fusion of heavy nuclei. *Phys. Lett. B*, 451:289–295, 1999.

[13] A. Diaz-Torres, G. G. Adamian, N. V. Antonenko, and W. Scheid. Melting or nucleon transfer in fusion of heavy nuclei? *Phys. Lett. B*, 481:228–235, 2000.

[14] V. I. Zagrebaev. Synthesis of superheavy nuclei: Nucleon collectivization as a mechanism for compound nucleus formation. *Phys. Rev. C*, 64:034606, 2001.

[15] A. Diaz-Torres, G. G. Adamian, N. V. Antonenko, and W. Scheid. Quasifission process in a transport model for a dinuclear system. *Phys. Rev. C*, 64:024604, 2001.

[16] Yoshihiro Aritomo and Masahisa Ohta. Dynamical calculation for fusion-fission probability in superheavy mass region, where mass symmetric fission events originate. *Nucl. Phys. A*, 744:3–14, 2004.

[17] A. Diaz-Torres. Competition between fusion and quasifission in a heavy fusing system: Diffusion of nuclear shapes through a dynamical collective potential energy landscape. *Phys. Rev. C*, 74:064601, 2006.

[18] G. N. Knyazheva, E. M. Kozulin, R. N. Sagaidak, A. Yu. Chizhov, M. G. Itkis, N. A. Kondratiev, V. M. Voskressensky, A. M. Stefanini, B. R. Behera, L. Corradi, E. Fioretto, A. Gadea, A. Latina, S. Szilner, M. Trotta, S. Beghini, G. Montagnoli, F. Scarlassara, F. Haas, N. Rowley, P. R. S. Gomes, and A. Szanto de Toledo. Quasifission processes in ^{40,48}Ca + ^{144,154}Sm reactions. *Phys. Rev. C*, 75:064602, 2007.

[19] Minghui Huang, Zaiguo Gan, Xiaohong Zhou, Junqing Li, and Werner Scheid. Competing fusion and quasifission reaction mechanisms in the production of superheavy nuclei. *Phys. Rev. C*, 82:044614, 2010.

[20] Minghui Huang, Zhiyuan Zhang, Zaiguo Gan, Xiaohong Zhou, Junqing Li, and Werner Scheid. Dynamical deformation in heavy ion collisions and formation of superheavy nuclei. *Phys. Rev. C*, 84:064619, 2011.

[21] Nan Wang, En-Guang Zhao, Werner Scheid, and Shan-Gui Zhou. Theoretical study of the synthesis of superheavy nuclei with $Z = 119$ and 120 in heavy-ion reactions with trans-uranium targets. *Phys. Rev. C*, 85:041601, 2012.

[22] Jinjuan Zhang, Chengbin Wang, and Zhongzhou Ren. Calculation of evaporation residue cross sections for the synthesis of superheavy nuclei in hot fusion reactions. *Nucl. Phys. A*, 909:36–49, 2013.

[23] Nan Wang, Enguang Zhao, and Shan-Gui Zhou. Study of nuclear dynamical deformation in the synthesis of super-heavy nuclei. *J. Phys: Conf. Ser.*, 515:012022, 2014.

[24] Tathagata Banerjee, S. Nath, and Santanu Pal. Fusion probability in heavy nuclei. *Phys. Rev. C*, 91:034619, 2015.

[25] K. Siwek-Wilczyńska, E. Siemaszko, and J. Wilczyński. Can we predict capture and fusion excitation functions? *Acta Phys. Pol. B*, 33:451–456, 2002.

[26] Ning Wang, Kai Zhao, Werner Scheid, and Xizhen Wu. Fusion-fission reactions with a modified Woods-Saxon potential. *Phys. Rev. C*, 77:014603, 2008.

[27] Long Zhu, Wen-Jie Xie, and Feng-Shou Zhang. Production cross sections of superheavy elements $Z = 119$ and 120 in hot fusion reactions. *Phys. Rev. C*, 89:024615, 2014.

[28] R. G. Stokstad, Y. Eisen, S. Kaplanis, D. Pelte, U. Smilansky, and I. Tserruya. Fusion of ^{16}O + ^{148,150,152,154}Sm at sub-barrier energies. *Phys. Rev. C*, 21:2427–2435, 1980.

[29] C. H. Dasso, S. Landowne, and A. Winther. Channel-coupling effects in heavy-ion fusion reactions. *Nucl. Phys. A*, 405:381–396, 1983.

[30] C. H. Dasso, S. Landowne, and A. Winther. A study of Q-value effects on barrier penetration. *Nucl. Phys. A*, 407:221–232, 1983.

[31] R. A. Broglia, C. H. Dasso, S. Landowne, and A. Winther. Possible effect of transfer reactions on heavy ion fusion at sub-barrier energies. *Phys. Rev. C*, 27:2433–2435, 1983.

[32] Ian J. Thompson. Coupled reaction channels calculations in nuclear physics. *Comput. Phys. Rep.*, 7:167–212, 1988.

[33] K. Hagino, N. Rowley, and A. T. Kruppa. A program for coupled-channel calculations with all order couplings for heavy-ion fusion reactions. *Comput. Phys. Commun.*, 123:143–152, 1999.

[34] Kouichi Hagino and Noboru Takigawa. Subbarrier fusion reactions and many-particle quantum tunneling. *Prog. Theo. Phys.*, 128:1001–1060, 2012.

[35] M. Beckerman. Sub-barrier fusion of two nuclei. *Rep. Prog. Phys.*, 51:1047, 1988.

[36] V. I. Zagrebaev, Y. Aritomo, M. G. Itkis, Yu. Ts. Oganessian, and M. Ohta. Synthesis of superheavy nuclei: How accurately can we describe it and calculate the cross sections? *Phys. Rev. C*, 65:014607, 2001.

[37] V. I. Zagrebaev and V. V. Samarin. Near-barrier fusion of heavy nuclei: Coupling of channels. *Phys. At. Nucl.*, 67:1462–1477, 2004.

[38] Min Liu, Ning Wang, Zhuxia Li, Xizhen Wu, and Enguang Zhao. Applications of Skyrme energy-density functional to fusion reactions spanning the fusion barriers. *Nucl. Phys. A*, 768:80–98, 2006.

[39] Long Zhu, Zhao-Qing Feng, Cheng Li, and Feng-Shou Zhang. Orientation effects on evaporation residue cross sections in ^{48}Ca-induced hot fusion reactions. *Phys. Rev. C*, 90:014612, 2014.

[40] W. Reisdorf, F. P. Hessberger, K. D. Hildenbrand, S. Hofmann, G. Münzenberg, K.-H. Schmidt, J. H. R. Schneider, W. F. W. Schneider, K. Sümmerer, G. Wirth, J. V. Kratz, and K. Schlitt. Fusion near the threshold: A comparative study of the systems ^{40}Ar + ^{112,116,122}Sn and ^{40}Ar + ^{144,148,154}Sm. *Nucl. Phys. A*, 438:212–252, 1985.

[41] Debasis Atta and D. N. Basu. Fusion cross sections for reactions involving medium and heavy nucleus-nucleus systems. *Phys. Rev. C*, 90:064622, 2014.

[42] N. Rowley, G. R. Satchler, and P. H. Stelson. On the "distribution of barriers" interpretation of heavy-ion fusion.

Phys. Lett. B, 254:25–29, 1991.

[43] N. Rowley. Sub-barrier fusion: Probing reaction dynamics with barrier distributions. *Nucl. Phys. A*, 538:205c–220c, 1992.

[44] A. S. Umar and V. E. Oberacker. Heavy-ion interaction potential deduced from density-constrained time-dependent Hartree-Fock calculation. *Phys. Rev. C*, 74:021601, 2006.

[45] A. S. Umar, V. E. Oberacker, J. A. Maruhn, and P.-G. Reinhard. Microscopic composition of ion-ion interaction potentials. *Phys. Rev. C*, 85:017602, 2012.

[46] Jörg Aichelin. "quantum" molecular dynamics-a dynamical microscopic n-body approach to investigate fragment formation and the nuclear equation of state in heavy ion collisions. *Phys. Rep.*, 202:233–360, 1991.

[47] Ning Wang, Zhuxia Li, and Xizhen Wu. Improved quantum molecular dynamics model and its applications to fusion reaction near barrier. *Phys. Rev. C*, 65:064608, 2002.

[48] Ning Wang, Zhuxia Li, Xizhen Wu, Junlong Tian, YingXun Zhang, and Min Liu. Further development of the improved quantum molecular dynamics model and its application to fusion reactions near the barrier. *Phys. Rev. C*, 69:034608, 2004.

[49] YingXun Zhang, ChengShuang Zhou, JiXian Chen, Ning Wang, Kai Zhao, and ZhuXia Li. Correlation between the fragmentation modes and light charged particles emission in heavy ion collisions. *Sci. China Phys. Mech. Astron.*, 58:112002, 2015.

[50] Zhao-Qing Feng, Feng-Shou Zhang, Gen-Ming Jin, and Xi Huang. Improved isospin dependent quantum molecular dynamics model and its application to fusion reactions near Coulomb barrier. *Nucl. Phys. A*, 750:232–244, 2005.

[51] Zhao-Qing Feng, Gen-Ming Jin, and Feng-Shou Zhang. Dynamical analysis on heavy-ion fusion reactions near Coulomb barrier. *Nucl. Phys. A*, 802:91–106, 2008.

[52] Lu Guo, J. A. Maruhn, and P.-G. Reinhard. Boost-invariant mean field approximation and the nuclear Landau-Zener effect. *Phys. Rev. C*, 76:014601, 2007.

[53] Lu Guo, J. A. Maruhn, P.-G. Reinhard, and Y. Hashimoto. Conservation properties in the time-dependent Hartree Fock theory. *Phys. Rev. C*, 77:041301, 2008.

[54] Bao-An Bian, Feng-Shou Zhang, and Hong-Yu Zhou. Entrance channel mass asymmetry dependence of compound nucleus formation. *Phys. Lett. B*, 665:314–317, 2008.

[55] Bao-An Bian, Feng-Shou Zhang, and Hong-Yu Zhou. Fusion enhancement in the reactions of neutron-rich nuclei. *Nucl. Phys. A*, 829:1–12, 2009.

[56] Kai Wen, Fumihiko Sakata, Zhu-Xia Li, Xi-Zhen Wu, Ying-Xun Zhang, and Shan-Gui Zhou. Non-gaussian fluctuations and non-markovian effects in the nuclear fusion process: Langevin dynamics emerging from quantum molecular dynamics simulations. *Phys. Rev. Lett.*, 111:12501, 2013.

[57] Long Zhu, Jun Su, Wen-Jie Xie, and Feng-Shou Zhang. Study of the dynamical potential barriers in heavy ion collisions. *Nucl. Phys. A*, 915:90–105, 2013.

[58] Kai Wen, Fumihiko Sakata, Zhu-Xia Li, Xi-Zhen Wu, Ying-Xun Zhang, and Shan-Gui Zhou. Energy dependence of the nucleus-nucleus potential and the friction parameter in fusion reactions. *Phys. Rev. C*, 90:054613, 2014.

[59] Gao-Feng Dai, Lu Guo, En-Guang Zhao, and Shan-Gui Zhou. Effect of tensor force on dissipation dynamics in time-dependent Hartree-Fock theory. *Sci. China Phys. Mech. Astron.*, 57:1618, 2014.

[60] Gao-Feng Dai, Lu Guo, En-Guang Zhao, and Shan-Gui Zhou. Dissipation dynamics and spin-orbit force in time-dependent Hartree-Fock theory. *Phys. Rev. C*, 90:044609, 2014.

[61] Ning Wang, Kai Zhao, and Zhuxia Li. Systematic study of ^{16}O-induced fusion with the improved quantum molecular dynamics model. *Phys. Rev. C*, 90:054610, 2014.

[62] Xiang Jiang, Joachim A. Maruhn, and Shiwei Yan. Microscopic study of noncentral effects in heavy-ion fusion reactions with spherical nuclei. *Phys. Rev. C*, 90:064618, 2014.

[63] V. E. Oberacker and A. S. Umar. Microscopic analysis of sub-barrier fusion enhancement in ^{132}Sn + ^{40}Ca versus ^{132}Sn + ^{48}Ca. *Phys. Rev. C*, 87:034611, 2013.

[64] Ning Wang, Kai Zhao, and ZhuXia Li. Fusion and quasi-fission dynamics in nearly-symmetric reactions. *Sci. China Phys. Mech. Astron.*, 58:112001, 2015.

[65] D. Bourgin, C. Simenel, S. Courtin, and F. Haas. Microscopic study of ^{40}Ca + ^{58,64}Ni fusion reactions. *Phys. Rev. C*, 93:034604, 2016.

[66] V. V. Sargsyan, Z. Kanokov, G. G. Adamian, N. V. Antonenko, and W. Scheid. Capture process in nuclear reactions with a quantum master equation. *Phys. Rev. C*, 80:034606, 2009.

[67] V. V. Sargsyan, G. G. Adamian, N. V. Antonenko, and W. Scheid. Peculiarities of the sub-barrier fusion with the quantum diffusion approach. *Eur. Phys. J. A*, 45:125–130, 2010.

[68] V. V. Sargsyan, G. G. Adamian, N. V. Antonenko, W. Scheid, and H. Q. Zhang. Effects of nuclear deformation and neutron transfer in capture processes, and fusion hindrance at deep sub-barrier energies. *Phys. Rev. C*, 84:064614, 2011.

[69] A. Diaz-Torres, D. J. Hinde, M. Dasgupta, G. J. Milburn, and J. A. Tostevin. Dissipative quantum dynamics in low-energy collisions of complex nuclei. *Phys. Rev. C*, 78:064604, 2008.

[70] A. Diaz-Torres. Coupled-channels density-matrix approach to low-energy nuclear collision dynamics: A technique for quantifying quantum decoherence effects on reaction observables. *Phys. Rev. C*, 82:054617, 2010.

[71] A. Diaz-Torres, G. G. Adamian, V. V. Sargsyan, N. V. Antonenko. Energy-shifting formulae yield reliable reaction and capture probabilities. *Phys. Lett. B*, 739:348–351, 2014.

[72] V. V. Sargsyan, G. G. Adamian, N. V. Antonenko, and P. R. S. Gomes. Derivation of reaction cross sections from experimental elastic backscattering probabilities. *Phys. Rev. C*, 88:044606, 2013.

[73] V. V. Sargsyan, G. G. Adamian, N. V. Antonenko, A. Diaz-Torres, P. R. S. Gomes, and H. Lenske. Deriving capture and reaction cross sections from observed quasi-elastic and elastic backscattering. *Phys. Rev. C*, 90:064601, 2014.

[74] V. V. Sargsyan, G. G. Adamian, N. V. Antonenko, A. Diaz-Torres, P. R. S. Gomes, and H. Lenske. Derivation

of breakup probabilities of weakly bound nuclei from experimental elastic and quasi-elastic scattering angular distributions. *Phys. Rev. C*, 92:054620, 2015.

[75] Bing Wang, Wei-Juan Zhao, En-Guang Zhao, and Shan-Gui Zhou. Theoretical study of fusion reactions ^{32}S + ^{94,96}Zr and ^{40}Ca + ^{94,96}Zr and quadrupole deformation of ^{94}Zr. *Sci. China Phys. Mech. Astron.*, 59:642002, 2016.

[76] Bing Wang, Wei-Juan Zhao, Alexis Diaz-Torres, En-Guang Zhao, and Shan-Gui Zhou. Systematic study of suppression of complete fusion in reactions involving weakly bound nuclei at energies above the Coulomb barrier. *Phys. Rev. C*, 93:014615, 2016.

[77] J. O. Newton, R. D. Butt, M. Dasgupta, D. J. Hinde, I. I. Gontchar, C. R. Morton, and K. Hagino. Systematic failure of the Woods-Saxon nuclear potential to describe both fusion and elastic scattering: Possible need for a new dynamical approach to fusion. *Phys. Rev. C*, 70:024605, 2004.

[78] J. O. Newton, R. D. Butt, M. Dasgupta, D. J. Hinde, I. I. Gontchar, C. R. Morton, and K. Hagino. Systematics of precise nuclear fusion cross sections: the need for anew dynamical treatment of fusion? *Phys. Lett. B*, 586(3–4):219–224, 2004.

[79] D. L. Hill and J. A. Wheeler. Nuclear constitution and the interpretation of fission phenomena. *Phys. Rev.*, 89:1102, 1953.

[80] Lu-Lu Li, Shan-Gui Zhou, En-Guang Zhao, and Werner Scheid. A new barrier penetration formula and its application to α-decay half-lives. *Int. J. Mod. Phys. E*, 19(03):359–370, 2010.

[81] C. Y. Wong. Interaction barrier in charged-particle nuclear reactions. *Phys. Rev. Lett.*, 31:766–769, 1973.

[82] William H. Press, Saul A. Teukolsky, William T. Vetterling, and Brian P. Flannery. *Numerical Recipes in Fortran 90*, volume 2. Cambridge University Press, 1996.

[83] Aage Bohr and Ben R. Mottelson. *Nuclear structure*, volume 2. World Scientific, 1998.

[84] M. Beckerman, M. Salomaa, A. Sperduto, H. Enge, J. Ball, A. DiRienzo, S. Gazes, Yan Chen, J. D. Molitoris, and Mao Nai-feng. Dynamic influence of valence neutrons upon the complete fusion of massive nuclei. *Phys. Rev. Lett.*, 45:1472–1475, 1980.

[85] H. Timmers, L. Corradi, A. M. Stefanini, D. Ackermann, J. H. He, S. Beghini, G. Montagnoli, F. Scarlassara, G. F. Segato, and N. Rowley. Strong isotopic dependence of the fusion of ^{40}Ca + ^{90,96}Zr. *Phys. Lett. B*, 399:35–39, 1997.

[86] A. M. Stefanini, B. R. Behera, S. Beghini, L. Corradi, E. Fioretto, A. Gadea, G. Montagnoli, N. Rowley, F. Scarlassara, S. Szilner, and M. Trotta. Sub-barrier fusion of ^{40}Ca + ^{94}Zr: Interplay of phonon and transfer couplings. *Phys. Rev. C*, 76:014610, 2007.

[87] H. Q. Zhang, C. J. Lin, F. Yang, H. M. Jia, X. X. Xu, Z. D. Wu, F. Jia, S. T. Zhang, Z. H. Liu, A. Richard, and C. Beck. Near-barrier fusion of ^{32}S + ^{90,96}Zr: The effect of multi-neutron transfers in sub-barrier fusion reactions. *Phys. Rev. C*, 82:054609, 2010.

[88] J. J. Kolata, A. Roberts, A. M. Howard, D. Shapira, J. F. Liang, C. J. Gross, R. L. Varner, Z. Kohley, A. N. Villano, H. Amro, W. Loveland, and E. Chavez. Fusion of ^{124,132}Sn with ^{40,48}Ca. *Phys. Rev. C*, 85:054603, 2012.

[89] Z. Kohley, J. F. Liang, D. Shapira, C. J. Gross, R. L. Varner, J. M. Allmond, J. J. Kolata, P. E. Mueller, and A. Roberts. Sub-barrier fusion enhancement with radioactive ^{134}Te. *Phys. Rev. C*, 87:064612, 2013.

[90] H. M. Jia, C. J. Lin, F. Yang, X. X. Xu, H. Q. Zhang, Z. H. Liu, Z. D. Wu, L. Yang, N. R. Ma, P. F. Bao, and L. J. Sun. Fusion of $^{32}\mathrm{S} + ^{94}\mathrm{Zr}$: Further exploration of the effect of the positive Q_{xn} value neutron transfer channels. *Phys. Rev. C*, 89:064605, 2014.

[91] V. I. Zagrebaev. Sub-barrier fusion enhancement due to neutron transfer. *Phys. Rev. C*, 67:061601, 2003.

[92] V. I. Zagrebaev. Sequential fusion: Sub-barrier fusion enhancement due to neutron transfer. *Prog. Theor. Phys. Suppl.*, 154:122–129, 2004.

[93] V. A. Rachkov, A. V. Karpov, A. S. Denikin, and V. I. Zagrebaev. Examining the enhancement of sub-barrier fusion cross sections by neutron transfer with positive Q values. *Phys. Rev. C*, 90:014614, 2014.

[94] P. H. Stelson, H. J. Kim, M. Beckerman, D. Shapira, and R. L. Robinson. Fusion cross sections for ^{46,50}Ti+^{90}Zr,^{93}Nb and some systematics of heavy-ion fusion at barrier and subbarrier energies. *Phys. Rev. C*, 41:1584–1599, 1990.

[95] H. M. Jia, C. J. Lin, F. Yang, X. X. Xu, H. Q. Zhang, Z. H. Liu, L. Yang, S. T. Zhang, P. F. Bao, and L. J. Sun. Fusion of the ^{16}O+^{76}Ge and ^{18}O+^{74}Ge systems and the role of positive Q-value neutron transfers. *Phys. Rev. C*, 86:044621, 2012.

[96] C. L. Jiang, K. E. Rehm, B. B. Back, H. Esbensen, R. V. F. Janssens, A. M. Stefanini, and G. Montagnoli. Influence of heavy-ion transfer on fusion reactions. *Phys. Rev. C*, 89:051603, 2014.

[97] G. Scamps, V. V. Sargsyan, G. G. Adamian, N. V. Antonenko, and D. Lacroix. Analysis of the dependence of the few-neutron transfer probability on the Q-value magnitudes. *Phys. Rev. C*, 91:024601, 2015.

[98] G. L. Zhang, X. X. Liu, and C. J. Lin. Systematic analysis of the effect of a positive Q-value neutron transfer in fusion reactions. *Phys. Rev. C*, 89:054602, 2014.

[99] V. V. Sargsyan, G. G. Adamian, N. V. Antonenko, W. Scheid, and H. Q. Zhang. Influence of neutron transfer in reactions with weakly and strongly bound nuclei on the sub-barrier capture process. *Phys. Rev. C*, 86(1):014602, 2012.

[100] V. V. Sargsyan, G. Scamps, G. G. Adamian, N. V. Antonenko, and D. Lacroix. Neutron-pair transfer in the sub-barrier capture process. *Phys. Rev. C*, 88:064601, 2013.

[101] V. V. Sargsyan, G. G. Adamian, N. V. Antonenko, W. Scheid, and H. Q. Zhang. Examination of the different roles of neutron transfer in the sub-barrier fusion reactions $^{32}\mathrm{S} + ^{94,96}$ Zr and $^{40}\mathrm{Ca} + ^{94,96}$ Zr. *Phys. Rev. C*, 91:014613, 2015.

[102] G. Audi, M. Wang, A. H. Wapstra, F. G. Kondev, M. MacCormick, X. Xu, and B. Pfeiffer. The AME2012 atomic mass evaluation (I). Evaluation of input data, adjustment procedures. *Chin. Phys. C.*, 36:1287–1602, 2012.

[103] M. Wang, G. Audi, A.H. Wapstra, F.G. Kondev, M. MacCormick, X. Xu, and B. Pfeiffer. The AME2012 atomic mass evaluation (II). Tables, graphs and references. *Chin. Phys. C.*, 36:1603–2014, 2012.

[104] P. Möller, J. R. Nix, W. D. Myers, and W. J. Swiatecki. Nuclear ground-state masses and deformations. *At. Data*

Nucl. Data Tables, 59:185–381, 1995.

[105] Bing-Nan Lu, En-Guang Zhao, and Shan-Gui Zhou. Potential energy surfaces of actinide nuclei from a multidimensional constrained covariant density functional theory: Barrier heights and saddle point shapes. *Phys. Rev. C*, 85:011301, 2012.

[106] Bing-Nan Lu, Jie Zhao, En-Guang Zhao, and Shan-Gui Zhou. Multidimensionally-constrained relativistic mean-field models and potential-energy surfaces of actinide nuclei. *Phys. Rev. C*, 89:014323, 2014.

[107] Shan-Gui Zhou. Multidimensionally constrained covariant density functional theories—nuclear shapes and potential energy surfaces. *Phys. Scr.*, 91:063008, 2016.

[108] S. Goriely, M. Samyn, P.-H. Heenen, J. M. Pearson, and F. Tondeur. Hartree-Fock mass formulas and extrapolation to new mass data. *Phys. Rev. C*, 66:024326, 2002.

[109] V. I. Zagrebaev, A. S. Denikin, A. V. Karpov, A. P. Alekseev, V. V. Samarin, V. A. Rachkov, and M. A. Naumenko. Low-energy nuclear knowledge base (Nuclear Reaction Video). http://nrv.jinr.ru/nrv/.

[110] A. Diaz-Torres and I. J. Thompson. Effect of continuum couplings in fusion of halo ^{11}Be on ^{208}Pb around the Coulomb barrier. *Phys. Rev. C*, 65:024606, 2002.

[111] A. Diaz-Torres, D. J. Hinde, J. A. Tostevin, M. Dasgupta, and L. R. Gasques. Relating breakup and incomplete fusion of weakly bound nuclei through a classical trajectory model with stochastic breakup. *Phys. Rev. Lett.*, 98:152701, 2007.

[112] P. R. S. Gomes, J. Lubian, and L. F. Canto. Breakup effects in fusion reactions of stable weakly bound nuclei and light targets. *Phys. Rev. C*, 79:027606, 2009.

[113] P. R. S. Gomes, D. R. Otomar, T. Correa, L. F. Canto, J. Lubian, R. Linares, D. H. Luong, M. Dasgupta, D. J. Hinde, and M. S. Hussein. Complete fusion enhancement and suppression of weakly bound nuclei at near barrier energies. *J. Phys. G*, 39:115103, 2012.

[114] P. R. S. Gomes, L. F. Canto, L. Lubian, P. Lotti, L. C. Chamon, E. Crema, and J. M. B. Shorto. Breakup coupling effects on fusion of weakly bound nuclei. *Nucl. Phys. A*, 834:151c–154c, 2010.

[115] Bing Wang, Wei-Juan Zhao, P. R. S. Gomes, En-Guang Zhao, and Shan-Gui Zhou. Systematic study of breakup effects on complete fusion at energies above the Coulomb barrier. *Phys. Rev. C*, 90:034612, 2014.

[116] Jinjuan Zhang, Chengbin Wang, and Zhongzhou Ren. A systematic study of the fission and evaporation residue excitation functions in complete fusion reactions with weakly bound stable nuclei. *Nucl. Phys. A*, 864(1):128–139, 2011.

[117] Y. D. Fang, P. R. S. Gomes, J. Lubian, X. H. Zhou, Y. H. Zhang, J. L. Han, M. L. Liu, Y. Zheng, S. Guo, J. G. Wang, Y. H. Qiang, Z. G. Wang, X. G. Wu, C. Y. He, Y. Zheng, C. B. Li, S. P. Hu, and S. H. Yao. Fusion and one-neutron stripping reactions in the ^{9}Be + ^{181}W system above the Coulomb barrier. *Phys. Rev. C*, 87:024604, 2013.

[118] Y. D. Fang, P. R. S. Gomes, J. Lubian, M. L. Liu, X. H. Zhou, D. R. Mendes Junior, N. T. Zhang, Y. H. Zhang, G. S. Li, J. G. Wang, S. Guo, Y. H. Qiang, B. S. Gao, Y. Zheng, X. G. Lei, and Z. G. Wang. Complete and

incomplete fusion of ^{9}Be + ^{169}Tm, ^{187}Re at near-barrier energies. *Phys. Rev. C*, 91:014608, 2015.

[119] C. L. Guo, G. L. Zhang, S. P. Hu, J. C. Yang, H. Q. Zhang, P. R. S. Gomes, J. Lubian, X. G. Wu, J. Zhong, C. Y. He, Y. Zheng, C. B. Li, G. S. Li, W. W. Qu, F. Wang, L. Zheng, L. Yu, Q. M. Chen, P. W. Luo, H. W. Li, Y. H. Wu, W. K. Zhou, B. J. Zhu, and H. B. Sun. Coupling effects on the fusion of ^{6}Li+^{154}Sm at energies slightly above the Coulomb barrier. *Phys. Rev. C*, 92:014615, 2015.

[120] S. P. Hu, G. L. Zhang, J. C. Yang, H. Q. Zhang, P. R. S. Gomes, J. Lubian, X. G. Wu, J. Zhong, C. Y. He, Y. Zheng, C. B. Li, G. S. Li, W. W. Qu, F. Wang, L. Zheng, L. Yu, Q. M. Chen, P. W. Luo, H. W. Li, Y. H. Wu, W. K. Zhou, B. J. Zhu, and H. B. Sun. Small suppression of the complete fusion of the ^{6}Li+^{96}Zr system at near-barrier energies. *Phys. Rev. C*, 91:044619, 2015.

[121] S. P. Hu, G. L. Zhang, J. C. Yang, H. Q. Zhang, P. R. S. Gomes, J. Lubian, J. L. Ferreira, X. G. Wu, J. Zhong, C. Y. He, Y. Zheng, C. B. Li, G. S. Li, W. W. Qu, F. Wang, L. Zheng, L. Yu, Q. M. Chen, P. W. Luo, H. W. Li, Y. H. Wu, W. K. Zhou, B. J. Zhu, and H. B. Sun. One-neutron stripping processes to excited states of the ^{6}Li +^{96} Zr reaction at near-barrier energies. *Phys. Rev. C*, 93:014621, 2016.

[122] Y. D. Fang, P. R. S. Gomes, J. Lubian, J. L. Ferreira, D. R. Mendes Junior, X. H. Zhou, M. L. Liu, N. T. Zhang, Y. H. Zhang, G. S. Li, J. G. Wang, S. Guo, Y. H. Qiang, B. S. Gao, Y. Zheng, X. G. Lei, and Z. G. Wang. One-neutron stripping from ^{9}Be to ^{169}Tm, ^{181}Ta, and ^{187}Re at near-barrier energies. *Phys. Rev. C*, 93:034615, 2016.

[123] M. R. Cortes, P. R. S. Gomes, J. Lubian, D. Mendes Jr. Search of a systematic behaviour for the weakly bound complete fusion suppression caused by breakup. *J. Phys: Conf. Ser.*, 630:012017, 2015.

[124] J. R. Leigh, M. Dasgupta, D. J. Hinde, J. C. Mein, C. R. Morton, R. C. Lemmon, J. P. Lestone, J. O. Newton, H. Timmers, J. X. Wei, and N. Rowley. Barrier distributions from the fusion of oxygen ions with ^{144,148,154}Sm and ^{186}W. *Phys. Rev. C*, 52:3151–3166, 1995.

[125] Y. Nagashima, J. Schimizu, T. Nakagawa, Y. Fukuchi, W. Yokota, K. Furuno, M. Yamanouchi, S. M. Lee, N. X. Dai, T. Mikumo, and T. Motobayashi. Effects of entrance channel and compound nucleus in the fusion cross sections for ^{28}Si+^{28}Si, ^{16}O+^{40}Ca, ^{32}S+^{30}Si, and ^{12}C+^{50}Cr. *Phys. Rev. C*, 33:176–184, 1986.

[126] P. Eudes, Z. Basrak, F. Sébille, V. de la Mota, and G. Royer. Comprehensive analysis of fusion data well above the barrier. *Phys. Rev. C*, 90:034609, 2014.

[127] Ş. Mişicu and H. Esbensen. Hindrance of heavy-ion fusion due to nuclear incompressibility. *Phys. Rev. Lett.*, 96:112701, 2006.

[128] M. Dasgupta, D. J. Hinde, A. Diaz-Torres, B. Bouriquet, Catherine I. Low, G. J. Milburn, and J. O. Newton. Beyond the coherent coupled channels description of nuclear fusion. *Phys. Rev. Lett.*, 99:192701, 2007.

[129] Takatoshi Ichikawa, Kouichi Hagino, and Akira Iwamoto. Existence of a one-body barrier revealed in deep sub-barrier fusion. *Phys. Rev. C*, 75:057603, 2007.

[130] Takatoshi Ichikawa, Kouichi Hagino, and Akira Iwamoto. Signature of smooth transition from sudden to adiabatic states in heavy-ion fusion reactions at deep sub-barrier energies. *Phys. Rev. Lett.*, 103:202701, 2009.

[131] V. Yu. Denisov. Nucleus-nucleus potential with shell-correction contribution and deep sub-barrier fusion of heavy nuclei. *Phys. Rev. C*, 89:044604, 2014.

[132] M. Beckerman, M. Salomaa, A. Sperduto, J. D. Molitoris, and A. DiRienzo. Sub-barrier fusion of ^{58,64}Ni with ^{64}Ni and ^{74}Ge. *Phys. Rev. C*, 25:837–849, 1982.

[133] D. E. DiGregorio, M. diTada, D. Abriola, M. Elgue, A. Etchegoyen, M. C. Etchegoyen, J. O. Fernández Niello, A. M. J. Ferrero, S. Gil, A. O. Macchiavelli, A. J. Pacheco, J. E. Testoni, P. R. Silveira Gomes, V. R. Vanin, R. Liguori Neto, E. Crema, and R. G. Stokstad. Subbarrier fusion of ^{16}O + ^{147,149}Sm. *Phys. Rev. C*, 39:516–523, 1989.

[134] P. R. S. Gomes, J. Lubian, I. Padron, and R. M. Anjos. Uncertainties in the comparison of fusion and reaction cross sections of different systems involving weakly bound nuclei. *Phys. Rev. C*, 71(1):017601, 2005.

[135] L. F. Canto, P. R. S. Gomes, J. Lubian, L. C. Chamon, and E. Crema. Disentangling static and dynamic effects of low breakup threshold in fusion reactions. *JPG*, 36(1):015109, 2009.

[136] L. F. Canto, P. R. S. Gomes, J. Lubian, L. C. Chamon, and E. Crema. Dynamic effects of breakup on fusion reactions of weakly bound nuclei. *Nucl. Phys. A*, 821:51–71, 2009.

[137] Roman Wolski. Compound nucleus aspect of sub-barrier fusion: A new energy scaling behavior. *Phys. Rev. C*, 88(4):041603, 2013.

[138] W. W. Qu, G. L. Zhang, H. Q. Zhang, and R. Wolski. Comparative studies of Coulomb barrier heights for nuclear models applied to sub-barrier fusion. *Phys. Rev. C*, 90:064603, 2014.

[139] L. F. Canto, D. R. Mendes Junior, P. R. S. Gomes, and J. Lubian. Reduction of fusion and reaction cross sections at near-barrier energies. *Phys. Rev. C*, 92:014626, 2015.

[140] P. R. S. Gomes, D. R. Mendes Junior, L. F. Canto, J. Lubian, and P. N. de Faria. Reduction Methods for Total Reaction Cross Sections. *Few-Body Syst.*, 57:205, 2016.

[141] P. R. S. Gomes, J. Lubian, L. F. Canto, D. R. Otomar, D. R. Mendes Junior, P. N. de Faria, R. Linares, L. Sigaud, J. Rangel, J. L. Ferreira, E. Ferioli, B. Paes, E. N. Cardozo, M. R. Cortes, M. J. Ermamatov, P. Lotti, and M. S. Hussein. Reactions with Weakly Bound Nuclei, at near Barrier Energies, and the Breakup and Transfer Influences on the Fusion and Elastic Scattering. *Few-Body Syst.*, 57:165, 2015.

[142] M. A. Cândido Ribeiro, L. C. Chamon, D. Pereira, M. S. Hussein, and D. Galetti. Pauli nonlocality in heavy-ion rainbow scattering: A further test of the folding model. *Phys. Rev. Lett.*, 78(17):3270–3273, 1997.

[143] L. C. Chamon, D. Pereira, M. S. Hussein, M. A. Cândido Ribeiro, and D. Galetti. Nonlocal description of the nucleus-nucleus interaction. *Phys. Rev. Lett.*, 79(1):5218–5221, 1997.

[144] L. C. Chamon, B. V. Carlson, L. R. Gasques, D. Pereira, C. De Conti, M. A. G. Alvarez, M. S. Hussein, M. A. Cândido Ribeiro, E. S. Rossi, and C. P. Silva. Toward a global description of the nucleus-nucleus interaction. *Phys. Rev. C*, 66:014610, 2002.

[145] A. V. Karpov, V. A. Rachkov, and V. V. Samarin. Quantum coupled-channels model of nuclear fusion with a semiclassical consideration of neutron rearrangement. *Phys. Rev. C*, 92:064603, 2015.

[146] H. Esbensen, G. Montagnoli, and A. M. Stefanini. Revised analysis of ^{40}Ca + ^{96}Zr fusion reactions. *Phys. Rev. C*, 93:034609, 2016.

[147] C. S. Palshetkar, S. Santra, A. Chatterjee, K. Ramachandran, Shital Thakur, S. K. Pandit, K. Mahata, A. Shrivastava, V. V. Parkar, and V. Nanal. Fusion of the weakly bound projectile ^{9}Be with ^{89}Y. *Phys. Rev. C*, 82:044608, 2010.

[148] J. O. Newton, C. R. Morton, M. Dasgupta, J. R. Leigh, J. C. Mein, D. J. Hinde, H. Timmers, and K. Hagino. Experimental barrier distributions for the fusion of ^{12}C, ^{16}O, ^{28}Si, and ^{35}Cl with ^{92}Zr and coupled-channels analyses. *Phys. Rev. C*, 64:064608, 2001.

[149] D. Abriola, A. A. Sonzogni, M. di Tada, A. Etchegoyen, M. C. Etchegoyen, J. O. Fernández Niello, S. Gil, A. O. Macchiavelli, A. J. Pacheco, R. Piegaia, and J. E. Testoni. Fusion and elastic scattering for the ^{12}C+^{144}Sm system at energies near to the Coulomb barrier. *Phys. Rev. C*, 46:244–249, 1992.

[150] R. Broda, M. Ishihara, B. Herskind, and H. Oeschler. Heavy-ion fusion cross sections. *Nucl. Phys. A*, 248:356–376, 1975.

[151] S. Gil, R. Vandenbosch, A. J. Lazzarini, D.-K. Lock, and A. Ray. Spin distribution of the compound nucleus in heavy ion reactions at near-barrier energies. *Phys. Rev. C*, 31:1752–1762, 1985.

[152] M. Crippa, E. Gadioli, P. Vergani, G. Ciavola, C. Marchetta, and M. Bonardi. Excitation functions for production of heavy residues in the interaction of ^{12}C with ^{181}Ta. *Z. Phys. A*, 350:121–129, 1994.

[153] A. Shrivastava, S. Kailas, A. Chatterjee, A. Navin, A. M. Samant, P. Singh, S. Santra, K. Mahata, B. S. Tomar, and G. Pollarolo. Collectivity against nucleon transfer in sub-barrier fusion of ^{12}C+^{194,198}Pt. *Phys. Rev. C*, 63:054602, 2001.

[154] R. N. Sagaidak, G. N. Kniajeva, I. M. Itkis, M. G. Itkis, N. A. Kondratiev, E. M. Kozulin, I. V. Pokrovsky, A. I. Svirikhin, V. M. Voskressensky, A. V. Yeremin, L. Corradi, A. Gadea, A. Latina, A. M. Stefanini, S. Szilner, M. Trotta, A. M. Vinodkumar, S. Beghini, G. Montagnoli, F. Scarlassara, D. Ackermann, F. Hanappe, N. Rowley, and L. Stuttgé. Fusion suppression in mass-asymmetric reactions leading to Ra compound nuclei. *Phys. Rev. C*, 68:014603, 2003.

[155] A. Mukherjee, D. J. Hinde, M. Dasgupta, K. Hagino, J. O. Newton, and R. D. Butt. Failure of the Woods-Saxon nuclear potential to simultaneously reproduce precise fusion and elastic scattering measurements. *Phys. Rev. C*, 75:044608, 2007.

[156] Zuhua Liu, Huanqiao Zhang, Jincheng Xu, Yu Qiao, Xing Qian, and Chengjian Lin. Fission before K equilibration. *Phys. Rev. C*, 54:761–766, 1996.

[157] Victor E. Viola and Torbjørn Sikkeland. Total cross sections for fission of U^{238} induced by He^{4} and heavy ions. *Phys. Rev.*, 128:767–774, 1962.

[158] P. R. S. Gomes, T. J. P. Penna, E. F. Chagas, R. Liguori Neto, J. C. Acquadro, P. R. Pascholati, E. Crema, C. Tenreiro, N. Carlin Filho, and M. M. Coimbra. Fusion of ^{59}Co with light projectiles at near barrier energies. *Nucl. Phys. A*, 534:429–444, 1991.

[159] Bivash R. Behera, M. Satpathy, S. Jena, S. Kailas, R. G. Thomas, K. Mahata, A. Chatterjee, Subinit Roy, P. Basu, M. K. Sharan, and S. K. Datta. Fission fragment angular distributions for the systems ^{14}N + ^{232}Th and ^{11}B + ^{235}U at near and sub-barrier energies. *Phys. Rev. C*, 69:064603, 2004.

[160] H. Funaki and E. Arai. Anomaly in the ^{15}N, ^{16}O, ^{19}F + ^{54,56}Fe fusion cross sections around the Coulomb barrier energy. *Nucl. Phys. A*, 556:307–316, 1993.

[161] E. Vulgaris, L. Grodzins, S. G. Steadman, and R. Ledoux. Fusion, transfer, and elastic scattering at sub-barrier energies for ^{16,18}O ions on ^{208}Pb and ^{15}N and ^{16}O ions on ^{209}Bi. *Phys. Rev. C*, 33:2017–2027, 1986.

[162] N. Keeley, J. S. Lilley, J. X. Wei, M. Dasgupta, D. J. Hinde, J. R. Leigh, J. C. Mein, C. R. Morton, H. Timmers, and N. Rowley. Fusion excitation function measurements for the ^{16}O+^{58}Ni and ^{16}O+^{62}Ni systems. *Nucl. Phys. A*, 628:1–16, 1998.

[163] E. F. Aguilera, J. J. Kolata, and R. J. Tighe. Nuclear structure effects in the sub-barrier fusion of ^{16}O + ^{70,72,73,74,76}Ge. *Phys. Rev. C*, 52:3103–3113, 1995.

[164] D. Ackermann, L. Corradi, D. R. Napoli, C. M. Petrache, P. Spolaore, A. M. Stefanini, F. Scarlassara, S. Beghini, G. Montagnoli, G. F. Segato, and C. Signorini. Subbarrier fusion of ^{16}O + ^{112}Cd: Cross sections and mean angular momenta. *Nucl. Phys. A*, 575:374–380, 1994.

[165] G. Duchêne, P. Romain, F. A. Beck, Ph. Benet, D. Disdier, B. Haas, B. Lott, V. Rauch, F. Scheibling, J. P. Vivien, S. K. Basu, E. Bozek, K. Zuber, D. Di Gregorio, and J. Fernandez-Niello. Angular momentum distributions for ^{16}O+^{144}Nd. *Phys. Rev. C*, 47:2043–2054, 1993.

[166] J. O. Fernández Niello, M. di Tada, A. O. Macchiavelli, A. J. Pacheco, D. Abriola, M. Elgue, A. Etchegoyen, M. C. Etchegoyen, S. Gil, and J. E. Testoni. Hexadecapole deformation effects in subbarrier fusion reactions. *Phys. Rev. C*, 43:2303–2306, 1991.

[167] R. C. Lemmon, J. R. Leigh, J. X. Wei, C. R. Morton, D. J. Hinde, J. O. Newton, J. C. Mein, M. Dasgupta, and N. Rowley. Strong dependence of sub-barrier fusion on the nuclear hexadecapole deformation. *Phys. Lett. B*, 316:32–37, 1993.

[168] C. R. Morton, A. C. Berriman, M. Dasgupta, D. J. Hinde, J. O. Newton, K. Hagino, and I. J. Thompson. Coupled-channels analysis of the ^{16}O+^{208}Pb fusion barrier distribution. *Phys. Rev. C*, 60:044608, 1999.

[169] Huanqiao Zhang, Jincheng Xu, Zuhua Liu, Jun Lu, Ming Ruan, and Kan Xu. Anomalous anisotropies of fission fragments for the ^{16}O+^{232}Th sub-barrier fusion-fission reaction. *Phys. Rev. C*, 42:1086–1091, 1990.

[170] B. B. Back, R. R. Betts, J. E. Gindler, B. D. Wilkins, S. Saini, M. B. Tsang, C. K. Gelbke, W. G. Lynch, M. A. McMahan, and P. A. Baisden. Angular distributions in heavy-ion-induced fission. *Phys. Rev. C*, 32:195–213, 1985.

[171] E. Bozek, D. M. De Castro-Rizzo, S. Cavallaro, B. Delaunay, J. Delaunay, H. Dumont, A. D'onofrio, M-G. Saint-Laurent, L. Sperduto, and F. Terrasi. De-excitation of ^{58,60,62}Ni compound nuclei formed via symmetric and asymmetric entrance channels. *Nucl. Phys. A*, 451:171–188, 1986.

[172] P. Jacobs, Z. Fraenkel, G. Mamane, and I. Tserruya. Sub-Coulomb barrier fusion of O+Sn. *Phys. Lett. B*, 175:271–274, 1986.

[173] R. J. Charity, J. R. Leigh, and J. J. M. Bokhorst. Heavy-ion induced fusion-fission systematics and the effect of the compound-nucleus spin distribution on fission-barrier determination. *Nucl. Phys. A*, 457:441–460, 1986.

[174] N. V. S. V. Prasad, A. M. Vinodkumar, A. K. Sinha, K. M. Varier, D. L. Sastry, N. Madhavan, P. Sugathan, D. O. Kataria, and J. J. Das. Study of transfer channel coupling and entrance channel effects for the near and sub-barrier fusion of ^{46}Ti+^{64}Ni, ^{50}Ti+^{60}Ni and ^{19}F+^{93}Nb systems. *Nucl. Phys. A*, 603:176–202, 1996.

[175] D. J. Hinde, A. C. Berriman, M. Dasgupta, J. R. Leigh, J. C. Mein, C. R. Morton, and J. O. Newton. Limiting angular momentum for statistical model description of fission. *Phys. Rev. C*, 60:054602, 1999.

[176] A. M. Samant, S. Kailas, A. Chatterjee, A. Shrivastava, A. Navin, and P. Singh. Fission fragment anisotropies for ^{19}F +^{209}Bi system. *Eur. Phys. J. A*, 7:59–64, 2000.

[177] R. Butsch, H. Jänsch, D. Krämer, K.-H. Möbius, W. Ott, E. Steffens, G. Tungate, Weller, A., K. Becker, K. Blatt, H. Leucker, W. Luck, D. Fick, and P. Paul. Fusion evaporation and fusion-fission with aligned ^{23}Na ions at energies near and below the fusion barrier. *Phys. Rev. C*, 36:1351–1363, 1987.

[178] C. L. Jiang, K. E. Rehm, H. Esbensen, B. B. Back, R. V. F. Janssens, P. Collon, C. M. Deibel, B. DiGiovine, J. M. Figueira, J. P. Greene, D. J. Henderson, H. Y. Lee, M. Notani, S. T. Marley, R. C. Pardo, N. Patel, D. Seweryniak, X. D. Tang, C. Ugalde, and S. Zhu. Fusion hindrance for ^{27}Al + ^{45}Sc and other systems with a positive Q value. *Phys. Rev. C*, 81:024611, 2010.

[179] E. F. Aguilera, J. J. Vega, J. J. Kolata, A. Morsad, R. G. Tighe, and X. J. Kong. Sub-barrier fusion of ^{27}Al+^{70,72,73,74,76}Ge: Evidence for shape transition and structure effects. *Phys. Rev. C*, 41:910–919, 1990.

[180] Y. X. Watanabe, A. Yoshida, T. Fukuda, T. Sekine, Y. Watanabe, H. Ikezoe, Y. Nagame, T. Ikuta, I. Nishinaka, Y. Mizoi, J. Nakano, M. Hirai, H. Sakurai, H. Kobinata, Y. Pu, K. Kimura, and M. Ishihara. Measurement of fusion excitation functions of ^{27,29,31}Al + ^{197}Au. *Eur. Phys. J. A*, 10:373–379, 2001.

[181] G. Montagnoli, A. M. Stefanini, H. Esbensen, C. L. Jiang, L. Corradi, S. Courtin, E. Fioretto, J. Grebosz, F. Haas, H. M. Jia, M. Mazzocco, C. Michelagnoli, T. Mijatović, D. Montanari, C. Parascandolo, F. Scarlassara, E. Strano, S. Szilner, and D. Torresi. Fusion of ^{28}Si + ^{28,30}Si: Different trends at sub-barrier energies. *Phys. Rev. C*, 90:044608, 2014.

[182] M. Dasgupta, A. Navin, Y. K. Agarwal, C. V. K. Baba, H. C. Jain, M. L. Jhingan, and A. Roy. Fusion of ^{28}Si + ^{68}Zn, ^{32}S + ^{64}Ni, ^{37}Cl + ^{59}Co and ^{45}Sc + ^{51}V in the vicinity of the Coulomb barrier. *Nucl. Phys. A*, 539:351–369, 1992.

[183] Sunil Kalkal, S. Mandal, N. Madhavan, E. Prasad, Shashi Verma, A. Jhingan, Rohit Sandal, S. Nath, J. Gehlot, B. R. Behera, Mansi Saxena, Savi Goyal, Davinder Siwal, Ritika Garg, U. D. Pramanik, Suresh Kumar, T. Varughese, K. S. Golda, S. Muralithar, A. K. Sinha, and R. Singh. Channel coupling effects on the fusion excitation functions for ^{28}Si + ^{90,94}Zr in sub- and near-barrier regions. *Phys. Rev. C*, 81:044610, 2010.

[184] Lagy T. Baby, Vandana Tripathi, D. O. Kataria, J. J. Das, P. Sugathan, N. Madhavan, A. K. Sinha, M. C. Radhakrishna, N. M. Badiger, N. G. Puttaswamy, A. M. Vinodkumar, and N. V. S. V. Prasad. Transfer and higher-order phonon coupling effects in the sub-barrier fusion of ^{28}Si and ^{93}Nb. *Phys. Rev. C*, 56:1936–1942, 1997.

[185] S. Gil, F. Hasenbalg, J. E. Testoni, D. Abriola, M. C. Berisso, M. di Tada, A. Etchegoyen, J. O. Fernández Niello, A. J. Pacheco, A. Charlop, A. A. Sonzogni, and R. Vandenbosch. Fusion cross sections in systems leading to ^{170}Hf at near-barrier energies. *Phys. Rev. C*, 51:1336–1344, 1995.

[186] S. Gil, D. Abriola, D. E. DiGregorio, M. di Tada, M. Elgue, A. Etchegoyen, M. C. Etchegoyen, J. Fernández Niello, A. M. J. Ferrero, A. O. Macchiavelli, A. J. Pacheco, J. E. Testoni, P. Silveira Gomes, V. R. Vanin, A. Charlop, A. Garca, S. Kailas, S. J. Luke, E. Renshaw, and R. Vandenbosch. Observation of mean-spin barrier bump in sub-barrier fusion of ^{28}Si with ^{154}Sm. *Phys. Rev. Lett.*, 65:3100–3103, 1990.

[187] D. J. Hinde, R. J. Charity, G. S. Foote, J. R. Leigh, J. O. Newton, S. Ogaza, and A. Chattejee. Neutron multiplicities in heavy-ion-induced fission: Timescale of fusion-fission. *Nucl. Phys. A*, 452:550–572, 1986.

[188] K. Nishio, H. Ikezoe, S. Mitsuoka, and J. Lu. Fusion of deformed nuclei in the reactions of ^{76}Ge+^{150}Nd and ^{28}Si+^{198}Pt at the Coulomb barrier region. *Phys. Rev. C*, 62:014602, 2000.

[189] D. J. Hinde, C. R. Morton, M. Dasgupta, J. R. Leigh, J. C. Mein, and H. Timmers. Competition between fusion-fission and quasi-fission in the reaction ^{28}Si+^{208}Pb. *Nucl. Phys. A*, 592:271–289, 1995.

[190] K. Nishio, H. Ikezoe, I. Nishinaka, S. Mitsuoka, K. Hirose, T. Ohtsuki, Y. Watanabe, Y. Aritomo, and S. Hofmann. Evidence for quasifission in the sub-barrier reaction of ^{30}Si+^{238}U. *Phys. Rev. C*, 82:044604, 2010.

[191] G. M. Berkowitz, P. Braun-Munzinger, J. S. Karp, R. H. Freifelder, T. R. Renner, and H. W. Wilschut. Fusion near and below the barrier for the systems ^{32,34}S+^{24,25,26}Mg and ^{32}S+^{27}Al. *Phys. Rev. C*, 28:667–678, 1983.

[192] H. H. Gutbrod, W. G. Winn, and M. Blann. Measurement and interpretation of heavy ion fusion excitation functions. *Nucl. Phys. A*, 213:267–284, 1973.

[193] G. Montagnoli, A. M. Stefanini, H. Esbensen, C. L. Jiang, L. Corradi, S. Courtin, E. Fioretto, A. Goasduff, J. Grebosz, F. Haas, M. Mazzocco, C. Michelagnoli, T. Mijatovic, D. Montanari, C. Parascandolo, K. E. Rehm, F. Scarlassara, S. Szilner, X. D. Tang, and C. A. Ur. Effects of transfer channels on near- and sub-barrier fusion of ^{32}S + ^{48}Ca. *Phys. Rev. C*, 87:014611, 2013.

[194] A. Mukherjee, M. Dasgupta, D. J. Hinde, K. Hagino, J. R. Leigh, J. C. Mein, C. R. Morton, J. O. Newton, and H. Timmers. Dominance of collective over proton transfer couplings in the fusion of ^{32}S and ^{34}S with ^{89}Y. *Phys. Rev. C*, 66:034607, 2002.

[195] R. Pengo, D. Evers, K. E. G. Löbner, U. Quade, K. Rudolph, S. J. Skorka, and I. Weidl. Nuclear structure effects in sub-barrier fusion cross sections. *Nucl. Phys. A*, 411:255–274, 1983.

[196] P. R. S. Gomes, I. C. Charret, R. Wanis, G. M. Sigaud, V. R. Vanin, R. Liguori Neto, D. Abriola, O. A. Capurro, D. E. DiGregorio, M. di Tada, G. Duchene, M. Elgue, A. Etchegoyen, J. O. Fernández Niello, A. M. J. Ferrero, S. Gil, A. O. Macchiavelli, A. J. Pacheco, and J. E. Testoni. Fusion of ^{32}S+^{154}Sm at sub-barrier energies. *Phys. Rev. C*, 49:245–249, 1994.

[197] S. Mitsuoka, H. Ikezoe, K. Nishio, and J. Lu. Sub-barrier fusion of deformed nuclei in ^{60}Ni+^{154}Sm and ^{32}S+^{182}W reactions. *Phys. Rev. C*, 62:054603, 2000.

[198] H. Q. Zhang, C. L. Zhang, C. J. Lin, Z. H. Liu, F. Yang, A. K. Nasirov, G. Mandaglio, M. Manganaro, and

G. Giardina. Competition between fusion-fission and quasifission processes in the $^{32}S + ^{184}W$ reaction. *Phys. Rev. C*, 81:034611, 2010.

[199] D. J. Hinde, M. Dasgupta, N. Herrald, R. G. Neilson, J. O. Newton, and M. A. Lane. Isotopic dependence of fusion barrier energies in reactions forming heavy elements. *Phys. Rev. C*, 75:054603, 2007.

[200] L. Corradi, S. J. Skorka, U. Lenz, K. E. G. Löbner, P. R. Pascholati, U. Quade, K. Rudolph, W. Schomburg, M. Steinmayer, H. G. Thies, G. Montagnoli, D. R. Napoli, A. M. Stefanini, A. Tivelli, S. Beghini, F. Scarlassara, C. Signorini, and F. Soramel. Near-barrier transfer and fusion of the systems $^{33}S + ^{90,91,92}Zr$. *Z. Phys. A*, 335:55–72, 1990.

[201] C. R. Morton, A. C. Berriman, R. D. Butt, M. Dasgupta, A. Godley, D. J. Hinde, and J. O. Newton. Memory of the entrance-channel K distribution observed in fission at high angular momentum. *Phys. Rev. C*, 62:024607, 2000.

[202] Sl. Cavallaro, M. L. Sperduto, B. Delaunay, J. Delaunay, A. D'Onofrio, and H. Dumont. Sub-barrier fusion induced by $^{35}C1$ and $^{37}C1$ beams on $^{24,25,26}Mg$ isotopes. *Nucl. Phys. A*, 513:174–186, 1990.

[203] W. Scobel, H. H. Gutbrod, M. Blann, and A. Mignerey. Fusion and interaction barrier parameters and critical angular momenta from ^{35}Cl-induced reactions. *Phys. Rev. C*, 14:1808–1823, 1976.

[204] E. M. Szanto, R. Liguori Neto, M. C. S. Figueira, A. Szanto de Toledo, M. G. Herman, N. G. Nicolis, P. M. Stwertka, and T. M. Cormier. Search for valence proton effects in sub-barrier fusion reactions. *Phys. Rev. C*, 41:2164–2171, 1990.

[205] A. M. Stefanini, G. Montagnoli, R. Silvestri, S. Beghini, L. Corradi, S. Courtin, E. Fioretto, B. Guiot, F. Haas, D. Lebhertz, N. Mărginean, P. Mason, F. Scarlassara, R. N. Sagaidak, and S. Szilner. Fusion of the positive Q-value system $^{36}S + ^{48}Ca$ well below the Coulomb barrier. *Phys. Rev. C*, 78:044607, 2008.

[206] G. Montagnoli, A. M. Stefanini, L. Corradi, S. Courtin, E. Fioretto, F. Haas, D. Lebhertz, F. Scarlassara, R. Silvestri, and S. Szilner. Sub-barrier fusion of $^{36}S + ^{64}Ni$ and other medium-light systems. *Phys. Rev. C*, 82:064609, 2010.

[207] A. M. Stefanini, L. Corradi, A. M. Vinodkumar, Yang Feng, F. Scarlassara, G. Montagnoli, S. Beghini, and M. Bisogno. Near-barrier fusion of $^{36}S + ^{90,96}Zr$: the effect of the strong octupole vibration of ^{96}Zr. *Phys. Rev. C*, 62:014601, 2000.

[208] M. G. Itkis, I. M. Itkis, G. N. Knyazheva, and E. M. Kozulin. Fusion-fission and quasifission of superheavy systems in heavy-ion induced reactions. *NPA*, 834:374c–377c, 2010. The 10th International Conference on Nucleus-Nucleus Collisions (NN2009).

[209] E. Martínez-Quiroz, E. F. Aguilera, J. J. Kolata, and M. Zahar. Sub-barrier fusion of $^{37}Cl + ^{70,72,73,74,76}Ge$. *Phys. Rev. C*, 63:054611, 2001.

[210] J. C. Mahon, L. L. Lee Jr, J. F. Liang, C. R. Morton, N. T. P. Bateman, K. Yildiz, and B. M. Young. Fusion and transfer in $^{37}Cl + ^{98,100}Mo, ^{93}Nb$ at near barrier energies. *J. Phys. G*, 23:1215, 1997.

[211] H. A. Aljuwair, R. J. Ledoux, M. Beckerman, S. B. Gazes, J. Wiggins, E. R. Cosman, R. R. Betts, S. Saini, and

Ole Hansen. Isotopic effects in the fusion of ^{40}Ca with ^{40,44,48}Ca. *Phys. Rev. C*, 30:1223–1227, 1984.

[212] A. A. Sonzogni, J. D. Bierman, M. P. Kelly, J. P. Lestone, J. F. Liang, and R. Vandenbosch. Transfer and surface vibration couplings in the fusion of ^{40}Ca+^{46,48,50}Ti at near-barrier energies. *Phys. Rev. C*, 57:722–730, 1998.

[213] D. Bourgin, S. Courtin, F. Haas, A. M. Stefanini, G. Montagnoli, A. Goasduff, D. Montanari, L. Corradi, E. Fioretto, J. Huiming, F. Scarlassara, N. Rowley, S. Szilner, and T. Mijatović. Barrier distributions and signatures of transfer channels in the ^{40}Ca + ^{58,64}Ni fusion reactions at energies around and below the Coulomb barrier. *Phys. Rev. C*, 90:044610, 2014.

[214] H. Timmers, D. Ackermann, S. Beghini, L. Corradi, J. H. He, G. Montagnoli, F. Scarlassara, A. M. Stefanini, and N. Rowley. A case study of collectivity, transfer and fusion enhancement. *Nucl. Phys. A*, 633:421–445, 1998.

[215] J. D. Bierman, P. Chan, J. F. Liang, M. P. Kelly, A. A. Sonzogni, and R. Vandenbosch. Experimental fusion barrier distributions reflecting projectile octupole state coupling to prolate and oblate target nuclei. *Phys. Rev. Lett.*, 76:1587–1590, 1996.

[216] A. J. Pacheco, J. O. Fernández Niello, D. E. DiGregorio, M. di Tada, J. E. Testoni, Y. Chan, E. Chávez, S. Gazes, E. Plagnol, and R. G. Stokstad. Capture reactions in the ^{40,48}Ca+^{197}Au and ^{40,48}Ca+^{208}Pb systems. *Phys. Rev. C*, 45:2861–2869, 1992.

[217] M. Trotta, A. M. Stefanini, L. Corradi, A. Gadea, F. Scarlassara, S. Beghini, and G. Montagnoli. Sub-barrier fusion of the magic nuclei ^{40,48}Ca+^{48}Ca. *Phys. Rev. C*, 65:011601, 2001.

[218] A. M. Stefanini, F. Scarlassara, S. Beghini, G. Montagnoli, R. Silvestri, M. Trotta, B. R. Behera, L. Corradi, E. Fioretto, A. Gadea, Y. W. Wu, S. Szilner, H. Q. Zhang, Z. H. Liu, M. Ruan, F. Yang, and N. Rowley. Fusion of ^{48}Ca + ^{90,96}Zr above and below the Coulomb barrier. *Phys. Rev. C*, 73:034606, 2006.

[219] M. Trotta, A. M. Stefanini, S. Beghini, B. R. Behera, A. Yu. Chizhov, L. Corradi, S. Courtin, E. Fioretto, A. Gadea, P. R. S. Gomes, F. Haas, I. M. Itkis, M. G. Itkis, G. N. Kniajeva, N. A. Kondratiev, E. M. Kozulin, A. Latina, G. Montagnoli, I. V. Pokrovsky, N. Rowley, R. N. Sagaidak, F. Scarlassara, A. Szanto de Toledo, S. Szilner, V. M. Voskressensky, and Y. W. Wu. Fusion hindrance and quasi-fission in ^{48}Ca induced reactions. *Eur. Phys. J. A*, 25:615–618, 2005.

[220] A. M. Stefanini, G. Montagnoli, L. Corradi, S. Courtin, D. Bourgin, E. Fioretto, A. Goasduff, J. Grebosz, F. Haas, M. Mazzocco, T. Mijatović, D. Montanari, M. Pagliaroli, C. Parascandolo, F. Scarlassara, E. Strano, S. Szilner, N. Toniolo, and D. Torresi. Fusion of ^{48}Ti + ^{58}Fe and ^{58}Ni + ^{54}Fe below the Coulomb barrier. *Phys. Rev. C*, 92:064607, 2015.

[221] A. M. Vinodkumar, K. M. Varier, N. V. S. V. Prasad, D. L. Sastry, A. K. Sinha, N. Madhavan, P. Sugathan, D. O. Kataria, and J. J. Das. Absence of isotopic dependence in the sub-barrier fusion of ^{48}Ti+^{58,60,64}Ni systems. *Phys. Rev. C*, 53:803–810, 1996.

[222] A. M. Stefanini, G. Montagnoli, L. Corradi, S. Courtin, E. Fioretto, A. Goasduff, F. Haas, P. Mason, R. Silvestri, Pushpendra P. Singh, F. Scarlassara, and S. Szilner. Fusion hindrance for ^{58}Ni + ^{54}Fe. *Phys. Rev. C*, 82:014614, 2010.

[223] M. Beckerman, J. Ball, H. Enge, M. Salomaa, A. Sperduto, S. Gazes, A. DiRienzo, and J. D. Molitoris. Near- and sub-barrier fusion of ^{58}Ni with ^{58}Ni. *Phys. Rev. C*, 23:1581–1589, 1981.

[224] C. L. Jiang, A. M. Stefanini, H. Esbensen, K. E. Rehm, S. Almaraz-Calderon, M. L. Avila, B. B. Back, D. Bourgin, L. Corradi, S. Courtin, E. Fioretto, F. Galtarossa, A. Goasduff, F. Haas, M. M. Mazzocco, D. Montanari, G. Montagnoli, T. Mijatovic, R. Sagaidak, D. Santiago-Gonzalez, F. Scarlassara, E. E. Strano, and S. Szilner. Fusion reactions of $^{5}8, 64$Ni+$^{1}24$Sn. *Phys. Rev. C*, 91:044602, 2015.

[225] Z. Kohley, J. F. Liang, D. Shapira, R. L. Varner, C. J. Gross, J. M. Allmond, A. L. Caraley, E. A. Coello, F. Favela, K. Lagergren, and P. E. Mueller. Near-barrier fusion of Sn + Ni and Te + Ni systems: Examining the correlation between nucleon transfer and fusion enhancement. *Phys. Rev. Lett.*, 107:202701, 2011.

[226] J. F. Liang, D. Shapira, J. R. Beene, C. J. Gross, R. L. Varner, A. Galindo-Uribarri, J. Gomez del Campo, P. A. Hausladen, P. E. Mueller, D. W. Stracener, H. Amro, J. J. Kolata, J. D. Bierman, A. L. Caraley, K. L. Jones, Y. Larochelle, W. Loveland, and D. Peterson. Fusion of radioactive ^{132}Sn with ^{64}Ni. *Phys. Rev. C*, 75:054607, 2007.

[227] H. Sann, R. Bock, Y. T. Chu, A. Gobbi, A. Olmi, U. Lynen, W. Müller, S. Bjørnholm, and H. Esbensen. Deformability as a critical factor in initiating fusion between very heavy ions. *Phys. Rev. Lett.*, 47:1248–1251, 1981.

Explanation of Graphs

Graphs 1–11. **Excitation functions for 131 reaction systems with negative Q value for one neutron pair transfer**

For each reaction system, the results are shown in logarithmic scale (the left panel) and linear scale (the right panel). The solid line denotes the calculated cross section. The arrow indicates the central value of the barrier distribution $B_{\rm m}$ given in Eq. (16). The solid squares and circles are the experimental values which are given in Table 2. $\mathcal{D}$, defined in Eq. (24), denotes the average deviation of the calculated cross sections from the experimental values.

Graphs 12–19. **Excitation functions for 89 reaction systems with positive Q value for one neutron pair transfer**

For each reaction system, the results are shown in logarithmic scale (the left panel) and linear scale (the right panel). The solid line denotes the calculated cross section with the effect of one neutron pair transfer taken into account. The dotted line denotes the calculated cross section with the effect of neutron transfer neglected. The arrow indicates the central value of the barrier distribution $B_{\rm m}$ given in Eq. (16). The solid squares and circles are the experimental values which are given in Table 2. $\mathcal{D}$, defined in Eq. (24), denotes the average deviation of the calculated cross sections with the effect of one neutron pair transfer taken into account from the experimental values.

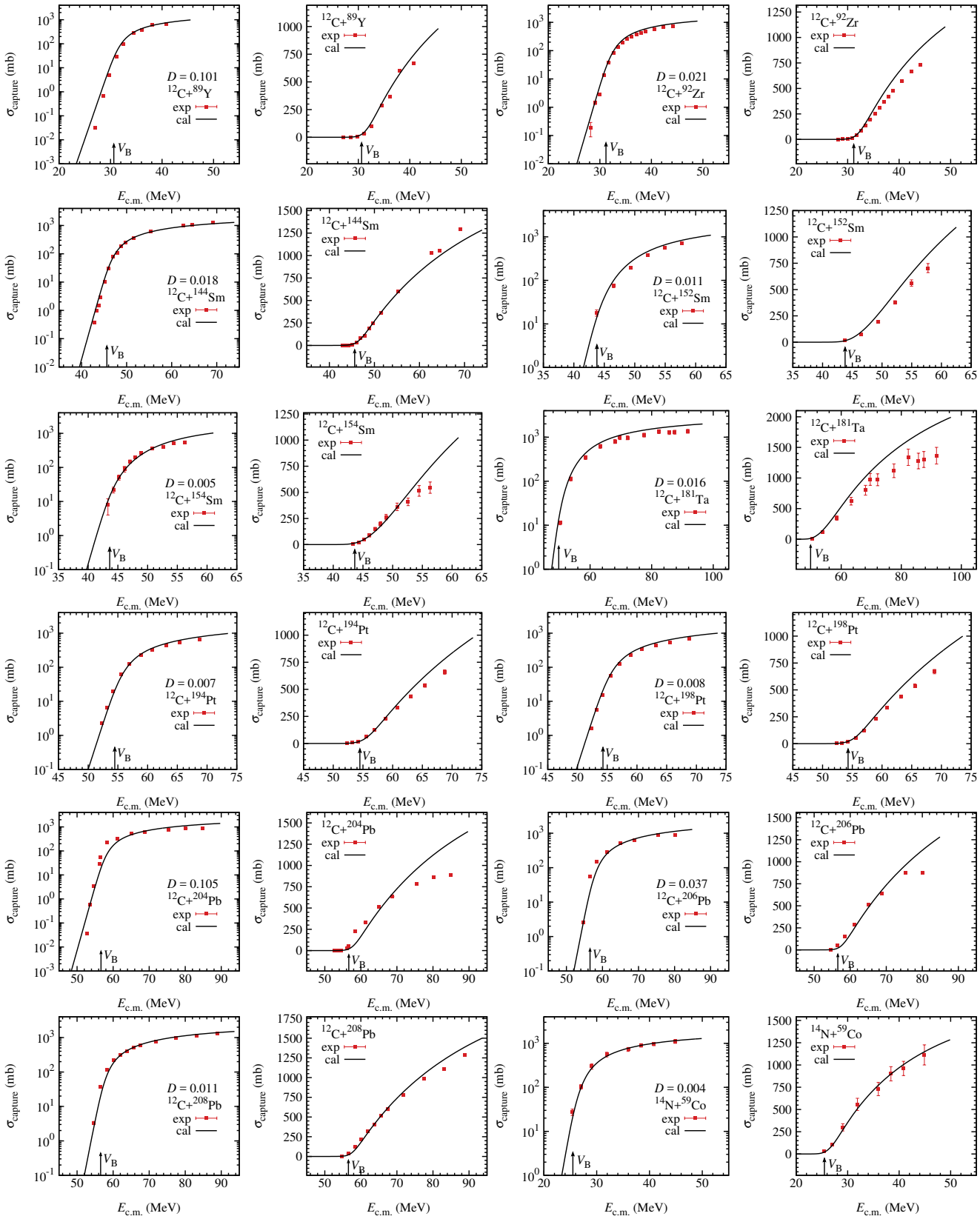

Graph 1

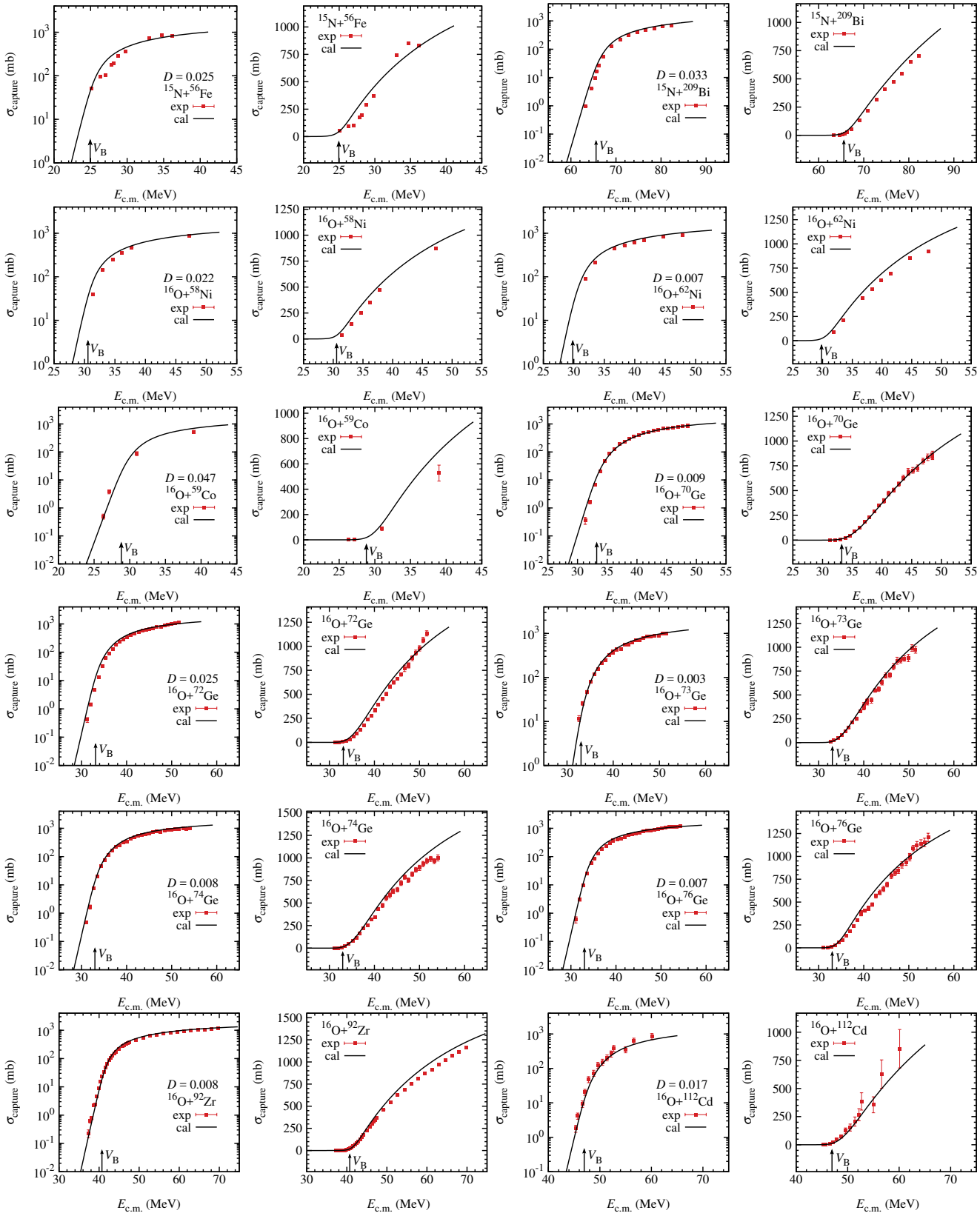

Graph 2

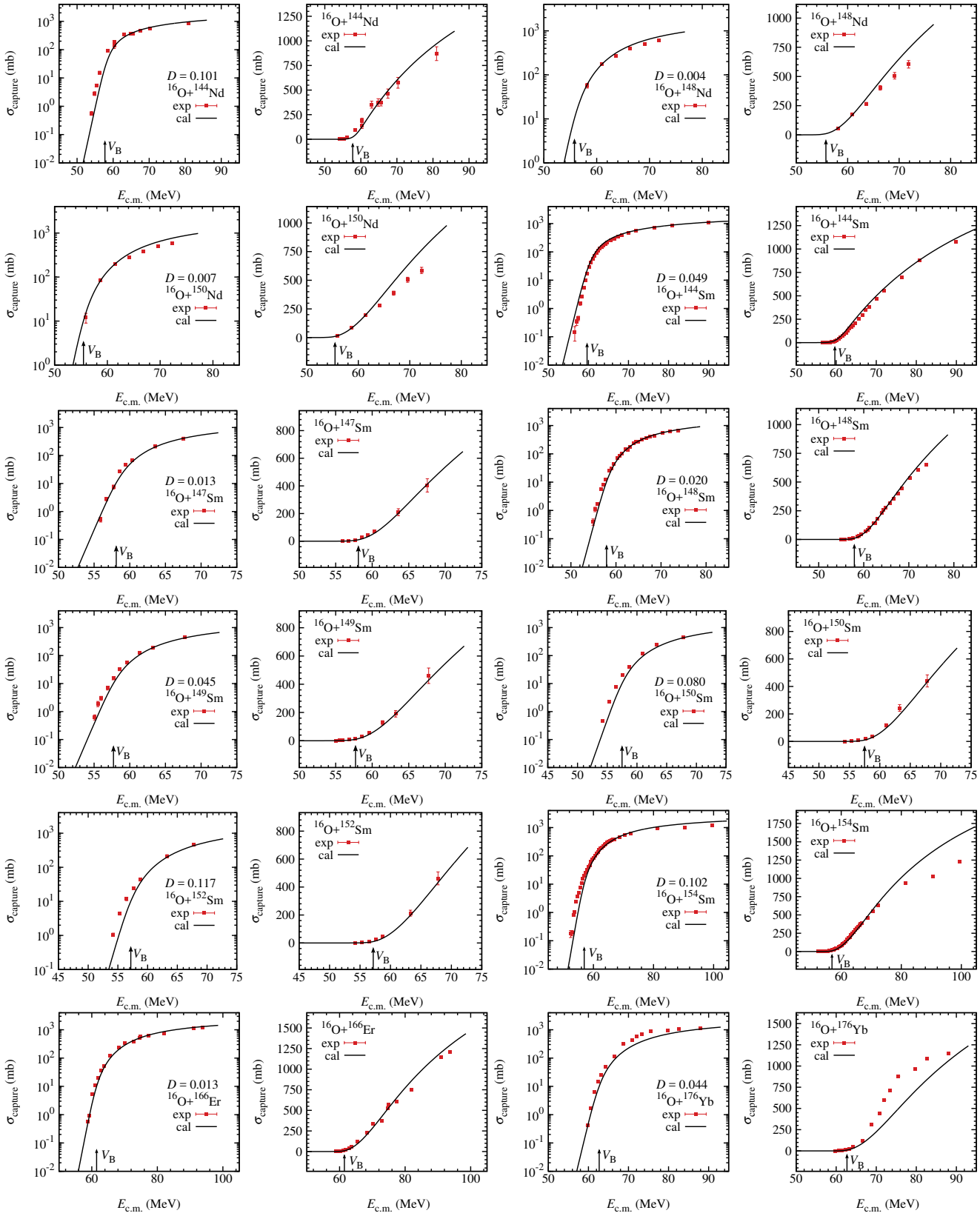

Graph 3

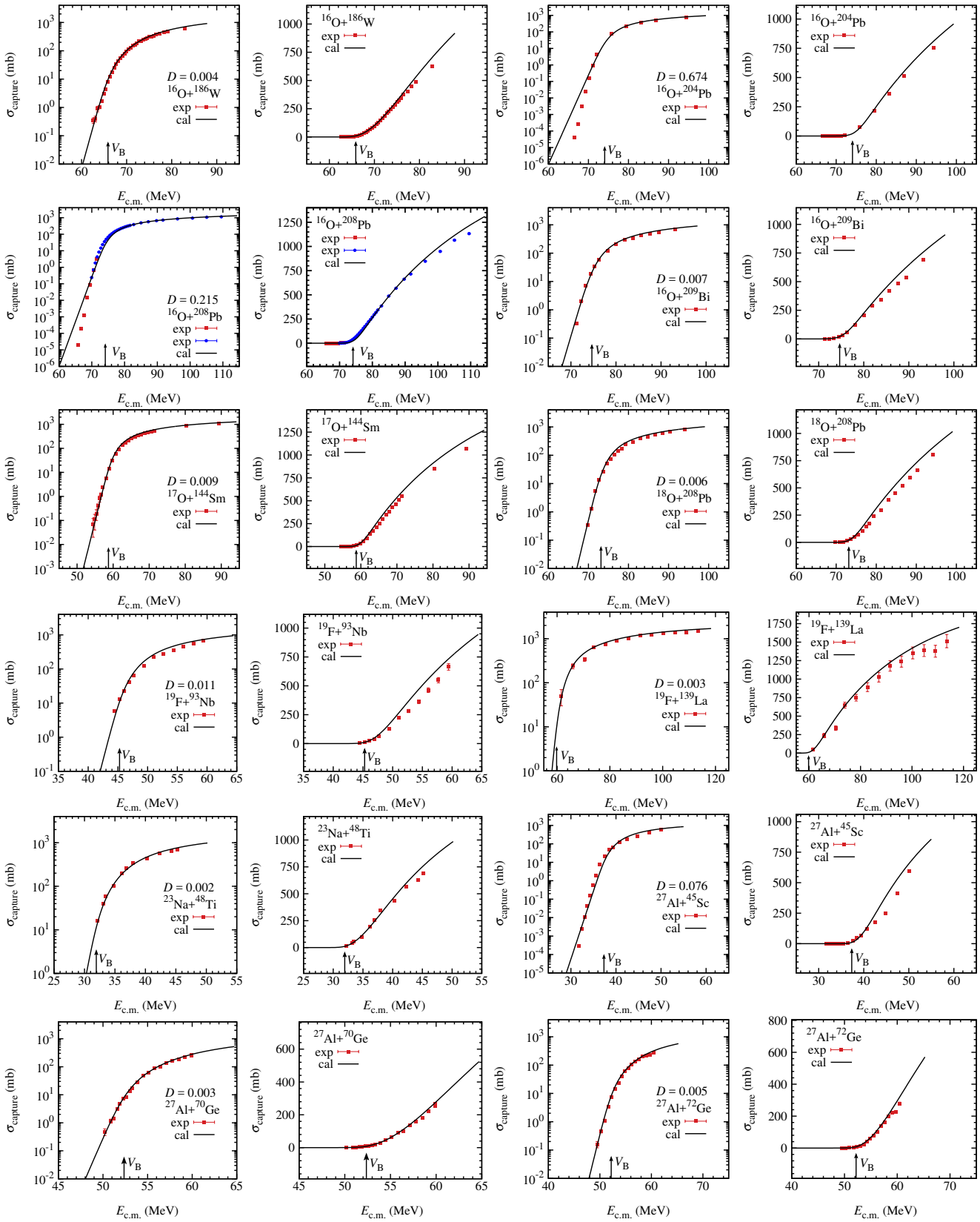

Graph 4

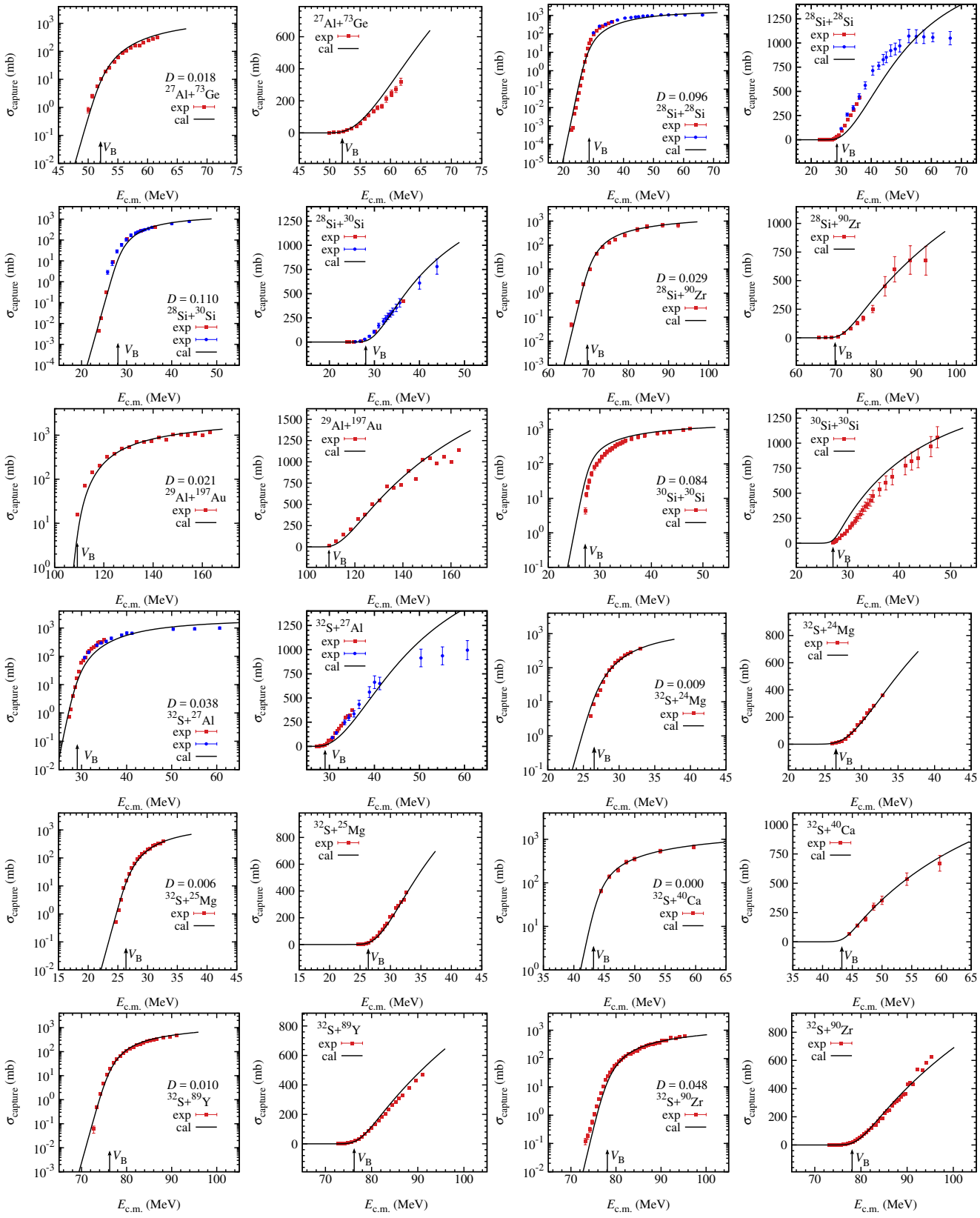

Graph 5

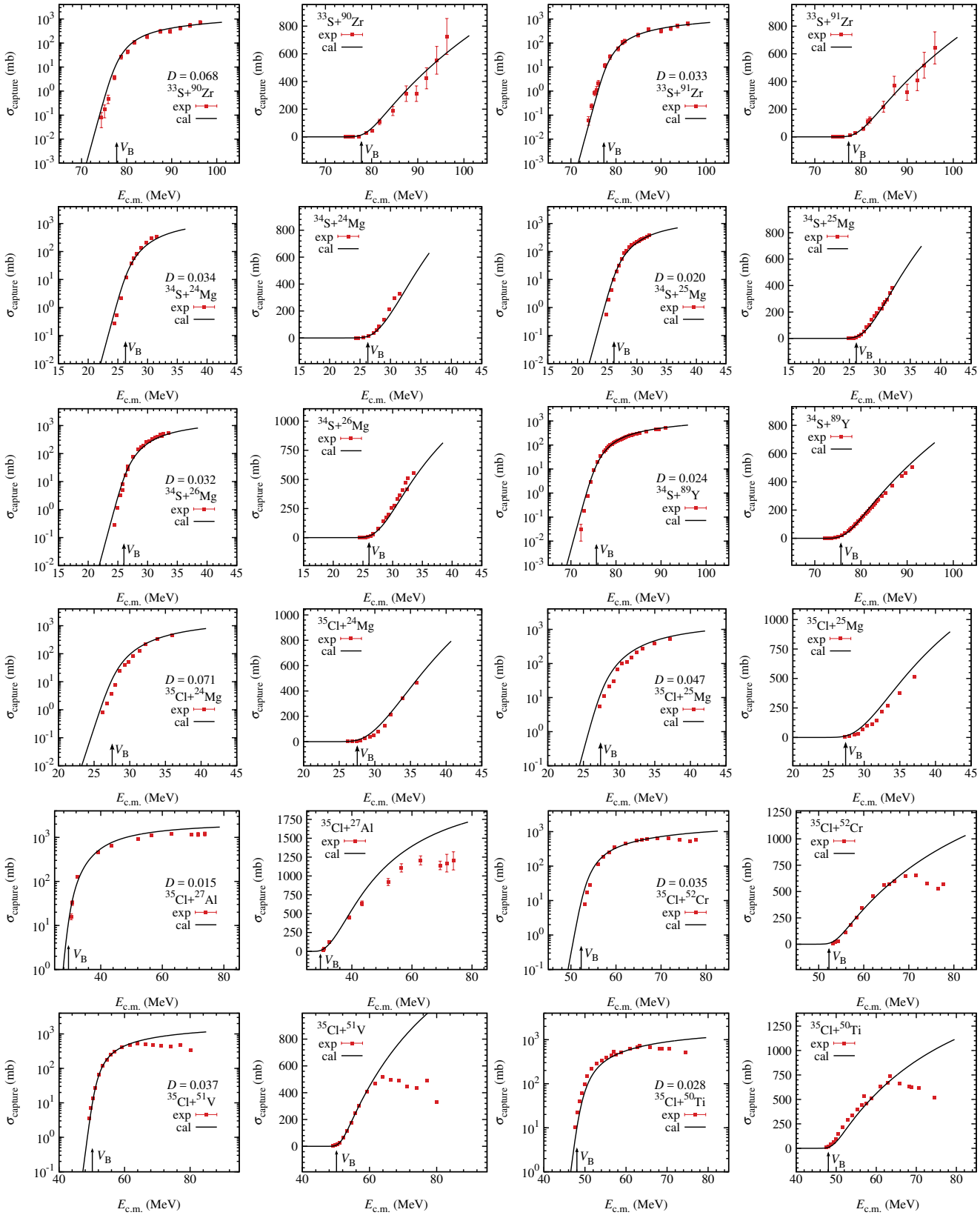

Graph 6

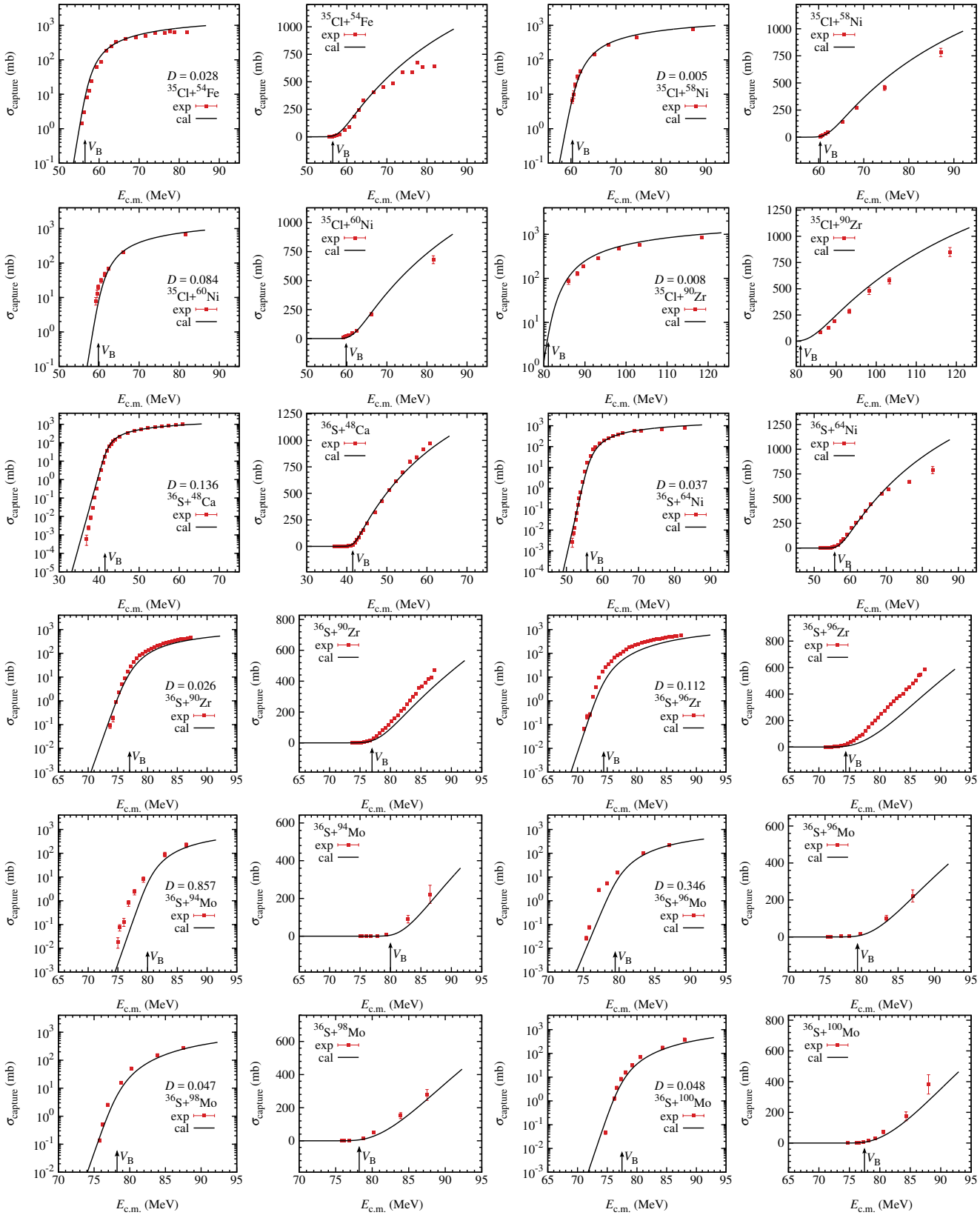

Graph 7

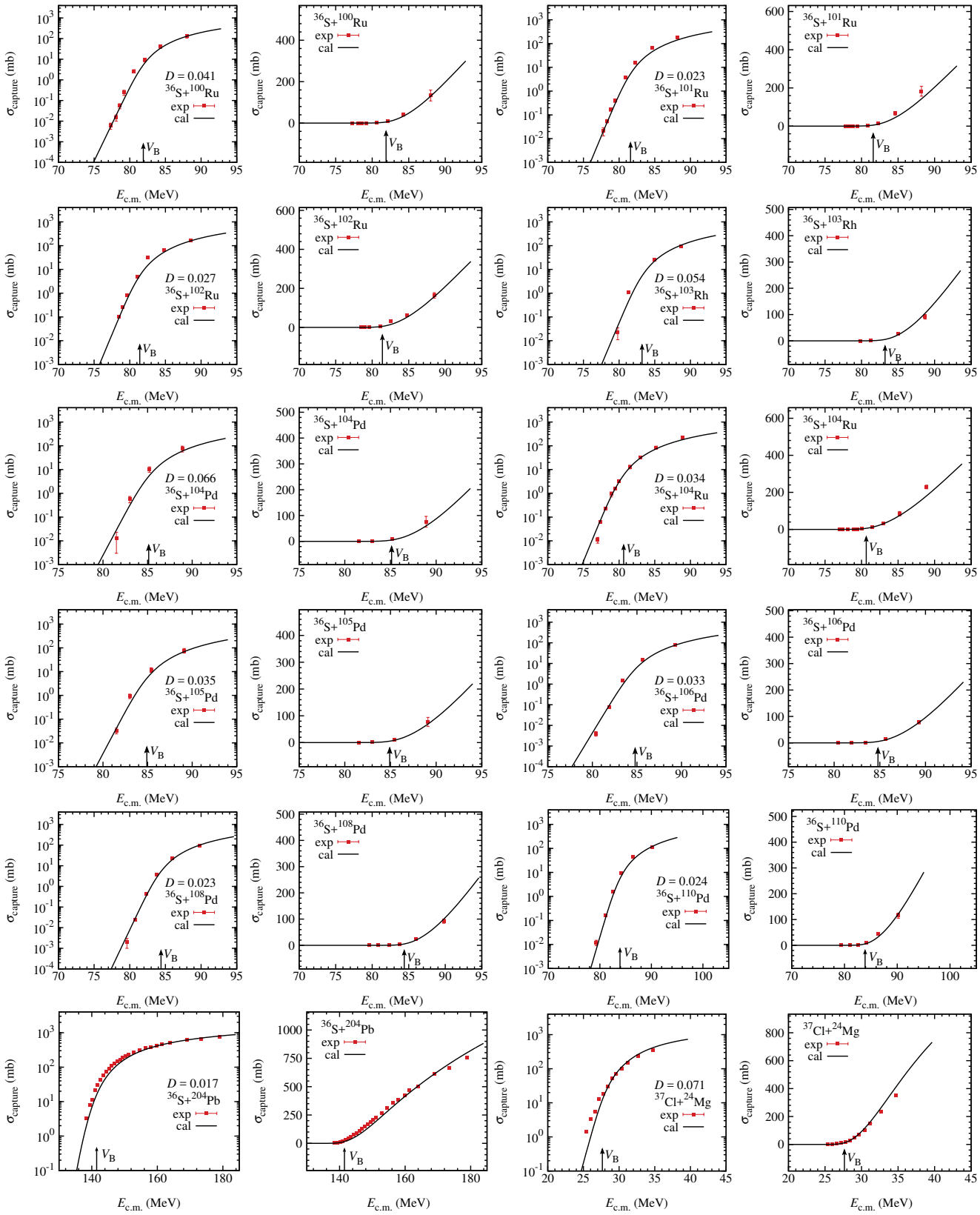

Graph 8

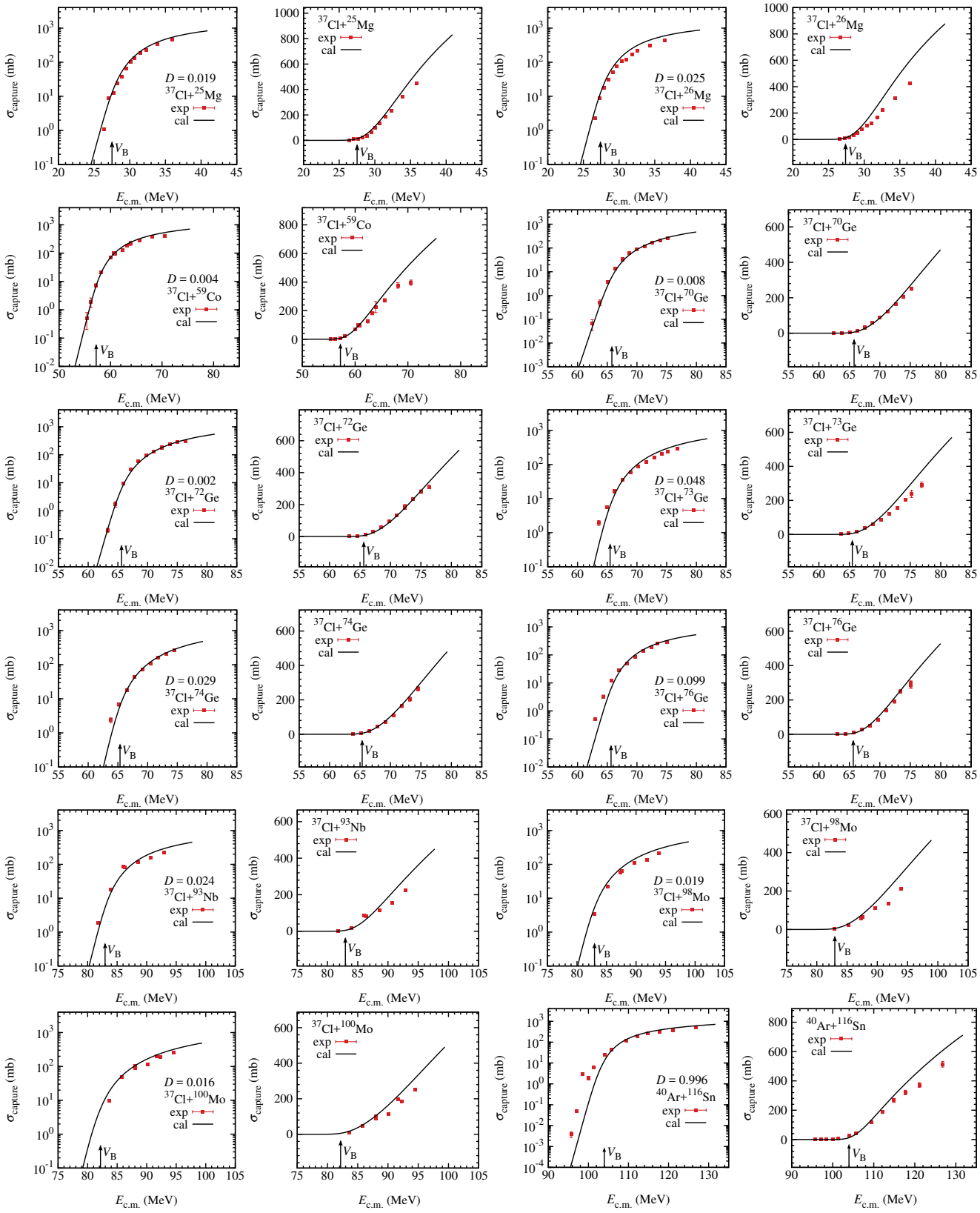

Graph 9

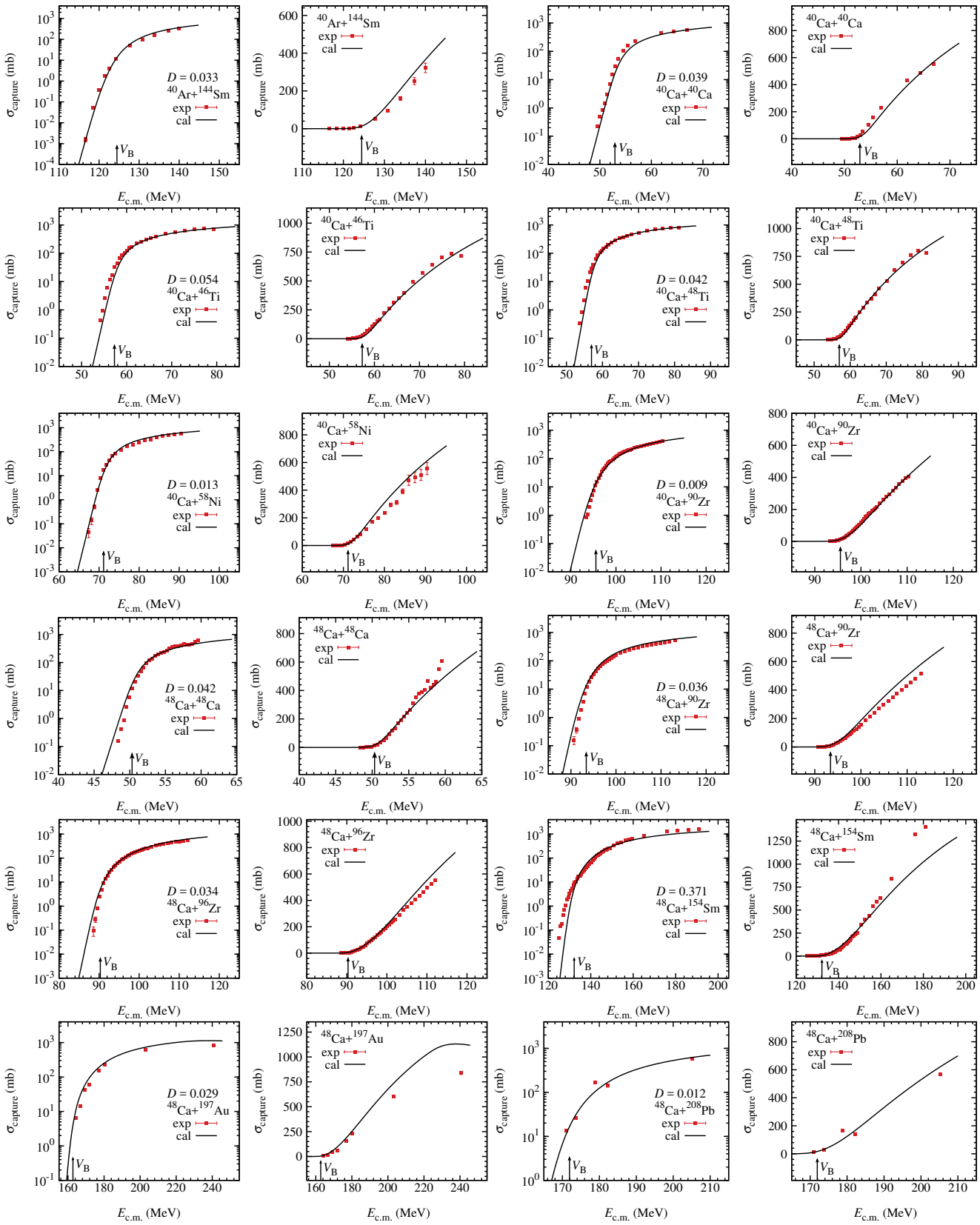

Graph 10

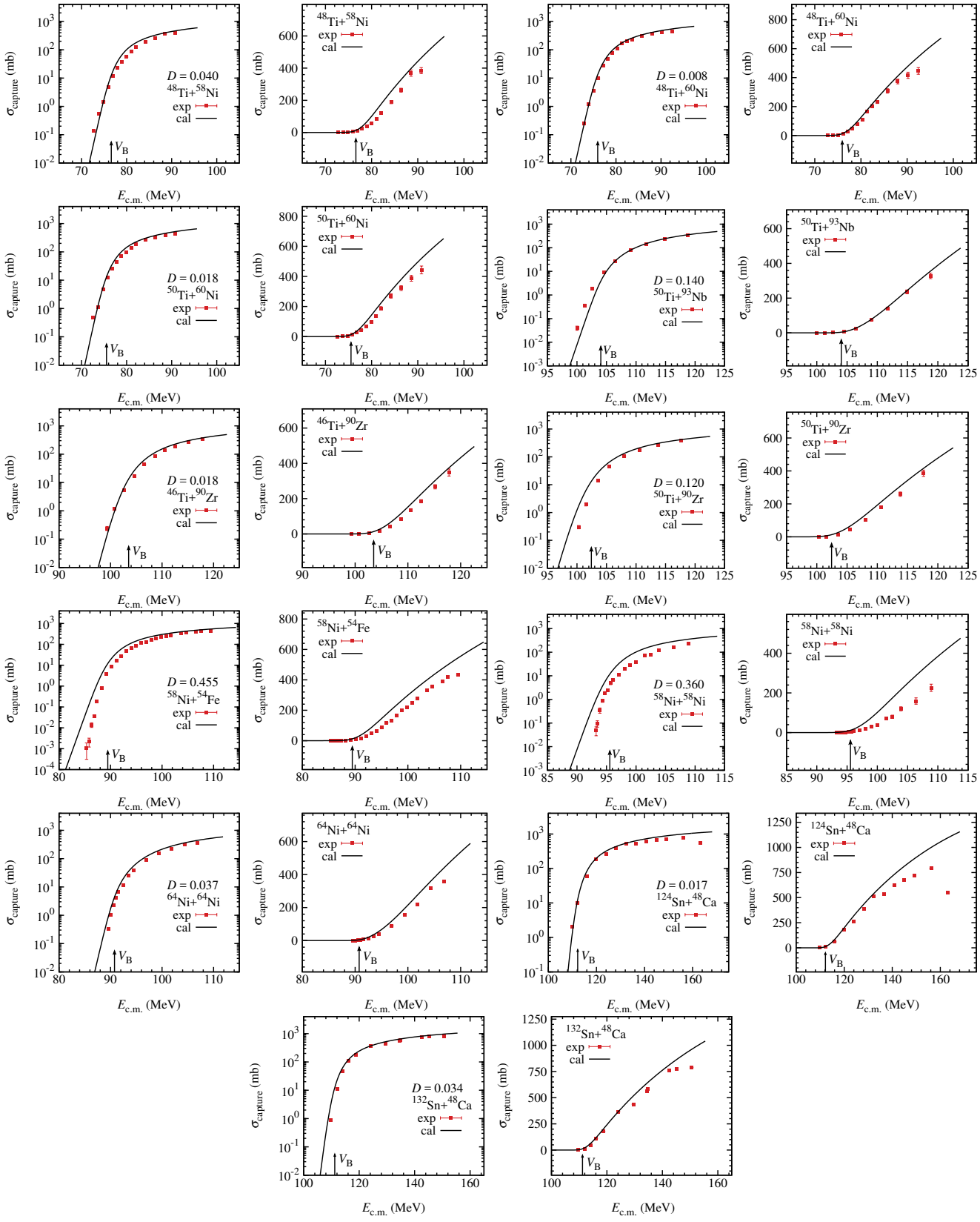

Graph 11

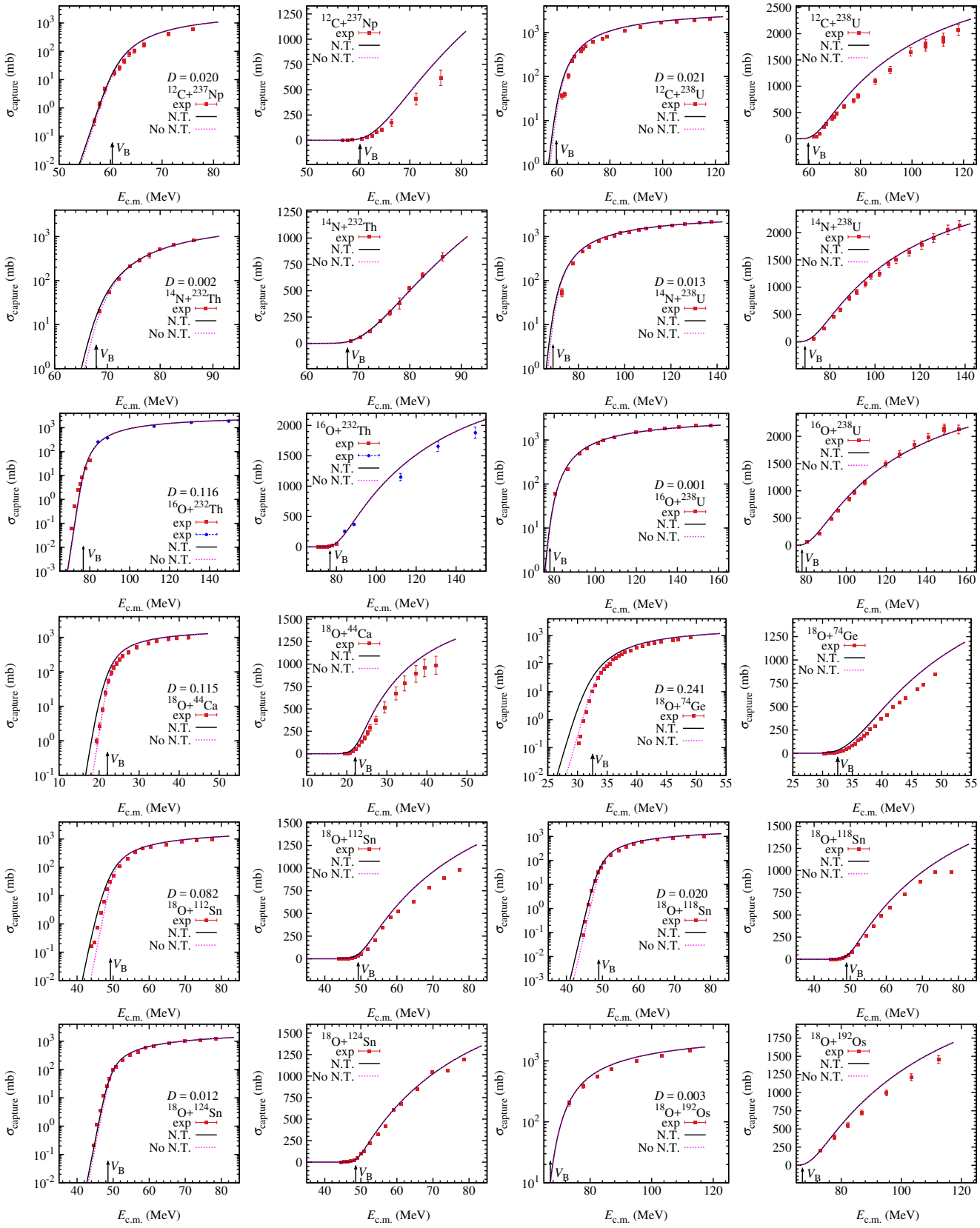

Graph 12

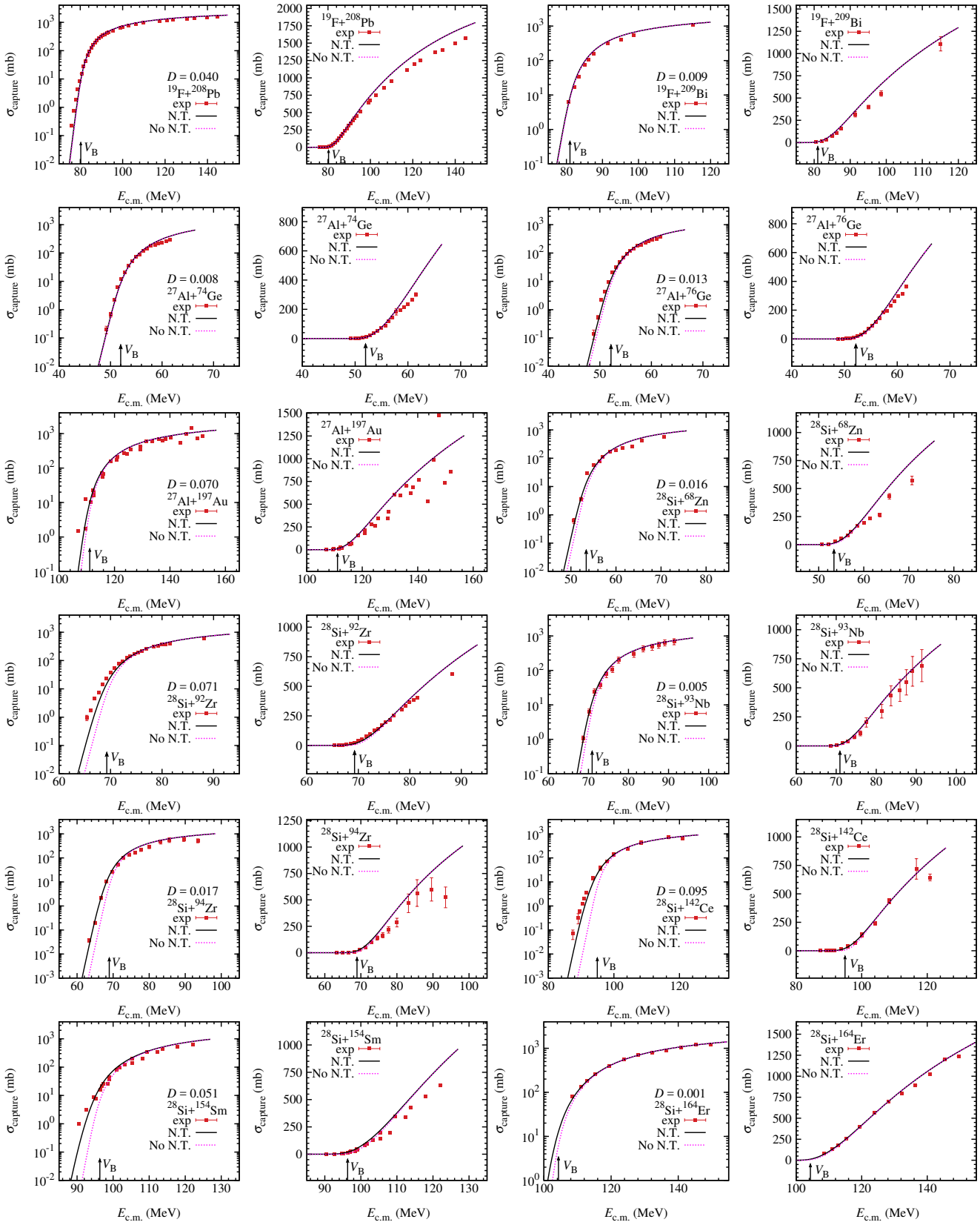

Graph 13

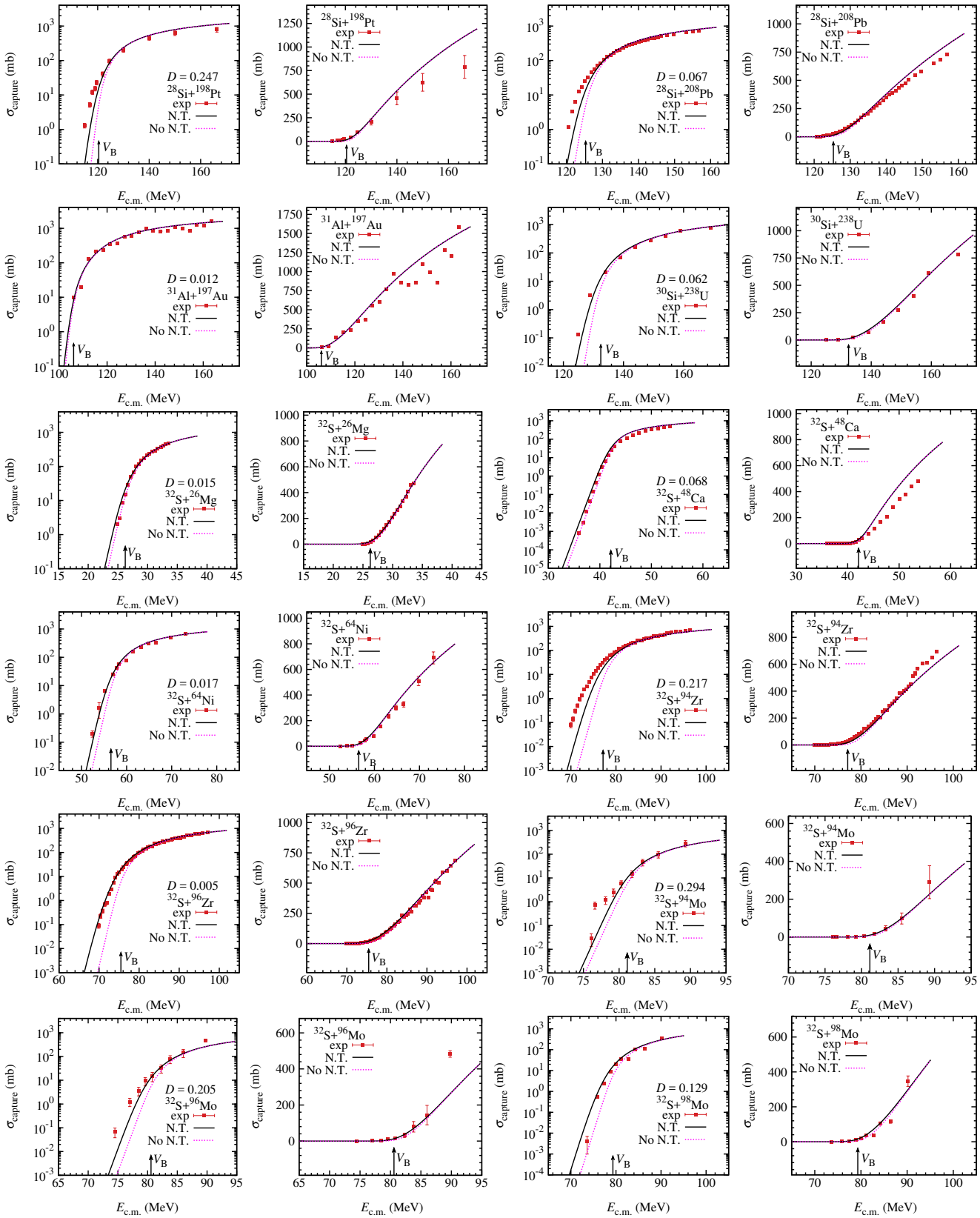

Graph 14

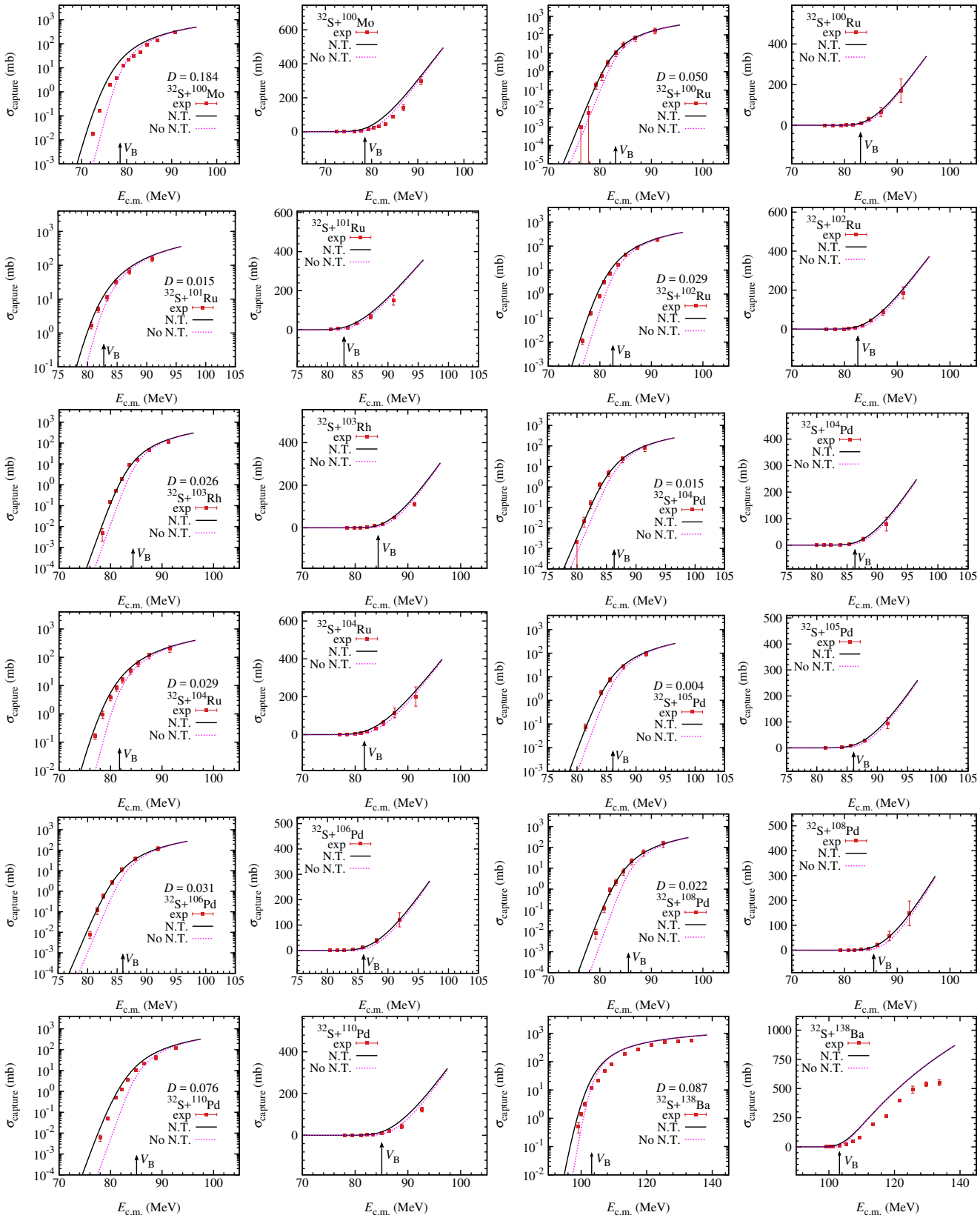

Graph 15

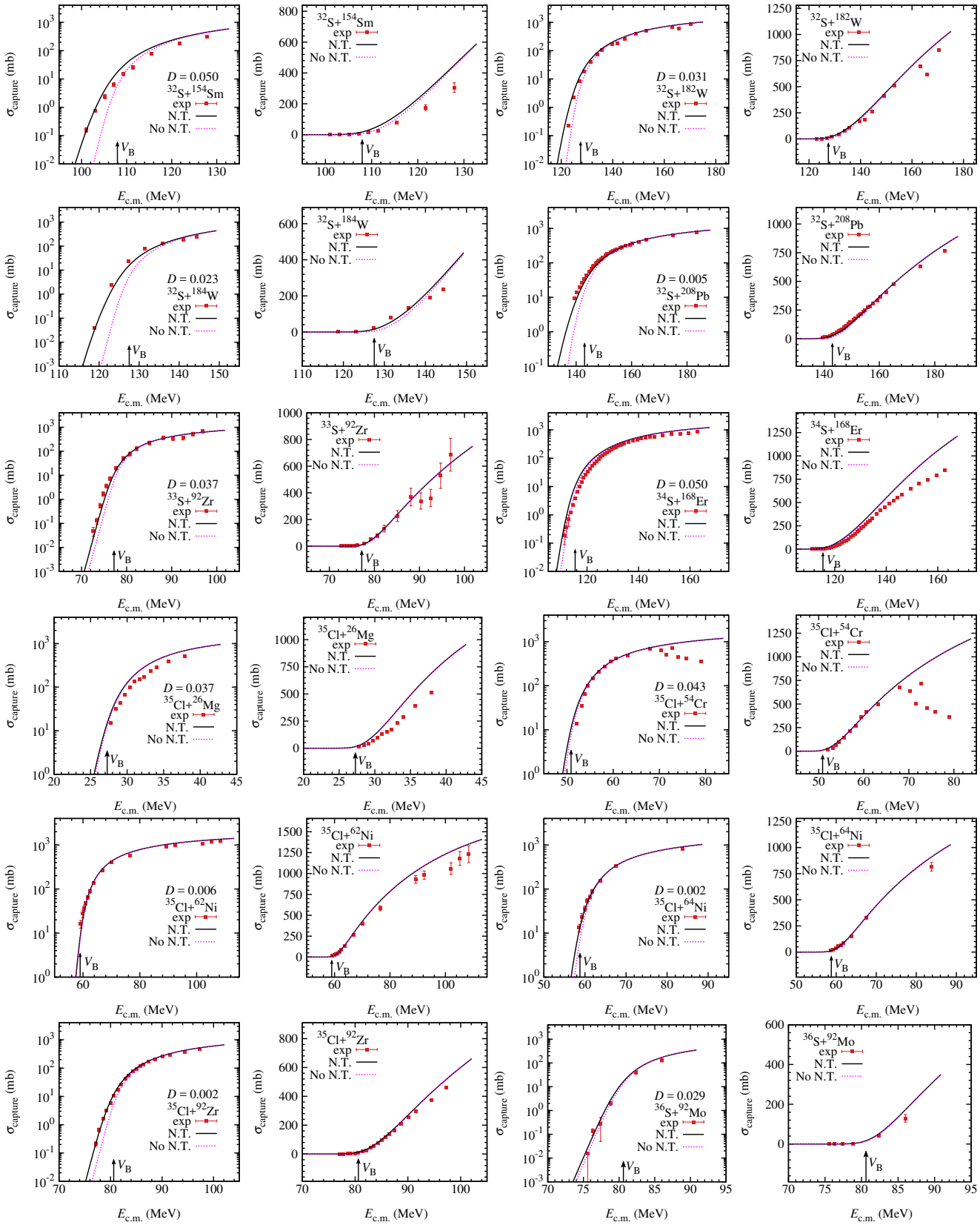

Graph 16

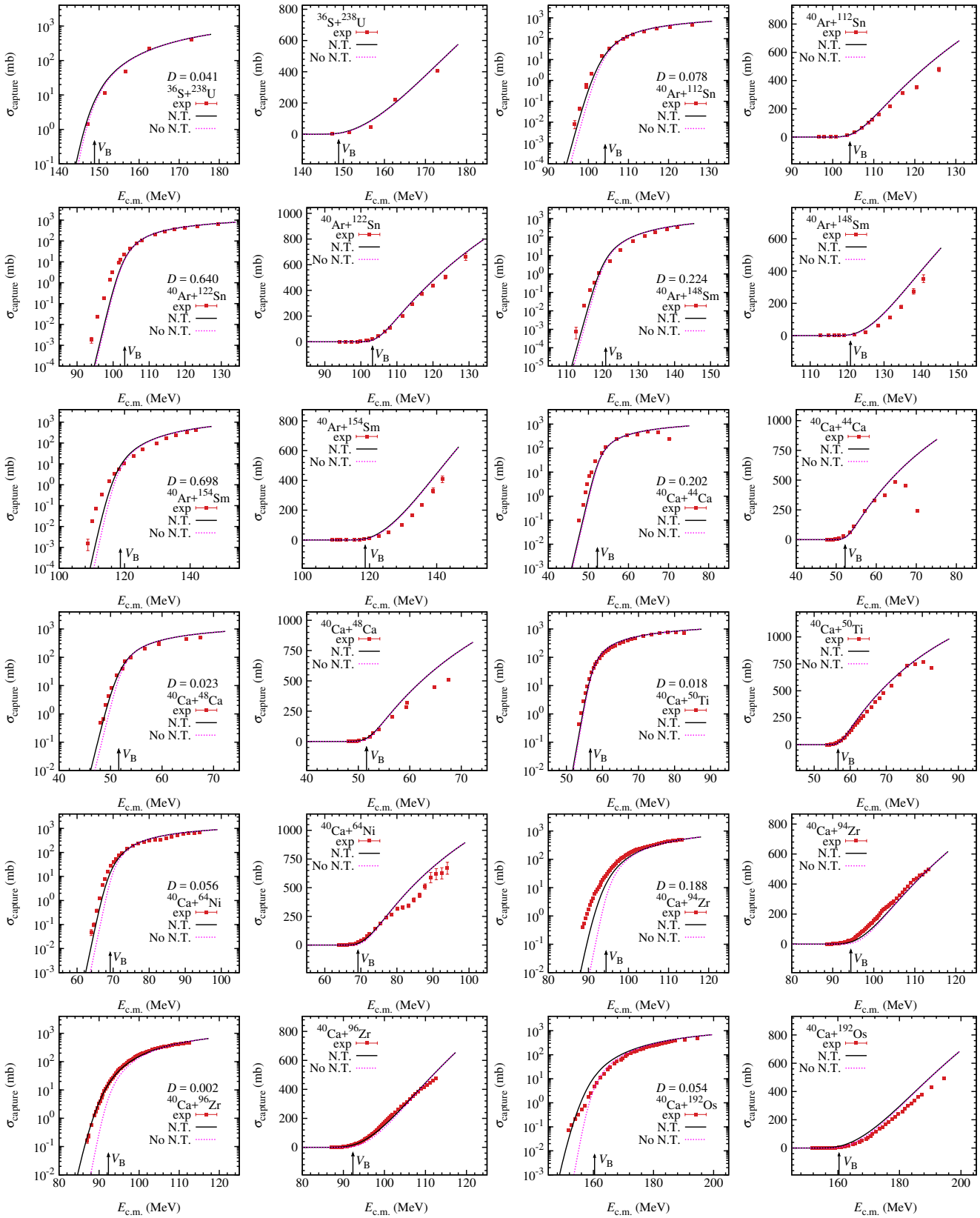

Graph 17

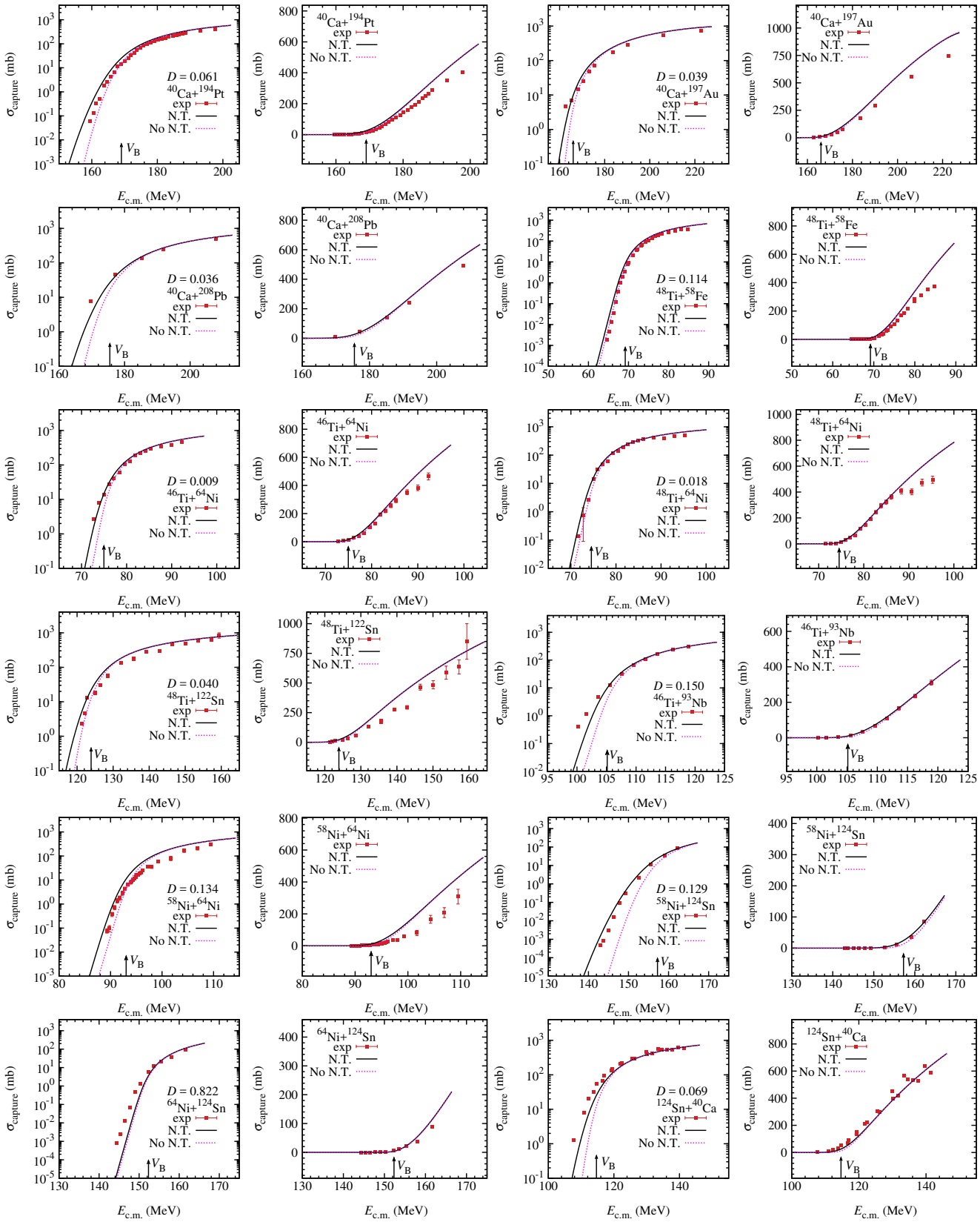

Graph 18

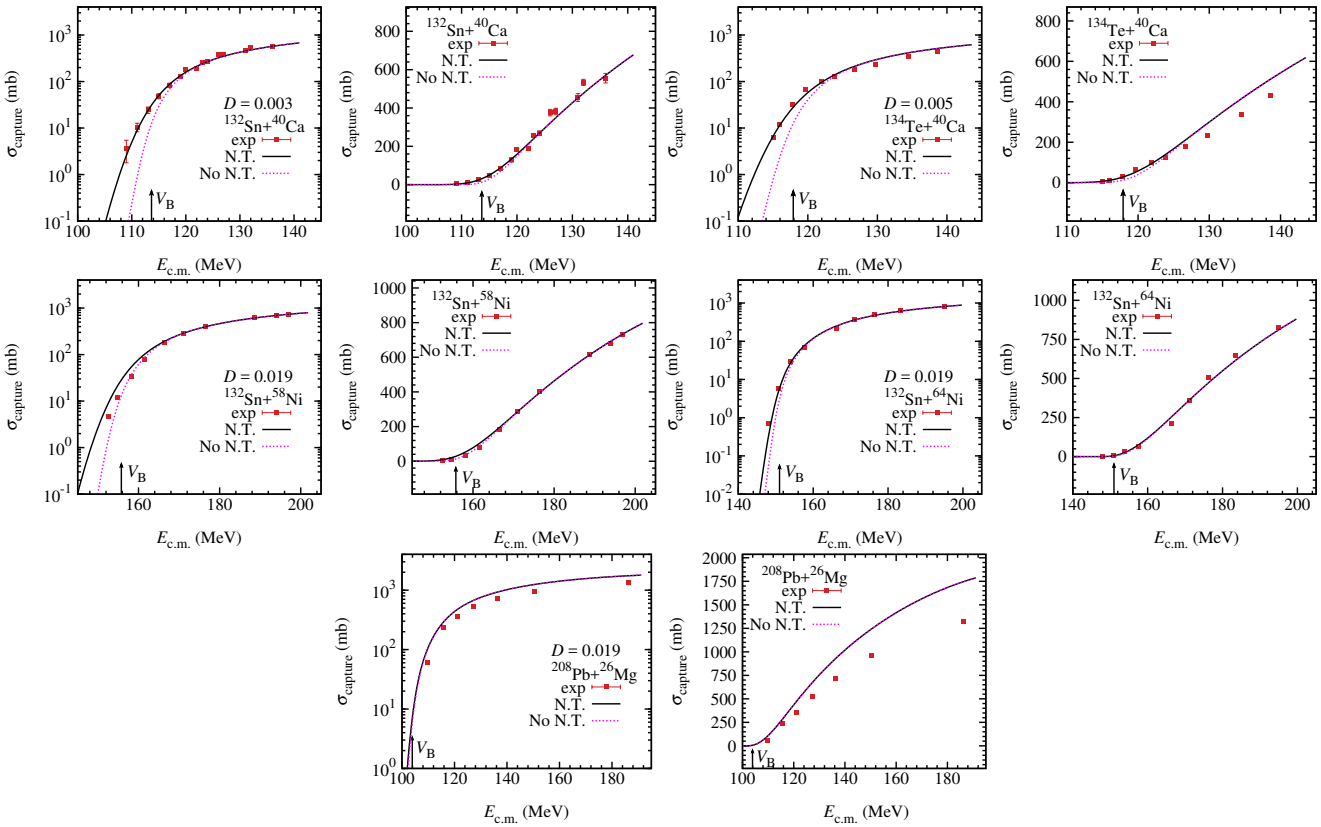

Graph 19

Explanation of Tables

Table 1. Fitted and calculated results for the parameters of the barrier distribution and average deviations of fitted and calculated cross sections from experimental values for a total of 220 reaction systems

For these 220 reaction systems, we tabulate the ground state quadrupole deformation parameters of the projectile and the target used in calculating the potential, the position and curvature of the potential approximated by a parabola, the fitted and calculated results for the parameters of the barrier distribution, the average deviations of fitted and calculated cross sections from experimental values and the corresponding references, and the Q value for one neutron pair transfer.

Reaction	Reaction system
$\beta_{\rm P}$	Ground state quadrupole deformation parameter of the projectile
$\beta_{\rm T}$	Ground state quadrupole deformation parameter of the target
$R_{\rm B}$	Position of the barrier
$\hbar\omega$	Curvature of the parabolic barrier
$B_{\rm m}^{\rm fit}$	Fitted results for the central value of the barrier distribution
$\Delta_1^{\rm fit}$	Fitted results for the left width of the barrier distribution
$\Delta_2^{\rm fit}$	Fitted results for the right width of the barrier distribution
$\mathcal{D}^{\rm fit}$	Average deviation of the fitted cross section from data
$B_{\rm m}^{\rm cal}$	Calculated results for the central value of the barrier distribution
$\Delta_1^{\rm cal}$	Calculated results for the left width of the barrier distribution
$\Delta_2^{\rm cal}$	Calculated results for the right width of the barrier distribution
$\mathcal{D}^{\rm cal}$	Average deviation of the calculated cross section from data
$Q(2n)$	Q value obtained from experimental masses for the one neutron pair transfer
Ref(s).	References(s) where the data are taken from

Table 2. The experimental and calculated excitation functions for a total of 220 reaction systems

For these 220 reaction systems, we tabulate the experimental excitation function together with the corresponding references. The detected particles in the experiment are the evaporation residual (EvR), fission fragments (FF), and/or quasifission (QF). There are two ways to extract the data: "authors' graph" denotes that the data are extracted from authors' graph and "authors' table" denotes that the data are obtained from authors' table. In the table, we also indicate how the collision energy was given in the corresponding reference: "$E_{\rm c.m.}$" denotes that the collision energy was given in the center-of-mass frame and then we calculate the energy in the laboratory frame by $E_{\rm lab} = E_{\rm c.m.}(A_{\rm P}+A_{\rm T})/A_{\rm T}$; "$E_{\rm lab}$" denotes that the collision energy was given in the laboratory frame and that in the center-of-mass frame is calculated by $E_{\rm c.m.} = E_{\rm lab}A_{\rm T}/(A_{\rm P}+A_{\rm T})$; "$E_{\rm lab}$ & $E_{\rm c.m.}$" denotes that the collision energy was given both in the laboratory frame and in the center-of-mass frame. The cross section and its errors are in the unit of mb. The calculated cross section at the corresponding energy is listed in the last column.

Reaction	Reaction system
Detected particles	Particles detected in the experiment
Data obtained	Data taken from authors' table or extracted from authors' graph and the corresponding reference
$E_{\rm lab}$	Collision energy in the laboratory frame
$E_{\rm c.m.}$	Collision energy in the center-of-mass frame
σ	Cross section
$\delta\sigma$	Error of cross section
$\sigma^{\rm cal}$	Calculated cross section

Table 1
Fitted and calculated results for the parameters of the barrier distribution and average deviations of fitted and calculated cross sections from experimental values for a total of 220 reaction systems. See page 59 for Explanation of Tables.

Reaction	β_P	β_T	R_B (fm)	$\hbar\omega$ (MeV)	B_m^{fit} (MeV)	Δ_1^{fit} (MeV)	Δ_2^{fit} (MeV)	$\mathcal{D}^{fit}$	B_m^{cal} (MeV)	Δ_1^{cal} (MeV)	Δ_2^{cal} (MeV)	$\mathcal{D}^{cal}$	$Q(2n)$ (MeV)	Ref(s).
$^{12}C+^{89}Y$	−0.320	0.035	10.53	4.18	31.46	0.254	0.555	0.0362	30.64	0.182	1.700	0.101	−7.71	[147]
$^{12}C+^{92}Zr$	−0.320	0.053	10.65	4.19	31.24	0.005	2.682	0.0073	31.19	0.202	1.882	0.021	−2.71	[148]
$^{12}C+^{144}Sm$	−0.320	0.000	11.10	4.63	45.76	0.028	1.856	0.0044	45.62	0.184	1.713	0.018	−6.00	[149]
$^{12}C+^{152}Sm$	−0.320	0.243	12.25	4.39	47.15	3.984	6.186	0.0001	43.79	0.691	6.453	0.011	−0.73	[150]
$^{12}C+^{154}Sm$	−0.320	0.270	12.40	4.36	42.97	0.005	8.038	0.0044	43.62	0.788	7.358	0.005	−0.71	[151]
$^{12}C+^{181}Ta$	−0.320	0.269	12.72	4.58	49.00	0.007	13.890	0.0043	49.81	0.820	7.652	0.016	−1.10	[152]
$^{12}C+^{194}Pt$	−0.320	0.000	11.66	4.90	53.67	0.106	4.015	0.0012	54.48	0.220	2.055	0.007	−1.49	[153]
$^{12}C+^{198}Pt$	−0.320	0.000	11.71	4.88	54.01	0.044	3.264	0.0017	54.29	0.217	2.025	0.008	−0.28	[153]
$^{12}C+^{204}Pb$	−0.320	0.008	11.78	4.96	57.40	0.051	1.468	0.1800	56.65	0.246	2.297	0.105	−2.19	[154]
$^{12}C+^{206}Pb$	−0.320	0.008	11.81	4.95	56.54	0.014	0.992	0.0184	56.55	0.244	2.277	0.037	−1.70	[154]
$^{12}C+^{208}Pb$	−0.320	0.000	11.80	4.95	56.18	0.029	1.670	0.0028	56.54	0.231	2.157	0.011	−0.98	[155]
$^{12}C+^{237}Np$	−0.320	0.215	13.09	4.94	60.23	1.311	13.458	0.0027	60.34	0.994	7.124	0.020	0.81	[156]
$^{12}C+^{238}U$	−0.320	0.215	13.11	4.91	62.20	1.908	5.887	0.0034	59.72	1.324	7.446	0.021	1.84	[157]
$^{14}N+^{59}Co$	0.000	0.143	10.10	3.77	27.29	2.042	0.565	0.0004	25.49	0.239	2.234	0.004	−5.70	[158]
$^{14}N+^{232}Th$	0.000	0.207	12.76	4.84	70.76	3.533	5.435	0.0002	67.89	1.446	8.796	0.002	1.76	[159]
$^{14}N+^{238}U$	0.000	0.215	12.85	4.85	69.62	0.012	8.769	0.0002	68.93	1.577	9.271	0.013	2.04	[157]
$^{15}N+^{56}Fe$	0.000	0.000	9.68	3.79	28.31	3.875	0.295	0.0047	24.95	0.131	0.380	0.025	−3.70	[160]
$^{15}N+^{209}Bi$	0.000	0.008	11.66	4.87	65.35	0.058	3.317	0.0008	65.59	0.807	2.345	0.033	−5.97	[161]
$^{16}O+^{58}Ni$	0.021	0.000	9.70	3.97	30.70	0.032	1.510	0.0004	30.57	0.220	0.638	0.022	−8.50	[162]
$^{16}O+^{62}Ni$	0.021	0.096	10.13	3.86	29.69	0.016	3.373	0.0002	29.82	0.197	1.840	0.007	−6.23	[162]
$^{16}O+^{59}Co$	0.021	0.143	10.21	3.79	28.26	0.496	7.011	0.0207	28.81	0.272	2.538	0.047	−6.84	[158]
$^{16}O+^{70}Ge$	0.021	0.241	10.74	3.79	33.27	0.007	3.955	0.0011	33.23	0.559	5.221	0.009	−7.54	[163]
$^{16}O+^{72}Ge$	0.021	0.224	10.74	3.78	33.85	0.702	5.070	0.0004	33.11	0.517	4.821	0.025	−5.98	[163]
$^{16}O+^{73}Ge$	0.021	0.224	10.77	3.77	33.49	1.479	6.014	0.0003	33.04	0.519	4.843	0.003	−5.35	[163]
$^{16}O+^{74}Ge$	0.021	0.224	10.80	3.76	32.74	0.021	5.729	0.0016	32.97	0.521	4.864	0.008	−4.79	[163]
$^{16}O+^{76}Ge$	0.021	0.143	10.59	3.80	32.74	0.064	4.675	0.0010	33.00	0.318	2.968	0.007	−3.74	[163]
$^{16}O+^{92}Zr$	0.021	0.053	10.50	4.17	39.91	0.048	4.082	0.0016	40.72	0.200	1.862	0.008	−3.64	[148]
$^{16}O+^{112}Cd$	0.021	0.144	11.13	4.18	46.41	0.012	3.720	0.0044	46.96	0.454	4.233	0.017	−4.18	[164]
$^{16}O+^{144}Nd$	0.021	0.000	10.97	4.56	56.95	0.747	1.884	0.0060	57.73	0.579	1.682	0.101	−1.75	[165]
$^{16}O+^{148}Nd$	0.021	0.206	11.89	4.38	54.88	0.645	11.069	0.0013	55.78	0.750	6.997	0.004	−0.44	[150]
$^{16}O+^{150}Nd$	0.021	0.243	12.09	4.34	54.53	0.040	11.887	0.0033	55.48	0.890	8.303	0.007	−0.23	[150]
$^{16}O+^{144}Sm$	0.021	0.000	10.94	4.63	59.66	0.097	1.996	0.0106	59.66	0.645	1.874	0.049	−6.93	[124]
$^{16}O+^{147}Sm$	0.021	0.143	11.59	4.50	57.96	0.001	3.469	0.0096	58.11	0.566	5.278	0.013	−2.57	[133]
$^{16}O+^{148}Sm$	0.021	0.161	11.68	4.48	56.98	0.391	7.951	0.0014	57.91	0.618	5.770	0.020	−2.29	[124]
$^{16}O+^{149}Sm$	0.021	0.180	11.78	4.46	56.44	0.003	7.883	0.0034	57.72	0.678	6.324	0.045	−1.82	[133]
$^{16}O+^{150}Sm$	0.021	0.206	11.90	4.44	57.19	1.201	7.450	0.0007	57.50	0.765	7.138	0.080	−1.67	[28]
$^{16}O+^{152}Sm$	0.021	0.243	12.09	4.40	57.15	1.774	9.420	0.0009	57.17	0.902	8.417	0.117	−1.67	[28]
$^{16}O+^{154}Sm$	0.021	0.270	12.24	4.37	55.84	1.148	12.680	0.0046	56.93	1.013	9.458	0.102	−1.65	[124]
$^{16}O+^{166}Er$	0.021	0.283	12.43	4.49	60.15	0.131	11.353	0.0041	61.47	1.109	10.355	0.013	−2.94	[166]
$^{16}O+^{176}Yb$	0.021	0.278	12.56	4.51	62.38	0.582	5.146	0.0064	62.69	1.118	10.431	0.044	−0.50	[166]
$^{16}O+^{186}W$	0.021	0.230	12.46	4.62	66.93	1.711	7.953	0.0024	65.87	0.958	8.941	0.004	−0.76	[167]
$^{16}O+^{204}Pb$	0.021	0.008	11.62	4.94	75.37	0.058	1.937	0.3745	74.07	1.047	3.042	0.674	−3.12	[128]
$^{16}O+^{208}Pb$	0.021	0.000	11.63	4.93	74.97	0.397	2.205	0.3504	73.97	0.963	2.799	0.215	−1.92	[128, 168]
$^{16}O+^{209}Bi$	0.021	0.008	11.67	4.95	73.70	0.008	4.293	0.0057	74.66	1.050	3.052	0.007	−2.16	[161]
$^{16}O+^{232}Th$	0.021	0.207	12.84	4.87	78.93	3.489	11.532	0.0054	76.76	1.217	9.673	0.116	0.63	[169, 170]
$^{16}O+^{238}U$	0.021	0.215	12.94	4.89	88.35	10.209	2.038	0.0002	77.93	1.352	10.196	0.001	0.91	[157]
$^{17}O+^{144}Sm$	0.107	0.000	11.20	4.40	59.55	1.469	3.856	0.0006	58.72	0.292	2.728	0.009	−4.63	[124]
$^{18}O+^{44}Ca$	0.021	0.000	9.63	3.44	20.92	0.193	4.800	0.0012	22.09	1.927	2.171	0.115	5.62	[171]
$^{18}O+^{74}Ge$	0.021	0.224	10.95	3.57	31.84	0.186	8.109	0.0198	32.54	1.711	5.986	0.241	3.74	[95]
$^{18}O+^{112}Sn$	0.021	0.018	10.76	4.15	48.90	1.655	5.817	0.0090	49.27	2.406	3.422	0.082	5.86	[172]
$^{18}O+^{118}Sn$	0.021	0.000	10.81	4.12	47.54	0.165	4.744	0.0071	48.99	1.517	2.335	0.020	3.40	[172]
$^{18}O+^{124}Sn$	0.021	0.000	10.92	4.08	46.73	0.015	5.448	0.0014	48.58	0.957	1.724	0.012	1.74	[172]
$^{18}O+^{192}Os$	0.021	0.155	12.33	4.35	62.70	0.627	19.704	0.0002	67.10	0.864	6.707	0.003	0.51	[173]
$^{18}O+^{208}Pb$	0.021	0.000	11.77	4.55	71.66	0.029	6.621	0.0011	73.14	0.941	2.734	0.006	−2.54	[161]
$^{19}F+^{93}Nb$	0.275	0.053	11.17	3.94	46.46	2.112	6.718	0.0004	45.28	0.502	4.685	0.011	−2.01	[174]
$^{19}F+^{139}La$	0.275	0.000	11.60	4.21	58.36	0.446	10.225	0.0014	59.82	0.504	4.708	0.003	−1.53	[173]
$^{19}F+^{208}Pb$	0.275	0.000	12.29	4.51	81.47	2.612	7.410	0.0008	80.25	0.898	6.784	0.040	0.60	[175]
$^{19}F+^{209}Bi$	0.275	0.008	12.33	4.52	83.35	3.097	7.453	0.0011	80.99	0.857	7.048	0.009	0.36	[176]
$^{23}Na+^{48}Ti$	0.366	0.000	10.58	3.45	31.21	0.002	6.626	0.0013	31.94	0.584	5.447	0.002	−4.41	[177]
$^{27}Al+^{45}Sc$	−0.448	0.000	10.30	3.57	37.21	0.005	5.264	0.1722	37.34	0.459	4.285	0.076	−3.88	[178]
$^{27}Al+^{70}Ge$	−0.448	0.241	11.54	3.62	53.14	1.428	7.246	0.0013	52.36	0.836	7.799	0.003	−2.58	[179]
$^{27}Al+^{72}Ge$	−0.448	0.224	11.54	3.61	53.20	1.492	6.889	0.0010	52.20	0.802	7.490	0.005	−1.02	[179]
$^{27}Al+^{73}Ge$	−0.448	0.224	11.57	3.61	52.30	1.524	11.235	0.0008	52.09	0.807	7.535	0.018	−0.38	[179]
$^{27}Al+^{74}Ge$	−0.448	0.224	11.60	3.60	50.53	0.046	12.695	0.0006	51.98	0.867	7.635	0.008	0.17	[179]

Continued on next page

Table 1 (continued)

Reaction	β_P	β_T	R_B (fm)	$\hbar\omega$ (MeV)	B_m^{fit} (MeV)	Δ_1^{fit} (MeV)	Δ_2^{fit} (MeV)	$\mathcal{D}^{fit}$	B_m^{cal} (MeV)	Δ_1^{cal} (MeV)	Δ_2^{cal} (MeV)	$\mathcal{D}^{cal}$	$Q(2n)$ (MeV)	Ref(s).
^{27}Al+^{76}Ge	−0.448	0.143	11.38	3.63	50.72	0.253	9.973	0.0011	52.16	1.025	6.319	0.013	1.22	[179]
^{27}Al+^{197}Au	−0.448	0.131	12.86	4.26	109.47	0.713	18.568	0.0794	111.07	1.727	9.622	0.070	2.44	[180]
^{28}Si+^{28}Si	−0.478	−0.478	10.51	3.32	27.08	0.008	6.403	0.0555	28.58	1.545	14.421	0.096	−11.41	[125, 181]
^{28}Si+^{30}Si	−0.478	0.000	10.02	3.41	27.96	0.032	3.771	0.1459	28.08	0.561	5.236	0.110	−14.71	[171, 181]
^{28}Si+^{68}Zn	−0.478	0.156	11.28	3.68	51.67	0.303	12.970	0.0084	53.39	1.298	7.229	0.016	1.83	[182]
^{28}Si+^{90}Zr	−0.478	0.035	11.20	3.91	71.83	2.408	4.836	0.0026	69.73	0.536	5.007	0.029	−2.21	[183]
^{28}Si+^{92}Zr	−0.478	0.053	11.31	3.89	68.93	2.300	8.407	0.0010	69.27	1.606	6.314	0.071	3.25	[148]
^{28}Si+^{93}Nb	−0.478	0.053	11.32	3.92	70.11	1.003	9.996	0.0019	70.93	1.322	6.031	0.005	2.37	[184]
^{28}Si+^{94}Zr	−0.478	0.062	11.39	3.87	66.49	0.492	16.540	0.0107	68.93	1.903	6.752	0.017	4.13	[183]
^{28}Si+^{142}Ce	−0.478	0.000	11.75	4.12	94.98	3.405	9.197	0.0016	94.92	2.614	7.103	0.095	6.49	[185]
^{28}Si+^{154}Sm	−0.478	0.270	13.03	4.02	100.36	6.338	15.409	0.0041	96.32	3.033	14.318	0.051	5.25	[186]
^{28}Si+^{164}Er	−0.478	0.273	13.14	4.14	105.91	5.211	15.022	0.0002	104.34	2.475	14.218	0.001	3.33	[187]
^{28}Si+^{198}Pt	−0.478	0.000	12.30	4.32	117.08	2.360	21.830	0.0028	120.44	2.487	8.062	0.247	5.68	[188]
^{28}Si+^{208}Pb	−0.478	0.000	12.38	4.37	122.33	1.743	16.068	0.0003	125.33	2.306	8.252	0.067	4.98	[189]
^{29}Al+^{197}Au	0.000	0.131	12.41	4.15	106.25	0.001	14.518	0.0024	109.24	1.169	10.912	0.021	−1.82	[180]
^{31}Al+^{197}Au	0.239	0.131	13.11	3.94	110.89	5.605	13.649	0.0120	106.07	1.863	14.176	0.012	1.20	[180]
^{30}Si+^{30}Si	0.000	0.000	9.53	3.38	27.38	0.150	2.456	0.0054	27.15	0.169	0.491	0.084	−3.30	[171]
^{30}Si+^{238}U	0.000	0.215	13.19	4.24	132.76	4.343	25.349	0.0029	132.44	3.333	19.093	0.062	4.51	[190]
^{32}S+^{27}Al	−0.448	0.448	11.09	3.28	28.49	0.151	5.738	0.0078	29.05	1.141	10.651	0.038	−4.36	[191, 192]
^{32}S+^{24}Mg	0.000	0.374	10.20	3.48	26.48	0.006	4.256	0.0006	26.50	0.591	5.516	0.009	−9.62	[191]
^{32}S+^{25}Mg	0.000	0.333	10.17	3.35	26.17	0.005	3.791	0.0035	26.36	0.511	4.770	0.006	−3.80	[191]
^{32}S+^{26}Mg	0.000	0.310	10.18	3.34	25.75	0.069	4.548	0.0016	26.24	0.995	4.924	0.015	1.64	[191]
^{32}S+^{40}Ca	0.000	0.000	9.68	3.85	42.43	0.014	2.470	0.0004	43.24	0.405	1.177	0.000	−8.26	[192]
^{32}S+^{48}Ca	0.000	0.000	9.98	3.54	40.51	0.055	6.275	0.0171	42.13	1.261	1.939	0.068	2.83	[193]
^{32}S+^{64}Ni	0.000	0.087	10.49	3.74	55.94	1.634	8.262	0.0016	56.52	1.524	4.721	0.017	3.56	[182]
^{32}S+^{89}Y	0.000	0.035	10.68	3.98	75.14	0.014	4.586	0.0124	76.23	1.202	3.494	0.010	−0.77	[194]
^{32}S+^{90}Zr	0.000	0.035	10.69	4.02	77.94	1.848	4.900	0.0017	78.08	1.258	3.657	0.048	−1.23	[87]
^{32}S+^{94}Zr	0.000	0.062	10.88	3.98	76.83	3.131	7.475	0.0008	77.14	2.157	6.517	0.217	5.10	[90]
^{32}S+^{96}Zr	0.000	0.217	11.49	3.79	75.15	2.523	12.751	0.0014	75.45	2.856	11.346	0.005	5.74	[87]
^{32}S+^{94}Mo	0.000	0.053	10.80	4.07	81.58	2.014	6.080	0.1268	81.14	1.291	5.884	0.294	2.31	[195]
^{32}S+^{96}Mo	0.000	0.080	10.94	3.95	83.51	3.898	2.375	0.0088	80.58	1.746	6.870	0.205	3.54	[195]
^{32}S+^{98}Mo	0.000	0.180	11.36	3.88	76.25	0.098	20.852	0.0297	79.32	2.397	10.121	0.129	4.59	[195]
^{32}S+^{100}Mo	0.000	0.244	11.64	3.83	80.12	3.175	15.510	0.0056	78.56	3.045	12.843	0.184	5.84	[195]
^{32}S+^{100}Ru	0.000	0.161	11.29	3.96	81.02	0.023	12.574	0.0173	83.04	1.841	9.403	0.050	2.92	[195]
^{32}S+^{101}Ru	0.000	0.180	11.39	3.94	84.06	2.961	10.994	0.0020	82.73	2.120	10.230	0.015	3.58	[195]
^{32}S+^{102}Ru	0.000	0.189	11.44	3.93	82.83	2.224	11.117	0.0043	82.53	2.297	10.675	0.029	4.04	[195]
^{32}S+^{103}Rh	0.000	0.180	11.41	3.97	81.12	0.004	22.924	0.0273	84.37	2.052	10.352	0.026	3.30	[195]
^{32}S+^{104}Pd	0.000	0.162	11.35	4.01	83.62	0.085	19.650	0.0128	86.30	1.741	9.706	0.015	2.45	[195]
^{32}S+^{104}Ru	0.000	0.253	11.73	3.88	82.20	2.770	13.903	0.0007	81.75	2.839	13.363	0.029	4.93	[195]
^{32}S+^{105}Pd	0.000	0.171	11.40	4.00	85.50	1.809	14.620	0.0001	86.09	1.941	10.160	0.004	2.98	[195]
^{32}S+^{106}Pd	0.000	0.171	11.42	4.00	83.33	0.015	15.354	0.0180	85.97	2.074	10.280	0.031	3.40	[195]
^{32}S+^{108}Pd	0.000	0.190	11.54	3.97	83.75	1.220	15.655	0.0081	85.55	2.429	11.208	0.022	4.30	[195]
^{32}S+^{110}Pd	0.000	0.218	11.69	3.95	84.22	2.181	22.709	0.0013	85.05	2.799	12.503	0.076	5.11	[195]
^{32}S+^{138}Ba	0.000	0.000	11.19	4.18	103.68	3.159	15.016	0.0024	103.21	3.064	6.135	0.087	4.54	[185]
^{32}S+^{154}Sm	0.000	0.270	12.51	4.04	110.68	5.387	26.643	0.0005	107.96	3.775	18.642	0.050	6.22	[196]
^{32}S+^{182}W	0.000	0.259	12.76	4.14	125.03	1.417	28.589	0.0015	127.52	3.705	20.425	0.031	5.31	[197]
^{32}S+^{184}W	0.000	0.240	12.71	4.15	124.25	2.614	30.489	0.0047	127.52	3.978	19.913	0.023	6.46	[198]
^{32}S+^{208}Pb	0.000	0.000	11.84	4.34	140.82	3.985	13.597	0.0002	143.06	4.896	10.598	0.005	5.95	[199]
^{33}S+^{90}Zr	0.000	0.035	10.73	3.92	77.83	0.734	4.483	0.0056	77.79	1.244	3.614	0.068	−2.88	[200]
^{33}S+^{91}Zr	0.000	0.053	10.82	3.90	76.22	0.052	6.937	0.0034	77.33	0.505	4.713	0.033	−0.76	[200]
^{33}S+^{92}Zr	0.000	0.053	10.84	3.90	74.80	0.019	10.719	0.0037	77.20	1.325	5.505	0.037	2.57	[200]
^{34}S+^{24}Mg	0.000	0.374	10.29	3.32	26.60	0.014	2.279	0.0011	26.29	0.582	5.432	0.034	−1.64	[191]
^{34}S+^{25}Mg	0.000	0.333	10.26	3.32	26.31	0.014	2.925	0.0054	26.15	0.503	4.693	0.020	−2.52	[191]
^{34}S+^{26}Mg	0.000	0.310	10.27	3.31	26.39	0.036	2.108	0.0088	26.02	0.464	4.327	0.032	−1.55	[191]
^{34}S+^{89}Y	0.000	0.035	10.78	3.87	75.00	0.059	3.493	0.0087	75.67	1.174	3.413	0.024	−3.96	[194]
^{34}S+^{168}Er	0.000	0.294	12.86	3.95	118.28	4.029	21.016	0.0010	115.41	2.874	19.707	0.050	2.67	[201]
^{35}Cl+^{24}Mg	0.100	0.374	10.56	3.36	29.77	1.731	3.378	0.0034	27.54	0.681	6.359	0.071	−5.73	[202]
^{35}Cl+^{25}Mg	0.100	0.333	10.53	3.36	29.58	1.926	4.482	0.0021	27.40	0.601	5.613	0.047	−4.97	[202]
^{35}Cl+^{26}Mg	0.100	0.310	10.54	3.35	26.67	0.057	9.913	0.0004	27.27	0.711	5.390	0.037	0.47	[202]
^{35}Cl+^{27}Al	0.100	0.448	10.87	3.28	28.59	0.066	14.593	0.0121	29.53	0.938	8.753	0.015	−5.53	[203]
^{35}Cl+^{54}Cr	0.100	0.180	10.93	3.52	49.10	0.226	21.513	0.0510	50.88	1.038	6.405	0.043	1.23	[204]
^{35}Cl+^{52}Cr	0.100	0.000	10.32	3.74	52.61	0.001	3.383	0.0110	52.28	0.325	3.031	0.035	−2.41	[204]
^{35}Cl+^{51}V	0.100	0.000	10.32	3.67	47.53	0.169	21.236	0.0586	50.16	0.306	2.855	0.037	−1.49	[204]
^{35}Cl+^{50}Ti	0.100	0.000	10.32	3.60	47.38	0.149	2.657	0.0092	48.04	0.288	2.684	0.028	−0.19	[204]
^{35}Cl+^{54}Fe	0.100	0.000	10.32	3.77	57.77	1.193	3.496	0.0036	56.48	0.364	3.400	0.028	−3.66	[204]
^{35}Cl+^{58}Ni	0.100	0.000	10.38	3.86	59.90	0.070	4.421	0.0040	60.35	0.396	3.699	0.005	−3.57	[203]

Continued on next page

Table 1 (continued)

Reaction	β_P	β_T	R_B (fm)	$\hbar\omega$ (MeV)	B_m^{fit} (MeV)	Δ_1^{fit} (MeV)	Δ_2^{fit} (MeV)	$\mathcal{D}^{fit}$	B_m^{cal} (MeV)	Δ_1^{cal} (MeV)	Δ_2^{cal} (MeV)	$\mathcal{D}^{cal}$	$Q(2n)$ (MeV)	Ref(s).
^{35}Cl+^{60}Ni	0.100	0.027	10.53	3.73	58.49	0.421	7.393	0.0023	59.82	0.426	3.980	0.084	−1.50	[203]
^{35}Cl+^{62}Ni	0.100	0.096	10.81	3.68	57.32	0.004	9.572	0.0008	58.99	0.697	5.236	0.006	0.47	[203]
^{35}Cl+^{64}Ni	0.100	0.087	10.84	3.66	57.19	0.125	8.265	0.0005	58.78	1.287	5.623	0.002	2.40	[203]
^{35}Cl+^{90}Zr	0.100	0.035	11.03	3.87	79.58	0.301	12.449	0.0006	81.09	0.636	5.933	0.008	−2.40	[203]
^{35}Cl+^{92}Zr	0.100	0.053	11.14	3.84	80.88	1.919	8.021	0.0009	80.62	1.648	7.217	0.002	3.06	[148]
^{36}S+^{48}Ca	0.000	0.000	10.16	3.39	41.89	0.021	1.514	0.0674	41.47	0.333	0.969	0.136	−4.89	[205, 206]
^{36}S+^{64}Ni	0.000	0.087	10.67	3.52	56.00	0.021	1.667	0.0419	55.68	0.366	3.411	0.037	−1.82	[206]
^{36}S+^{90}Zr	0.000	0.035	10.86	3.80	76.95	0.146	0.012	0.0075	76.97	1.202	3.493	0.026	−1.05	[207]
^{36}S+^{96}Zr	0.000	0.217	11.67	3.59	73.98	0.288	2.667	0.0087	74.41	0.987	9.209	0.112	−1.98	[207]
^{36}S+^{92}Mo	0.000	0.035	10.87	3.87	80.19	1.329	7.046	0.0235	80.61	1.593	4.099	0.029	0.87	[195]
^{36}S+^{94}Mo	0.000	0.053	10.98	3.77	79.41	1.306	5.364	0.0214	80.00	0.527	4.923	0.857	−0.35	[195]
^{36}S+^{96}Mo	0.000	0.080	11.12	3.74	78.66	0.580	5.827	0.0686	79.45	0.590	5.504	0.346	−1.41	[195]
^{36}S+^{98}Mo	0.000	0.180	11.54	3.68	77.65	0.102	5.205	0.0260	78.22	0.895	8.356	0.047	−2.66	[195]
^{36}S+^{100}Mo	0.000	0.244	11.82	3.63	77.12	0.080	5.063	0.0289	77.48	1.141	10.646	0.048	−1.88	[195]
^{36}S+^{100}Ru	0.000	0.161	11.47	3.75	81.28	0.334	7.480	0.0276	81.90	0.875	8.170	0.041	−0.85	[195]
^{36}S+^{101}Ru	0.000	0.180	11.56	3.74	80.68	0.040	6.518	0.0030	81.60	0.940	8.774	0.023	−1.42	[195]
^{36}S+^{102}Ru	0.000	0.189	11.62	3.73	80.29	0.072	8.921	0.0097	81.40	0.972	9.072	0.027	−1.74	[195]
^{36}S+^{103}Rh	0.000	0.180	11.59	3.76	82.52	0.202	9.812	0.0741	83.22	0.962	8.982	0.054	−0.91	[195]
^{36}S+^{104}Pd	0.000	0.162	11.52	3.80	84.98	0.146	4.675	0.0794	85.12	0.923	8.610	0.066	−0.22	[195]
^{36}S+^{104}Ru	0.000	0.253	11.91	3.68	79.85	0.112	9.043	0.0306	80.64	1.226	11.442	0.034	−2.50	[195]
^{36}S+^{105}Pd	0.000	0.171	11.58	3.79	84.16	0.202	7.864	0.0272	84.92	0.953	8.890	0.035	−0.78	[195]
^{36}S+^{106}Pd	0.000	0.171	11.60	3.79	84.22	0.103	7.507	0.0297	84.80	0.951	8.879	0.033	−1.12	[195]
^{36}S+^{108}Pd	0.000	0.190	11.72	3.69	83.68	0.224	9.382	0.0199	84.38	1.019	9.514	0.023	−1.93	[195]
^{36}S+^{110}Pd	0.000	0.218	11.87	3.67	82.68	0.433	12.873	0.0044	83.90	1.129	10.537	0.024	−2.61	[195]
^{36}S+^{204}Pb	0.000	0.008	12.00	4.08	138.95	1.384	9.334	0.0004	141.49	3.048	8.859	0.017	−2.06	[199]
^{36}S+^{238}U	0.000	0.215	13.32	3.99	157.03	6.824	9.193	0.0040	148.85	2.503	20.538	0.041	1.06	[208]
^{37}Cl+^{24}Mg	0.000	0.374	10.38	3.38	28.88	2.138	6.003	0.0010	27.65	0.589	5.496	0.071	−0.47	[202]
^{37}Cl+^{25}Mg	0.000	0.333	10.35	3.38	27.15	0.042	5.991	0.0099	27.51	0.510	4.756	0.019	−1.35	[202]
^{37}Cl+^{26}Mg	0.000	0.310	10.36	3.26	26.91	0.119	7.970	0.0011	27.39	0.470	4.390	0.025	−3.94	[202]
^{37}Cl+^{59}Co	0.000	0.143	10.71	3.64	56.48	0.074	7.049	0.0023	57.22	0.507	4.731	0.004	−2.08	[182]
^{37}Cl+^{70}Ge	0.000	0.241	11.23	3.62	64.46	0.081	11.193	0.0006	65.78	0.915	8.544	0.008	−0.72	[209]
^{37}Cl+^{72}Ge	0.000	0.224	11.23	3.61	64.64	0.025	8.768	0.0008	65.62	0.862	8.043	0.002	−1.91	[209]
^{37}Cl+^{73}Ge	0.000	0.224	11.26	3.61	66.08	2.303	12.179	0.0005	65.49	0.863	8.058	0.048	−2.19	[209]
^{37}Cl+^{74}Ge	0.000	0.224	11.29	3.60	67.61	3.030	6.549	0.0004	65.36	0.865	8.073	0.029	−2.80	[209]
^{37}Cl+^{76}Ge	0.000	0.143	11.07	3.63	65.48	1.479	9.051	0.0010	65.64	0.612	5.709	0.099	−1.75	[209]
^{37}Cl+^{93}Nb	0.000	0.053	10.96	3.82	81.71	0.128	8.738	0.0092	82.95	0.558	5.205	0.024	−2.54	[210]
^{37}Cl+^{98}Mo	0.000	0.180	11.52	3.76	81.85	0.026	14.705	0.0014	82.97	0.959	8.953	0.019	−1.28	[210]
^{37}Cl+^{100}Mo	0.000	0.244	11.81	3.65	81.76	0.184	13.550	0.0038	82.18	1.210	11.291	0.016	−0.04	[210]
^{40}Ar+^{112}Sn	0.000	0.018	11.12	3.89	101.84	1.674	12.608	0.0011	104.19	2.369	5.924	0.078	1.58	[40]
^{40}Ar+^{116}Sn	0.000	0.000	11.12	3.88	101.04	1.578	14.597	0.0718	103.96	1.681	4.886	0.996	−0.20	[40]
^{40}Ar+^{122}Sn	0.000	0.000	11.24	3.79	102.27	2.715	9.678	0.0007	103.22	1.770	4.815	0.640	0.54	[40]
^{40}Ar+^{144}Sm	0.000	0.000	11.41	3.94	122.24	1.496	15.567	0.0064	124.46	2.375	6.902	0.033	−1.29	[40]
^{40}Ar+^{148}Sm	0.000	0.161	12.16	3.85	123.36	3.677	20.235	0.0057	120.91	1.770	13.735	0.224	1.04	[40]
^{40}Ar+^{154}Sm	0.000	0.270	12.73	3.78	118.37	3.650	43.070	0.0171	118.72	2.478	18.622	0.698	1.69	[40]
^{40}Ca+^{40}Ca	0.000	0.000	9.84	3.83	53.12	0.468	0.122	0.0055	52.92	0.579	1.684	0.039	−9.09	[211]
^{40}Ca+^{44}Ca	0.000	0.000	10.00	3.78	50.36	0.744	8.313	0.0224	52.23	0.794	1.833	0.202	0.78	[211]
^{40}Ca+^{46}Ti	0.000	0.000	9.99	3.83	56.11	0.341	3.008	0.0009	57.31	0.653	1.899	0.054	−2.88	[212]
^{40}Ca+^{48}Ca	0.000	0.000	10.14	3.64	49.30	0.087	7.901	0.0042	51.60	1.351	2.332	0.023	2.61	[211]
^{40}Ca+^{48}Ti	0.000	0.000	10.06	3.81	56.25	0.746	2.762	0.0011	56.97	0.635	1.845	0.042	−0.66	[212]
^{40}Ca+^{50}Ti	0.000	0.000	10.13	3.70	55.10	0.325	5.689	0.0006	56.64	0.861	2.038	0.018	0.76	[212]
^{40}Ca+^{58}Ni	0.000	0.000	10.18	3.95	70.31	0.073	4.064	0.0109	71.13	0.953	2.769	0.013	−2.62	[213]
^{40}Ca+^{64}Ni	0.000	0.087	10.64	3.76	66.19	0.130	12.425	0.0037	69.20	1.574	5.758	0.056	3.35	[213]
^{40}Ca+^{90}Zr	0.000	0.035	10.82	3.96	94.21	0.046	4.897	0.0011	95.55	1.750	5.086	0.009	−1.44	[214]
^{40}Ca+^{94}Zr	0.000	0.062	11.01	3.85	93.86	3.147	7.950	0.0004	94.40	2.275	8.194	0.188	4.89	[86]
^{40}Ca+^{96}Zr	0.000	0.217	11.63	3.76	91.90	2.596	12.839	0.0004	92.33	3.015	13.396	0.002	5.53	[214]
^{40}Ca+^{192}Os	0.000	0.155	12.51	3.97	167.35	7.228	13.803	0.0030	160.38	4.123	21.075	0.054	6.53	[215]
^{40}Ca+^{194}Pt	0.000	0.000	11.79	4.03	169.11	4.917	18.011	0.0022	169.02	5.621	13.145	0.061	5.23	[215]
^{40}Ca+^{197}Au	0.000	0.131	12.43	4.00	175.75	11.131	17.917	0.0018	166.02	3.680	20.668	0.039	5.13	[216]
^{40}Ca+^{208}Pb	0.000	0.000	11.92	4.04	175.67	8.467	20.859	0.0001	175.50	6.044	14.066	0.036	5.74	[216]
^{48}Ca+^{48}Ca	0.000	0.000	10.44	3.31	50.47	0.007	0.764	0.0118	50.33	0.460	1.336	0.042	−5.72	[217]
^{48}Ca+^{90}Zr	0.000	0.035	11.12	3.62	92.08	0.014	7.145	0.0011	93.41	1.615	4.693	0.036	−1.40	[218]
^{48}Ca+^{96}Zr	0.000	0.217	11.92	3.44	89.98	0.210	10.453	0.0045	90.30	1.173	10.951	0.034	−2.81	[218]
^{48}Ca+^{154}Sm	0.000	0.270	12.92	3.58	134.36	4.761	22.998	0.0087	132.17	2.090	19.505	0.371	−2.33	[219]
^{48}Ca+^{197}Au	0.000	0.131	12.73	3.68	165.82	3.999	20.495	0.0039	162.72	1.936	18.072	0.029	−3.13	[216]
^{48}Ca+^{208}Pb	0.000	0.000	12.22	3.68	174.92	6.607	9.554	0.0131	171.92	3.980	11.566	0.012	−2.60	[216]
^{48}Ti+^{58}Fe	0.000	0.199	11.08	3.56	68.17	0.055	12.134	0.0064	69.19	1.220	7.677	0.114	1.39	[220]

Continued on next page

Table 1 (continued)

Reaction	$\beta_{\rm P}$	$\beta_{\rm T}$	$R_{\rm B}$ (fm)	$\hbar\omega$ (MeV)	$B_{\rm m}^{\rm fit}$ (MeV)	$\Delta_1^{\rm fit}$ (MeV)	$\Delta_2^{\rm fit}$ (MeV)	$\mathcal{D}^{\rm fit}$	$B_{\rm m}^{\rm cal}$ (MeV)	$\Delta_1^{\rm cal}$ (MeV)	$\Delta_2^{\rm cal}$ (MeV)	$\mathcal{D}^{\rm cal}$	$Q(2n)$ (MeV)	Ref(s).
^{48}Ti+^{58}Ni	0.000	0.000	10.39	3.78	78.69	2.794	3.968	0.0010	76.60	1.055	3.065	0.040	−0.12	[221]
^{48}Ti+^{60}Ni	0.000	0.027	10.54	3.75	77.53	2.226	2.606	0.0010	75.95	1.151	3.347	0.008	−1.31	[221]
^{46}Ti+^{64}Ni	0.000	0.087	10.78	3.70	76.38	3.297	7.348	0.0014	74.96	1.836	6.436	0.009	4.01	[174]
^{48}Ti+^{64}Ni	0.000	0.087	10.85	3.61	74.86	1.305	6.328	0.0049	74.54	1.368	5.871	0.018	2.59	[221]
^{48}Ti+^{122}Sn	0.000	0.000	11.33	3.75	123.54	3.065	15.750	0.0063	123.90	3.531	7.762	0.040	4.10	[185]
^{50}Ti+^{60}Ni	0.000	0.027	10.61	3.66	76.99	2.336	3.882	0.0023	75.54	1.125	3.271	0.018	−0.67	[174]
^{46}Ti+^{93}Nb	0.000	0.053	11.06	3.85	108.71	4.839	5.140	0.0002	105.12	2.024	8.783	0.150	3.79	[94]
^{50}Ti+^{93}Nb	0.000	0.053	11.21	3.69	104.10	1.660	9.875	0.0017	104.04	0.781	7.294	0.140	−2.54	[94]
^{46}Ti+^{90}Zr	0.000	0.035	10.95	3.84	105.35	3.320	6.133	0.0005	103.51	1.971	5.729	0.018	−0.78	[94]
^{50}Ti+^{90}Zr	0.000	0.035	11.09	3.68	102.13	0.780	7.072	0.0001	102.44	1.897	5.514	0.120	−3.25	[94]
^{58}Ni+^{54}Fe	0.000	0.000	10.44	3.92	89.58	0.287	6.041	0.0474	89.47	1.406	4.085	0.455	−1.97	[222]
^{58}Ni+^{58}Ni	0.000	0.000	10.49	3.86	93.88	0.083	14.077	0.0822	95.56	1.577	4.582	0.360	−2.08	[223]
^{58}Ni+^{64}Ni	0.000	0.087	10.96	3.71	92.20	1.367	23.646	0.0050	93.04	1.991	8.209	0.134	3.89	[132]
^{58}Ni+^{124}Sn	0.000	0.000	11.43	3.66	157.04	4.647	11.753	0.0081	157.24	5.161	11.369	0.129	5.95	[224]
^{64}Ni+^{64}Ni	0.087	0.087	11.42	3.50	90.05	0.028	12.073	0.0029	90.77	0.879	8.203	0.037	−1.44	[84]
^{64}Ni+^{124}Sn	0.087	0.000	11.90	3.48	151.86	2.442	23.232	0.0056	152.33	1.563	12.952	0.822	0.62	[224]
^{124}Sn+^{40}Ca	0.000	0.000	11.17	3.93	113.80	4.485	7.892	0.0017	114.67	3.673	7.376	0.069	5.41	[88]
^{132}Sn+^{40}Ca	0.000	0.000	11.31	3.90	115.79	5.701	4.844	0.0009	113.65	4.159	7.641	0.003	7.29	[88, 98]
^{134}Te+^{40}Ca	0.000	0.000	11.31	3.95	114.49	1.561	14.100	0.0024	117.90	4.015	7.794	0.005	6.35	[89]
^{124}Sn+^{48}Ca	0.000	0.000	11.47	3.62	111.83	2.343	12.593	0.0097	112.19	1.807	5.252	0.017	−2.93	[88]
^{132}Sn+^{48}Ca	0.000	0.000	11.61	3.54	112.18	1.698	4.461	0.0015	111.20	1.702	4.945	0.034	−1.05	[88]
^{132}Sn+^{58}Ni	0.000	0.000	11.58	3.60	161.34	7.669	3.695	0.0001	155.77	5.598	11.492	0.019	7.83	[225]
^{132}Sn+^{64}Ni	0.000	0.087	12.04	3.42	152.06	3.304	13.500	0.0015	151.01	2.099	12.936	0.019	2.50	[226]
^{208}Pb+^{26}Mg	0.000	0.310	12.59	4.22	102.72	0.121	19.467	0.0034	103.91	1.407	10.889	0.019	0.84	[227]

Table 2
The experimental and calculated excitation functions for a total of 220 reaction systems. See page 59 for Explanation of Tables.

Reaction	Detected particles	Data obtained	E_{lab} (MeV)	$E_{c.m.}$ (MeV)	σ (mb)	$\delta\sigma$ (mb)	σ^{cal} (mb)
$^{12}C+^{89}Y$	EvR	authors' graph	30.682	27.037	0.033	—	0.195
		[147]	32.403	28.554	0.668	—	1.697
		E_{lab}	33.789	29.774	4.757	—	9.135
			35.387	31.183	29.865	—	47.223
			36.912	32.526	96.919	—	132.929
			39.174	34.520	287.692	—	302.095
			41.019	36.145	369.296	—	434.894
			43.207	38.074	597.752	—	575.375
			46.281	40.783	665.270	—	744.850
$^{12}C+^{92}Zr$	EvR	authors' table	31.88	28.20	0.19	0.1	0.456
		[148]	32.88	29.09	1.45	0.2	1.613
		$E_{c.m.}$	33.89	29.98	2.91	0.2	5.554
			34.89	30.86	13.2	0.5	17.351
			35.89	31.75	38.6	1.1	45.991
			36.89	32.63	83.6	1.2	95.738
			37.89	33.52	136	3	163.147
			38.89	34.40	197	2	237.855
			39.90	35.30	253	3	315.353
			40.90	36.18	308	3	388.645
			41.91	37.07	366	3	459.032
			42.90	37.95	421	3	524.753
			43.89	38.83	476	4	586.786
			45.90	40.60	570	5	701.389
			47.91	42.38	664	5	804.554
			49.91	44.15	731	9	896.774
$^{12}C+^{144}Sm$	EvR	authors' graph	46.464	42.890	0.377	—	0.815
		[149]	46.968	43.355	0.975	—	1.489
		E_{lab}	47.407	43.760	1.458	—	2.508
			47.895	44.210	2.933	—	4.434
			48.919	45.156	9.959	—	13.789
			49.895	46.057	29.568	—	35.079
			50.871	46.958	79.905	—	72.962
			51.896	47.904	107.382	—	127.901
			52.872	48.805	186.270	—	187.889
			53.847	49.705	250.323	—	249.787
			55.848	51.552	359.775	—	372.427
			59.898	55.290	599.433	—	591.509
			67.851	62.632	1025.933	—	928.056
			69.852	64.478	1053.872	—	997.567
			74.877	69.118	1289.154	—	1151.361
$^{12}C+^{152}Sm$	EvR	authors' table	47.2	43.75	18	3	13.701
		[150]	50.2	46.53	75	7	99.161
		E_{lab}	53.3	49.40	195	10	268.312
			56.3	52.18	378	16	463.518
			59.3	54.96	562	30	656.140
			62.3	57.74	704	43	832.511
$^{12}C+^{154}Sm$	EvR	authors' table	46.7	43.32	8	4	10.434
		[151]	47.7	44.25	22	4.2	24.915
		E_{lab}	48.7	45.18	51	8.6	49.214
			49.7	46.11	89	16	83.397
			49.7	46.11	93	12	83.397
			50.7	47.03	150	15	126.393
			51.7	47.96	199	20	176.742
			52.7	48.89	263	26	232.886
			54.7	50.75	361	36	356.567
			56.7	52.60	409	36	486.904
			58.7	54.46	514	51	616.366
			60.7	56.31	545	54	740.500
$^{12}C+^{181}Ta$	EvR	authors' table	53.6	50.27	11.3	1.1	20.506
		[152]	57.3	53.74	112.9	11.3	140.683
		E_{lab}	62.4	58.52	345.6	34.6	433.558
			67.5	63.30	620.5	62.1	746.158
			72.6	68.09	799.9	80.0	1020.155
			74.3	69.68	977.2	97.7	1101.736
			76.9	72.12	971.1	97.1	1217.973

Continued on next page

Table 2 (continued)

Reaction	Detected particles	Data obtained	$E_{\rm lab}$ (MeV)	$E_{\rm c.m.}$ (MeV)	σ (mb)	$\delta\sigma$ (mb)	$\sigma^{\rm cal}$ (mb)
			82.7	77.56	1118.3	111.8	1444.913
			87.8	82.34	1338.6	133.9	1613.780
			91.4	85.72	1277.8	127.8	1718.709
			93.3	87.50	1302.4	130.2	1769.920
			97.8	91.72	1364.7	136.5	1881.003
^{12}C+^{194}Pt	EvRFF	authors' table [153] $E_{\rm lab}$	55.5	52.27	2.3	0.15	1.671
			56.5	53.21	6.7	0.2	5.176
			57.5	54.15	19.6	0.6	14.817
			59.0	55.56	62.0	1.8	53.027
			60.5	56.98	126.0	4.0	123.702
			62.5	58.86	229.6	7.0	241.814
			64.5	60.74	330.8	10.0	360.315
			67.0	63.10	435.0	14.0	497.678
			69.5	65.45	535.3	16.0	622.875
			73.0	68.75	660.0	20.0	780.234
^{12}C+^{198}Pt	EvRFF	authors' table [153] $E_{\rm lab}$	55.5	52.33	1.6	0.07	2.298
			56.5	53.27	5.5	0.11	7.055
			57.5	54.21	15.6	0.25	19.613
			59.0	55.63	55.5	1.5	65.077
			60.5	57.04	125.0	4.0	141.825
			62.5	58.93	230.2	7.0	263.070
			64.5	60.81	332.0	10.0	382.248
			67.0	63.17	437.0	14.0	519.913
			69.5	65.53	538.0	17.0	645.353
			73.0	68.83	670.0	20.0	803.029
^{12}C+^{204}Pb	EvRFF	authors' graph [154] $E_{\rm c.m.}$[1]	55.814	52.713	0.037	—	0.201
			56.790	53.635	0.600	—	0.621
			57.775	54.565	3.465	—	1.921
			59.547	56.239	28.717	—	13.001
			59.793	56.471	53.328	—	16.507
			61.811	58.377	226.038	—	77.032
			64.814	61.213	332.804	—	242.677
			68.851	65.026	515.936	—	471.515
			72.838	68.792	634.162	—	668.423
			79.878	75.440	779.478	—	956.856
			84.903	80.186	864.183	—	1126.287
			89.871	84.879	886.761	—	1270.280
^{12}C+^{206}Pb	EvRFF	authors' graph [154] $E_{\rm c.m.}$[2]	57.835	54.651	2.632	—	2.391
			59.798	56.507	54.729	—	18.914
			61.863	58.458	151.329	—	86.200
			64.812	61.245	289.817	—	252.654
			68.843	65.053	509.937	—	481.723
			72.825	68.816	639.254	—	678.622
			79.805	75.412	872.246	—	965.333
			84.818	80.150	872.246	—	1135.019
^{12}C+^{208}Pb	EvRFF	authors' table [155] $E_{\rm lab}$ & $E_{\rm c.m.}$	57.87	54.67	3.32	0.36	2.534
			59.80	56.49	37.6	1.2	19.276
			61.73	58.32	118	5	81.922
			63.66	60.15	217	5	187.383
			65.59	61.97	318	7	302.498
			67.52	63.80	408	8	413.456
			69.50	65.67	519	12	519.327
			71.50	67.56	598	17	618.957
			76.00	71.82	778	15	819.662
			82.00	77.49	986	13	1044.328
			88.00	83.16	1110	13	1230.635
			94.00	88.83	1286	15	1386.686
^{12}C+^{237}Np	FF	authors' table [156] $E_{\rm c.m.}$	59.78	56.90	0.34	0.10	0.389
			60.83	57.90	1.35	0.36	1.293
			61.84	58.86	4.5	1.0	3.837
			63.79	60.72	17.3	3.6	21.829

Continued on next page

[1] In the authors' graph, the capture excitation function was plotted as a function of the excitation energy $E^*_{\rm CN}$ of the compound nucleus. $E_{\rm c.m.}$ is obtained by $E_{\rm c.m.} = E^*_{\rm CN} - Q$ and $Q = -28.401$ MeV is calculated with the nuclear masses taken from Refs. [102, 103].

[2] Similar to the reaction system ^{12}C+^{204}Pb, but the Q value is -30.437 MeV.

Table 2 (continued)

Reaction	Detected particles	Data obtained	E_{lab} (MeV)	$E_{c.m.}$ (MeV)	σ (mb)	$\delta\sigma$ (mb)	σ^{cal} (mb)
			64.85	61.72	25.8	4.8	43.436
			65.85	62.68	45.5	8.4	73.129
			66.82	63.60	80	15	109.187
			67.85	64.58	103	17	154.611
			69.85	66.48	174	34	258.036
			74.85	71.24	407	58	552.044
			79.86	76.01	617	76	831.008
$^{12}C+^{238}U$	FF	authors' table [157] E_{lab}	65.0	61.88	35.6	5.0	74.117
			66.0	62.83	39.2	5.0	110.849
			67.5	64.26	102	14	178.051
			69.1	65.78	226	18	261.714
			70.0	66.64	280	20	312.438
			72.5	69.02	374	22	459.934
			72.5	69.02	401	25	459.934
			73.0	69.50	413	25	489.794
			73.5	69.97	426	29	519.585
			74.3	70.73	479	33	566.957
			77.3	73.59	616	38	738.687
			81.2	77.30	725	41	942.982
			83.0	79.02	812	49	1029.722
			90.0	85.68	1094	60	1327.017
			96.2	91.58	1311	68	1546.066
			104.5	99.48	1653	79	1788.827
			110.6	105.29	1758	90	1937.835
			110.6	105.29	1801	90	1937.835
			117.8	112.15	1858	95	2087.951
			117.8	112.15	1915	95	2087.951
			124.0	118.05	2068	100	2198.584
$^{14}N+^{59}Co$	EvR	authors' table [158] E_{lab} & $E_{c.m.}$	32	25.39	27.5	4.5	19.293
			—	27.02	103	12	97.782
			36.5	29.06	299	40	270.372
			—	31.90	558	68	508.336
			45	35.96	730	75	772.632
			48	38.40	901	80	897.825
			51	40.85	961	80	1004.414
			56	44.90	1113	113	1147.999
$^{14}N+^{232}Th$	FF	authors' table [159] E_{lab}	72.6	68.47	20.3	2	23.214
			74.6	70.35	54	4	64.198
			76.6	72.24	111	7	127.042
			78.7	74.22	214	11	210.877
			80.7	76.11	290	27	301.718
			82.7	77.99	380	53	397.994
			84.7	79.88	518	24	495.616
			87.5	82.52	650	26	629.408
			91.6	86.39	823	40	812.446
$^{14}N+^{238}U$	FF	authors' table [157] E_{lab}	77.1	72.82	50.0	7.3	108.723
			77.1	72.82	57.3	7.9	108.723
			82.0	77.44	244	18	310.553
			86.6	81.79	456	27	531.823
			89.7	84.72	585	32	677.730
			93.9	88.68	800	40	861.348
			97.4	91.99	914	45	1000.554
			101.3	95.67	1057	50	1141.801
			104.0	98.22	1200	55	1231.839
			107.9	101.91	1254	57	1351.878
			112.4	106.16	1420	63	1477.260
			115.8	109.37	1500	67	1563.701
			121.9	115.13	1640	72	1703.109
			127.8	120.70	1770	76	1821.247
			133.4	125.99	1900	81	1920.287
			140.2	132.41	2050	87	2025.695
			145.5	137.42	2132	90	2097.917
$^{15}N+^{56}Fe$	EvR	authors' graph [160] $E_{c.m.}$	31.821	25.098	50.513	—	52.182
			33.374	26.323	93.725	—	147.307
			34.253	27.017	101.282	—	211.254
			35.296	27.839	175.325	—	285.887

Continued on next page

Table 2 (continued)

Reaction	Detected particles	Data obtained	E_{lab} (MeV)	$E_{c.m.}$ (MeV)	σ (mb)	$\delta\sigma$ (mb)	σ^{cal} (mb)
			35.662	28.128	196.709	—	311.188
			36.462	28.758	288.753	—	364.403
			37.798	29.812	367.986	—	447.253
			41.906	33.053	745.488	—	660.651
			44.026	34.725	847.594	—	751.105
			45.827	36.145	832.719	—	819.505
$^{15}N+^{209}Bi$	FF	authors' graph [161] $E_{c.m.}$	67.875	63.330	0.964	—	2.120
			69.275	64.636	4.110	—	9.396
			70.000	65.312	9.739	—	18.405
			70.514	65.792	16.617	—	28.103
			70.979	66.226	26.558	—	39.523
			72.027	67.204	54.192	—	74.436
			73.959	69.007	129.766	—	162.176
			76.056	70.963	220.054	—	268.091
			78.069	72.841	313.491	—	366.532
			80.031	74.672	408.787	—	456.955
			82.113	76.614	475.136	—	546.979
			84.144	78.510	542.568	—	629.436
			86.192	80.420	653.348	—	707.549
			88.204	82.297	705.589	—	779.863
$^{16}O+^{58}Ni$	EvR	authors' graph [162] $E_{c.m.}$	40.081	31.415	39.763	—	79.423
			42.141	33.029	144.785	—	199.243
			44.188	34.634	251.310	—	318.487
			46.162	36.181	349.866	—	421.974
			48.193	37.773	468.998	—	517.257
			60.291	47.255	872.497	—	919.802
$^{16}O+^{62}Ni$	EvR	authors' graph [162] $E_{c.m.}$	40.151	31.915	90.320	—	134.468
			42.187	33.533	210.476	—	264.904
			46.156	36.688	440.075	—	498.982
			48.196	38.310	527.866	—	601.166
			50.186	39.891	622.607	—	690.699
			52.221	41.509	693.091	—	773.334
			56.218	44.686	853.498	—	913.516
			60.215	47.863	920.135	—	1029.919
$^{16}O+^{59}Co$	EvR	authors' table [158] E_{lab} & $E_{c.m.}$	34	26.30	0.5	0.1	0.451
			35	27.10	3.8	0.6	1.580
			40	31.00	88	14	127.017
			50	39.00	527	63	699.662
$^{16}O+^{70}Ge$	EvR	authors' table [163] $E_{c.m.}$	38.45	31.3	0.36	0.10	0.861
			39.44	32.1	1.63	0.23	2.883
			40.54	33.0	6.84	0.37	9.753
			41.53	33.8	19.98	0.97	23.661
			42.51	34.6	46.6	1.7	47.170
			43.49	35.4	86.7	3.3	80.168
			44.47	36.2	123.6	4.6	121.271
			45.58	37.1	187.0	7.2	174.946
			46.56	37.9	230.9	8.3	227.225
			47.55	38.7	287	10	282.050
			48.53	39.5	353	10	337.999
			49.51	40.3	405	14	393.944
			49.51	40.3	394	20	393.944
			50.49	41.1	469	24	449.053
			51.60	42.0	505	20	509.354
			52.58	42.8	565	21	561.067
			53.57	43.6	630	24	610.823
			54.55	44.4	680	26	658.562
			54.55	44.4	689	34	658.562
			55.53	45.2	704	29	704.299
			56.51	46.0	727	31	748.090
			57.62	46.9	797	29	795.129
			58.60	47.7	836	33	835.062
			59.59	48.5	863	34	873.322
			59.59	48.5	840	27	873.322
			59.59	48.5	848	29	873.322
$^{16}O+^{72}Ge$	EvR	authors' table [163]	38.26	31.3	0.41	0.08	1.035
			39.23	32.1	1.44	0.18	3.457

Continued on next page

Table 2 (continued)

Reaction	Detected particles	Data obtained	E_{lab} (MeV)	$E_{c.m.}$ (MeV)	σ (mb)	$\delta\sigma$ (mb)	σ^{cal} (mb)
		$E_{c.m.}$	40.21	32.9	4.69	0.27	10.219
			41.31	33.8	13.45	0.63	27.554
			42.29	34.6	31.7	1.5	53.939
			43.27	35.4	62.6	2.8	90.254
			44.12	36.1	90.3	3.3	128.830
			45.10	36.9	130.0	5.0	178.798
			46.08	37.7	180.1	6.6	233.029
			47.06	38.5	237	10	289.648
			48.03	39.3	274	10	347.108
			49.01	40.1	336	13	404.233
			49.01	40.1	330	14	404.233
			49.01	40.1	341	12	404.233
			49.99	40.9	394	10	460.201
			51.09	41.8	452	17	521.135
			52.19	42.7	503	18	579.543
			53.17	43.5	581	17	629.214
			54.14	44.3	624	19	676.769
			55.12	45.1	660	13	722.262
			56.10	45.9	706	17	765.780
			57.08	46.7	770	33	807.421
			58.18	47.6	798	24	852.146
			58.18	47.6	803	25	852.146
			59.16	48.4	875	25	890.125
			60.13	49.2	933	27	926.526
			61.11	50.0	978	28	961.436
			62.09	50.8	1066	28	994.936
			63.07	51.6	1134	27	1027.098
$^{16}O+^{73}Ge$	EvR	authors' table [163] $E_{c.m.}$	39.75	32.6	11.7	1.8	7.626
			40.72	33.4	25.7	2.6	19.809
			41.82	34.3	46.6	3.9	45.459
			42.79	35.1	79.1	5.4	79.216
			43.77	35.9	117.7	7.8	121.784
			44.74	36.7	157.3	9.6	171.105
			45.72	37.5	212	16	225.060
			46.82	38.4	249	14	288.909
			46.82	38.4	250	17	288.909
			47.79	39.2	328	15	346.707
			48.77	40.0	364	21	404.226
			48.77	40.0	392	28	404.226
			49.74	40.8	436	25	460.621
			49.74	40.8	419	24	460.621
			50.84	41.7	442	29	522.056
			51.82	42.5	547	19	574.551
			52.79	43.3	560	23	624.927
			53.77	44.1	630	26	673.168
			54.74	44.9	704	27	719.323
			55.84	45.8	706	24	768.855
			56.81	46.6	797	32	810.865
			57.79	47.4	859	37	851.079
			58.76	48.2	862	26	889.596
			59.74	49.0	882	28	926.509
			60.84	49.9	887	37	966.227
			61.81	50.7	992	34	1000.014
			62.79	51.5	973	35	1032.452
$^{16}O+^{74}Ge$	EvR	authors' table [163] $E_{c.m.}$	37.82	31.1	0.47	0.01	0.937
			38.80	31.9	1.67	0.27	3.164
			39.77	32.7	7.64	0.61	9.507
			40.74	33.5	19.8	1.3	23.682
			41.72	34.3	44.7	2.2	48.167
			42.81	35.2	76.7	3.9	87.907
			43.78	36.0	116.0	5.6	132.286
			44.76	36.8	164.5	8.2	183.006
			45.73	37.6	220.0	7.8	237.969
			46.82	38.5	256.3	7.3	302.554
			47.80	39.3	317.1	9.1	360.727
			48.77	40.1	346	11	418.431

Continued on next page

Table 2 (continued)

Reaction	Detected particles	Data obtained	E_{lab} (MeV)	$E_{c.m.}$ (MeV)	σ (mb)	$\delta\sigma$ (mb)	σ^{cal} (mb)
			49.74	40.9	434	16	474.882
			50.84	41.8	473	22	536.282
			51.81	42.6	553	26	588.700
			52.78	43.4	589	31	638.978
			53.76	44.2	631	26	687.114
			54.85	45.1	649	24	738.778
			55.82	45.9	722	28	782.585
			56.80	46.7	788	24	824.503
			57.77	47.5	754	24	864.633
			58.86	48.4	821	24	907.763
			59.84	49.2	868	26	944.412
			60.81	50.0	890	29	979.561
			61.78	50.8	932	29	1013.290
			62.76	51.6	965	30	1045.676
			63.85	52.5	989	28	1080.589
			64.82	53.3	964	27	1110.344
			65.80	54.1	1000	34	1138.958
$^{16}O+^{76}Ge$	EvR	authors' table [163] $E_{c.m.}$	37.65	31.1	0.60	0.15	1.015
			38.74	32.0	3.07	0.41	4.032
			39.71	32.8	9.90	0.74	12.365
			40.67	33.6	25.2	1.3	31.517
			41.76	34.5	57.6	2.6	69.905
			42.73	35.3	86.1	3.8	117.491
			43.70	36.1	132.3	5.4	173.715
			44.67	36.9	180.5	8.0	234.473
			45.76	37.8	236.0	9.0	304.251
			46.73	38.6	299	12	365.270
			47.69	39.4	388	15	424.217
			47.69	39.4	364	14	424.217
			48.78	40.3	404	15	487.524
			49.75	41.1	426	17	541.031
			49.75	41.1	441	16	541.031
			50.72	41.9	473	19	592.009
			51.69	42.7	566	22	640.589
			52.78	43.6	606	25	692.549
			53.75	44.4	644	28	736.495
			54.72	45.2	691	26	778.465
			55.81	46.1	787	29	823.468
			56.77	46.9	820	31	861.622
			57.74	47.7	846	32	898.141
			58.71	48.5	907	35	933.116
			59.80	49.4	934	33	970.726
			60.77	50.2	988	38	1002.699
			60.77	50.2	1000	32	1002.699
			61.74	51.0	1090	30	1033.377
			62.71	51.8	1119	44	1062.827
			63.79	52.7	1138	44	1094.570
			64.76	53.5	1153	46	1121.616
			65.73	54.3	1207	46	1147.619
$^{16}O+^{92}Zr$	EvR	authors' table [148] $E_{c.m.}$	43.85	37.35	0.23	0.07	0.177
			44.34	37.77	0.62	0.09	0.325
			44.84	38.20	0.79	0.1	0.607
			45.34	38.62	2.22	0.1	1.113
			45.84	39.05	2.41	0.2	2.057
			46.33	39.47	4.62	0.3	3.710
			46.84	39.90	8.7	0.4	6.663
			47.34	40.33	15.2	0.5	11.625
			47.84	40.75	23.1	0.5	19.242
			48.34	41.18	33.8	0.6	30.637
			48.85	41.61	49.2	0.5	46.081
			49.34	42.03	65.7	0.7	65.001
			49.84	42.46	86.2	0.9	87.800
			50.35	42.89	105	1	113.314
			50.84	43.31	128	1	140.065
			51.35	43.74	151	1	168.588
			51.85	44.17	174	2	197.653

Continued on next page

Table 2 (continued)

Reaction	Detected particles	Data obtained	E_{lab} (MeV)	$E_{c.m.}$ (MeV)	σ (mb)	$\delta\sigma$ (mb)	σ^{cal} (mb)
			52.85	45.02	223	2	255.081
			53.85	45.87	270	2	311.019
			54.35	46.30	299	2	338.498
			54.86	46.73	325	2	365.386
			55.35	47.15	347	3	391.071
			55.76	47.50	367	3	412.045
			57.76	49.20	459	3	508.579
			59.86	50.99	543	3	601.431
			61.87	52.70	626	5	682.655
			63.86	54.40	687	5	756.954
			65.87	56.11	754	6	825.879
			67.86	57.81	813	6	889.205
			69.87	59.52	867	6	948.185
			71.88	61.23	912	7	1002.879
			73.87	62.93	971	7	1053.394
			75.88	64.64	1022	7	1100.668
			77.88	66.34	1071	7	1144.450
			79.88	68.05	1110	8	1185.527
			81.89	69.76	1159	8	1223.874
$^{16}O+^{112}Cd$	EvR	authors' table [164] $E_{c.m.}$	51.77	45.3	1.8	0.41	1.410
			52.23	45.7	4.2	0.86	2.454
			53.26	46.6	9.4	2.0	7.854
			53.83	47.1	20.6	4.1	13.888
			54.63	47.8	48.0	9.6	27.519
			55.77	48.8	73.2	14.7	58.649
			56.69	49.6	124	25	92.632
			57.71	50.5	153	31	138.324
			58.74	51.4	206	41	189.355
			59.66	52.2	267	54	237.236
			60.23	52.7	385	77	267.711
			62.86	55.0	355	71	406.442
			64.69	56.6	628	126	497.459
			68.69	60.1	853	171	676.581
$^{16}O+^{144}Nd$	EvR	authors' table [165] E_{lab} & $E_{c.m.}$	60.0	54.0	0.564	0.085	0.226
			61.0	54.9	2.84	0.43	0.751
			61.5	55.35	5.44	0.55	1.361
			62.5	56.25	15.4	2.0	4.327
			65.0	58.5	92	9	44.821
			67.0	60.3	140	30	127.172
			67.0	60.3	193	20	127.172
			70.0	63.0	352	35	273.954
			72.0	64.8	374	38	366.264
			72.9	65.6	374	35	405.275
			75.0	67.5	464	47	493.231
			78.0	70.3	574	55	611.858
			90.0	81.0	870	70	970.337
$^{16}O+^{148}Nd$	EvR	authors' table [150] E_{lab}	64.5	58.21	57	7	60.471
			67.5	60.91	177	10	170.554
			70.5	63.62	265	13	311.835
			73.5	66.33	402	19	460.319
			76.6	69.13	506	28	607.153
			79.6	71.83	604	32	738.081
$^{16}O+^{150}Nd$	EvR	authors' table [150] E_{lab}	61.9	55.93	12	3	15.433
			65.0	58.73	86	6	83.665
			68.0	61.45	197	9	198.323
			71.0	64.16	281	12	338.852
			74.0	66.87	387	18	486.532
			77.0	69.58	504	22	629.745
			80.0	72.29	586	27	763.316
$^{16}O+^{144}Sm$	EvR	authors' table [124] E_{lab}	62.88	56.59	0.15	0.08	0.577
			63.38	57.04	0.33	0.08	1.037
			63.88	57.49	0.45	0.08	1.852
			64.38	57.94	1.5	0.2	3.267
			64.88	58.39	2.7	0.3	5.653
			65.38	58.84	5.5	0.3	9.513
			65.88	59.29	10.2	0.4	15.429

Continued on next page

Table 2 (continued)

Reaction	Detected particles	Data obtained	$E_{\rm lab}$ (MeV)	$E_{\rm c.m.}$ (MeV)	σ (mb)	$\delta\sigma$ (mb)	$\sigma^{\rm cal}$ (mb)
			66.38	59.74	17.5	0.3	23.945
			66.88	60.19	28.6	0.3	35.412
			67.38	60.64	41.3	0.4	49.892
			67.88	61.09	55.5	0.4	67.154
			68.38	61.54	71.2	0.5	86.748
			68.88	61.99	90.6	0.6	108.125
			69.38	62.44	108	1	130.729
			69.88	62.89	131	1	154.075
			70.38	63.34	150	1	177.778
			70.88	63.79	169	1	201.557
			71.38	64.24	184	1	225.221
			71.88	64.69	208	1	248.649
			72.88	65.59	253	2	294.550
			73.88	66.49	295	2	339.012
			74.88	67.39	348	2	382.002
			75.88	68.29	383	2	423.559
			77.88	70.09	469	3	502.599
			79.88	71.89	552	3	576.592
			84.88	76.39	700	5	742.155
			89.88	80.89	876	4	884.162
			99.88	89.89	1076	15	1113.206
^{16}O+^{147}Sm	EvR	authors' table [133] $E_{\rm lab}$	62.0	55.91	0.52	0.1	0.749
			62.9	56.73	2.8	0.4	2.150
			64.0	57.72	7.6	1.2	7.008
			65.0	58.62	27.3	3.3	17.304
			65.9	59.43	47.3	5.7	33.266
			66.9	60.33	69.0	8.0	58.868
			70.5	63.58	210.0	25.0	202.000
			74.9	67.55	404.0	48.0	413.016
^{16}O+^{148}Sm	EvR	authors' table [124] $E_{\rm lab}$	60.86	54.92	0.4	0.1	0.254
			61.36	55.37	1.1	0.2	0.467
			61.86	55.82	1.7	0.2	0.852
			62.86	56.73	5.8	0.2	2.715
			63.36	57.18	7.9	0.4	4.667
			63.91	57.67	12.6	0.3	8.112
			64.86	58.53	25.0	0.4	18.538
			65.36	58.98	31.0	0.7	26.759
			65.86	59.43	43.4	0.4	36.985
			66.86	60.34	70.7	0.7	63.277
			67.40	60.82	83.0	0.8	80.453
			67.86	61.24	105	1	96.543
			68.86	62.14	145	2	135.475
			69.36	62.59	140	2	156.622
			69.86	63.04	179	2	178.655
			70.86	63.95	233	3	224.731
			71.36	64.40	260	3	248.475
			71.86	64.85	274	3	272.513
			72.86	65.75	318	4	321.024
			73.86	66.65	356	4	369.516
			74.86	67.56	399	4	417.451
			75.86	68.46	442	4	464.470
			77.86	70.26	536	5	554.988
			79.86	72.07	605	6	640.360
			81.86	73.87	652	7	720.630
^{16}O+^{149}Sm	EvR	authors' table [133] $E_{\rm lab}$	61.0	55.08	0.63	0.13	0.409
			61.5	55.54	1.9	0.4	0.748
			62.0	55.99	3.0	0.5	1.353
			63.0	56.89	7.0	1.1	4.142
			63.9	57.70	15.4	1.8	10.039
			64.9	58.61	32.6	3.9	22.569
			66.0	59.60	56.6	6.8	44.995
			68.0	61.41	127.0	15.0	107.377
			70.0	63.21	191.0	23.0	190.208
			75.0	67.73	460.0	55.0	429.166
^{16}O+^{150}Sm	EvR	authors' table [28]	59.98	54.20	0.472	0.047	0.168
			61.24	55.34	2.22	0.22	0.785

Continued on next page

Table 2 (continued)

Reaction	Detected particles	Data obtained	$E_{\rm lab}$ (MeV)	$E_{\rm c.m.}$ (MeV)	σ (mb)	$\delta\sigma$ (mb)	$\sigma^{\rm cal}$ (mb)
		$E_{\rm lab}$	62.49	56.47	7.75	0.78	3.283
			63.75	57.61	20.2	2.0	11.190
			65.00	58.73	38.4	3.8	28.491
			67.51	61.00	117.0	11.7	95.328
			70.01	63.26	243.0	24.3	194.600
			75.02	67.79	440.0	44.0	432.429
^{16}O+^{152}Sm	EvR	authors' table	59.92	54.21	1.06	0.11	0.282
		[28]	61.17	55.34	4.40	0.44	1.270
		$E_{\rm lab}$	62.42	56.48	11.7	1.2	4.927
			63.68	57.62	24.4	2.4	14.943
			64.93	58.75	43.9	4.4	34.259
			69.94	63.28	213.0	21.3	198.367
			74.95	67.81	462.0	46.2	432.629
^{16}O+^{154}Sm	EvR	authors' table	57.86	52.41	0.18	0.05	0.035
		[124]	58.36	52.87	0.19	0.04	0.065
		$E_{\rm lab}$	58.86	53.32	0.81	0.06	0.123
			59.36	53.77	1.06	0.09	0.230
			59.86	54.23	2.4	0.2	0.427
			60.36	54.68	3.6	0.3	0.781
			60.86	55.13	5.1	0.3	1.401
			61.36	55.58	7.7	0.3	2.444
			61.86	56.04	11.0	0.4	4.116
			62.36	56.49	15.4	0.5	6.652
			62.86	56.94	19.4	0.4	10.289
			63.36	57.40	25.2	0.4	15.235
			63.86	57.85	31.9	0.4	21.629
			64.36	58.30	39.8	0.5	29.527
			64.86	58.76	46.8	1.2	38.921
			65.36	59.21	61.5	0.7	49.774
			65.86	59.66	74.3	0.8	62.027
			66.36	60.11	87.1	1.0	75.607
			66.86	60.57	103	1	90.442
			67.36	61.02	118	1	106.450
			67.86	61.47	138	1	123.546
			68.36	61.93	165	2	141.648
			68.86	62.38	186	2	160.670
			69.36	62.83	201	2	180.526
			69.86	63.28	222	2	201.133
			70.36	63.74	247	4	222.408
			70.72	64.06	263	3	238.094
			71.36	64.64	295	3	266.641
			71.86	65.10	318	3	289.445
			72.36	65.55	341	4	312.612
			72.86	66.00	354	4	336.072
			73.36	66.46	375	4	359.762
			73.86	66.91	391	4	383.622
			75.86	68.72	463	5	479.708
			77.86	70.53	555	6	574.812
			79.86	72.34	630	6	667.054
			89.86	81.40	933	9	1064.883
			99.86	90.46	1025	10	1366.567
			109.86	99.52	1229	13	1598.770
^{16}O+^{166}Er	EvR	authors' graph	64.455	58.788	0.585	—	0.497
		[166]	64.928	59.220	0.899	—	0.864
		$E_{\rm c.m.}$	65.923	60.128	5.360	—	2.573
			66.918	61.035	10.732	—	6.671
			67.865	61.899	20.115	—	14.218
			68.901	62.844	36.417	—	27.727
			69.849	63.708	53.559	—	45.104
			71.838	65.523	118.429	—	95.974
			74.870	68.288	229.426	—	203.207
			76.860	70.103	333.720	—	286.703
			79.844	72.825	376.733	—	421.509
			81.881	74.683	524.356	—	515.351
			82.118	74.899	566.411	—	526.214
			84.865	77.405	605.133	—	650.053

Continued on next page

Table 2 (continued)

Reaction	Detected particles	Data obtained	$E_{\rm lab}$ (MeV)	$E_{\rm c.m.}$ (MeV)	σ (mb)	$\delta\sigma$ (mb)	$\sigma^{\rm cal}$ (mb)
			89.887	81.984	746.093	—	860.170
			99.787	91.015	1146.738	—	1203.915
			102.771	93.737	1211.703	—	1291.367
^{16}O+^{176}Yb	EvR	authors' graph [166] $E_{\rm c.m.}$	65.193	59.760	0.410	—	0.370
			66.183	60.668	1.646	—	1.175
			67.079	61.489	6.454	—	3.067
			68.068	62.396	14.751	—	7.711
			69.011	63.260	25.594	—	15.979
			70.095	64.254	50.687	—	31.247
			72.593	66.544	115.847	—	89.542
			75.044	68.791	312.366	—	172.526
			77.354	70.908	439.585	—	266.877
			78.579	72.031	598.500	—	321.010
			80.040	73.370	713.916	—	387.689
			82.412	75.544	880.216	—	497.875
			87.016	79.765	961.349	—	706.577
			90.127	82.616	1085.256	—	837.827
			96.019	88.017	1146.737	—	1060.389
^{16}O+^{186}W	EvRFF	authors' table [167] $E_{\rm lab}$	68.0	62.61	0.35	0.08	0.224
			68.5	63.07	0.40	0.09	0.408
			69.0	63.53	0.9	0.2	0.735
			69.5	64.00	1.0	0.1	1.300
			70.0	64.46	1.7	0.2	2.248
			70.5	64.92	3.0	0.2	3.769
			71.0	65.38	4.5	0.3	6.086
			71.5	65.84	8.0	0.3	9.432
			72.0	66.30	12.0	0.4	14.013
			72.5	66.76	17.9	0.5	19.977
			73.0	67.22	24.9	0.4	27.394
			73.5	67.68	33.4	0.3	36.274
			74.0	68.14	43.9	0.7	46.590
			74.5	68.60	55.1	0.5	58.290
			75.0	69.06	67.2	0.7	71.306
			75.5	69.52	81.0	0.8	85.566
			76.0	69.98	95.6	0.9	100.987
			76.5	70.44	111	1	117.487
			77.0	70.90	130	1	134.979
			77.5	71.36	149	2	153.377
			78.0	71.82	165	2	172.593
			78.5	72.28	183	2	192.542
			79.0	72.74	214	2	213.139
			79.5	73.20	222	2	234.301
			80.0	73.66	244	3	255.951
			80.5	74.12	267	3	278.010
			81.0	74.58	285	3	300.409
			81.5	75.04	310	3	323.079
			82.0	75.50	323	3	345.957
			82.5	75.97	340	3	368.984
			83.0	76.43	373	4	392.106
			84.0	77.35	405	6	438.441
			85.0	78.27	445	5	484.622
			86.0	79.19	490	5	530.379
			90.0	82.87	626	6	705.786
^{16}O+^{204}Pb	EvRFF	authors' graph [128] $E_{\rm c.m.}$	71.796	66.575	3.576E − 5	—	0.003
			72.790	67.496	2.726E − 4	—	0.011
			73.788	68.422	0.003	—	0.034
			74.787	69.348	0.023	—	0.107
			75.786	70.274	0.165	—	0.337
			76.784	71.200	0.963	—	1.039
			77.783	72.126	4.433	—	3.064
			81.777	75.829	74.113	—	66.860
			85.728	79.493	217.155	—	227.667
			89.765	83.237	363.805	—	399.033
			93.759	86.940	513.178	—	551.467
			101.748	94.348	755.688	—	811.170
^{16}O+^{208}Pb	EvRFF	authors' graph	70.906	65.841	1.556E − 5	—	0.001

Continued on next page

Table 2 (continued)

Reaction	Detected particles	Data obtained	$E_{\rm lab}$ (MeV)	$E_{\rm c.m.}$ (MeV)	σ (mb)	$\delta\sigma$ (mb)	$\sigma^{\rm cal}$ (mb)
		[128]	71.896	66.761	1.878E − 4	—	0.005
		$E_{\rm c.m.}$	72.944	67.734	0.001	—	0.015
			73.919	68.639	0.014	—	0.047
			74.895	69.545	0.089	—	0.146
			75.942	70.518	0.700	—	0.486
			76.918	71.424	3.043	—	1.459
		authors' table	75.35	69.97	0.24	0.01	0.247
		[168]	75.96	70.53	0.70	0.004	0.493
		$E_{\rm c.m.}$	76.56	71.09	1.83	0.01	0.977
			77.15	71.64	4.28	0.02	1.885
			77.75	72.20	8.27	0.04	3.598
			78.36	72.76	14.5	0.07	6.630
			78.95	73.31	23.4	0.1	11.548
			79.55	73.87	35.4	0.2	19.221
			80.16	74.43	50.0	0.3	30.116
			80.76	74.99	67.0	0.3	44.459
			81.35	75.54	87.0	0.4	61.782
			81.95	76.10	107	0.5	82.322
			82.56	76.66	129	0.7	105.234
			83.15	77.21	152	0.8	129.455
			83.75	77.77	175	0.9	155.297
			84.36	78.33	197	1	181.839
			84.95	78.88	223	1	208.214
			85.55	79.44	245	1	235.099
			86.15	80.00	270	1	261.823
			86.76	80.56	295	2	288.263
			87.35	81.11	318	2	313.884
			87.95	81.67	343	2	339.579
			89.15	82.78	385	2	389.285
			91.55	85.01	487	3	484.257
			93.95	87.24	568	3	573.087
			96.63	89.73	662	3	665.641
			98.75	91.70	715	4	734.318
			103.55	96.15	847	4	876.200
			108.47	100.72	949	5	1005.106
			113.14	105.06	1065	6	1113.968
			117.94	109.52	1133	6	1213.904
^{16}O+^{209}Bi	FF	authors' graph	76.789	71.329	0.330	—	0.600
		[161]	77.887	72.348	1.996	—	2.024
		$E_{\rm c.m.}$	78.938	73.325	7.025	—	5.987
			80.140	74.441	19.121	—	17.441
			81.041	75.278	34.317	—	33.503
			82.093	76.255	58.921	—	61.363
			84.126	78.144	122.943	—	137.043
			86.164	80.037	203.186	—	225.798
			88.217	81.944	290.410	—	315.407
			90.200	83.786	340.632	—	398.108
			92.188	85.632	417.639	—	476.605
			94.275	87.571	484.229	—	554.552
			96.313	89.464	538.559	—	626.488
			100.319	93.185	688.362	—	757.067
^{16}O+^{232}Th	FF	authors' graph	75.588	70.711	0.062	—	0.011
		[169]	77.492	72.492	0.517	—	0.101
		$E_{\rm lab}$	79.472	74.345	2.571	—	0.960
			80.462	75.271	4.341	—	2.686
			81.452	76.197	8.496	—	6.646
			83.432	78.050	20.201	—	26.467
			85.489	79.973	42.852	—	67.561
		authors' table	90	84.19	255	15	216.633
		[170]	95	88.87	370	20	428.911
		$E_{\rm lab}$	120	112.26	1150	60	1313.917
			140	130.97	1655	85	1747.773
			160	149.68	1880	95	2036.888
^{16}O+^{238}U	FF	authors' table	86.0	80.58	59.2	4.4	53.593
		[157]	92.6	86.77	219.3	10.8	271.957
		$E_{\rm lab}$	98.8	92.58	484.8	21	538.179

Continued on next page

Table 2 (continued)

Reaction	Detected particles	Data obtained	$E_{\rm lab}$ (MeV)	$E_{\rm c.m.}$ (MeV)	σ (mb)	$\delta\sigma$ (mb)	$\sigma^{\rm cal}$ (mb)
			102.4	95.95	635.2	26	689.189
			108.4	101.57	848.2	34	918.779
			111.0	104.01	971.5	38	1009.159
			116.6	109.26	1152	45	1186.771
			127.8	119.75	1493	57	1483.244
			135.2	126.68	1675	64	1644.403
			143.0	133.99	1849	70	1790.182
			150.4	140.93	1977	75	1909.137
			159.0	148.98	2116	80	2027.168
			159.0	148.98	2142	81	2027.168
			166.6	156.11	2126	80	2115.696
^{17}O+^{144}Sm	EvR	authors' table [124] $E_{\rm lab}$	60.88	54.45	0.07	0.05	0.044
			61.38	54.90	0.11	0.07	0.082
			61.88	55.35	0.19	0.09	0.153
			62.38	55.79	0.40	0.09	0.284
			62.88	56.24	0.81	0.23	0.528
			63.38	56.69	1.2	0.2	0.977
			63.88	57.13	2.4	0.2	1.792
			64.88	58.03	5.7	0.3	5.734
			65.88	58.92	13.9	0.5	16.048
			66.88	59.82	30.8	0.6	36.758
			67.88	60.71	57.2	0.7	68.820
			68.88	61.61	90.5	0.9	109.822
			70.01	62.62	137	1	162.424
			70.88	63.40	171	1	204.788
			71.88	64.29	209	1	253.617
			72.88	65.18	253	2	301.583
			73.88	66.08	296	2	348.224
			74.88	66.97	345	2	393.395
			75.88	67.87	383	2	437.089
			76.88	68.76	428	2	479.347
			77.88	69.66	463	3	520.228
			78.88	70.55	508	3	559.789
			79.88	71.45	548	3	598.087
			89.88	80.39	852	4	922.083
			99.88	89.33	1072	7	1163.922
^{18}O+^{44}Ca	EvR	authors' table [171] $E_{\rm lab}$ & $E_{\rm c.m.}$	27.39	19.44	1.0	0.2	6.411
			28.40	20.15	2.7	0.6	14.804
			29.40	20.86	8.0	1.0	30.648
			30.41	21.58	24	4.0	57.317
			31.41	22.29	53	8.0	95.673
			32.42	23.01	92	14	146.100
			33.43	23.72	134	18	204.396
			34.43	24.43	176	23	267.405
			35.44	25.15	229	29	332.485
			36.44	25.86	288	35	395.264
			38.45	27.29	372	45	512.613
			41.46	29.42	516	62	662.355
			45.48	32.28	673	73	824.397
			48.49	34.41	784	83	922.752
			52.51	37.26	891	93	1031.635
			55.52	39.40	956	98	1099.782
			59.54	42.25	987	100	1176.189
^{18}O+^{74}Ge	EvR	authors' table [95] $E_{\rm c.m.}$	37.55	30.2	0.14	0.01	2.962
			37.92	30.5	0.25	0.01	4.329
			38.54	31.0	0.89	0.03	7.789
			39.16	31.5	1.84	0.05	13.222
			39.78	32.0	4.56	0.08	21.177
			40.41	32.5	10.0	0.1	32.082
			41.03	33.0	16.7	0.2	46.196
			41.65	33.5	31.5	0.3	63.571
			42.27	34.0	46.9	0.4	84.075
			42.89	34.5	63.1	0.6	107.465
			43.51	35.0	82.6	0.8	133.448
			44.14	35.5	99.4	0.9	161.705
			44.76	36.0	136.5	1.2	191.906

Continued on next page

Table 2 (continued)

Reaction	Detected particles	Data obtained	$E_{\rm lab}$ (MeV)	$E_{\rm c.m.}$ (MeV)	σ (mb)	$\delta\sigma$ (mb)	$\sigma^{\rm cal}$ (mb)
			45.38	36.5	156.7	1.3	223.721
			46.00	37.0	190.1	1.6	256.827
			46.62	37.5	211.9	2.0	290.916
			47.24	38.0	254.8	1.8	325.699
			48.36	38.9	292.5	2.7	389.231
			49.61	39.9	371.3	2.3	459.886
			50.85	40.9	409.9	3.3	529.301
			52.09	41.9	497.9	3.7	596.550
			53.46	43.0	545.6	4.4	667.367
			54.70	44.0	593.4	4.8	728.594
			57.19	46.0	686.5	7.4	841.906
			58.31	46.9	731.6	7.6	889.076
			60.92	49.0	847.9	7.9	990.720
^{18}O+^{112}Sn	EvR	authors' graph [172] $E_{\rm c.m.}$	51.034	43.968	0.160	—	0.327
			52.048	44.841	0.215	—	0.973
			53.062	45.715	0.718	—	2.644
			54.153	46.655	2.521	—	6.901
			55.128	47.495	6.080	—	14.591
			56.143	48.369	16.979	—	28.501
			57.116	49.208	31.037	—	49.017
			58.169	50.115	51.448	—	79.679
			60.236	51.896	108.900	—	161.617
			62.732	54.046	202.340	—	280.096
			65.150	56.129	346.520	—	395.071
			67.645	58.279	457.180	—	505.193
			70.141	60.429	520.870	—	605.671
			75.092	64.695	633.420	—	780.039
			80.083	68.995	782.950	—	928.019
			84.896	73.141	892.020	—	1049.441
			89.849	77.408	983.680	—	1156.591
^{18}O+^{118}Sn	EvR	authors' graph [172] $E_{\rm c.m.}$	51.489	44.674	0.078	—	0.235
			52.069	45.178	0.279	—	0.484
			53.076	46.051	1.425	—	1.620
			54.238	47.059	5.424	—	5.790
			55.206	47.899	13.963	—	14.548
			56.212	48.773	31.548	—	32.365
			57.180	49.612	48.992	—	59.985
			58.226	50.519	82.545	—	100.856
			60.239	52.266	166.392	—	199.465
			62.833	54.517	262.647	—	333.143
			65.195	56.566	375.953	—	446.025
			67.596	58.649	487.994	—	550.708
			70.228	60.934	583.841	—	655.102
			75.107	65.166	733.525	—	824.034
			80.063	69.466	877.598	—	968.790
			84.903	73.666	983.684	—	1089.082
			90.012	78.099	983.684	—	1197.627
^{18}O+^{124}Sn	EvR	authors' graph [172] $E_{\rm c.m.}$	50.986	44.523	0.208	—	0.146
			52.025	45.431	1.134	—	0.562
			53.179	46.438	3.493	—	2.409
			54.141	47.278	11.670	—	7.441
			55.218	48.219	25.522	—	22.156
			56.142	49.025	46.654	—	46.811
			57.219	49.966	95.589	—	90.443
			58.257	50.873	124.070	—	143.140
			60.181	52.552	215.970	—	249.315
			62.643	54.702	319.390	—	379.368
			65.182	56.920	421.390	—	501.086
			67.644	59.070	603.190	—	608.125
			70.106	61.220	676.100	—	705.649
			75.107	65.587	849.440	—	878.852
			80.032	69.887	1049.900	—	1022.478
			84.917	74.153	1067.200	—	1143.719
			89.996	78.588	1196.200	—	1251.397
^{18}O+^{192}Os	EvRFF	authors' table [173]	80	73.14	201.3	20.6	206.103
			85	77.71	388.4	31.2	440.444

Continued on next page

Table 2 (continued)

Reaction	Detected particles	Data obtained	$E_{\rm lab}$ (MeV)	$E_{\rm c.m.}$ (MeV)	σ (mb)	$\delta\sigma$ (mb)	$\sigma^{\rm cal}$ (mb)
		$E_{\rm lab}$	90	82.29	553	33	663.184
			95	86.86	725	33	859.065
			104	95.09	995	38	1152.787
			113	103.31	1212	47	1387.588
			123	112.46	1455	55	1596.434
^{18}O+^{208}Pb	FF	authors' graph	75.861	69.819	0.346	—	0.397
		[161]	76.903	70.778	1.280	—	1.400
		$E_{\rm c.m.}$	77.957	71.748	5.460	—	4.652
			78.968	72.679	13.174	—	12.860
			80.064	73.687	26.612	—	31.459
			81.075	74.618	49.922	—	59.274
			82.087	75.549	72.278	—	95.950
			83.140	76.519	104.646	—	140.437
			84.152	77.450	143.859	—	186.163
			85.121	78.342	173.099	—	230.771
			86.133	79.273	239.732	—	276.955
			88.156	81.134	294.935	—	366.257
			90.178	82.996	387.842	—	450.749
			92.117	84.780	449.719	—	527.338
			94.098	86.603	521.468	—	601.461
			96.163	88.504	595.779	—	674.608
			98.186	90.366	660.824	—	742.461
			102.232	94.089	806.997	—	867.887
^{19}F+^{93}Nb	EvR	authors' table	53.47	44.4	5.75	0.4	3.562
		[174]	54.55	45.3	12.9	0.8	11.219
		$E_{\rm c.m.}$	55.52	46.1	22.1	1.3	25.588
			56.48	46.9	41.0	2.4	48.614
			57.45	47.7	64.6	3.5	79.894
			59.49	49.4	125	6	167.113
			61.42	51.0	224	10	263.376
			63.47	52.7	282	14	368.821
			65.51	54.4	362	16	470.700
			67.44	56.0	463	20	560.884
			69.49	57.7	549	23	650.193
			71.54	59.4	664	28	733.133
^{19}F+^{139}La	EvR	authors' table	70	61.58	50	20	45.051
		[173]	75	65.98	238	30	245.103
		$E_{\rm lab}$	80	70.38	337	30	475.430
			84	73.90	648	40	639.409
			89	78.30	749	45	818.495
			94	82.70	892	60	973.485
			99	87.09	1026	65	1108.467
			104	91.49	1178	70	1226.641
			109	95.89	1237	75	1330.545
			114	100.29	1354	80	1422.216
			119	104.69	1386	80	1503.305
			124	109.09	1377	80	1575.160
			129	113.49	1514	90	1638.890
^{19}F+^{208}Pb	EvRFF	authors' table	82.94	76.0	0.22	0.02	0.047
		[175]	83.92	76.9	0.74	0.03	0.160
		$E_{\rm c.m.}$	85.02	77.9	1.83	0.04	0.608
			86.00	78.8	4.22	0.06	1.903
			86.98	79.7	8.17	0.09	5.297
			87.96	80.6	15.4	0.1	12.526
			88.94	81.5	27.3	0.2	24.983
			89.93	82.4	43.6	0.2	43.079
			91.02	83.4	68.2	0.3	69.397
			92.00	84.3	95.7	0.5	97.949
			92.98	85.2	126	0.6	130.292
			93.96	86.1	163	0.8	165.610
			94.95	87.0	197	1	203.120
			95.93	87.9	234	1	242.110
			97.02	88.9	271	1	286.430
			98.00	89.8	313	2	326.671
			98.99	90.7	344	2	366.849
			99.97	91.6	382	2	406.679

Continued on next page

Table 2 (continued)

Reaction	Detected particles	Data obtained	E_{lab} (MeV)	$E_{c.m.}$ (MeV)	σ (mb)	$\delta\sigma$ (mb)	σ^{cal} (mb)
			100.95	92.5	418	2	445.963
			101.93	93.4	454	2	484.569
			104.01	95.3	515	3	563.529
			108.04	99.0	643	3	706.913
			109.03	99.9	679	3	739.778
			111.97	102.6	749	4	833.970
			116.01	106.3	856	4	953.133
			119.94	109.9	953	5	1059.177
			128.01	117.3	1116	6	1250.707
			131.94	120.9	1200	6	1332.696
			135.00	123.7	1250	6	1392.005
			142.31	130.4	1364	7	1519.740
			146.13	133.9	1403	7	1579.300
			152.68	139.9	1493	7	1671.265
			157.92	144.7	1567	8	1736.470
$^{19}F+^{209}Bi$	FF	authors' table [176] E_{lab} & $E_{c.m.}$	88.0	80.5	6.3	0.6	5.236
			89.7	82.2	16.8	1.1	22.942
			91.0	83.4	34.0	2.0	46.933
			92.7	85.1	75.0	5.0	95.913
			94.0	86.2	108.0	6.0	135.042
			95.5	87.5	159.0	9.0	186.594
			99.7	91.4	318.0	30.0	356.690
			103.7	95.1	399.0	20.0	516.323
			107.6	98.6	551.0	30.0	656.005
			125.6	115.1	1109.0	80.0	1173.328
$^{23}Na+^{48}Ti$	EvR	authors' graph [177] $E_{c.m.}$	47.601	32.181	16.197	—	15.177
			49.012	33.135	39.698	—	38.821
			49.491	33.458	57.757	—	50.001
			51.549	34.850	100.360	—	114.019
			53.512	36.177	196.310	—	193.048
			54.565	36.889	258.775	—	239.849
			56.145	37.957	344.498	—	312.835
			59.544	40.255	436.542	—	469.768
			62.560	42.294	564.204	—	599.141
			65.576	44.333	628.885	—	715.623
			66.868	45.207	687.284	—	761.641
$^{27}Al+^{45}Sc$	EvR	authors' graph [178] $E_{c.m.}$	50.794	31.746	2.803E − 4	—	0.001
			51.927	32.454	0.002	—	0.004
			52.873	33.045	0.010	—	0.010
			53.856	33.660	0.042	—	0.028
			54.839	34.275	0.151	—	0.080
			55.747	34.842	0.564	—	0.210
			56.806	35.504	1.991	—	0.639
			58.319	36.449	8.002	—	2.933
			60.172	37.608	21.437	—	14.308
			61.571	38.482	47.567	—	34.680
			63.046	39.404	65.427	—	68.418
			65.164	40.728	122.003	—	134.293
			67.963	42.477	172.746	—	238.547
			71.670	44.794	248.166	—	380.765
			75.868	47.417	412.106	—	527.837
			80.104	50.065	592.028	—	657.351
$^{27}Al+^{70}Ge$	EvR	authors' table [179] $E_{c.m.}$	69.56	50.2	0.48	0.13	0.385
			70.53	50.9	1.16	0.19	1.163
			70.95	51.2	1.44	0.17	1.818
			71.50	51.6	3.12	0.35	3.185
			71.92	51.9	4.78	0.34	4.706
			72.47	52.3	7.47	0.73	7.584
			72.89	52.6	8.31	0.50	10.497
			73.44	53.0	13.4	1.3	15.518
			73.86	53.3	16.83	0.86	20.182
			74.69	53.9	28.0	1.2	31.847
			75.52	54.5	47.6	2.0	46.533
			76.35	55.1	62.4	2.4	64.042
			77.32	55.8	89.1	3.3	87.714
			78.15	56.4	98.6	3.0	110.480

Continued on next page

Table 2 (continued)

Reaction	Detected particles	Data obtained	E_{lab} (MeV)	$E_{c.m.}$ (MeV)	σ (mb)	$\delta\sigma$ (mb)	σ^{cal} (mb)
			79.12	57.1	134.6	4.3	139.542
			80.09	57.8	160.8	5.4	170.877
			81.06	58.5	181.1	5.9	204.053
			82.03	59.2	224.0	6.8	238.661
			82.03	59.2	220.6	8.2	238.661
			83.00	59.9	267.8	8.4	274.317
			83.00	59.9	255.1	9.3	274.317
$^{27}Al+^{72}Ge$	EvR	authors' table	68.06	49.5	0.16	0.04	0.152
		[179]	69.03	50.2	0.46	0.06	0.484
		$E_{c.m.}$	69.99	50.9	1.11	0.12	1.450
			71.09	51.7	3.29	0.31	4.449
			71.91	52.3	7.38	0.65	9.093
			72.88	53.0	14.70	0.52	18.155
			73.84	53.7	23.61	0.85	31.590
			74.66	54.3	39.1	1.4	46.528
			75.49	54.9	60.8	2.3	64.409
			76.45	55.6	79.7	2.6	88.644
			77.28	56.2	102.5	3.2	111.979
			78.24	56.9	135.8	4.0	141.773
			79.20	57.6	160.4	5.0	173.880
			80.16	58.3	198.2	6.6	207.837
			81.12	59.0	222.6	6.8	243.205
			82.09	59.7	223.8	6.2	279.579
			83.05	60.4	279.2	8.4	316.597
$^{27}Al+^{73}Ge$	EvR	authors' table	68.49	50.0	0.81	0.18	0.422
		[179]	69.45	50.7	2.54	0.39	1.278
		$E_{c.m.}$	70.55	51.5	5.78	0.44	3.995
			71.51	52.2	10.17	0.58	9.270
			72.47	52.9	18.9	1.1	18.450
			73.42	53.6	26.0	1.6	32.016
			74.52	54.4	43.2	2.3	52.754
			75.48	55.1	59.5	3.3	75.093
			76.44	55.8	86.2	6.3	100.894
			77.26	56.4	108.4	8.7	125.413
			78.36	57.2	135	11	161.013
			79.32	57.9	157	12	194.385
			80.27	58.6	166	12	229.360
			81.23	59.3	210	19	265.519
			82.47	60.2	242	16	313.138
			82.47	60.2	250	17	313.138
			83.42	60.9	271	19	350.641
			84.52	61.7	319	22	393.606
$^{27}Al+^{74}Ge$	EvR	authors' table	67.15	49.2	0.20	0.06	0.150
		[179]	68.24	50.0	0.67	0.13	0.560
		$E_{c.m.}$	69.20	50.7	2.18	0.21	1.657
			70.15	51.4	6.22	0.55	4.366
			71.11	52.1	12.16	0.75	9.922
			72.06	52.8	20.8	1.0	19.405
			73.02	53.5	35.4	1.6	33.244
			73.98	54.2	50.2	2.0	51.324
			74.93	54.9	71.9	2.8	73.305
			76.02	55.7	89.5	3.0	102.667
			76.98	56.4	117.8	3.9	131.559
			77.93	57.1	141.2	4.7	162.952
			78.89	57.8	183	22	196.387
			79.98	58.6	193.1	6.5	236.534
			80.94	59.3	214.4	6.9	272.896
			81.89	60.0	235.3	8.4	310.021
			82.98	60.8	266.9	8.8	352.966
			83.94	61.5	301	12	390.680
$^{27}Al+^{76}Ge$	EvR	authors' table	66.14	48.8	0.14	0.05	0.095
		[179]	67.22	49.6	0.54	0.08	0.355
		$E_{c.m.}$	68.17	50.3	2.21	0.25	1.070
			69.12	51.0	4.21	0.38	2.949
			70.07	51.7	9.58	0.68	7.148
			71.02	52.4	20.2	1.2	14.978

Continued on next page

Table 2 (continued)

Reaction	Detected particles	Data obtained	E_{lab} (MeV)	$E_{c.m.}$ (MeV)	σ (mb)	$\delta\sigma$ (mb)	σ^{cal} (mb)
			71.96	53.1	30.9	1.1	27.353
			72.91	53.8	48.1	1.7	44.484
			73.86	54.5	69.1	2.5	66.095
			74.81	55.2	94.3	3.0	91.707
			75.76	55.9	119.3	3.7	120.752
			76.71	56.6	142.4	4.4	152.635
			77.66	57.3	184.3	5.7	186.760
			78.61	58.0	197.3	6.2	222.562
			79.69	58.8	233.1	7.1	264.864
			80.64	59.5	261.3	7.9	302.581
			81.59	60.2	297.1	9.0	340.547
			82.67	61.0	311.7	9.0	383.842
			83.62	61.7	364	11	421.366
$^{27}Al+^{197}Au$	FF	authors' graph [180] $E_{c.m.}$	121.679	107.012	1.483	—	0.120
			124.537	109.526	1.725	—	2.567
			124.620	109.598	12.565	—	2.763
			126.705	111.432	10.224	—	12.859
			127.583	112.205	22.920	—	20.865
			127.958	112.534	16.094	—	25.027
			127.956	112.533	19.735	—	25.009
			131.249	115.428	69.570	—	79.471
			131.442	115.598	54.734	—	83.562
			131.916	116.015	68.694	—	93.965
			134.750	118.508	154.355	—	165.276
			137.373	120.814	177.157	—	241.036
			137.612	121.025	211.239	—	248.227
			140.235	123.332	275.202	—	328.750
			141.607	124.538	258.435	—	371.294
			142.960	125.728	341.116	—	413.103
			146.936	129.225	341.149	—	533.035
			147.172	129.433	417.437	—	539.984
			149.510	131.489	601.865	—	607.315
			152.020	133.696	594.366	—	676.864
			154.664	136.021	700.238	—	747.059
			156.271	137.435	617.232	—	788.230
			157.279	138.321	682.803	—	813.499
			159.566	140.332	764.932	—	869.254
			163.381	143.687	530.563	—	957.702
			165.785	145.802	984.587	—	1010.673
			167.980	147.732	1474.123	—	1057.249
			170.398	149.859	736.536	—	1106.676
			172.630	151.822	856.979	—	1150.630
$^{28}Si+^{28}Si$	EvR	authors' graph [181] $E_{c.m.}$	45.553	22.777	6.153E − 4	—	0.003
			46.135	23.067	7.880E − 4	—	0.004
			47.182	23.591	4.580E − 3	—	0.011
			48.166	24.083	0.010	—	0.027
			49.182	24.591	0.027	—	0.065
			50.197	25.099	0.061	—	0.155
			51.149	25.575	0.158	—	0.336
			52.197	26.098	0.398	—	0.754
			53.181	26.590	1.026	—	1.522
			54.196	27.098	2.950	—	2.940
			55.180	27.590	6.806	—	5.196
			56.195	28.098	15.703	—	8.697
			57.211	28.606	31.748	—	13.595
			58.227	29.113	50.392	—	20.106
			60.226	30.113	95.375	—	38.549
			62.225	31.113	144.867	—	63.237
			64.225	32.112	210.568	—	93.283
			66.288	33.144	251.088	—	129.051
			68.255	34.128	306.067	—	166.932
			70.255	35.127	364.964	—	208.544
			72.286	36.143	435.196	—	253.310
		authors' table [125] $E_{c.m.}$	60.00	30.0	115	8	36.097
			64.00	32.0	260	17	89.631
			68.00	34.0	330	22	161.800

Continued on next page

Table 2 (continued)

Reaction	Detected particles	Data obtained	E_{lab} (MeV)	$E_{c.m.}$ (MeV)	σ (mb)	$\delta\sigma$ (mb)	σ^{cal} (mb)
			72.00	36.0	446	29	246.846
			76.00	38.0	562	37	339.797
			81.00	40.5	715	47	460.861
			85.00	42.5	765	36	557.524
			88.00	44.0	828	54	628.296
			90.00	45.0	852	56	674.307
			93.00	46.5	922	60	740.997
			96.00	48.0	938	61	804.637
			99.00	49.5	970	63	865.018
			105.00	52.5	1072	70	975.593
			110.00	55.0	1068	69	1057.591
			115.00	57.5	1064	70	1130.995
			121.00	60.5	1058	45	1208.874
			132.60	66.3	1050	69	1332.925
^{28}Si+^{30}Si	EvR	authors' graph [181] $E_{c.m.}$	46.131	23.861	0.004	—	0.010
			47.143	24.385	0.018	—	0.026
			49.168	25.432	0.306	—	0.165
			52.205	27.003	9.060	—	2.421
			58.219	30.113	111.254	—	72.977
			64.262	33.239	280.284	—	258.489
			70.306	36.365	425.727	—	467.583
		authors' table [171] E_{lab} & $E_{c.m.}$	49.86	25.79	2.9	0.6	0.310
			51.86	26.82	8.0	2.0	1.798
			53.86	27.86	29	5.0	8.664
			55.86	28.89	59	10	28.310
			57.86	29.93	105	16	64.911
			59.86	30.96	170	25	115.595
			61.86	32.00	214	29	177.207
			62.86	32.51	242	31	209.957
			63.86	33.03	265	33	244.424
			64.86	33.55	292	34	279.545
			65.86	34.06	315	36	314.262
			67.37	34.85	353	39	367.883
			68.87	35.62	405	44	419.249
			77.37	40.02	610	63	678.368
			84.87	43.90	780	79	855.688
^{28}Si+^{68}Zn	EvR	authors' table [182] E_{lab} & $E_{c.m.}$	71.6	50.7	0.62	0.13	0.453
			73.7	52.2	3.6	0.5	3.682
			75.7	53.6	29	2	15.807
			77.7	55.0	56	4	42.885
			79.7	56.4	79	4	84.992
			80.6	57.1	114	8	110.796
			82.7	58.6	171	9	174.260
			84.7	60.0	194	10	240.467
			86.7	61.4	234	13	310.197
			89.8	63.6	264	16	421.071
			92.8	65.7	431	24	523.532
			99.8	70.7	572	38	742.516
^{28}Si+^{90}Zr	EvR	authors' table [183] $E_{c.m.}$	86.14	65.7	0.049	0.009	0.018
			88.24	67.3	0.435	0.058	0.218
			90.20	68.8	2.317	0.287	2.072
			92.30	70.4	9.770	1.19	14.057
			94.40	72.0	42.60	5.19	46.880
			96.50	73.6	81.18	9.79	99.040
			98.60	75.2	129.2	15.5	163.269
			100.56	76.7	169.1	20.6	228.295
			103.71	79.1	251.5	31.7	332.692
			107.77	82.2	450.3	85.1	459.402
			110.92	84.6	599.0	110.8	549.672
			116.03	88.5	680.1	125.0	682.919
			121.15	92.4	674.3	126.4	801.570
^{28}Si+^{92}Zr	EvR	authors' table [148] $E_{c.m.}$	85.30	65.40	0.96	0.2	0.152
			86.30	66.16	1.73	0.2	0.463
			87.30	66.93	4.49	0.3	1.316
			88.30	67.70	7.21	0.5	3.353
			89.30	68.46	14.0	0.4	7.456

Continued on next page

Table 2 (continued)

Reaction	Detected particles	Data obtained	$E_{\rm lab}$ (MeV)	$E_{\rm c.m.}$ (MeV)	σ (mb)	$\delta\sigma$ (mb)	$\sigma^{\rm cal}$ (mb)
			90.30	69.23	23.6	0.6	14.728
			91.30	70.00	38.8	0.6	25.849
			92.30	70.76	54.2	1.5	40.818
			93.37	71.58	77.8	0.9	61.199
			94.30	72.30	94.9	1.3	82.344
			95.47	73.19	125	1	112.057
			96.30	73.83	141	1	135.442
			97.30	74.60	170	2	165.331
			98.30	75.36	197	2	196.244
			99.30	76.13	216	2	228.534
			100.30	76.90	252	2	261.395
			102.30	78.43	302	2	327.101
			103.30	79.20	335	3	359.891
			104.30	79.96	365	3	391.850
			105.30	80.73	383	3	423.710
			106.30	81.50	404	3	454.974
			115.00	88.17	603	6	698.545
^{28}Si+^{93}Nb	EvR	authors' table [184] $E_{\rm c.m.}$	89.32	68.65	1.04	0.21	0.908
			91.32	70.19	6.3	1.3	6.052
			93.08	71.54	24	5	20.302
			94.94	72.97	37	7	49.232
			96.93	74.5	77	15	94.464
			98.92	76.03	108	21	150.426
			100.85	77.51	202	40	210.623
			105.86	81.36	299	59	373.406
			108.86	83.67	431	86	466.500
			111.79	85.92	478	95	551.611
			113.88	87.53	547	109	609.126
			115.87	89.06	642	128	661.293
			118.91	91.39	691	138	736.375
^{28}Si+^{94}Zr	EvR	authors' table [183] $E_{\rm c.m.}$	82.16	63.3	0.037	0.006	0.021
			84.36	65.0	0.201	0.029	0.261
			86.44	66.6	2.160	0.310	2.077
			88.51	68.2	10.70	1.48	10.351
			90.46	69.7	26.57	3.68	30.303
			92.54	71.3	52.04	7.28	67.236
			94.61	72.9	100.2	13.9	118.004
			96.69	74.5	138.8	19.3	178.640
			98.77	76.1	165.4	23.1	245.069
			100.84	77.7	216.0	29.6	313.831
			103.83	80.0	285.6	41.1	411.956
			107.98	83.2	467.7	87.9	540.977
			111.10	85.6	565.0	126.4	630.416
			116.29	89.6	599.2	110.0	765.975
			121.35	93.5	524.0	98.2	883.699
^{28}Si+^{142}Ce	EvR	authors' table [185] $E_{\rm lab}$	104.7	87.46	0.07	0.03	0.010
			106.7	89.13	0.33	0.15	0.096
			107.2	89.54	0.6	0.1	0.163
			108.2	90.38	1.2	0.1	0.445
			108.7	90.80	2.0	0.2	0.713
			109.7	91.63	3.7	0.3	1.708
			112.2	93.72	14.4	0.8	10.060
			112.2	93.72	14.2	0.5	10.060
			114.7	95.81	34	3	34.156
			114.7	95.81	39	2	34.156
			117.2	97.90	71	1	77.399
			119.7	99.98	146	6	136.107
			119.7	99.98	134	7	136.107
			124.7	104.16	244	7	277.264
			124.7	104.16	235	5	277.264
			124.7	104.16	242	5	277.264
			129.7	108.34	429	12	421.746
			129.7	108.34	449	6	421.746
			139.7	116.69	719	90	677.467
			144.7	120.87	644	30	788.177
^{28}Si+^{154}Sm	EvR	authors' graph	106.905	90.458	0.998	—	0.151

Continued on next page

Table 2 (continued)

Reaction	Detected particles	Data obtained	$E_{\rm lab}$ (MeV)	$E_{\rm c.m.}$ (MeV)	σ (mb)	$\delta\sigma$ (mb)	$\sigma^{\rm cal}$ (mb)
		[186]	109.396	92.566	3.129	—	1.346
		$E_{\rm lab}$	111.914	94.697	8.685	—	7.252
			112.532	95.220	7.617	—	10.128
			113.888	96.366	16.264	—	19.041
			114.514	96.897	21.137	—	24.502
			114.921	97.241	25.376	—	28.557
			116.316	98.421	26.391	—	45.434
			116.929	98.940	37.563	—	54.180
			116.876	98.895	44.520	—	53.400
			119.424	101.051	81.274	—	97.705
			120.246	101.746	95.082	—	114.575
			122.026	103.253	126.839	—	154.835
			124.533	105.374	142.635	—	218.859
			124.467	105.319	195.216	—	217.097
			127.814	108.150	195.236	—	312.107
			129.426	109.514	347.195	—	360.476
			132.732	112.312	338.275	—	462.302
			134.432	113.750	427.974	—	515.068
			139.333	117.897	527.554	—	664.774
			144.345	122.138	633.610	—	810.040
^{28}Si+^{164}Er	EvRFF	authors' graph	127.049	108.521	82.246	—	71.567
		[187][1]	129.990	111.033	134.046	—	129.667
		$E_{\rm c.m.}$	132.205	112.925	179.355	—	182.182
			135.062	115.365	257.802	—	258.049
			139.843	119.449	400.315	—	397.281
			145.056	123.902	562.327	—	554.034
			150.001	128.126	701.458	—	698.303
			154.942	132.346	791.913	—	833.991
			159.709	136.418	894.966	—	955.709
			164.975	140.916	1021.998	—	1079.934
			170.059	145.259	1202.045	—	1190.346
			175.096	149.561	1237.054	—	1291.330
^{28}Si+^{198}Pt	FF	authors' table	131.15	114.9	1.3	0.2	0.089
		[188]	133.43	116.9	5.2	0.8	0.914
		$E_{\rm c.m.}$	134.69	118.0	12.1	1.7	2.665
			135.83	119.0	15.4	2.3	6.113
			136.51	119.6	23.1	3.5	9.425
			139.25	122.0	40.7	6.1	35.010
			142.22	124.6	95.3	14.3	85.322
			148.38	130.0	204	31	236.725
			159.80	140.0	456	68	535.817
			171.21	150.0	625	94	788.612
			189.82	166.3	789	121	1113.081
^{28}Si+^{208}Pb	FF	authors' graph	136.881	120.641	1.173	—	0.174
		[189]	138.006	121.632	3.269	—	0.561
		$E_{\rm c.m.}$	138.989	122.499	6.228	—	1.414
			140.128	123.503	12.333	—	3.618
			140.959	124.235	16.943	—	6.549
			141.978	125.133	24.846	—	12.218
			142.986	126.021	32.434	—	20.508
			144.057	126.966	45.343	—	32.437
			145.028	127.822	55.165	—	45.948
			145.909	128.598	70.653	—	60.266
			146.937	129.504	83.751	—	79.218
			147.981	130.424	104.538	—	100.657
			148.979	131.303	126.565	—	122.874
			150.030	132.230	145.432	—	147.770
			150.943	133.035	168.986	—	170.412
			151.954	133.926	189.233	—	196.270
			152.988	134.837	206.531	—	223.321
			154.026	135.752	233.723	—	250.908
			154.990	136.601	256.433	—	276.665

Continued on next page

[1]In the authors' graph, the capture excitation function was plotted as a function of the excitation energy $E^*_{\rm CN}$ of the compound nucleus. $E_{\rm c.m.}$ is obtained by $E_{\rm c.m.} = E^*_{\rm CN} - Q$ and $Q = -64.869$ MeV is calculated with the nuclear masses taken from Refs. [102, 103].

Table 2 (continued)

Reaction	Detected particles	Data obtained	E_{lab} (MeV)	$E_{c.m.}$ (MeV)	σ (mb)	$\delta\sigma$ (mb)	σ^{cal} (mb)
			155.879	137.385	278.522	—	300.461
			156.828	138.221	299.333	—	325.789
			157.865	139.135	321.765	—	353.287
			158.875	140.025	345.846	—	379.798
			159.771	140.815	373.665	—	403.077
			160.770	141.695	389.315	—	428.710
			161.808	142.610	409.990	—	454.980
			162.842	143.522	436.165	—	480.751
			163.766	144.336	452.187	—	503.427
			164.921	145.354	473.650	—	531.332
			165.879	146.198	509.104	—	554.091
			167.925	148.002	547.232	—	601.541
			169.881	149.726	576.136	—	645.490
			173.864	153.236	648.779	—	730.845
			175.940	155.065	686.546	—	773.253
			177.932	156.821	726.666	—	812.673
^{29}Al+^{197}Au	FF	authors' graph [180] $E_{c.m.}$	125.290	109.213	15.513	—	5.016
			128.745	112.225	70.433	—	35.029
			132.205	115.240	141.436	—	94.952
			135.637	118.233	203.358	—	175.494
			139.107	121.257	330.192	—	268.869
			142.472	124.190	384.133	—	363.561
			145.912	127.189	504.522	—	459.618
			149.368	130.201	544.235	—	552.624
			152.905	133.284	714.758	—	643.039
			156.290	136.235	693.413	—	724.840
			159.704	139.211	725.665	—	802.748
			163.201	142.259	897.216	—	878.029
			166.640	145.257	794.651	—	947.921
			170.045	148.225	1028.012	—	1013.312
			173.487	151.226	1044.035	—	1075.774
			176.879	154.182	982.365	—	1133.957
			180.364	157.220	1060.255	—	1190.467
			183.831	160.242	997.336	—	1243.544
			187.251	163.223	1143.012	—	1292.990
^{31}Al+^{197}Au	FF	authors' graph [180] $E_{c.m.}$	122.913	106.202	9.878	—	8.871
			126.370	109.188	19.335	—	42.115
			129.887	112.227	132.156	—	102.756
			133.346	115.215	208.148	—	182.685
			136.949	118.329	231.224	—	280.420
			140.392	121.304	353.450	—	381.348
			143.877	124.315	369.843	—	486.044
			147.245	127.225	556.565	—	586.264
			150.683	130.196	600.346	—	685.519
			154.163	133.202	764.947	—	781.663
			157.634	136.201	974.670	—	872.808
			161.093	139.190	850.445	—	958.834
			164.696	142.303	825.150	—	1043.551
			168.217	145.346	850.461	—	1121.740
			171.622	148.287	1100.642	—	1193.272
			175.153	151.339	989.541	—	1263.502
			178.616	154.330	850.408	—	1328.661
			182.050	157.298	1280.346	—	1389.897
			185.550	160.322	1205.112	—	1449.000
			188.983	163.288	1582.041	—	1503.904
^{30}Si+^{30}Si	EvR	authors' table [171] E_{lab} & $E_{c.m.}$	54.36	27.18	4.4	0.9	34.074
			54.86	27.43	13	2	46.578
			55.36	27.68	21	3	61.585
			55.86	27.93	32	5	78.770
			56.86	28.43	52	8	117.745
			57.86	28.93	79	12	159.714
			58.86	29.43	98	14	202.076
			59.86	29.93	123	17	243.557
			60.86	30.43	159	21	283.658
			61.86	30.93	190	26	322.236
			62.86	31.43	224	32	359.293

Continued on next page

Table 2 (continued)

Reaction	Detected particles	Data obtained	$E_{\rm lab}$ (MeV)	$E_{\rm c.m.}$ (MeV)	σ (mb)	$\delta\sigma$ (mb)	$\sigma^{\rm cal}$ (mb)
			63.86	31.93	257	36	394.878
			64.86	32.43	284	38	429.060
			65.86	32.93	328	43	461.909
			66.86	33.43	365	46	493.494
			67.86	33.93	394	49	523.879
			68.86	34.43	429	58	553.126
			69.86	34.93	469	60	581.291
			72.36	36.18	539	67	647.314
			74.87	37.43	603	70	707.646
			77.37	38.68	662	78	762.920
			82.37	41.18	772	88	860.403
			84.87	42.43	822	90	903.487
			87.37	43.68	848	94	943.290
			92.37	46.18	965	101	1014.256
			94.87	47.43	1059	106	1045.934
^{30}Si+^{238}U	FF	authors' graph [190] $E_{\rm c.m.}$	140.736	124.982	0.131	—	0.030
			145.184	128.932	3.201	—	1.465
			150.904	134.011	20.801	—	24.226
			156.517	138.996	68.002	—	90.596
			162.130	143.981	163.384	—	192.472
			167.850	149.060	275.147	—	319.486
			173.463	154.045	401.964	—	454.630
			179.076	159.030	615.725	—	590.842
			190.303	169.001	780.325	—	846.315
^{32}S+^{27}Al	EvR	authors' graph [191] $E_{\rm c.m.}$	59.491	27.225	0.743	—	1.202
			60.405	27.643	1.352	—	2.274
			61.348	28.075	4.035	—	4.157
			62.448	28.578	8.223	—	7.768
			63.328	28.980	17.175	—	12.056
			64.388	29.465	29.493	—	19.217
			65.316	29.890	58.811	—	27.500
			66.462	30.415	69.899	—	40.337
			67.369	30.830	90.025	—	52.343
			68.443	31.321	134.786	—	68.562
			69.455	31.785	156.468	—	85.739
			70.356	32.197	185.815	—	102.411
			71.393	32.671	210.969	—	123.051
			72.486	33.171	233.956	—	146.440
			73.425	33.601	294.436	—	167.715
			74.365	34.031	315.564	—	189.937
			75.460	34.533	322.854	—	216.946
			76.511	35.014	374.979	—	243.861
		authors' table [192] $E_{\rm lab}$	67	30.66	90	—	47.243
			69	31.58	139	—	77.937
			73	33.41	248	—	158.122
			75	34.32	296	—	205.347
			77.5	35.47	336	—	270.132
			80	36.61	434	—	338.301
			85	38.90	561	—	480.991
			87.5	40.04	663	—	552.424
			90	41.19	650	—	623.431
			110	50.34	914	—	1099.136
			120.4	55.10	936	—	1278.122
			132.5	60.64	995	—	1441.465
^{32}S+^{24}Mg	EvR	authors' graph [191] $E_{\rm c.m.}$	60.699	26.014	3.873	—	6.782
			61.698	26.442	8.580	—	11.944
			62.801	26.915	15.250	—	20.666
			63.757	27.325	22.385	—	31.140
			64.855	27.795	38.607	—	46.589
			65.855	28.224	59.518	—	63.732
			66.697	28.584	84.040	—	80.255
			67.752	29.037	102.878	—	103.387
			68.791	29.482	139.715	—	128.498
			69.798	29.913	161.353	—	154.688
			70.747	30.320	189.946	—	180.770
			71.765	30.757	230.155	—	209.972

Continued on next page

Table 2 (continued)

Reaction	Detected particles	Data obtained	$E_{\rm lab}$ (MeV)	$E_{\rm c.m.}$ (MeV)	σ (mb)	$\delta\sigma$ (mb)	$\sigma^{\rm cal}$ (mb)
			72.779	31.191	253.131	—	239.998
			73.787	31.623	281.308	—	270.560
			76.844	32.933	360.942	—	364.983
^{32}S+^{25}Mg	EvR	authors' graph [191] $E_{\rm c.m.}$	56.166	24.634	0.503	—	0.838
			57.260	25.114	1.326	—	1.912
			58.239	25.543	3.110	—	3.864
			59.221	25.974	8.595	—	7.445
			60.198	26.403	15.425	—	13.384
			61.317	26.894	27.153	—	23.958
			62.251	27.303	44.288	—	36.215
			63.371	27.795	64.361	—	55.072
			64.350	28.224	88.311	—	74.991
			65.376	28.673	110.135	—	98.963
			66.309	29.083	139.904	—	123.170
			67.249	29.495	158.534	—	149.448
			68.360	29.982	205.340	—	182.536
			69.384	30.432	217.529	—	214.507
			70.361	30.860	271.148	—	245.956
			71.361	31.299	287.215	—	278.749
			72.336	31.726	319.140	—	311.033
			73.358	32.175	334.801	—	344.932
			74.388	32.626	390.375	—	378.913
^{32}S+^{26}Mg	EvR	authors' graph [191] $E_{\rm c.m.}$	55.502	24.880	2.025	—	3.689
			56.558	25.354	3.024	—	7.290
			57.624	25.832	8.684	—	13.458
			58.654	26.293	14.995	—	22.571
			59.608	26.721	28.777	—	34.209
			60.727	27.222	49.779	—	51.909
			61.647	27.635	67.544	—	69.641
			62.648	28.084	98.177	—	91.912
			63.657	28.536	118.964	—	117.147
			64.613	28.965	151.115	—	143.283
			65.661	29.434	169.614	—	173.970
			66.658	29.881	207.431	—	204.792
			67.644	30.323	232.714	—	236.405
			68.704	30.798	266.113	—	271.311
			69.707	31.248	292.935	—	304.826
			70.665	31.677	331.732	—	337.075
			71.939	32.249	365.110	—	379.899
			72.709	32.593	409.633	—	405.555
			73.668	33.024	459.631	—	437.211
			74.702	33.487	473.325	—	470.775
^{32}S+^{40}Ca	EvR	authors' table [192] $E_{\rm lab}$	80	44.44	65	—	64.917
			82.5	45.83	139	—	139.322
			85	47.22	196	—	217.013
			87.5	48.61	300	—	290.268
			90	50.00	354	—	358.386
			97.5	54.17	535	—	535.804
			107.5	59.72	670	—	722.857
^{32}S+^{48}Ca	EvR	authors' graph [193] $E_{\rm c.m.}$	59.924	35.954	7.839E − 4	—	0.003
			61.317	36.790	0.003	—	0.011
			62.335	37.401	0.012	—	0.033
			63.356	38.014	0.042	—	0.093
			64.369	38.621	0.137	—	0.261
			65.375	39.225	0.425	—	0.708
			66.339	39.803	1.186	—	1.771
			67.354	40.412	3.105	—	4.354
			68.410	41.046	6.195	—	10.089
			69.378	41.627	14.016	—	19.708
			70.358	42.215	26.818	—	35.021
			71.362	42.817	39.079	—	57.024
			73.386	44.031	74.768	—	117.329
			75.367	45.220	116.012	—	186.927
			77.356	46.414	165.636	—	257.519
			79.406	47.644	208.541	—	326.901
			81.389	48.833	279.468	—	389.937

Continued on next page

Table 2 (continued)

Reaction	Detected particles	Data obtained	$E_{\rm lab}$ (MeV)	$E_{\rm c.m.}$ (MeV)	σ (mb)	$\delta\sigma$ (mb)	$\sigma^{\rm cal}$ (mb)
			83.418	50.051	344.547	—	450.469
			85.415	51.249	374.615	—	506.406
			87.372	52.423	442.831	—	558.034
			89.414	53.649	481.559	—	608.776
^{32}S+^{64}Ni	EvR	authors' table [182] $E_{\rm lab}$ & $E_{\rm c.m.}$	78.6	52.4	0.20	0.05	0.098
			80.8	53.9	1.6	0.9	0.952
			82.7	55.1	6.6	0.5	4.510
			85.3	56.9	25	3	24.958
			86.7	57.8	43	3	45.305
			87.3	58.2	57	4	56.542
			89.8	59.9	78	5	116.637
			92.1	61.4	154	10	180.733
			94.8	63.2	234	15	262.675
			97.2	64.8	301	18	334.918
			99.8	66.5	327	21	408.359
			104.7	69.8	509	36	538.779
			109.8	73.1	690	47	654.117
^{32}S+^{89}Y	EvR	authors' table [194] $E_{\rm lab}$ & $E_{\rm c.m.}$	99.00	72.68	0.06	0.02	0.151
			100.00	73.42	0.50	0.07	0.457
			101.00	74.16	1.7	0.1	1.317
			102.00	74.89	4.6	0.2	3.425
			103.00	75.63	10.7	0.3	8.007
			104.00	76.36	19.6	0.3	16.187
			105.00	77.17	33.6	0.4	30.448
			106.00	77.83	47.9	0.5	46.125
			107.00	78.57	66.4	0.7	67.483
			108.00	79.30	86.2	0.9	91.636
			109.00	80.00	109	1	116.817
			110.00	80.78	132	1	146.290
			111.00	81.51	157	2	174.514
			112.00	82.25	183	2	203.238
			113.00	82.98	205	2	231.358
			114.00	83.72	234	2	259.447
			115.00	84.46	261	3	287.010
			116.00	85.20	282	3	314.001
			117.00	85.93	309	3	340.053
			118.00	86.67	331	3	365.883
			120.00	88.12	378	4	414.850
			122.00	89.60	427	4	462.682
			124.00	91.07	468	5	508.157
^{32}S+^{90}Zr	EvR	authors' table [87] $E_{\rm c.m.}$	99.23	73.2	0.12	0.03	0.022
			99.90	73.7	0.18	0.04	0.047
			100.58	74.2	0.31	0.06	0.100
			101.26	74.7	0.57	0.10	0.212
			101.94	75.2	1.09	0.16	0.444
			102.62	75.7	2.07	0.25	0.904
			103.29	76.2	3.66	0.37	1.781
			103.97	76.7	5.89	0.41	3.352
			104.65	77.2	10.58	0.42	5.975
			105.33	77.7	17.46	0.35	10.034
			106.00	78.2	23.41	0.35	15.859
			106.68	78.7	32.89	0.34	23.652
			107.36	79.2	40.22	0.39	33.466
			108.04	79.7	54.96	0.55	45.213
			108.72	80.2	63.69	0.62	58.713
			109.39	80.7	77.96	0.80	73.726
			110.07	81.2	91.59	0.92	89.986
			110.75	81.7	105.94	1.10	107.224
			111.43	82.2	122.84	1.08	125.185
			112.10	82.7	142.10	1.37	143.641
			112.78	83.2	143.85	1.38	162.397
			113.46	83.7	167.85	1.25	181.291
			114.14	84.2	189.70	1.75	200.200
			114.82	84.7	190.06	1.64	219.030
			115.49	85.2	224.93	1.95	237.713
			116.17	85.7	244.09	2.02	256.203

Continued on next page

Table 2 (continued)

Reaction	Detected particles	Data obtained	$E_{\rm lab}$ (MeV)	$E_{\rm c.m.}$ (MeV)	σ (mb)	$\delta\sigma$ (mb)	$\sigma^{\rm cal}$ (mb)
			116.85	86.2	246.27	2.81	274.471
			117.53	86.7	277.99	2.29	292.498
			118.20	87.2	298.07	2.85	310.276
			118.88	87.7	309.41	2.80	327.799
			119.56	88.2	322.27	3.07	345.067
			120.24	88.7	342.70	2.94	362.083
			120.92	89.2	357.17	2.84	378.849
			121.59	89.7	363.05	3.22	395.369
			122.27	90.2	429.44	3.58	411.648
			122.95	90.7	442.29	3.03	427.689
			123.63	91.2	430.00	3.37	443.497
			124.98	92.2	535.48	4.70	474.431
			126.47	93.3	528.80	3.93	507.442
			127.69	94.2	582.98	4.63	533.687
			129.18	95.3	623.51	4.00	564.866
^{32}S+^{94}Zr	EvR	authors' table [90] $E_{\rm c.m.}$	93.83	70.0	0.08	0.02	0.004
			94.50	70.5	0.14	0.03	0.008
			95.17	71.0	0.30	0.06	0.018
			95.84	71.5	0.51	0.09	0.038
			96.51	72.0	0.92	0.14	0.078
			97.18	72.5	1.32	0.16	0.156
			97.85	73.0	2.42	0.27	0.306
			98.52	73.5	3.21	0.30	0.580
			99.33	74.1	4.82	0.51	1.192
			100.00	74.6	7.64	0.63	2.078
			100.67	75.1	11.00	0.43	3.477
			101.34	75.6	13.89	0.35	5.573
			102.01	76.1	18.86	0.32	8.558
			102.68	76.6	25.00	0.23	12.606
			103.35	77.1	30.50	0.30	17.854
			104.02	77.6	39.73	0.31	24.392
			104.69	78.1	46.01	0.34	32.253
			105.36	78.6	62.66	0.51	41.421
			106.03	79.1	67.44	0.64	51.840
			106.70	79.6	82.58	0.64	63.435
			107.50	80.2	91.87	0.85	78.772
			108.17	80.7	120.09	1.06	92.625
			108.84	81.2	120.47	1.21	107.341
			109.51	81.7	138.67	1.33	122.813
			110.18	82.2	152.07	1.53	138.934
			110.85	82.7	173.43	1.62	155.600
			111.52	83.2	191.05	1.74	172.710
			112.19	83.7	211.77	1.98	190.170
			112.86	84.2	205.49	1.96	207.891
			113.53	84.7	250.37	1.96	225.795
			114.20	85.2	261.45	1.74	243.808
			114.87	85.7	260.86	2.11	261.868
			115.54	86.2	291.18	2.38	279.920
			116.21	86.7	311.20	2.61	297.916
			116.89	87.2	323.80	2.52	315.818
			117.69	87.8	346.00	2.61	337.129
			118.36	88.3	387.17	2.83	354.717
			119.03	88.8	386.07	2.88	372.127
			119.70	89.3	404.10	2.71	389.345
			120.37	89.8	411.25	3.69	406.359
			121.04	90.3	436.50	2.35	423.161
			121.71	90.8	452.09	3.39	439.748
			122.38	91.3	512.76	2.82	456.114
			123.05	91.8	531.09	4.13	472.260
			123.05	91.8	534.23	3.87	472.260
			123.72	92.3	569.45	2.95	488.185
			125.06	93.3	607.63	4.67	519.379
			126.40	94.3	609.22	3.03	549.711
			127.88	95.4	649.90	5.12	582.110
			129.22	96.4	691.71	3.18	610.711
^{32}S+^{96}Zr	EvR	authors' table	93.20	69.9	0.09	0.02	0.159

Continued on next page

Table 2 (continued)

Reaction	Detected particles	Data obtained	$E_{\rm lab}$ (MeV)	$E_{\rm c.m.}$ (MeV)	σ (mb)	$\delta\sigma$ (mb)	$\sigma^{\rm cal}$ (mb)
		[87]	93.87	70.4	0.23	0.05	0.290
		$E_{\rm c.m.}$	94.53	70.9	0.37	0.07	0.511
			95.20	71.4	0.69	0.12	0.872
			95.87	71.9	0.79	0.12	1.440
			96.67	72.5	1.94	0.23	2.516
			97.33	73.0	2.95	0.30	3.865
			98.13	73.6	5.53	0.39	6.195
			98.67	74.0	8.95	0.36	8.269
			99.47	74.6	13.12	0.26	12.287
			100.00	75.0	15.32	0.23	15.623
			100.93	75.7	20.18	0.03	22.827
			101.33	76.0	23.82	0.03	26.479
			102.27	76.7	31.81	0.34	36.371
			102.67	77.0	37.01	0.31	41.180
			103.60	77.7	46.28	0.51	53.646
			104.13	78.1	50.41	0.43	61.537
			104.93	78.7	66.85	0.70	74.362
			105.47	79.1	72.13	0.66	83.527
			106.27	79.7	90.53	0.83	98.163
			106.80	80.1	99.28	0.85	108.483
			107.73	80.8	117.57	1.21	127.519
			108.13	81.1	130.62	1.09	136.038
			109.07	81.8	145.06	1.51	156.694
			109.47	82.1	161.35	1.34	165.847
			110.40	82.8	179.30	1.82	187.839
			110.93	83.2	182.87	1.85	200.775
			111.73	83.8	231.63	1.93	220.606
			112.27	84.2	222.32	1.83	234.080
			113.07	84.8	231.95	2.18	254.629
			113.60	85.2	244.76	1.78	268.515
			114.40	85.8	282.11	2.51	289.571
			114.93	86.2	264.38	2.37	303.739
			115.87	86.9	313.05	2.37	328.715
			116.27	87.2	314.40	2.44	339.468
			117.33	88.0	338.00	2.74	368.236
			117.73	88.3	354.74	2.11	379.039
			118.53	88.9	393.91	2.55	400.634
			119.07	89.3	382.96	3.02	415.008
			119.87	89.9	424.93	3.13	436.508
			120.40	90.3	381.53	2.95	450.782
			121.20	90.9	448.78	3.14	472.084
			121.73	91.3	439.19	3.38	486.201
			122.67	92.0	510.25	3.57	510.716
			123.07	92.3	519.80	4.10	521.142
			124.00	93.0	505.50	3.00	545.264
			125.20	93.9	591.22	4.33	575.821
			126.67	95.0	601.59	3.70	612.420
			127.87	95.9	644.56	7.76	641.717
			129.47	97.1	683.96	3.93	679.841
^{32}S+^{94}Mo	EvR	authors' table	102.01	76.1	0.029	0.016	0.013
		[195]	102.68	76.6	0.72	0.23	0.028
		$E_{\rm c.m.}$	104.69	78.1	1.19	0.42	0.264
			106.16	79.2	2.54	0.89	1.202
			107.64	80.3	5.7	1.9	4.444
			109.65	81.8	15.1	4.6	17.063
			111.66	83.3	46	14	42.362
			114.61	85.5	98	29	99.391
			119.70	89.3	290	87	226.379
^{32}S+^{96}Mo	EvR	authors' table	99.33	74.5	0.068	0.030	0.006
		[195]	102.67	77.0	1.25	0.47	0.252
		$E_{\rm c.m.}$	104.67	78.5	3.6	1.4	1.757
			106.13	79.6	9.4	3.6	5.614
			107.73	80.8	15.0	6.3	15.118
			109.73	82.3	32	12	37.133
			111.73	83.8	79	29	69.991
			114.67	86.0	144	54	133.078

Continued on next page

Table 2 (continued)

Reaction	Detected particles	Data obtained	$E_{\rm lab}$ (MeV)	$E_{\rm c.m.}$ (MeV)	σ (mb)	$\delta\sigma$ (mb)	$\sigma^{\rm cal}$ (mb)
			119.73	89.8	483	18	262.390
^{32}S+^{98}Mo	EvR	authors' table	97.63	73.6	0.004	0.003	0.044
		[195]	100.68	75.9	0.562	0.054	0.835
		$E_{\rm c.m.}$	102.67	77.4	2.39	0.21	3.790
			104.66	78.9	8.74	0.77	12.098
			106.12	80.0	19.8	1.7	23.257
			107.71	81.2	35.5	3.0	40.968
			109.70	82.7	36.3	3.2	70.651
			111.69	84.2	104.4	9.0	107.554
			114.61	86.4	116	10	171.814
			119.65	90.2	347	30	299.279
^{32}S+^{100}Mo	EvR	authors' table	95.70	72.5	0.018	0.003	0.122
		[195]	97.68	74.0	0.158	0.012	0.644
		$E_{\rm c.m.}$	100.72	76.3	1.90	0.15	4.907
			102.70	77.8	3.70	0.31	13.189
			104.68	79.3	12.2	1.0	28.133
			106.13	80.4	22.3	1.8	43.962
			107.71	81.6	31.8	2.9	65.570
			109.69	83.1	45.8	3.6	98.338
			111.67	84.6	88.0	7.3	136.643
			114.71	86.9	141	17	203.882
			119.72	90.7	300	24	329.192
^{32}S+^{100}Ru	EvR	authors' table	100.72	76.3	≤ 0.001	—	0.002
		[195]	102.70	77.8	0.006	0.007	0.022
		$E_{\rm c.m.}$	104.68	79.3	0.192	0.079	0.196
			106.13	80.4	0.61	0.27	0.830
			107.71	81.6	3.1	1.1	3.166
			109.69	83.1	10.4	3.7	11.411
			111.67	84.6	30	10	28.452
			114.71	86.9	65	22	71.965
			119.72	90.7	170	58	177.846
^{32}S+^{101}Ru	EvR	authors' table	106.14	80.6	1.69	0.37	2.117
		[195]	107.72	81.8	5.03	0.89	6.356
		$E_{\rm c.m.}$	109.69	83.3	11.0	2.0	17.989
			111.67	84.8	33.1	5.8	38.317
			114.70	87.1	67	12	85.085
			119.70	90.9	152	26	192.556
^{32}S+^{102}Ru	EvR	authors' table	100.63	76.6	0.011	0.003	0.024
		[195]	102.73	78.2	0.161	0.030	0.217
		$E_{\rm c.m.}$	104.97	79.9	0.83	0.14	1.584
			106.15	80.8	3.14	0.52	3.768
			107.73	82.0	7.2	1.2	9.752
			109.70	83.5	16.7	2.7	24.060
			111.67	85.0	43.9	7.2	46.829
			114.69	87.3	86	14	96.243
			119.68	91.1	186	31	205.700
^{32}S+^{103}Rh	EvR	authors' table	102.76	78.4	0.005	0.003	0.012
		[195]	104.72	79.9	0.154	0.015	0.106
		$E_{\rm c.m.}$	106.17	81.0	0.528	0.046	0.457
			107.74	82.2	1.95	0.15	1.826
			109.70	83.7	8.97	0.75	7.225
			111.67	85.2	16.3	1.6	19.720
			114.68	87.5	47.2	3.8	55.382
			119.67	91.3	110.6	8.3	149.772
^{32}S+^{104}Pd	EvR	authors' table	104.62	80.0	≤ 0.002	—	0.003
		[195]	106.18	81.2	0.022	0.011	0.021
		$E_{\rm c.m.}$	107.62	82.3	0.151	0.062	0.107
			109.72	83.9	1.23	0.42	0.909
			111.68	85.4	4.9	1.7	4.538
			114.68	87.7	22.5	7.3	23.666
			119.65	91.5	79	26	98.304
^{32}S+^{104}Ru	EvR	authors' table	100.69	77.0	0.164	0.037	0.344
		[195]	102.65	78.5	0.97	0.28	1.604
		$E_{\rm c.m.}$	104.62	80.0	3.76	0.87	5.581
			106.18	81.2	8.1	1.8	12.319
			107.62	82.3	15.7	3.4	22.120

Continued on next page

Table 2 (continued)

Reaction	Detected particles	Data obtained	$E_{\rm lab}$ (MeV)	$E_{\rm c.m.}$ (MeV)	σ (mb)	$\delta\sigma$ (mb)	$\sigma^{\rm cal}$ (mb)
			109.72	83.9	32.5	7.4	43.469
			111.68	85.4	61	14	70.502
			114.42	87.5	114	26	118.164
			119.65	91.5	201	51	232.571
^{32}S+^{105}Pd	EvR	authors' table	106.21	81.4	0.076	0.024	0.061
		[195]	109.73	84.1	2.20	0.48	1.905
		$E_{\rm c.m.}$	111.69	85.6	7.6	1.6	7.562
			114.69	87.9	27.1	5.9	31.015
			119.65	91.7	95	21	110.274
^{32}S+^{106}Pd	EvR	authors' table	104.67	80.4	0.008	0.003	0.023
		[195]	106.23	81.6	0.118	0.044	0.129
		$E_{\rm c.m.}$	107.67	82.7	0.60	0.14	0.539
			109.62	84.2	2.73	0.62	2.804
			111.70	85.8	11.5	2.7	10.560
			114.70	88.1	38.8	8.0	37.470
			119.64	91.9	121	28	120.832
^{32}S+^{108}Pd	EvR	authors' table	102.67	79.2	0.008	0.004	0.018
		[195]	104.74	80.8	0.114	0.039	0.164
		$E_{\rm c.m.}$	106.17	81.9	0.86	0.31	0.620
			107.72	83.1	2.28	0.77	2.168
			109.67	84.6	6.9	2.4	7.620
			111.74	86.2	21.5	7.2	20.567
			114.72	88.5	57	19	54.823
			119.65	92.3	148	50	145.100
^{32}S+^{110}Pd	EvR	authors' table	100.69	78.0	0.006	0.002	0.018
		[195]	102.63	79.5	0.050	0.008	0.128
		$E_{\rm c.m.}$	104.69	81.1	0.492	0.062	0.778
			106.11	82.2	1.24	0.17	2.232
			107.66	83.4	3.59	0.30	5.879
			109.73	85.0	10.5	1.3	16.155
			111.66	86.5	21.8	1.9	33.023
			114.63	88.8	43	11	72.637
			119.67	92.7	123	11	169.951
^{32}S+^{138}Ba	EvRFF	authors' table	122.2	99.20	0.5	0.2	1.490
		[185]	123.2	100.01	1.4	0.2	3.037
		$E_{\rm lab}$	124.7	101.23	3.2	0.5	7.690
			127.2	103.26	11.9	0.4	25.546
			129.7	105.29	22	0.5	59.263
			132.2	107.32	47	1.7	106.990
			134.7	109.34	80	5	163.809
			139.7	113.40	191	6	286.092
			144.7	117.46	262	10	403.510
			149.7	121.52	398	12	511.183
			154.7	125.58	490	30	609.515
			159.7	129.64	538	20	699.424
			164.7	133.70	551	25	781.724
^{32}S+^{154}Sm	EvRFF	authors' table	121.99	101.0	0.16	0.03	0.142
		[196]	124.52	103.1	0.76	0.02	0.936
		$E_{\rm c.m.}$	127.06	105.2	2.4	0.4	4.208
			129.48	107.2	6.4	1.0	12.519
			132.01	109.3	15	2	28.980
			134.55	111.4	26	4	54.684
			139.50	115.5	80	8	127.020
			146.99	121.7	176	18	276.694
			154.48	127.9	305	31	450.401
^{32}S+^{182}W	FF	authors' graph	144.472	122.868	0.219	—	0.834
		[197]	146.807	124.855	2.213	—	3.454
		$E_{\rm c.m.}$	149.345	127.013	8.427	—	11.088
			151.376	128.740	17.902	—	22.106
			154.591	131.474	39.262	—	50.310
			157.467	133.921	74.221	—	85.190
			159.498	135.648	103.135	—	114.563
			164.236	139.677	168.046	—	195.673
			166.655	141.734	186.240	—	242.445
			169.989	144.570	262.429	—	310.948
			175.268	149.060	408.292	—	424.908

Continued on next page

Table 2 (continued)

Reaction	Detected particles	Data obtained	E_{lab} (MeV)	$E_{c.m.}$ (MeV)	σ (mb)	$\delta\sigma$ (mb)	σ^{cal} (mb)
			179.973	153.061	512.138	—	528.060
			191.818	163.135	696.709	—	775.557
			194.864	165.725	619.942	—	834.457
			200.279	170.330	852.364	—	933.664
$^{32}S+^{184}W$	FF	authors' table [198] $E_{c.m.}$	139.46	118.8	0.04	—	0.031
			144.51	123.1	2.35	—	1.398
			149.44	127.3	22.97	—	14.504
			154.37	131.5	81.01	—	54.378
			159.42	135.8	132.27	—	122.772
			165.64	141.1	189.33	—	234.703
			169.51	144.4	237.06	—	314.335
$^{32}S+^{208}Pb$	FF	authors' graph [199] $E_{c.m.}$	160.852	139.405	9.367	—	6.179
			161.868	140.286	14.128	—	9.462
			162.926	141.202	19.988	—	14.137
			163.983	142.118	26.215	—	20.283
			164.958	142.964	34.272	—	27.360
			165.894	143.774	43.794	—	35.465
			166.910	144.655	56.247	—	45.764
			167.845	145.466	68.333	—	56.555
			168.536	146.065	78.222	—	65.301
			168.984	146.452	83.715	—	71.292
			169.797	147.157	96.534	—	82.818
			169.959	147.298	99.098	—	85.218
			170.569	147.827	109.719	—	94.482
			170.935	148.144	115.945	—	100.233
			171.830	148.919	132.060	—	114.861
			172.521	149.518	144.512	—	126.673
			173.903	150.716	167.586	—	151.449
			174.554	151.280	180.038	—	163.565
			175.814	152.372	200.548	—	187.711
			176.505	152.971	213.366	—	201.259
			176.952	153.359	218.128	—	210.119
			177.928	154.204	238.637	—	229.653
			178.497	154.698	247.793	—	241.148
			179.880	155.896	277.826	—	269.255
			180.612	156.530	281.854	—	284.190
			181.953	157.693	308.590	—	311.559
			183.864	159.349	333.495	—	350.286
			184.921	160.265	365.358	—	371.485
			187.605	162.591	404.913	—	424.301
			190.735	165.304	473.401	—	483.771
			201.753	174.853	633.084	—	673.146
			211.755	183.521	765.665	—	819.853
$^{33}S+^{90}Zr$	EvR	authors' table [200] $E_{c.m.}$	101.68	74.4	0.079	0.049	0.185
			102.64	75.1	0.171	0.094	0.532
			103.73	75.9	0.49	0.19	1.652
			105.64	77.3	3.70	0.74	8.825
			107.69	78.8	26.2	5.0	31.249
			109.61	80.2	43.5	7.8	68.050
			111.66	81.7	108	19	119.286
			115.62	84.6	187	33	229.468
			119.58	87.5	312	56	335.499
			122.59	89.7	312	56	410.253
			125.60	91.9	423	76	480.315
			128.60	94.1	553	100	546.052
			131.61	96.3	725	130	607.801
$^{33}S+^{91}Zr$	EvR	authors' table [200] $E_{c.m.}$	100.70	73.9	0.062	0.024	0.037
			101.65	74.6	0.235	0.061	0.113
			102.61	75.3	0.85	0.20	0.337
			103.15	75.7	1.14	0.40	0.622
			103.70	76.1	2.18	0.57	1.132
			105.74	77.6	11.7	2.3	8.030
			107.24	78.7	26.6	5.9	22.331
			109.69	80.5	58.2	11.6	65.075
			110.92	81.4	107	21	93.401
			111.60	81.9	122	22	110.490

Continued on next page

Table 2 (continued)

Reaction	Detected particles	Data obtained	$E_{\rm lab}$ (MeV)	$E_{\rm c.m.}$ (MeV)	σ (mb)	$\delta\sigma$ (mb)	$\sigma^{\rm cal}$ (mb)
			115.69	84.9	218	39	222.032
			118.82	87.2	371	67	307.545
			122.64	90.0	322	58	405.274
			125.64	92.2	407	73	476.734
			127.68	93.7	518	93	522.925
			130.81	96.0	643	116	590.037
^{33}S+^{92}Zr	EvR	authors' table [200] $E_{\rm c.m.}$	98.64	72.6	0.049	0.020	0.024
			99.73	73.4	0.129	0.036	0.084
			100.68	74.1	0.56	0.12	0.246
			101.63	74.8	1.71	0.36	0.684
			102.58	75.5	3.63	0.69	1.764
			103.67	76.3	7.4	1.4	4.594
			105.57	77.7	19.9	3.8	16.939
			107.61	79.2	51.3	9.7	43.767
			109.65	80.7	77.9	15.0	83.389
			111.68	82.2	131	25	132.040
			115.62	85.1	226	41	237.565
			119.70	88.1	368	66	346.745
			122.69	90.3	339	61	422.200
			125.68	92.5	361	65	493.147
			128.67	94.7	528	95	559.780
			131.66	96.9	686	123	622.405
^{34}S+^{24}Mg	EvR	authors' graph [191] $E_{\rm c.m.}$	58.881	24.365	0.280	—	0.601
			59.782	24.737	0.547	—	1.154
			61.800	25.573	2.181	—	4.559
			63.897	26.440	11.959	—	15.138
			65.913	27.275	36.754	—	36.428
			66.922	27.692	58.592	—	51.606
			67.955	28.119	84.221	—	70.086
			69.963	28.950	136.602	—	113.483
			71.975	29.783	212.275	—	164.895
			73.999	30.620	297.305	—	222.235
			76.056	31.472	326.915	—	284.001
^{34}S+^{25}Mg	EvR	authors' graph [191] $E_{\rm c.m.}$	58.644	24.849	0.579	—	1.753
			59.574	25.243	1.941	—	3.388
			60.632	25.691	4.263	—	6.827
			61.623	26.112	9.763	—	12.360
			62.661	26.551	18.996	—	21.316
			63.634	26.964	32.161	—	33.074
			64.701	27.416	54.471	—	49.824
			65.647	27.817	86.092	—	67.871
			66.631	28.234	104.135	—	89.569
			67.630	28.657	139.742	—	114.251
			68.613	29.073	168.926	—	140.804
			69.675	29.523	190.625	—	171.541
			70.659	29.940	226.536	—	201.524
			71.677	30.372	228.555	—	233.675
			72.293	30.633	260.135	—	253.529
			72.743	30.823	278.725	—	268.173
			73.688	31.224	293.655	—	299.182
			74.749	31.673	342.966	—	334.196
			75.622	32.043	380.455	—	362.951
^{34}S+^{26}Mg	EvR	authors' graph [191] $E_{\rm c.m.}$	56.464	24.468	0.277	—	1.125
			57.546	24.937	1.171	—	2.527
			58.580	25.385	3.303	—	5.253
			59.597	25.825	4.916	—	10.168
			59.549	25.804	8.112	—	9.869
			60.634	26.275	16.901	—	18.442
			61.619	26.702	27.901	—	30.007
			61.636	26.709	34.335	—	30.236
			63.659	27.586	75.994	—	66.114
			65.707	28.473	139.135	—	116.934
			66.699	28.903	169.758	—	145.625
			67.690	29.332	196.546	—	176.300
			68.841	29.831	254.722	—	213.860
			69.770	30.234	277.746	—	245.176

Continued on next page

Table 2 (continued)

Reaction	Detected particles	Data obtained	E_{lab} (MeV)	$E_{c.m.}$ (MeV)	σ (mb)	$\delta\sigma$ (mb)	σ^{cal} (mb)
			70.992	30.763	330.045	—	287.245
			72.054	31.223	366.136	—	324.127
			73.067	31.662	406.146	—	359.226
			74.739	32.387	413.166	—	416.472
			74.207	32.156	474.446	—	398.413
			75.234	32.601	512.711	—	433.131
			77.334	33.511	554.237	—	501.978
$^{34}S+^{89}Y$	EvR	authors' table [194] E_{lab} & $E_{c.m.}$	100.00	72.23	0.03	0.02	0.153
			101.00	72.95	0.18	0.02	0.465
			102.00	73.67	0.73	0.06	1.337
			103.00	74.40	3.0	0.1	3.560
			104.00	75.12	8.8	0.2	8.271
			105.00	75.84	19.9	0.4	16.759
			106.00	76.57	35.2	0.5	30.009
			107.00	77.29	53.6	0.5	47.658
			107.50	77.66	63.3	0.6	58.316
			108.00	78.02	75.5	0.8	69.579
			108.50	78.38	85.3	0.8	81.606
			109.00	78.74	97.8	1.0	94.275
			109.50	79.10	107	1	107.470
			110.00	79.46	121	1	121.077
			110.50	79.82	132	1	134.995
			111.00	80.18	146	1	149.132
			111.50	80.55	159	1	163.808
			112.00	80.93	172	2	178.959
			112.50	81.27	183	2	192.530
			113.00	81.63	196	2	206.872
			113.50	82.00	208	2	221.548
			114.00	82.36	223	2	235.738
			114.50	82.72	238	2	249.820
			115.00	83.08	246	2	263.780
			115.50	83.44	262	3	277.608
			116.00	83.80	273	3	291.299
			117.00	84.53	300	3	318.625
			118.00	85.25	322	3	344.997
			120.00	86.70	375	4	396.389
			123.00	88.88	444	4	469.530
			124.00	89.60	464	5	492.658
			126.00	91.05	505	5	537.768
$^{34}S+^{168}Er$	EvRFF	authors' table [201] $E_{c.m.}$	133.69	111.19	0.19	0.1	0.398
			134.69	112.02	0.36	0.2	0.902
			135.69	112.85	0.69	0.3	1.873
			136.69	113.68	1.21	0.1	3.562
			137.68	114.51	2.28	0.09	6.209
			138.69	115.35	3.93	0.2	10.016
			139.69	116.18	6.43	0.2	15.019
			140.69	117.01	9.94	0.2	21.585
			141.71	117.86	14.7	0.3	29.994
			142.73	118.71	20.0	0.3	39.642
			143.70	119.51	26.9	0.4	49.867
			144.69	120.34	34.2	0.6	61.896
			145.69	121.17	43.4	0.5	75.059
			146.69	122.00	53.8	0.8	89.155
			147.70	122.84	65.9	0.6	104.632
			148.70	123.67	79.5	1.0	121.003
			149.70	124.50	94.2	0.9	138.117
			150.69	125.33	110	1	156.114
			151.70	126.17	128	1	175.287
			152.70	127.00	144	2	194.849
			153.70	127.83	164	2	215.003
			154.75	128.70	184	2	236.916
			155.70	129.49	205	2	257.298
			156.69	130.32	228	2	279.062
			157.70	131.16	246	3	301.588
			158.70	131.99	268	3	324.254
			159.70	132.82	290	3	347.119

Continued on next page

Table 2 (continued)

Reaction	Detected particles	Data obtained	$E_{\rm lab}$ (MeV)	$E_{\rm c.m.}$ (MeV)	σ (mb)	$\delta\sigma$ (mb)	$\sigma^{\rm cal}$ (mb)
			160.71	133.66	307	3	370.519
			161.71	134.49	333	3	393.914
			163.70	136.15	375	4	440.956
			165.70	137.81	414	4	488.327
			167.71	139.48	449	5	535.854
			169.70	141.14	488	5	582.826
			171.71	142.81	523	5	629.554
			173.71	144.47	554	6	675.298
			175.72	146.14	582	6	720.524
			179.72	149.47	650	7	807.851
			183.72	152.80	707	7	891.070
			187.72	156.12	744	7	969.785
			191.72	159.45	790	8	1044.487
			195.72	162.78	849	9	1115.061
^{35}Cl+^{24}Mg	EvR	authors' table [202] $E_{\rm c.m.}$	64.41	26.2	0.8	—	1.771
			65.88	26.8	1.7	—	4.544
			67.36	27.4	3.8	—	10.401
			68.83	28.0	7.7	—	20.844
			70.31	28.6	24.8	—	36.725
			72.03	29.3	39.5	—	62.101
			73.26	29.8	50.1	—	84.352
			74.98	30.5	80.5	—	120.503
			77.19	31.4	124.2	—	173.959
			79.16	32.2	216.2	—	226.366
			83.34	33.9	343.0	—	346.196
			88.25	35.9	462.9	—	489.608
^{35}Cl+^{25}Mg	EvR	authors' table [202] $E_{\rm c.m.}$	65.52	27.3	5.4	—	11.102
			66.96	27.9	11.2	—	22.543
			68.64	28.6	21.2	—	43.547
			70.08	29.2	29.8	—	68.021
			71.52	29.8	68.0	—	97.826
			72.96	30.4	99.6	—	132.163
			74.64	31.1	110.3	—	176.820
			76.08	31.7	146.7	—	218.082
			78.00	32.5	216.2	—	275.972
			79.92	33.3	270.9	—	335.656
			84.00	35.0	378.3	—	462.627
			89.04	37.1	515.8	—	610.335
^{35}Cl+^{26}Mg	EvR	authors' table [202] $E_{\rm c.m.}$	65.22	27.8	15.1	—	26.731
			66.87	28.5	31.3	—	49.886
			68.27	29.1	44.1	—	76.276
			69.68	29.7	66.8	—	107.980
			71.32	30.4	98.7	—	150.538
			72.73	31.0	132.5	—	190.765
			74.37	31.7	152.5	—	240.851
			75.78	32.3	170.8	—	285.569
			77.89	33.2	236.0	—	354.140
			79.77	34.0	287.9	—	415.221
			83.76	35.7	389.2	—	540.978
			88.92	37.9	515.9	—	689.336
^{35}Cl+^{27}Al	EvRFF	authors' table [203] $E_{\rm c.m.}$	69.81	30.4	15.9	2.4	27.640
			70.73	30.8	32.4	3.9	37.856
			74.63	32.5	128	9	99.928
			89.79	39.1	450	23	493.603
			99.66	43.4	637	32	756.472
			119.64	52.1	920	46	1155.303
			129.74	56.5	1107	55	1299.477
			144.44	62.9	1206	60	1462.417
			159.36	69.4	1140	57	1586.792
			164.41	71.6	1170	117	1621.685
			169.47	73.8	1200	120	1653.525
^{35}Cl+^{54}Cr	EvR	authors' graph [204] $E_{\rm c.m.}$	85.866	52.098	13.744	—	31.227
			87.730	53.230	35.243	—	61.920
			88.781	53.867	64.538	—	83.629
			89.793	54.481	98.708	—	107.084
			91.738	55.661	145.638	—	157.817

Continued on next page

Table 2 (continued)

Reaction	Detected particles	Data obtained	E_{lab} (MeV)	$E_{c.m.}$ (MeV)	σ (mb)	$\delta\sigma$ (mb)	σ^{cal} (mb)
			93.762	56.889	210.272	—	216.149
			95.903	58.188	268.617	—	281.090
			97.965	59.439	358.297	—	344.555
			99.950	60.644	416.794	—	404.952
			104.075	63.147	491.871	—	524.864
			111.897	67.892	680.155	—	725.009
			115.906	70.325	637.462	—	814.445
			117.929	71.552	506.254	—	856.594
			119.952	72.780	715.326	—	896.887
			121.977	74.009	457.690	—	935.452
			125.091	75.898	419.806	—	991.559
			130.188	78.991	360.885	—	1075.783
$^{35}Cl+^{52}Cr$	EvR	authors' graph [204] $E_{c.m.}$	88.847	53.104	7.834	—	23.039
			89.670	53.596	17.318	—	35.886
			90.756	54.245	27.657	—	57.762
			93.653	55.976	113.320	—	135.022
			95.661	57.176	184.258	—	195.551
			97.767	58.435	254.784	—	258.968
			99.742	59.616	348.102	—	316.289
			103.889	62.095	458.777	—	428.101
			107.971	64.534	562.626	—	527.394
			109.946	65.715	569.419	—	571.997
			111.888	66.876	597.426	—	613.853
			115.838	69.236	649.791	—	693.318
			119.788	71.597	653.702	—	765.908
			123.902	74.056	579.764	—	835.009
			127.984	76.496	529.853	—	897.697
			130.025	77.716	569.419	—	927.041
$^{35}Cl+^{51}V$	EvR	authors' graph [204] $E_{c.m.}$	82.880	49.150	3.537	—	2.188
			83.875	49.740	7.096	—	5.320
			84.970	50.389	13.568	—	12.634
			85.998	50.999	26.572	—	24.796
			87.889	52.120	65.370	—	61.633
			90.012	53.379	117.004	—	119.618
			91.970	54.540	175.970	—	180.129
			93.927	55.701	249.236	—	241.504
			95.917	56.881	303.824	—	302.044
			99.898	59.242	407.696	—	414.643
			103.846	61.583	468.041	—	515.447
			107.927	64.003	518.314	—	609.633
			111.974	66.403	496.991	—	694.249
			115.889	68.725	488.123	—	768.740
			119.936	71.125	446.101	—	839.020
			124.979	74.115	432.913	—	918.125
			130.022	77.106	488.123	—	988.985
			135.031	80.077	330.455	—	1052.228
$^{35}Cl+^{50}Ti$	EvR	authors' graph [204] $E_{c.m.}$	80.812	47.536	10.192	—	4.918
			81.748	48.087	21.972	—	10.654
			82.818	48.717	39.803	—	22.515
			83.788	49.287	60.949	—	38.945
			84.825	49.897	97.920	—	62.135
			85.862	50.507	150.846	—	89.986
			87.634	51.550	218.843	—	144.320
			89.842	52.848	288.422	—	216.166
			91.915	54.068	333.106	—	282.544
			93.889	55.229	394.059	—	342.885
			95.962	56.448	444.314	—	402.991
			96.899	56.999	535.167	—	429.059
			97.902	57.590	457.849	—	456.273
			99.876	58.750	510.079	—	507.733
			103.789	61.052	629.306	—	602.306
			106.799	62.823	672.253	—	668.948
			107.769	63.393	740.007	—	689.384
			111.882	65.813	660.258	—	770.916
			115.963	68.213	629.306	—	844.292
			116.899	68.764	621.798	—	860.174

Continued on next page

Table 2 (continued)

Reaction	Detected particles	Data obtained	E_{lab} (MeV)	$E_{c.m.}$ (MeV)	σ (mb)	$\delta\sigma$ (mb)	σ^{cal} (mb)
			119.976	70.574	614.380	—	910.020
			126.766	74.568	516.239	—	1008.578
$^{35}Cl+^{54}Fe$	EvR	authors' graph [204] $E_{c.m.}$	91.804	55.701	1.458	—	2.741
			92.797	56.304	2.945	—	6.371
			93.905	56.976	7.969	—	14.299
			94.825	57.534	12.816	—	24.866
			95.851	58.157	24.431	—	41.109
			97.905	59.403	61.015	—	85.446
			99.851	60.584	85.303	—	136.818
			101.986	61.879	181.531	—	197.133
			103.932	63.060	246.292	—	252.104
			105.689	64.126	329.185	—	300.297
			109.823	66.634	404.104	—	406.516
			113.932	69.127	451.108	—	502.325
			117.904	71.537	483.826	—	586.681
			121.904	73.964	588.029	—	664.355
			125.849	76.358	588.022	—	734.592
			127.931	77.621	673.034	—	769.319
			130.011	78.883	633.838	—	802.528
			134.985	81.901	640.202	—	876.353
$^{35}Cl+^{58}Ni$	EvR	authors' table [203] $E_{c.m.}$	96.69	60.3	6.7	1.3	7.134
			97.17	60.6	10.0	2.5	10.191
			97.65	60.9	18.5	2.8	14.136
			98.61	61.5	31.8	4.8	24.920
			99.57	62.1	46.9	4.7	39.581
			104.71	65.3	143	7	161.894
			109.68	68.4	271	14	297.525
			119.62	74.6	454	23	532.304
			139.66	87.1	781	39	876.116
$^{35}Cl+^{60}Ni$	EvR	authors' table [203] $E_{c.m.}$	93.73	59.2	8.0	2.0	3.155
			94.21	59.5	13.1	3.3	4.792
			94.68	59.8	20.0	3.0	7.086
			95.79	60.5	31.0	4.7	15.681
			97.22	61.4	47.2	7.1	34.391
			98.80	62.4	68.0	6.8	64.714
			104.66	66.1	210	15	222.315
			129.20	81.6	680	34	778.332
$^{35}Cl+^{62}Ni$	EvRFF	authors' table [203] $E_{c.m.}$	92.62	59.2	16.1	3.2	10.103
			93.71	59.9	27.6	5.5	20.007
			94.65	60.5	37.3	5.6	32.125
			95.28	60.9	47.6	4.8	42.015
			96.53	61.7	64.9	6.5	65.750
			97.63	62.4	89	8.9	90.251
			99.66	63.7	136	7	142.637
			104.67	66.9	268	13	288.259
			109.67	70.1	401	20	430.527
			119.69	76.5	585	29	673.649
			139.71	89.3	929	46	1027.417
			144.56	92.4	980	49	1093.590
			159.58	102.0	1058	70	1263.339
			164.59	105.2	1179	84	1309.987
			169.59	108.4	1231	100	1352.419
$^{35}Cl+^{64}Ni$	EvR	authors' table [203] $E_{c.m.}$	90.65	58.6	13.2	2.6	11.302
			91.58	59.2	23.1	4.6	19.287
			92.66	59.9	35.6	5.3	32.378
			93.59	60.5	54.7	5.5	46.802
			94.67	61.2	66.0	6.6	67.071
			95.60	61.8	89.3	8.9	87.055
			98.69	63.8	152	11	166.552
			104.57	67.6	328	16	338.965
			129.63	83.8	816	41	910.294
$^{35}Cl+^{90}Zr$	EvR	authors' table [203] $E_{c.m.}$	119.44	86.0	86	13	106.621
			122.36	88.1	129	13	178.934
			124.44	89.6	190	13	233.517
			129.58	93.3	286	20	365.775
			136.39	98.2	478	33	524.213

Continued on next page

Table 2 (continued)

Reaction	Detected particles	Data obtained	E_{lab} (MeV)	$E_{c.m.}$ (MeV)	σ (mb)	$\delta\sigma$ (mb)	σ^{cal} (mb)
			143.47	103.3	576	29	668.431
			164.44	118.4	850	43	999.512
$^{35}Cl+^{92}Zr$	EvR	authors' table [148] $E_{c.m.}$	106.46	77.12	0.21	0.04	0.207
			107.33	77.75	0.66	0.1	0.508
			108.47	78.58	1.68	0.1	1.503
			109.30	79.18	3.15	0.2	3.021
			110.48	80.03	5.97	0.3	7.094
			111.28	80.61	10.9	0.3	11.615
			112.46	81.47	17.7	0.4	21.436
			113.28	82.06	26.6	0.3	30.428
			114.47	82.92	42.6	0.6	46.691
			115.29	83.52	55.4	0.5	60.091
			116.47	84.37	76.4	0.9	81.645
			117.35	85.01	94.7	0.7	99.616
			118.48	85.83	118	1	124.474
			119.28	86.41	135	1	143.087
			120.66	87.41	165	1	176.711
			122.49	88.73	207	1	223.070
			124.49	90.18	254	2	275.149
			126.30	91.49	298	2	322.180
			130.31	94.40	376	2	423.588
			134.32	97.30	459	3	518.247
$^{36}S+^{48}Ca$	EvR	authors' table [205, 206][1] $E_{c.m.}$	64.52	36.87	0.00062	0.00035	0.008
			65.43	37.39	0.0025	0.0006	0.020
			66.33	37.90	0.0088	0.0020	0.049
			67.22	38.41	0.0296	0.0042	0.123
			68.13	38.93	0.104	0.014	0.313
			69.02	39.44	0.333	0.025	0.779
			69.91	39.95	1.107	0.077	1.920
			70.80	40.46	3.333	0.219	4.605
			71.70	40.97	8.571	0.538	10.463
			72.57	41.47	16.61	0.76	21.433
			73.48	41.99	35.47	1.48	40.034
			74.38	42.50	60.79	2.56	65.217
			75.25	43.00	83.83	2.20	94.742
			76.16	43.52	124.6	3.1	128.146
			77.03	44.02	150.9	3.9	161.125
			78.84	45.05	213.3	5.2	228.131
			82.43	47.10	323.1	8.2	351.777
			85.44	48.82	423.1	7.7	445.386
			88.43	50.53	533.4	7.2	530.356
			91.42	52.24	612.2	9.7	608.177
			94.43	53.96	699.0	13.4	680.034
			97.42	55.67	799.6	14.8	745.768
			100.43	57.39	840.4	14.7	806.736
			103.42	59.10	915.2	11.3	862.737
			106.42	60.81	972.7	12.1	914.577
$^{36}S+^{64}Ni$	EvR	authors' table [206] $E_{c.m.}$	80.67	51.63	0.0028	0.0013	0.009
			81.17	51.95	0.0070	0.0016	0.016
			81.67	52.27	0.013	0.002	0.027
			82.17	52.59	0.031	0.005	0.048
			82.67	52.91	0.063	0.008	0.084
			83.17	53.23	0.158	0.016	0.147
			83.67	53.55	0.323	0.032	0.257
			84.17	53.87	0.639	0.055	0.446
			85.17	54.51	2.01	0.12	1.318
			86.06	55.08	6.41	0.29	3.287
			87.06	55.72	17.14	0.43	8.251
			88.67	56.75	35.06	1.22	26.253
			89.67	57.39	71.56	2.09	44.563
			90.67	58.03	92.48	2.05	67.729
			92.38	59.12	139.1	2.8	115.419
			94.38	60.40	201.0	4.4	178.615

Continued on next page

[1]The experiment was reported in Ref. [205] and the data were shown in graphs. The data were given in tables in Ref. [206]

Table 2 (continued)

Reaction	Detected particles	Data obtained	$E_{\rm lab}$ (MeV)	$E_{\rm c.m.}$ (MeV)	σ (mb)	$\delta\sigma$ (mb)	$\sigma^{\rm cal}$ (mb)
			96.27	61.61	259.4	3.9	240.146
			98.38	62.96	312.0	5.9	307.316
			100.47	64.30	379.7	6.3	371.054
			102.56	65.64	446.5	3.9	431.586
			107.47	68.78	548.3	9.6	561.621
			110.47	70.70	590.3	8.9	633.790
			119.47	76.46	672.4	13.3	822.240
			129.47	82.86	788.9	35.9	991.680
^{36}S+^{90}Zr	EvR	authors' table	103.18	73.7	0.090	0.021	0.190
		[207]	103.88	74.2	0.18	0.05	0.414
		$E_{\rm c.m.}$	104.58	74.7	0.88	0.07	0.881
			105.28	75.2	2.28	0.16	1.802
			105.98	75.7	4.85	0.27	3.502
			106.68	76.2	9.12	0.30	6.400
			107.38	76.7	17.4	0.77	10.939
			108.08	77.2	27.3	0.70	17.480
			108.78	77.7	42.5	1.0	26.223
			109.48	78.2	61.9	1.2	37.182
			110.18	78.7	80.8	1.6	50.219
			110.88	79.2	97.5	1.9	65.096
			111.58	79.7	117.0	2.2	81.523
			112.28	80.2	140.2	3.8	99.187
			112.98	80.7	161.5	3.0	117.787
			113.68	81.2	176.5	3.4	137.043
			114.38	81.7	207.5	4.1	156.714
			115.08	82.2	223.1	4.2	176.601
			115.78	82.7	251.5	4.8	196.549
			116.48	83.2	273.4	5.3	216.440
			117.18	83.7	299.6	5.5	236.191
			117.88	84.2	317.6	4.8	255.744
			118.58	84.7	357.4	5.4	275.064
			119.14	85.1	367.6	4.7	290.336
			119.98	85.7	392.2	5.2	312.923
			120.68	86.2	411.5	5.8	331.448
			121.38	86.7	425.1	6.4	349.700
			122.08	87.2	469.7	5.0	367.681
^{36}S+^{96}Zr	EvR	authors' table	97.76	71.1	0.067	0.011	0.045
		[207]	98.45	71.6	0.22	0.05	0.104
		$E_{\rm c.m.}$	99.14	72.1	0.27	0.05	0.238
			99.83	72.6	1.45	0.10	0.529
			100.51	73.1	3.88	0.16	1.121
			101.20	73.6	9.65	0.31	2.231
			102.03	74.2	16.6	0.44	4.617
			102.71	74.7	26.4	0.65	7.797
			103.40	75.2	35.3	0.80	12.284
			104.09	75.7	47.4	1.0	18.161
			104.78	76.2	67.4	1.4	25.414
			105.46	76.7	82.8	1.8	34.007
			106.15	77.2	95.9	1.7	43.875
			106.84	77.7	122.0	2.4	54.949
			107.53	78.2	147.5	2.1	67.160
			108.21	78.7	176.0	3.1	80.424
			108.90	79.2	200.3	2.5	94.665
			109.59	79.7	220.9	3.8	109.801
			110.28	80.2	249.0	4.3	125.744
			111.10	80.8	273.7	4.8	145.834
			111.79	81.3	300.4	4.9	163.272
			112.47	81.8	326.2	5.6	181.262
			113.16	82.3	344.7	6.1	199.727
			113.85	82.8	368.7	6.2	218.591
			114.54	83.3	387.1	7.1	237.788
			115.22	83.8	400.6	6.5	257.248
			115.91	84.3	434.0	7.3	276.913
			116.60	84.8	453.5	6.6	296.725
			117.43	85.4	482.4	6.2	320.620
			118.11	85.9	504.4	6.8	340.580

Continued on next page

Table 2 (continued)

Reaction	Detected particles	Data obtained	E_{lab} (MeV)	$E_{c.m.}$ (MeV)	σ (mb)	$\delta\sigma$ (mb)	σ^{cal} (mb)
			118.80	86.4	543.4	7.5	360.536
			119.21	86.7	545.8	5.7	372.493
			120.18	87.4	586.2	6.6	400.297
$^{36}S+^{92}Mo$	EvR	authors' table	105.18	75.6	≤ 0.016	—	0.027
		[195]	106.16	76.3	0.13	0.04	0.081
		$E_{c.m.}$	107.69	77.4	0.28	0.23	0.424
			109.63	78.8	2.00	0.37	2.732
			114.64	82.4	40.2	6.2	51.992
			119.65	86.0	129	19	172.043
$^{36}S+^{94}Mo$	EvR	authors' table	103.72	75.0	0.019	0.009	0.002
		[195]	104.14	75.3	0.076	0.023	0.004
		$E_{c.m.}$	105.11	76.0	0.132	0.049	0.011
			106.21	76.8	0.80	0.22	0.042
			107.60	77.8	2.37	0.61	0.216
			109.67	79.3	8.0	2.0	2.178
			114.65	82.9	90	20	55.190
			119.63	86.5	222	48	177.086
$^{36}S+^{96}Mo$	EvR	authors' table	103.68	75.4	0.027	0.005	0.010
		[195]	104.22	75.8	0.077	0.013	0.020
		$E_{c.m.}$	106.15	77.2	2.89	0.43	0.200
			107.66	78.3	5.48	0.82	1.133
			109.72	79.8	15.7	2.4	8.088
			114.67	83.4	102	15	83.542
			119.62	87.0	222	33	212.960
$^{36}S+^{98}Mo$	EvR	authors' table	103.64	75.8	0.137	0.019	0.183
		[195]	104.19	76.2	0.508	0.070	0.348
		$E_{c.m.}$	105.15	76.9	2.56	0.34	1.013
			107.75	78.8	15.8	1.9	9.776
			109.66	80.2	51.0	6.0	27.826
			114.72	83.9	152	18	121.179
			119.64	87.5	277	33	249.846
$^{36}S+^{100}Mo$	EvR	authors' table	101.59	74.7	0.047	0.008	0.137
		[195]	103.63	76.2	1.26	0.21	1.319
		$E_{c.m.}$	104.18	76.6	3.60	0.59	2.212
			105.13	77.3	8.4	1.4	4.894
			106.22	78.1	15.9	2.6	10.330
			107.71	79.2	32.2	5.3	22.784
			109.62	80.6	71.5	11.0	46.696
			114.65	84.3	174	29	145.192
			119.68	88.0	382	63	275.721
$^{36}S+^{100}Ru$	EvR	authors' table	105.13	77.3	0.006	0.002	0.005
		[195]	106.22	78.1	0.015	0.005	0.019
		$E_{c.m.}$	106.90	78.6	0.055	0.015	0.044
			107.71	79.2	0.244	0.068	0.118
			109.62	80.6	2.64	0.49	1.023
			111.66	82.1	9.3	1.9	6.520
			114.65	84.3	41.3	8.0	33.961
			119.68	88.0	133	26	129.795
$^{36}S+^{101}Ru$	EvR	authors' table	105.53	77.8	0.021	0.008	0.021
		[195]	106.21	78.3	0.055	0.009	0.047
		$E_{c.m.}$	106.89	78.8	0.171	0.028	0.107
			107.70	79.4	0.397	0.059	0.278
			109.74	80.9	3.81	0.56	2.390
			111.63	82.3	15.9	2.4	10.496
			114.75	84.6	67.3	9.6	44.834
			119.64	88.2	183	26	142.538
$^{36}S+^{102}Ru$	EvR	authors' table	106.21	78.5	0.099	0.008	0.094
		[195]	106.88	79.0	0.268	0.024	0.209
		$E_{c.m.}$	107.69	79.6	0.835	0.074	0.531
			109.72	81.1	4.78	0.42	3.914
			111.62	82.5	32.9	1.7	14.559
			114.73	84.8	63.2	5.5	52.980
			119.74	88.5	164	14	157.662
$^{36}S+^{103}Rh$	EvR	authors' table	107.69	79.8	0.023	0.012	0.041
		[195]	109.72	81.3	1.07	0.10	0.441
		$E_{c.m.}$	114.71	85.0	26.6	2.5	22.842

Continued on next page

Table 2 (continued)

Reaction	Detected particles	Data obtained	$E_{\rm lab}$ (MeV)	$E_{\rm c.m.}$ (MeV)	σ (mb)	$\delta\sigma$ (mb)	$\sigma^{\rm cal}$ (mb)
			119.70	88.7	91.8	8.9	104.796
^{36}S+^{104}Pd	EvR	authors' table	109.71	81.5	0.013	0.010	0.029
		[195]	111.73	83.0	0.57	0.17	0.311
		$E_{\rm c.m.}$	114.69	85.2	10.3	2.7	5.615
			119.67	88.9	76	21	59.893
^{36}S+^{104}Ru	EvR	authors' table	103.65	77.0	0.011	0.003	0.039
		[195]	104.19	77.4	0.063	0.005	0.076
		$E_{\rm c.m.}$	105.13	78.1	0.225	0.019	0.231
			106.21	78.9	0.93	0.22	0.757
			106.88	79.4	1.53	0.09	1.482
			107.69	80.0	3.23	0.13	3.040
			109.71	81.5	13.0	2.3	12.207
			111.73	83.0	33.0	1.9	30.998
			114.69	85.2	85	12	74.725
			119.67	88.9	229	10	181.219
^{36}S+^{105}Pd	EvR	authors' table	109.44	81.5	0.033	0.009	0.041
		[195]	111.46	83.0	0.93	0.20	0.439
		$E_{\rm c.m.}$	114.68	85.4	11.9	2.6	8.407
			119.65	89.1	77	17	69.077
^{36}S+^{106}Pd	EvR	authors' table	107.71	80.4	0.004	0.001	0.008
		[195]	109.72	81.9	0.078	0.009	0.094
		$E_{\rm c.m.}$	111.72	83.4	1.45	0.13	0.935
			114.67	85.6	15.8	1.6	11.126
			119.63	89.3	78.0	6.3	77.373
^{36}S+^{108}Pd	EvR	authors' table	106.13	79.6	0.002	0.001	0.004
		[195]	107.73	80.8	0.024	0.003	0.030
		$E_{\rm c.m.}$	109.73	82.3	0.440	0.040	0.343
			111.73	83.8	3.69	0.33	2.763
			114.67	86.0	23.6	2.1	20.158
			119.73	89.8	92.2	8.0	100.108
^{36}S+^{110}Pd	EvR	authors' table	105.25	79.3	0.012	0.003	0.006
		[195]	107.64	81.1	0.159	0.012	0.126
		$E_{\rm c.m.}$	109.63	82.6	1.59	0.11	1.201
			111.62	84.1	9.57	0.84	6.654
			114.68	86.4	43.2	3.8	32.887
			119.72	90.2	115	10	121.578
^{36}S+^{204}Pb	FF	authors' graph	162.845	138.419	3.310	—	2.091
		[199]	164.047	139.440	7.903	—	4.605
		$E_{\rm c.m.}$	164.877	140.145	11.199	—	7.416
			165.871	140.991	21.087	—	12.254
			166.825	141.801	30.610	—	18.588
			167.861	142.682	43.062	—	27.495
			168.773	143.457	58.811	—	37.060
			169.851	144.373	74.193	—	50.336
			170.846	145.219	91.406	—	64.341
			171.841	146.065	111.550	—	79.860
			172.794	146.875	127.665	—	95.993
			173.831	147.756	150.006	—	114.737
			174.826	148.602	165.754	—	133.724
			175.779	149.412	191.025	—	152.664
			176.815	150.293	208.605	—	173.896
			177.810	151.139	225.819	—	194.748
			179.759	152.795	267.937	—	236.382
			181.749	154.486	313.718	—	279.260
			183.946	156.354	357.301	—	326.256
			185.811	157.939	384.769	—	365.474
			188.050	159.842	422.127	—	411.435
			189.791	161.322	468.274	—	446.263
			192.817	163.894	503.433	—	504.810
			198.786	168.968	614.039	—	613.060
			204.051	173.443	663.483	—	701.015
			210.518	178.940	757.974	—	800.136
^{36}S+^{238}U	FF	authors' graph	169.482	147.215	1.408	—	2.147

Continued on next page

Table 2 (continued)

Reaction	Detected particles	Data obtained	$E_{\rm lab}$ (MeV)	$E_{\rm c.m.}$ (MeV)	σ (mb)	$\delta\sigma$ (mb)	$\sigma^{\rm cal}$ (mb)
		[208][1]	174.411	151.495	11.189	—	22.991
		$E_{\rm c.m.}$	180.336	156.642	47.652	—	86.533
			187.177	162.585	222.438	—	200.045
			199.160	172.993	407.450	—	450.915
^{37}Cl+^{24}Mg	EvR	authors' table	64.56	25.4	1.4	—	0.351
		[202]	66.08	26.0	3.4	—	0.994
		$E_{\rm c.m.}$	67.61	26.6	5.5	—	2.694
			69.13	27.2	13.1	—	6.704
			70.66	27.8	18.2	—	14.751
			72.18	28.4	30.6	—	28.288
			73.71	29.0	51.9	—	47.830
			75.23	29.6	69.3	—	73.081
			77.27	30.4	99.8	—	114.438
			79.30	31.2	151.2	—	162.791
			83.11	32.7	236.4	—	265.500
			88.20	34.7	349.4	—	410.836
^{37}Cl+^{25}Mg	EvR	authors' table	65.47	26.4	1.1	—	2.434
		[202]	66.96	27.0	8.6	—	6.247
		$E_{\rm c.m.}$	68.70	27.7	12.3	—	16.139
			70.18	28.3	23.4	—	31.251
			71.67	28.9	37.2	—	53.119
			73.16	29.5	66.3	—	81.324
			74.65	30.1	99.7	—	114.978
			76.14	30.7	131.8	—	153.026
			78.12	31.5	183.3	—	208.738
			80.10	32.3	230.2	—	267.981
			84.07	33.9	341.4	—	389.436
			89.03	35.9	449.8	—	534.449
^{37}Cl+^{26}Mg	EvR	authors' table	64.45	26.6	2.3	—	3.823
		[202]	66.15	27.3	8.7	—	11.131
		$E_{\rm c.m.}$	67.60	27.9	17.6	—	23.747
			69.06	28.5	31.0	—	43.595
			70.51	29.1	51.5	—	70.589
			71.97	29.7	77.8	—	103.853
			73.66	30.4	107.1	—	148.998
			75.12	31.0	121.4	—	191.695
			77.05	31.8	166.6	—	252.237
			78.99	32.6	221.0	—	314.715
			83.11	34.3	311.9	—	446.072
			88.20	36.4	427.6	—	595.158
^{37}Cl+^{59}Co	EvR	authors' table	90.1	55.4	0.5	0.3	0.474
		[182]	91.5	56.2	1.9	0.7	1.705
		$E_{\rm lab}$ & $E_{\rm c.m.}$	93.0	57.2	7.3	1.0	6.968
			94.5	58.1	21	2	18.655
			97.6	60.0	68	2	69.773
			98.6	60.6	100	5	92.166
			99.1	60.9	96	10	104.198
			101.6	62.4	126	12	170.160
			102.8	63.2	181	10	207.644
			104.0	63.9	225	38	240.880
			106.8	65.6	272	12	320.930
			110.8	68.1	376	19	432.376
			114.8	70.6	396	18	534.386
^{37}Cl+^{70}Ge	EvR	authors' table	95.49	62.47	0.065	0.031	0.045
		[209]	97.49	63.78	0.51	0.14	0.394
		$E_{\rm c.m.}$	99.46	65.07	3.67	0.28	2.612
			101.39	66.33	13.25	0.88	10.560
			103.24	67.54	31.4	2.2	26.855
			103.24	67.54	35.2	2.4	26.855
			105.10	68.76	59.8	3.9	51.978
			107.02	70.01	88.7	5.2	85.581
			108.97	71.29	120.8	7.1	126.681

Continued on next page

[1] In the authors' graph, the capture excitation function was plotted as a function of the excitation energy $E^*_{\rm CN}$ of the compound nucleus. $E_{\rm c.m.}$ is obtained by $E_{\rm c.m.} = E^*_{\rm CN} - Q$ and $Q = -116.779$ MeV is calculated with the nuclear masses taken from Refs. [102, 103].

Table 2 (continued)

Reaction	Detected particles	Data obtained	E_{lab} (MeV)	$E_{c.m.}$ (MeV)	σ (mb)	$\delta\sigma$ (mb)	σ^{cal} (mb)
			110.97	72.60	165.3	6.9	174.015
			112.96	73.90	205.4	9.3	224.581
			114.95	75.20	249.9	8.6	277.228
$^{37}Cl+^{72}Ge$	EvR	authors' table	95.81	63.29	0.201	0.034	0.220
		[209]	97.80	64.60	1.72	0.37	1.686
		$E_{c.m.}$	97.80	64.60	1.72	0.16	1.686
			99.77	65.90	9.33	0.76	8.245
			101.70	67.18	30.4	1.7	24.270
			103.64	68.46	58.6	2.5	50.584
			103.64	68.46	57.8	2.5	50.584
			105.61	69.76	93.4	4.0	86.441
			107.59	71.07	131.7	4.9	129.976
			109.59	72.39	190	10	179.326
			109.59	72.39	180.3	7.6	179.326
			111.60	73.72	234.9	8.1	232.658
			113.59	75.03	281	11	287.062
			115.59	76.35	310	11	342.426
$^{37}Cl+^{73}Ge$	EvR	authors' table	95.81	63.58	1.94	0.31	0.437
		[209]	97.81	64.91	5.52	0.47	3.069
		$E_{c.m.}$	99.81	66.24	16.22	0.97	12.964
			99.81	66.24	16.9	1.1	12.964
			101.83	67.58	36.1	2.1	34.169
			103.82	68.90	59.8	3.4	65.654
			105.83	70.23	87.3	4.9	106.190
			107.83	71.56	121.1	5.4	153.482
			109.83	72.89	156.7	7.2	205.454
			111.84	74.22	204.0	6.6	260.224
			113.33	75.21	238	21	301.866
			115.83	76.87	292	16	371.837
$^{37}Cl+^{74}Ge$	EvR	authors' table	95.73	63.82	2.36	0.39	0.782
		[209]	97.73	65.15	6.82	0.73	4.852
		$E_{c.m.}$	99.73	66.49	18.2	1.8	17.869
			101.75	67.83	43.4	2.9	42.425
			103.74	69.16	70.9	4.0	77.100
			105.75	70.50	108.7	5.7	120.427
			107.75	71.83	163.4	8.3	169.621
			109.74	73.16	204	12	222.936
			111.75	74.50	265	13	278.991
$^{37}Cl+^{76}Ge$	EvR	authors' table	93.64	62.98	0.506	0.040	0.106
		[209]	95.65	64.33	3.26	0.44	0.978
		$E_{c.m.}$	95.65	64.33	3.24	0.31	0.978
			95.65	64.33	3.19	0.18	0.978
			97.64	65.67	12.4	1.1	6.450
			99.65	67.02	28.6	2.1	24.182
			101.67	68.38	48.5	3.0	57.038
			103.66	69.72	82.7	5.1	101.479
			105.66	71.06	138.0	7.7	154.081
			107.66	72.41	190.1	9.0	211.672
			109.15	73.41	250	11	255.553
			111.65	75.09	287	19	329.088
			111.65	75.09	288	17	329.088
			111.65	75.09	296	15	329.088
$^{37}Cl+^{93}Nb$	EvR	authors' graph	114.234	81.721	1.840	—	0.990
		[210]	117.318	83.928	18.234	—	14.404
		$E_{c.m.}$	120.203	85.991	85.076	—	55.014
			120.716	86.358	81.531	—	64.868
			123.833	88.588	116.562	—	135.743
			126.813	90.720	154.355	—	211.940
			129.929	92.949	224.464	—	291.785
$^{37}Cl+^{98}Mo$	EvR	authors' graph	114.238	82.928	3.461	—	5.049
		[210]	117.391	85.217	21.874	—	29.761
		$E_{c.m.}$	120.278	87.313	58.832	—	73.481
			120.614	87.557	63.616	—	79.676
			123.542	89.682	111.061	—	141.176
			126.513	91.839	135.145	—	213.352
			129.393	93.930	211.165	—	287.793

Continued on next page

Table 2 (continued)

Reaction	Detected particles	Data obtained	E_{lab} (MeV)	$E_{c.m.}$ (MeV)	σ (mb)	$\delta\sigma$ (mb)	σ^{cal} (mb)
$^{37}Cl+^{100}Mo$	EvR	authors' graph	114.579	83.634	9.757	—	17.927
		[210]	117.558	85.809	48.382	—	52.634
		$E_{c.m.}$	120.609	88.036	87.157	—	105.361
			120.579	88.014	101.772	—	104.769
			123.488	90.137	115.994	—	167.132
			125.576	91.661	195.165	—	217.030
			126.478	92.320	185.953	—	239.532
			129.518	94.539	250.231	—	317.834
$^{40}Ar+^{112}Sn$	EvRFF	authors' table	131.10	96.6	0.00836	0.0035	0.003
		[40]	132.73	97.8	0.0446	0.0082	0.016
		$E_{c.m.}$	135.04	99.5	0.479	0.051	0.180
			135.04	99.5	0.634	0.058	0.180
			136.66	100.7	2.17	0.098	0.797
			140.33	103.4	15.3	0.52	10.084
			142.77	105.2	34.6	1.1	30.089
			145.21	107.0	64.2	2.3	63.632
			147.52	108.7	99.8	3.5	105.163
			148.74	109.6	121	4.9	129.809
			150.91	111.2	159	4.9	176.239
			154.58	113.9	219	7.7	256.942
			158.92	117.1	310	9.3	349.694
			163.40	120.4	352	11	439.169
			170.86	125.9	478	15	574.382
$^{40}Ar+^{116}Sn$	EvRFF	authors' table	128.70	95.7	0.00383	0.0011	1.334E − 4
		[40]	130.58	97.1	0.0497	0.0052	0.001
		$E_{c.m.}$	132.47	98.5	2.94	0.015	0.012
			134.48	100.0	1.74	0.073	0.119
			134.62	100.1	1.93	0.066	0.139
			136.37	101.4	6.17	0.18	0.864
			140.00	104.1	25.6	0.79	14.034
			142.15	105.7	44.4	1.4	37.771
			147.12	109.4	118	6.8	132.741
			150.89	112.2	188	10	218.841
			154.52	114.9	267	14	300.363
			158.29	117.7	321	15	380.252
			162.86	121.1	372	16	470.677
			170.52	126.8	513	19	607.596
$^{40}Ar+^{122}Sn$	EvRFF	authors' table	124.82	94.0	0.00183	0.00056	2.840E − 5
		[40]	127.08	95.7	0.0235	0.0027	4.610E − 4
		$E_{c.m.}$	129.33	97.4	0.182	0.011	0.007
			131.59	99.1	1.36	0.068	0.109
			132.52	99.8	3.05	0.11	0.307
			134.78	101.5	9.29	0.31	2.743
			135.44	102.0	13.2	0.42	4.678
			136.90	103.1	21.9	0.69	12.561
			139.03	104.7	42.7	1.4	35.379
			141.55	106.6	77.1	2.3	78.975
			143.41	108.0	110	3.5	118.946
			148.19	111.6	202	6.3	232.269
			151.78	114.3	294	9	315.766
			155.36	117.0	372	11	394.627
			159.21	119.9	437	12	474.095
			163.86	123.4	504	15	563.319
			171.43	129.1	661	27	694.575
$^{40}Ar+^{144}Sm$	EvRFF	authors' table	148.99	116.6	0.00161	0.00040	0.001
		[40]	151.29	118.4	0.0519	0.0076	0.022
		$E_{c.m.}$	153.21	119.9	0.367	0.013	0.172
			155.12	121.4	1.75	0.066	1.028
			156.53	122.5	3.90	0.15	3.069
			158.70	124.2	11.7	1.5	11.486
			163.30	127.8	51.2	2.1	60.452
			167.26	130.9	95.7	5.1	130.123
			171.09	133.9	160	10	208.176
			175.44	137.3	252	19	297.746
			178.89	140.0	322	25	366.068
$^{40}Ar+^{148}Sm$	EvRFF	authors' table	143.16	112.7	0.000793	0.00049	7.340E − 5

Continued on next page

Table 2 (continued)

Reaction	Detected particles	Data obtained	$E_{\rm lab}$ (MeV)	$E_{\rm c.m.}$ (MeV)	σ (mb)	$\delta\sigma$ (mb)	$\sigma^{\rm cal}$ (mb)
		[40]	145.95	114.9	0.0195	0.0020	0.003
		$E_{\rm c.m.}$	147.99	116.5	0.130	0.0075	0.032
			149.51	117.7	0.333	0.019	0.183
			151.29	119.1	1.09	0.034	1.066
			154.97	122.0	5.11	0.36	12.009
			158.66	124.9	20.6	1.0	43.268
			163.23	128.5	59.7	3.8	106.928
			167.29	131.7	112	7.5	180.164
			171.11	134.7	178	10	257.319
			175.30	138.0	274	17	346.290
			178.73	140.7	353	24	419.348
^{40}Ar+^{154}Sm	EvRFF	authors' table	137.06	108.8	0.00158	0.00088	3.260E − 5
		[40]	138.70	110.1	0.0185	0.0029	2.717E − 4
		$E_{\rm c.m.}$	140.21	111.3	0.0720	0.0068	0.002
			142.48	113.1	0.337	0.023	0.027
			145.37	115.4	1.51	0.047	0.502
			147.39	117.0	3.45	0.10	2.370
			149.03	118.3	5.63	0.19	6.211
			151.04	119.9	10.3	0.33	15.059
			154.70	122.8	24.5	1.1	45.164
			158.22	125.6	49.2	1.9	88.886
			163.39	129.7	99.0	4.3	173.672
			167.29	132.8	165	8.2	249.529
			170.82	135.6	235	6.4	323.613
			175.10	139.0	332	17	417.268
			178.51	141.7	407	22	492.427
^{40}Ca+^{40}Ca	EvR	authors' graph	98.994	49.497	0.220	—	0.106
		[211]	99.966	49.983	0.500	—	0.230
		$E_{\rm c.m.}$	100.919	50.459	0.855	—	0.489
			101.872	50.936	1.416	—	1.034
			102.882	51.441	2.950	—	2.245
			103.952	51.976	6.789	—	4.903
			104.904	52.452	15.387	—	9.323
			105.934	52.967	29.472	—	17.305
			106.965	53.482	54.752	—	29.356
			108.986	54.493	104.874	—	64.514
			110.911	55.456	156.080	—	107.440
			113.807	56.904	228.764	—	176.908
			123.760	61.880	431.532	—	392.293
			128.756	64.378	487.692	—	484.298
			133.733	66.866	551.161	—	566.975
^{40}Ca+^{44}Ca	EvR	authors' graph	91.025	47.680	0.099	—	0.022
		[211]	92.973	48.700	0.426	—	0.114
		$E_{\rm c.m.}$	93.975	49.225	1.427	—	0.266
			94.903	49.711	3.234	—	0.580
			95.961	50.265	6.738	—	1.383
			96.851	50.732	9.800	—	2.802
			98.855	51.781	28.367	—	11.618
			101.861	53.356	63.313	—	52.348
			103.717	54.328	109.797	—	93.845
			108.913	57.050	245.061	—	227.888
			113.811	59.615	330.206	—	345.367
			118.766	62.211	373.180	—	451.536
			123.720	64.806	483.977	—	546.645
			128.656	67.391	451.791	—	631.858
			134.130	70.259	243.195	—	716.690
^{40}Ca+^{46}Ti	EvR	authors' graph	101.209	54.135	0.425	—	0.155
		[212]	102.162	54.645	0.932	—	0.350
		$E_{\rm c.m.}$	103.223	55.212	2.547	—	0.855
			104.169	55.718	6.001	—	1.860
			105.192	56.266	11.604	—	4.141
			106.215	56.812	17.235	—	8.628
			107.237	57.359	32.781	—	16.454
			108.222	57.886	43.384	—	27.903
			109.244	58.433	68.831	—	43.958
			110.229	58.960	85.281	—	62.892

Continued on next page

Table 2 (continued)

Reaction	Detected particles	Data obtained	$E_{\rm lab}$ (MeV)	$E_{\rm c.m.}$ (MeV)	σ (mb)	$\delta\sigma$ (mb)	$\sigma^{\rm cal}$ (mb)
			111.290	59.527	105.662	—	86.096
			112.274	60.054	124.598	—	109.286
			113.297	60.601	154.376	—	134.196
			114.319	61.148	167.639	—	159.350
			116.327	62.221	221.860	—	208.092
			118.334	63.295	261.619	—	255.125
			120.341	64.368	313.631	—	300.189
			122.311	65.422	351.991	—	342.538
			124.356	66.516	395.044	—	384.657
			128.294	68.623	489.455	—	460.802
			132.271	70.750	567.734	—	531.635
			136.248	72.877	637.174	—	596.998
			140.262	75.024	703.416	—	657.981
			144.277	77.171	739.077	—	714.413
			148.291	79.319	715.108	—	766.705
^{40}Ca+^{48}Ca	EvR	authors' graph [211] $E_{\rm c.m.}$	88.054	48.029	0.495	—	0.236
			89.034	48.564	0.664	—	0.558
			89.961	49.070	2.075	—	1.220
			90.977	49.624	4.226	—	2.734
			91.903	50.129	8.540	—	5.388
			93.846	51.188	22.725	—	18.022
			95.841	52.277	40.017	—	45.509
			96.839	52.821	71.008	—	65.078
			98.889	53.939	97.154	—	114.370
			103.842	56.641	200.879	—	250.201
			108.760	59.324	281.222	—	376.080
			108.939	59.421	317.820	—	380.372
			118.668	64.728	448.350	—	589.505
			123.764	67.508	510.588	—	682.040
^{40}Ca+^{48}Ti	EvR	authors' graph [212] $E_{\rm c.m.}$	98.516	53.736	0.344	—	0.137
			99.478	54.261	0.836	—	0.319
			100.602	54.874	2.236	—	0.844
			101.564	55.399	6.124	—	1.903
			102.580	55.953	10.381	—	4.305
			103.650	56.536	21.322	—	9.433
			104.559	57.032	28.435	—	16.946
			105.201	57.382	39.786	—	24.371
			106.538	58.112	62.761	—	45.656
			107.608	58.695	83.699	—	67.554
			108.784	59.337	111.622	—	95.057
			109.586	59.774	125.848	—	115.012
			110.602	60.329	148.861	—	140.921
			111.779	60.970	171.908	—	171.066
			112.688	61.466	198.523	—	194.137
			113.009	61.641	203.343	—	202.206
			114.613	62.516	246.367	—	241.791
			116.592	63.596	291.418	—	288.779
			118.624	64.704	336.536	—	334.935
			120.657	65.813	370.432	—	379.061
			122.635	66.892	407.742	—	420.181
			124.614	67.971	459.707	—	459.589
			128.625	70.159	530.880	—	534.577
			132.636	72.347	627.957	—	603.587
			136.647	74.535	691.205	—	667.223
			140.658	76.723	760.822	—	726.009
			144.723	78.940	798.218	—	781.090
			148.734	81.127	779.296	—	831.427
^{40}Ca+^{50}Ti	EvR	authors' graph [212] $E_{\rm c.m.}$	96.267	53.481	0.429	—	0.182
			97.429	54.127	1.047	—	0.525
			98.374	54.652	2.779	—	1.215
			99.423	55.235	5.543	—	2.955
			100.421	55.789	9.585	—	6.435
			101.418	56.343	17.384	—	12.834
			102.416	56.898	30.059	—	23.165
			103.465	57.481	41.953	—	38.774
			104.463	58.035	58.551	—	57.795

Continued on next page

Table 2 (continued)

Reaction	Detected particles	Data obtained	$E_{\rm lab}$ (MeV)	$E_{\rm c.m.}$ (MeV)	σ (mb)	$\delta\sigma$ (mb)	$\sigma^{\rm cal}$ (mb)
			105.145	58.414	69.171	—	72.744
			106.458	59.143	94.266	—	104.578
			107.612	59.785	116.796	—	134.503
			108.452	60.251	137.979	—	156.686
			109.502	60.834	163.005	—	184.404
			110.499	61.389	183.614	—	210.440
			111.444	61.914	206.829	—	234.693
			112.442	62.468	222.144	—	259.784
			113.439	63.022	244.343	—	284.329
			114.489	63.605	262.436	—	309.574
			116.536	64.742	310.035	—	357.112
			118.479	65.821	349.235	—	400.226
			120.526	66.959	393.389	—	443.705
			122.521	68.067	432.700	—	484.233
			124.463	69.146	475.939	—	522.051
			128.505	71.392	549.032	—	595.935
			132.494	73.608	648.613	—	663.019
			136.484	75.824	730.619	—	724.882
			140.473	78.041	748.226	—	782.031
			144.620	80.345	766.257	—	836.907
			148.610	82.561	713.428	—	885.736
^{40}Ca+^{58}Ni	EvR	authors' table [213] $E_{\rm c.m.}$	113.89	67.4043	0.0452063	0.0185513	0.080
			115.14	68.1441	0.136136	0.0434224	0.252
			116.39	68.8839	0.514438	0.0966851	0.771
			117.64	69.6237	2.5846	0.154385	2.222
			118.90	70.3694	8.24477	0.431715	5.819
			120.15	71.1092	17.5668	0.920312	13.125
			121.40	71.849	28.655	1.3522	25.428
			122.65	72.5888	45.1693	2.14054	42.959
			123.90	73.3286	65.1941	3.08011	64.967
			125.16	74.0743	82.6049	3.93189	90.426
			127.66	75.5539	118.789	5.3897	145.786
			130.17	77.0394	170.833	7.74169	202.366
			132.67	78.519	199.303	8.9576	256.860
			135.18	80.0045	235.982	10.6673	309.059
			137.68	81.4841	293.919	13.1304	358.569
			140.18	82.9637	311.411	13.893	405.737
			142.69	84.4492	391.593	17.494	450.878
			145.19	85.9288	471.873	37.0391	493.765
			147.70	87.4143	492.335	38.4844	534.861
			150.20	88.8939	510.356	39.8958	573.951
			152.71	90.3794	556.167	43.432	611.450
^{40}Ca+^{64}Ni	EvR	authors' table [213] $E_{\rm c.m.}$	103.90	63.9385	0.0479657	0.0129742	0.013
			105.15	64.7077	0.0989459	0.0174628	0.045
			106.41	65.4831	0.377938	0.0584998	0.151
			107.66	66.2523	1.23054	0.13627	0.478
			108.91	67.0215	4.59769	0.464655	1.379
			110.16	67.7908	7.87834	0.487811	3.536
			111.42	68.5662	15.6649	0.796171	7.961
			112.67	69.3354	27.6629	1.37448	15.539
			113.92	70.1046	39.6533	2.05691	26.880
			115.17	70.8738	54.5242	2.83184	42.063
			116.43	71.6492	75.8496	2.79015	60.964
			117.68	72.4185	96.315	4.40567	82.826
			120.18	73.9569	139.434	6.51987	133.702
			122.69	75.5015	190.343	9.02277	190.803
			125.19	77.04	241.534	11.2115	250.038
			127.70	78.5846	266.7	11.8037	309.331
			130.20	80.1231	316.888	14.3233	366.767
			132.71	81.6677	327.181	14.7511	422.141
			135.21	83.2062	342.691	15.6016	474.815
			137.72	84.7508	393.621	17.6151	525.230
			140.22	86.2892	433.909	19.3776	573.090
			142.72	87.8277	510.756	22.8318	618.733
			145.23	89.3723	587.969	45.5102	662.452
			147.73	90.9108	618.174	48.1976	704.020

Continued on next page

Table 2 (continued)

Reaction	Detected particles	Data obtained	$E_{\rm lab}$ (MeV)	$E_{\rm c.m.}$ (MeV)	σ (mb)	$\delta\sigma$ (mb)	$\sigma^{\rm cal}$ (mb)
			150.24	92.4554	625.271	48.7673	743.881
			152.74	93.9938	669.571	52.2409	781.817
^{40}Ca+^{90}Zr	EvR	authors' table [214] $E_{\rm lab}$	134.86	93.36	0.84	0.06	1.604
			135.36	93.71	1.05	0.08	2.392
			135.86	94.06	2.00	0.09	3.484
			136.37	94.41	3.40	0.09	4.985
			136.87	94.76	5.26	0.11	6.911
			137.37	95.10	7.41	0.13	9.350
			137.87	95.45	11.0	0.2	12.357
			138.37	95.79	15.0	0.2	15.972
			138.87	96.14	21.0	0.3	20.216
			139.37	96.49	26.8	0.3	25.098
			139.87	96.83	34.3	0.4	30.609
			140.37	97.18	41.4	0.3	36.731
			140.87	97.53	49.1	0.4	43.436
			141.37	97.87	58.8	0.4	50.692
			141.87	98.22	66.8	0.6	58.461
			142.37	98.56	75.7	0.6	66.703
			142.87	98.91	83.8	0.7	75.376
			143.37	99.26	95.0	0.6	84.437
			143.87	99.60	104.4	0.8	93.843
			144.37	99.95	117.7	1.0	103.550
			144.87	100.29	128.1	0.9	113.517
			145.37	100.64	139.2	0.9	123.704
			145.87	100.99	152.7	1.0	134.073
			146.37	101.33	161.4	1.3	144.590
			146.87	101.68	172.5	1.2	155.220
			147.38	102.03	179.3	1.5	166.151
			147.88	102.38	190.5	1.6	176.925
			148.38	102.72	196.8	1.5	187.734
			148.88	103.07	207.6	1.7	198.555
			149.38	103.42	215.3	1.6	209.372
			150.38	104.11	236.3	2.1	230.930
			151.38	104.80	260.1	2.8	252.311
			152.38	105.49	280.4	2.5	273.448
			153.38	106.19	295.0	2.5	294.299
			154.38	106.88	315.1	2.3	314.839
			155.38	107.57	335.0	3.0	335.052
			156.38	108.26	357.6	2.8	354.935
			157.38	108.96	375.1	2.6	374.488
			158.38	109.65	394.1	4.0	393.712
			159.38	110.34	407.0	3.8	412.613
^{40}Ca+^{94}Zr	EvR	authors' graph [86] $E_{\rm c.m.}$	126.307	88.603	0.396	—	0.024
			126.841	88.978	0.527	—	0.042
			127.319	89.313	0.832	—	0.069
			127.833	89.674	1.197	—	0.114
			128.311	90.009	1.737	—	0.179
			128.899	90.422	2.395	—	0.306
			129.414	90.783	3.275	—	0.480
			129.929	91.144	4.293	—	0.738
			130.407	91.479	6.072	—	1.080
			130.921	91.840	7.131	—	1.595
			131.436	92.201	8.884	—	2.304
			131.914	92.537	10.521	—	3.178
			132.429	92.898	12.780	—	4.401
			132.943	93.259	15.788	—	5.962
			133.458	93.620	19.017	—	7.907
			133.899	93.929	22.712	—	9.909
			134.414	94.290	26.002	—	12.664
			134.928	94.651	30.022	—	15.894
			135.443	95.012	35.856	—	19.618
			135.958	95.373	42.106	—	23.843
			136.436	95.709	48.615	—	28.210
			136.914	96.044	56.608	—	32.996
			137.465	96.431	64.809	—	39.025
			137.980	96.792	72.954	—	45.125

Continued on next page

Table 2 (continued)

Reaction	Detected particles	Data obtained	$E_{\rm lab}$ (MeV)	$E_{\rm c.m.}$ (MeV)	σ (mb)	$\delta\sigma$ (mb)	$\sigma^{\rm cal}$ (mb)
			138.494	97.153	82.820	—	51.662
			138.972	97.488	87.870	—	58.109
			139.413	97.797	96.436	—	64.366
			139.928	98.158	105.837	—	72.020
			140.479	98.545	118.135	—	80.620
			140.994	98.906	125.338	—	88.997
			141.472	99.242	137.556	—	97.057
			141.987	99.603	143.497	—	106.019
			142.501	99.964	154.844	—	115.252
			142.942	100.273	164.286	—	123.363
			143.457	100.634	171.382	—	133.036
			143.935	100.969	183.376	—	142.204
			144.450	101.330	192.920	—	152.255
			144.964	101.691	208.176	—	162.470
			145.442	102.027	219.010	—	172.084
			145.994	102.414	228.469	—	183.311
			146.472	102.749	236.329	—	193.139
			146.950	103.084	244.459	—	203.044
			147.464	103.445	252.869	—	213.780
			147.942	103.780	259.366	—	223.801
			148.457	104.141	268.289	—	234.633
			148.898	104.451	275.182	—	243.941
			149.486	104.863	287.066	—	256.371
			150.442	105.534	307.158	—	276.574
			151.435	106.230	325.888	—	297.497
			152.464	106.952	342.849	—	319.069
			153.420	107.623	363.756	—	338.937
			154.449	108.345	385.938	—	360.116
			155.442	109.041	409.472	—	380.296
			156.434	109.737	427.156	—	400.213
			157.427	110.434	438.131	—	419.854
			158.419	111.130	457.052	—	439.208
			159.449	111.852	464.848	—	458.968
			160.441	112.548	480.840	—	477.721
			161.471	113.270	497.382	—	496.855
^{40}Ca+^{96}Zr	EvR	authors' table [214] $E_{\rm lab}$	123.35	87.07	0.16	0.03	0.225
			123.85	87.42	0.24	0.04	0.333
			124.86	88.14	0.57	0.04	0.701
			125.86	88.84	1.23	0.07	1.376
			126.36	89.20	1.72	0.10	1.884
			126.86	89.55	2.34	0.09	2.539
			127.36	89.90	3.26	0.11	3.370
			127.86	90.25	3.88	0.10	4.406
			128.36	90.61	5.44	0.15	5.675
			128.86	90.96	6.72	0.15	7.202
			129.36	91.31	9.30	0.20	9.009
			129.86	91.67	10.9	0.2	11.112
			130.36	92.02	13.5	0.2	13.523
			130.86	92.37	16.5	0.3	16.256
			131.36	92.72	19.9	0.3	19.327
			131.86	93.08	23.8	0.4	22.759
			132.36	93.43	28.0	0.4	26.568
			132.86	93.78	32.8	0.5	30.745
			133.36	94.14	38.0	0.6	35.265
			133.86	94.49	42.9	0.6	40.105
			134.36	94.84	48.9	0.8	45.262
			134.86	95.20	54.6	0.8	50.745
			135.36	95.55	60.4	0.6	56.553
			135.86	95.90	68.4	0.6	62.666
			136.37	96.26	76.3	0.7	69.189
			136.87	96.61	82.0	0.7	75.857
			137.37	96.97	91.0	0.8	82.801
			137.87	97.32	100.1	1.0	90.022
			138.37	97.67	107.7	0.7	97.507
			138.87	98.03	116.8	1.0	105.230
			139.37	98.38	125.5	1.0	113.175

Continued on next page

Table 2 (continued)

Reaction	Detected particles	Data obtained	E_{lab} (MeV)	$E_{c.m.}$ (MeV)	σ (mb)	$\delta\sigma$ (mb)	σ^{cal} (mb)
			139.87	98.73	133.2	1.0	121.341
			140.37	99.08	143.5	1.1	129.732
			140.87	99.44	153.5	1.0	138.339
			141.37	99.79	162.2	1.2	147.139
			141.87	100.14	173.2	1.3	156.114
			142.37	100.50	182.4	1.4	165.255
			142.87	100.85	193.3	1.9	174.567
			143.37	101.20	203.8	1.9	184.042
			143.87	101.56	214.7	2.1	193.666
			144.37	101.91	223.8	1.6	203.417
			145.37	102.61	242.3	1.7	223.270
			146.37	103.32	261.6	2.2	243.570
			147.38	104.03	281.1	2.4	264.424
			148.38	104.74	298.7	2.5	285.349
			149.38	105.44	314.8	2.8	306.510
			150.38	106.15	333.5	2.6	327.816
			151.38	106.86	351.1	3.1	349.228
			152.38	107.56	366.9	3.5	370.697
			153.38	108.27	382.4	4.3	392.159
			154.38	108.97	402.0	3.0	413.591
			155.38	109.68	414.9	3.1	434.943
			156.38	110.39	429.9	3.5	456.181
			157.38	111.09	445.0	3.0	477.284
			158.38	111.80	459.2	4.3	498.216
			159.38	112.50	474.0	4.5	518.960
$^{40}Ca+^{192}Os$	FF	authors' graph [215] $E_{c.m.}$	183.340	151.730	0.075	—	0.031
			184.631	152.798	0.117	—	0.088
			186.125	154.034	0.205	—	0.264
			187.072	154.819	0.329	—	0.499
			188.603	156.085	0.541	—	1.264
			189.842	157.110	0.749	—	2.452
			191.299	158.316	1.805	—	4.846
			192.319	159.161	2.563	—	7.342
			193.850	160.427	4.847	—	12.500
			194.724	161.151	6.751	—	16.241
			196.145	162.327	11.028	—	23.935
			197.494	163.443	15.858	—	32.987
			199.133	164.800	24.773	—	45.687
			200.081	165.584	29.801	—	54.120
			201.793	167.001	41.775	—	70.890
			202.740	167.785	52.213	—	80.952
			204.344	169.112	63.212	—	99.534
			204.927	169.595	72.264	—	106.624
			206.238	170.680	85.831	—	123.187
			206.931	171.253	101.298	—	132.378
			208.279	172.369	113.610	—	150.978
			209.736	173.575	137.545	—	171.820
			210.830	174.480	149.425	—	188.124
			212.178	175.595	169.736	—	208.792
			213.307	176.530	182.061	—	226.451
			214.728	177.706	206.809	—	249.288
			215.822	178.611	220.417	—	267.132
			217.133	179.696	242.526	—	288.781
			218.627	180.933	258.484	—	313.859
			219.647	181.777	279.026	—	331.078
			220.923	182.833	299.287	—	352.707
			222.380	184.039	316.954	—	377.592
			223.401	184.883	337.809	—	394.992
			224.785	186.029	360.038	—	418.604
			226.243	187.235	378.868	—	443.431
			230.069	190.402	427.633	—	507.851
			235.061	194.533	491.992	—	589.490
$^{40}Ca+^{194}Pt$	FF	authors' graph [215] $E_{c.m.}$	192.410	159.519	0.062	—	0.254
			193.771	160.648	0.135	—	0.540
			194.535	161.281	0.328	—	0.803
			195.991	162.488	0.520	—	1.625

Continued on next page

Table 2 (continued)

Reaction	Detected particles	Data obtained	E_{lab} (MeV)	$E_{c.m.}$ (MeV)	σ (mb)	$\delta\sigma$ (mb)	σ^{cal} (mb)
			197.482	163.725	1.860	—	3.127
			198.683	164.720	2.591	—	5.046
			199.956	165.776	4.152	—	8.008
			201.266	166.862	6.324	—	12.287
			202.358	167.767	11.441	—	16.950
			203.886	169.034	14.577	—	25.281
			205.087	170.029	18.691	—	33.377
			206.396	171.115	25.871	—	43.817
			207.451	171.990	32.753	—	53.360
			208.579	172.925	41.465	—	64.635
			209.525	173.709	53.509	—	74.877
			210.799	174.765	68.611	—	89.742
			211.999	175.760	82.018	—	104.770
			213.309	176.846	96.803	—	122.180
			214.546	177.872	112.090	—	139.461
			216.075	179.139	126.522	—	161.756
			217.311	180.164	143.726	—	180.436
			218.731	181.341	159.159	—	202.396
			220.004	182.396	176.249	—	222.471
			221.350	183.512	192.702	—	243.948
			222.769	184.689	213.393	—	266.749
			224.079	185.775	234.805	—	287.851
			225.098	186.619	251.861	—	304.246
			226.371	187.675	265.038	—	324.671
			227.572	188.671	286.108	—	343.809
			232.993	193.165	350.850	—	427.973
			238.450	197.690	401.106	—	507.783
$^{40}Ca+^{197}Au$	FF	authors' table [216] $E_{c.m.}$	195.80	162.75	4.6	0.4	1.592
			199.00	165.41	7.1	0.4	7.460
			202.30	168.16	14.7	0.4	21.685
			205.20	170.57	25.2	0.6	41.879
			208.50	173.31	47	2	72.598
			211.19	175.55	73	3	103.085
			220.79	183.53	178	6	239.457
			228.70	190.10	290	8	368.214
			247.90	206.06	554	6	669.809
			267.89	222.68	747	8	914.842
$^{40}Ca+^{208}Pb$	FF	authors' table [216] $E_{c.m.}$	202.30	169.67	7.88	0.46	3.062
			211.21	177.14	45.5	1.5	40.359
			220.80	185.19	138	4	150.510
			228.70	191.81	242	4	271.450
			247.90	207.92	494	5	558.918
$^{48}Ca+^{48}Ca$	EvR	authors' graph [217] $E_{c.m.}$	96.699	48.349	0.153	—	0.654
			97.494	48.747	0.414	—	1.344
			98.305	49.153	0.882	—	2.752
			99.086	49.543	2.524	—	5.316
			99.897	49.949	5.585	—	10.037
			100.709	50.354	11.626	—	17.736
			101.489	50.745	19.903	—	28.541
			102.301	51.150	32.447	—	43.422
			103.144	51.572	48.562	—	62.341
			103.893	51.946	66.722	—	81.430
			104.736	52.368	92.801	—	104.586
			105.516	52.758	119.948	—	126.914
			106.296	53.148	135.537	—	149.583
			107.108	53.554	168.880	—	173.168
			107.951	53.975	193.176	—	197.440
			108.700	54.350	215.632	—	218.722
			109.543	54.771	240.698	—	242.277
			110.354	55.177	262.192	—	264.551
			111.135	55.567	311.109	—	285.585
			111.915	55.957	351.544	—	306.246
			112.726	56.363	378.286	—	327.344
			113.569	56.785	387.644	—	348.843
			114.318	57.159	407.061	—	367.609
			115.130	57.565	465.622	—	387.583

Continued on next page

Table 2 (continued)

Reaction	Detected particles	Data obtained	E_{lab} (MeV)	$E_{c.m.}$ (MeV)	σ (mb)	$\delta\sigma$ (mb)	σ^{cal} (mb)
			115.942	57.971	422.260	—	407.196
			116.753	58.377	443.411	—	426.455
			117.533	58.767	459.967	—	444.649
			118.345	59.173	552.493	—	463.241
			119.125	59.563	609.228	—	480.808
$^{48}Ca+^{90}Zr$	EvR	authors' table [218] $E_{c.m.}$	139.07	90.7	0.16	0.05	0.610
			139.84	91.2	0.36	0.08	1.224
			140.61	91.7	0.89	0.10	2.325
			141.37	92.2	1.89	0.17	4.165
			142.14	92.7	3.50	0.27	7.021
			142.75	93.1	6.80	0.56	10.211
			143.52	93.6	11.8	0.70	15.492
			144.29	94.1	17.7	1.1	22.315
			145.05	94.6	25.6	1.5	30.695
			145.82	95.1	33.7	0.8	40.574
			146.59	95.6	43.3	0.9	51.843
			147.35	96.1	54.0	1.0	64.362
			148.12	96.6	65.3	1.3	77.975
			148.89	97.1	77.1	1.5	92.517
			149.65	97.6	89.0	1.7	107.826
			150.27	98.0	100.9	1.8	120.517
			151.03	98.5	113.8	1.7	136.812
			151.80	99.0	127.2	1.8	153.461
			152.57	99.5	141.9	1.8	170.344
			153.33	100.0	157.7	1.6	187.361
			154.87	101.0	186.3	1.9	221.475
			156.40	102.0	214.0	2.3	255.317
			157.78	102.9	241.9	2.6	285.305
			159.31	103.9	269.1	2.2	317.967
			160.85	104.9	295.7	3.1	349.875
			162.38	105.9	322.8	3.5	381.012
			163.91	106.9	347.9	3.4	411.386
			165.29	107.8	374.5	4.0	438.083
			166.83	108.8	402.0	4.0	467.056
			168.36	109.8	426.5	4.1	495.323
			169.89	110.8	455.0	5.0	522.905
			171.43	111.8	479.8	5.2	549.822
			173.42	113.1	516.9	5.8	583.854
$^{48}Ca+^{96}Zr$	EvR	authors' table [218] $E_{c.m.}$	132.90	88.6	0.095	0.040	0.579
			133.65	89.1	0.28	0.07	1.191
			134.40	89.6	0.83	0.11	2.271
			135.15	90.1	2.59	0.25	4.009
			135.90	90.6	4.73	0.31	6.582
			136.65	91.1	8.73	0.40	10.153
			137.40	91.6	13.5	0.65	14.794
			138.15	92.1	18.9	0.6	20.461
			138.90	92.6	25.2	0.9	27.122
			139.65	93.1	31.5	1.0	34.769
			140.40	93.6	41.8	1.2	43.336
			141.15	94.1	49.8	1.5	52.774
			141.90	94.6	60.5	1.7	63.067
			142.65	95.1	73.0	2.4	74.147
			143.40	95.6	85.7	2.7	85.957
			144.15	96.1	96.6	3.1	98.472
			144.90	96.6	108.4	3.0	111.628
			145.65	97.1	121.0	2.7	125.363
			146.40	97.6	134.9	2.8	139.649
			147.15	98.1	149.4	2.8	154.426
			147.90	98.6	161.5	2.9	169.632
			148.65	99.1	174.9	2.9	185.237
			149.40	99.6	189.1	3.2	201.191
			150.15	100.1	203.9	3.4	217.436
			150.90	100.6	215.7	3.5	233.940
			151.65	101.1	230.0	3.3	250.664
			152.40	101.6	244.9	4.4	267.557
			153.15	102.1	257.4	2.7	284.591

Continued on next page

Table 2 (continued)

Reaction	Detected particles	Data obtained	E_{lab} (MeV)	$E_{c.m.}$ (MeV)	σ (mb)	$\delta\sigma$ (mb)	σ^{cal} (mb)
			154.65	103.1	289.9	3.2	318.945
			156.15	104.1	325.1	3.4	353.474
			157.65	105.1	349.4	4.4	387.968
			159.15	106.1	381.0	4.1	422.264
			160.65	107.1	407.4	4.5	456.221
			162.15	108.1	433.5	4.6	489.734
			163.65	109.1	464.9	4.8	522.728
			165.15	110.1	494.0	5.1	555.142
			166.65	111.1	522.0	5.2	586.941
			168.15	112.1	552.0	5.7	618.101
$^{48}Ca+^{154}Sm$	EvRFFQF	authors' graph [219] $E_{c.m.}$	164.125	125.125	0.049	—	0.001
			164.908	125.722	0.147	—	0.002
			165.788	126.392	0.185	—	0.005
			166.451	126.898	0.414	—	0.011
			167.285	127.534	0.684	—	0.029
			168.040	128.110	1.095	—	0.069
			168.903	128.768	1.906	—	0.174
			169.766	129.426	2.294	—	0.402
			170.413	129.919	3.273	—	0.715
			171.277	130.577	4.413	—	1.427
			172.032	131.153	5.621	—	2.427
			172.895	131.811	7.686	—	4.104
			173.650	132.387	9.651	—	6.088
			174.513	133.045	10.511	—	9.056
			175.161	133.538	13.773	—	11.915
			176.024	134.196	16.572	—	16.659
			176.995	134.937	18.835	—	22.972
			177.642	135.430	21.715	—	27.601
			178.397	136.006	25.394	—	33.499
			179.261	136.664	29.695	—	41.090
			180.016	137.240	35.728	—	48.435
			180.771	137.815	40.035	—	56.229
			181.742	138.556	47.489	—	66.834
			182.497	139.132	56.329	—	75.701
			183.360	139.790	64.024	—	86.572
			184.116	140.365	67.773	—	96.555
			184.871	140.941	79.254	—	106.846
			185.734	141.599	91.371	—	119.068
			186.489	142.175	106.850	—	130.295
			187.245	142.751	121.446	—	141.962
			188.216	143.491	132.268	—	157.366
			188.755	143.902	142.020	—	166.091
			189.726	144.643	152.490	—	182.239
			190.589	145.301	173.321	—	197.113
			191.344	145.876	191.471	—	210.395
			192.100	146.452	211.521	—	223.831
			193.071	147.192	220.744	—	241.405
			193.718	147.686	237.019	—	253.374
			194.581	148.344	247.354	—	269.581
			195.336	148.920	250.898	—	283.884
			197.602	150.647	343.107	—	327.537
			200.084	152.539	401.231	—	376.380
			202.565	154.431	436.986	—	425.837
			205.047	156.323	540.938	—	475.354
			207.420	158.132	589.142	—	522.497
			209.470	159.695	632.577	—	562.887
			216.591	165.124	840.790	—	698.722
			230.833	175.981	1325.581	—	942.851
			237.414	180.999	1403.204	—	1042.485
			243.887	185.934	1485.374	—	1132.782
			250.685	191.116	1550.144	—	1219.811
$^{48}Ca+^{197}Au$	FF	authors' table [216] $E_{c.m.}$	204.39	164.35	6.5	0.3	10.914
			207.30	166.69	14.3	1.2	28.620
			210.50	169.26	42.1	2.7	57.418
			213.80	171.91	60	4	95.931
			220.10	176.98	155	7	188.370

Continued on next page

Table 2 (continued)

Reaction	Detected particles	Data obtained	E_{lab} (MeV)	$E_{c.m.}$ (MeV)	σ (mb)	$\delta\sigma$ (mb)	σ^{cal} (mb)
			224.31	180.36	227	6	258.836
			252.50	203.03	605	11	732.578
			299.30	240.66	837	13	1128.397
^{48}Ca+^{208}Pb	FF	authors' table	210.50	171.03	13.3	0.8	11.238
		[216]	213.80	173.71	26.2	1.9	31.646
		$E_{c.m.}$	220.10	178.83	165	8	103.363
			224.30	182.24	141	10	167.715
			252.50	205.16	569	9	620.274
^{48}Ti+^{58}Fe	EvR	author's graph	118.100	64.621	0.002	—	0.100
		[220]	119.071	65.152	0.004	—	0.025
		$E_{c.m.}$	120.094	65.712	0.014	—	0.064
			121.098	66.261	0.036	—	0.160
			122.092	66.805	0.117	—	0.386
			123.114	67.364	0.382	—	0.907
			124.097	67.902	1.019	—	1.927
			125.100	68.451	2.016	—	3.832
			126.091	68.993	3.315	—	6.935
			127.624	69.832	8.116	—	14.840
			128.097	70.091	9.223	—	18.130
			130.104	71.189	21.331	—	36.545
			131.590	72.002	36.093	—	54.547
			132.103	72.283	39.874	—	61.556
			133.586	73.094	59.362	—	83.825
			134.101	73.376	65.561	—	92.221
			135.587	74.189	89.632	—	118.063
			137.071	75.001	107.809	—	145.941
			138.608	75.842	131.635	—	176.514
			140.110	76.664	172.346	—	207.624
			141.579	77.468	187.735	—	238.842
			143.084	78.291	216.329	—	271.265
			146.105	79.944	283.447	—	336.680
			146.119	79.952	267.846	—	336.995
			149.096	81.581	313.134	—	400.485
			152.075	83.211	350.818	—	462.043
			155.094	84.863	371.316	—	521.918
^{48}Ti+^{58}Ni	EvR	authors' table	132.92	72.73	0.14	0.01	0.053
		[221]	134.93	73.83	0.55	0.04	0.313
		$E_{c.m.}$	136.89	74.90	1.41	0.1	1.587
			138.91	76.01	4.87	0.3	6.747
			140.67	76.97	11.9	0.7	17.913
			142.42	77.93	22.5	1.0	37.189
			144.27	78.94	37.2	2.0	65.347
			146.21	80.00	57.2	2.95	100.828
			148.13	81.05	86.0	4.2	138.982
			149.97	82.06	123	5.5	176.454
			153.94	84.23	188	9	255.089
			157.87	86.38	263	12	328.396
			161.81	88.54	369	19.5	397.336
			165.84	90.74	384	19	463.069
^{48}Ti+^{60}Ni	EvR	authors' table	131.17	72.87	0.25	0.03	0.214
		[221]	133.18	73.99	1.18	0.10	1.199
		$E_{c.m.}$	135.02	75.01	3.54	0.30	4.743
			137.00	76.11	9.67	0.55	15.345
			138.89	77.16	27.2	1.5	34.912
			140.65	78.14	48.5	2.5	61.243
			142.54	79.19	78	4	95.820
			144.52	80.29	109	6	136.084
			146.48	81.38	166	9	177.504
			148.36	82.42	204	10	216.942
			150.35	83.53	232	10.5	258.147
			154.35	85.75	308	15	336.772
			158.35	87.97	373	16	410.255
			162.34	90.19	416	21.5	478.959
			166.37	92.43	446	23	543.838
^{46}Ti+^{64}Ni	EvR	authors' table	124.95	72.7	2.63	0.18	1.609
		[174]	127.02	73.9	7.88	0.55	5.930

Continued on next page

Table 2 (continued)

Reaction	Detected particles	Data obtained	$E_{\rm lab}$ (MeV)	$E_{\rm c.m.}$ (MeV)	σ (mb)	$\delta\sigma$ (mb)	$\sigma^{\rm cal}$ (mb)
		$E_{\rm c.m.}$	128.91	75.0	13.7	1.0	15.040
			130.80	76.1	27.9	1.8	30.679
			132.69	77.2	40.4	2.5	52.941
			134.75	78.4	60.2	4.0	83.800
			136.81	79.6	104	5.5	120.073
			138.70	80.7	129	8	156.729
			140.77	81.9	193	12	199.038
			142.66	83.0	219	13	238.889
			144.72	84.2	256	14	282.594
			146.61	85.3	294	16	322.279
			150.73	87.7	352	17	406.024
			154.69	90.0	383	20	481.588
			158.64	92.3	464	25	552.368
^{48}Ti+^{64}Ni	EvR	authors' table	125.28	71.59	0.14	0.01	0.252
		[221]	127.29	72.74	0.74	0.65	1.396
		$E_{\rm c.m.}$	129.31	73.89	2.68	0.20	5.712
			131.27	75.01	14.5	0.75	16.139
			132.93	75.96	30.6	1.5	31.213
			134.75	77.00	48	2.5	54.106
			136.80	78.17	62	3	86.625
			138.81	79.32	118	6	123.891
			140.70	80.40	143	9	162.116
			142.73	81.56	193	9.5	205.154
			144.71	82.69	245	12.5	247.856
			146.67	83.81	293	17	290.077
			148.66	84.95	322	15.5	332.376
			150.66	86.09	361	17	373.653
			154.65	88.37	406	21	452.571
			158.69	90.68	401	22.5	527.430
			162.72	92.98	473	26	597.125
			166.74	95.28	495	27.5	662.358
^{48}Ti+^{122}Sn	EvRFF	authors' table	169.1	121.35	2.3	0.2	5.318
		[185]	170.1	122.07	4.7	0.3	8.401
		$E_{\rm lab}$	171.1	122.79	13.4	0.6	12.668
			174.1	124.94	17.8	1.5	33.878
			174.1	124.94	18	1	33.878
			174.1	124.94	18.3	1	33.878
			176.1	126.38	30	1.3	55.274
			179.1	128.53	56	2	96.615
			179.1	128.53	57	5	96.615
			184.1	132.12	133	5	181.556
			189.1	135.71	172	9	273.508
			189.1	135.71	179	4	273.508
			194.1	139.30	278	10	363.369
			199.1	142.88	294	15	448.019
			204.1	146.47	465	25	527.050
			209.1	150.06	485	35	600.745
			214.1	153.65	587	55	669.462
			219.1	157.24	635	60	733.523
			222.1	159.39	850	150	769.840
^{50}Ti+^{60}Ni	EvR	authors' table	133.10	72.6	0.47	0.04	0.237
		[174]	135.12	73.7	1.12	0.09	1.333
		$E_{\rm c.m.}$	137.13	74.8	4.84	0.36	5.874
			138.97	75.8	12.4	0.8	16.815
			140.80	76.8	25.9	1.7	36.646
			142.63	77.8	44.6	2.8	64.783
			144.47	78.8	69.5	3.7	98.910
			146.48	79.9	97.2	5.5	140.277
			148.50	81.0	136	8	183.032
			150.33	82.0	188	11	221.711
			154.37	84.2	270	14	303.653
			158.40	86.4	322	16	380.380
			162.43	88.6	387	19	452.107
			166.47	90.8	443	26	519.240
^{46}Ti+^{93}Nb	EvR	authors' table	149.81	100.23	0.42	0.04	0.041
		[94]	151.79	101.56	1.15	0.08	0.268

Continued on next page

Table 2 (continued)

Reaction	Detected particles	Data obtained	$E_{\rm lab}$ (MeV)	$E_{\rm c.m.}$ (MeV)	σ (mb)	$\delta\sigma$ (mb)	$\sigma^{\rm cal}$ (mb)
		$E_{\rm c.m.}$	154.78	103.56	4.85	0.30	2.708
			157.77	105.56	12.50	0.60	13.210
			160.76	107.56	32.00	1.30	36.585
			163.86	109.63	66.00	3.00	73.466
			166.76	111.57	109.00	5.00	116.994
			169.74	113.57	166.00	10.00	167.850
			173.74	116.24	235.00	10.00	240.355
			177.71	118.90	311.00	14.00	313.347
^{50}Ti+^{93}Nb	EvR	authors' table	153.79	100.02	0.04	0.008	0.008
		[94]	155.78	101.31	0.36	0.050	0.070
		$E_{\rm c.m.}$	157.78	102.61	1.82	0.180	0.568
			160.76	104.55	8.90	0.500	6.676
			163.76	106.50	26.00	1.300	27.993
			167.74	109.09	77.00	5.000	79.628
			171.72	111.68	141.00	7.000	148.347
			176.72	114.93	236.00	11.000	243.692
			182.69	118.81	328.00	16.000	356.039
^{46}Ti+^{90}Zr	EvR	authors' table	150.10	99.33	0.24	0.04	0.139
		[94]	152.18	100.71	1.16	0.12	0.886
		$E_{\rm c.m.}$	155.09	102.63	5.30	0.40	6.644
			158.08	104.61	16.40	0.90	26.346
			161.05	106.58	43.00	2.00	62.801
			164.18	108.65	86.00	4.00	114.559
			167.07	110.56	136.00	7.00	168.824
			170.02	112.51	185.00	9.00	226.119
			174.03	115.17	267.00	12.00	302.831
			178.01	117.80	348.00	20.00	374.925
^{50}Ti+^{90}Zr	EvR	authors' table	156.01	100.29	0.30	0.04	1.721
		[94]	157.92	101.52	1.92	0.20	6.211
		$E_{\rm c.m.}$	161.06	103.54	14.4	0.80	26.967
			164.06	105.47	44.00	2.00	64.567
			168.05	108.03	104.00	6.00	133.207
			172.03	110.59	178.00	6.00	210.782
			177.02	113.80	259.00	13.00	307.580
			183.00	117.64	386.00	19.00	415.718
^{58}Ni+^{54}Fe	EvR	authors' table	177.04	85.36	0.0011	0.00079	0.064
		[222]	178.04	85.84	0.0022	0.0010	0.133
		$E_{\rm c.m.}$	179.03	86.32	0.0139	0.0035	0.274
			180.05	86.81	0.0358	0.0049	0.559
			181.05	87.29	0.178	0.019	1.086
			183.04	88.25	0.795	0.070	3.594
			185.05	89.22	3.91	0.12	9.717
			187.04	90.18	8.61	0.21	21.012
			189.03	91.14	15.93	0.34	38.013
			191.04	92.11	27.46	0.61	60.325
			193.03	93.07	46.73	0.86	86.275
			195.05	94.04	64.48	1.44	115.067
			197.04	95.00	85.61	1.91	144.938
			199.05	95.97	116.8	1.8	175.611
			201.04	96.93	132.9	3.0	205.864
			203.05	97.90	167.1	3.7	235.979
			205.04	98.86	198.1	4.3	265.163
			207.03	99.82	219.5	3.7	293.659
			209.05	100.79	250.5	3.5	321.734
			211.04	101.75	276.1	4.7	348.818
			215.04	103.68	332.5	8.7	401.222
			217.05	104.65	357.4	8.4	426.569
			221.03	106.57	390.7	6.2	474.884
			223.05	107.54	418.2	7.1	498.394
			227.05	109.47	435.1	5.0	543.462
^{58}Ni+^{58}Ni	EvR	authors' table	187.6	93.25	0.049	0.020	1.010
		[223]	188.0	93.45	0.096	0.029	1.309
		$E_{\rm lab}$ & $E_{\rm c.m.}$	189.0	93.88	0.348	0.087	2.221
			190.0	94.31	0.888	0.133	3.621
			191.0	94.76	1.86	0.28	5.775
			192.0	95.22	2.52	0.25	8.874

Continued on next page

Table 2 (continued)

Reaction	Detected particles	Data obtained	E_{lab} (MeV)	$E_{c.m.}$ (MeV)	σ (mb)	$\delta\sigma$ (mb)	σ^{cal} (mb)
			193.0	95.68	4.98	0.75	13.019
			194.0	96.15	6.47	0.25	18.424
			196.0	97.10	11.1	1.1	33.011
			198.0	98.05	19.5	2.1	52.099
			200.0	99.02	28.6	2.9	75.356
			202.0	100.0	37.3	3.0	101.647
			205.0	101.5	71.2	7.1	145.001
			207.0	102.5	79.9	8.0	174.739
			210.0	103.9	120	10	216.254
			215.0	106.4	159	16	287.966
			220.0	108.9	226	18	355.565
^{58}Ni+^{64}Ni	EvR	authors' table [132] $E_{c.m.}$	170.23	89.3	0.077	0.015	0.211
			171.18	89.8	0.098	0.029	0.418
			172.13	90.3	0.377	0.075	0.792
			173.09	90.8	0.722	0.144	1.432
			174.04	91.3	1.39	0.28	2.468
			174.99	91.8	1.80	0.36	4.044
			175.95	92.3	2.89	0.58	6.306
			176.90	92.8	4.41	0.66	9.379
			178.04	93.4	6.52	0.98	14.276
			179.00	93.9	7.93	1.19	19.435
			179.38	94.1	8.54	0.77	21.777
			179.95	94.4	9.90	0.99	25.584
			180.33	94.6	11.6	1.4	28.315
			180.90	94.9	13.1	1.3	32.696
			181.09	95.0	13.8	1.4	34.230
			181.28	95.1	16.6	2.0	35.801
			181.86	95.4	16.2	1.6	40.730
			182.24	95.6	18.4	2.2	44.191
			182.81	95.9	20.1	2.0	49.638
			183.38	96.2	25.5	2.6	55.381
			185.29	97.2	35.7	4.3	76.503
			186.81	98.0	35.7	5.4	95.348
			189.29	99.3	59.7	5.4	128.961
			193.87	101.7	80.6	16.1	197.507
			198.82	104.3	166	25	275.677
			203.78	106.9	208	31	353.127
			208.73	109.5	308	46	427.373
^{58}Ni+^{124}Sn	EvR	author's graph [224] $E_{c.m.}$	209.887	143.000	4.700E − 4	—	0.002
			210.915	143.700	0.001	—	0.003
			212.969	145.100	0.003	—	0.013
			214.877	146.400	0.016	—	0.043
			216.932	147.800	0.090	—	0.140
			218.987	149.200	0.297	—	0.404
			223.977	152.600	2.219	—	3.403
			228.381	155.600	11.710	—	13.604
			233.518	159.100	35.300	—	41.702
			238.215	162.300	86.140	—	83.466
^{64}Ni+^{64}Ni	EvR	authors' graph [84] $E_{c.m.}$	179.175	89.587	0.328	—	0.920
			180.108	90.054	1.043	—	1.797
			181.138	90.569	2.308	—	3.474
			182.071	91.035	4.146	—	5.859
			182.972	91.486	6.898	—	9.098
			184.999	92.499	11.386	—	20.018
			186.994	93.497	25.196	—	35.536
			188.957	94.478	39.104	—	54.985
			193.913	96.956	88.555	—	118.796
			198.739	99.370	156.689	—	194.049
			203.631	101.815	219.986	—	275.665
			208.715	104.357	316.079	—	360.532
			213.702	106.851	357.585	—	440.822
^{64}Ni+^{124}Sn	EvR	author's graph [224] $E_{c.m.}$	218.929	144.400	0.001	—	1.650E − 5
			220.445	145.400	0.002	—	9.940E − 5
			221.961	146.400	0.013	—	5.961E − 4
			223.932	147.700	0.071	—	0.006
			225.903	149.000	0.483	—	0.055

Continued on next page

Table 2 (continued)

Reaction	Detected particles	Data obtained	E_{lab} (MeV)	$E_{c.m.}$ (MeV)	σ (mb)	$\delta\sigma$ (mb)	σ^{cal} (mb)
			227.874	150.300	1.379	—	0.388
			230.906	152.300	6.022	—	3.558
			232.877	153.600	12.180	—	9.292
			235.606	155.400	20.570	—	23.135
			239.700	158.100	36.480	—	55.354
			245.006	161.600	89.800	—	113.308
^{124}Sn+^{40}Ca	EvR	authors' graph [88] $E_{c.m.}$	441.612	107.710	1.296	—	0.167
			454.730	110.910	8.104	—	2.866
			460.240	112.254	20.666	—	7.164
			466.709	113.831	32.170	—	17.259
			469.988	114.631	55.054	—	25.027
			478.276	116.653	66.805	—	53.278
			479.808	117.026	93.123	—	59.792
			488.904	119.245	134.900	—	105.354
			489.662	119.430	149.295	—	109.604
			499.614	121.857	209.572	—	169.743
			502.333	122.520	221.888	—	187.138
			514.477	125.482	301.826	—	266.410
			517.410	126.198	300.772	—	285.508
			532.486	129.875	452.787	—	380.833
			533.400	130.097	396.574	—	386.416
			539.661	131.625	420.369	—	424.041
			547.653	133.574	565.845	—	470.403
			551.690	134.559	540.072	—	493.128
			558.281	136.166	533.814	—	529.248
			564.789	137.754	527.629	—	563.760
			572.781	139.703	635.787	—	604.618
			579.783	141.411	585.979	—	639.101
^{132}Sn+^{40}Ca	EvR	authors' table [88, 98][1] $E_{c.m.}$	468.70	109	3.62	1.83	2.547
			477.30	111	10.50	2.20	8.963
			485.90	113	24.49	3.85	23.879
			494.50	115	48.65	6.03	50.082
			503.10	117	83.52	8.99	87.384
			511.70	119	129.43	11.85	133.416
			516.00	120	181.10	8.11	158.759
			524.60	122	186.47	8.35	212.213
			528.90	123	257.13	7.62	239.667
			533.20	124	268.64	12.03	267.249
			541.80	126	375.88	16.83	322.037
			546.10	127	381.41	17.08	348.981
			563.30	131	454.47	20.35	452.269
			567.60	132	533.67	15.82	476.861
			584.80	136	555.57	24.97	570.331
^{134}Te+^{40}Ca	EvR	authors' graph [89] $E_{c.m.}$	500.551	115.069	6.271	—	6.925
			504.523	115.982	11.673	—	11.546
			512.275	117.764	31.565	—	26.498
			520.604	119.679	67.356	—	52.441
			530.351	121.920	100.202	—	94.806
			538.719	123.844	126.675	—	138.988
			551.194	126.711	180.126	—	212.469
			564.392	129.745	235.262	—	293.144
			584.975	134.477	337.962	—	414.295
			603.177	138.661	432.631	—	513.071
^{124}Sn+^{48}Ca	EvR	authors' graph [88] $E_{c.m.}$	393.759	109.886	2.040	—	1.208
			402.070	112.206	9.947	—	12.579
			415.970	116.085	60.186	—	193.374
			429.272	119.797	183.675	—	318.630
			444.231	123.972	264.722	—	435.919
			459.368	128.196	383.882	—	541.703
			474.283	132.358	512.374	—	638.697
			489.197	136.520	537.082	—	729.637
			504.446	140.776	620.492	—	85.107
			519.481	144.971	674.322	—	811.890

Continued on next page

[1]The experiment was reported in Ref. [88] and the data were shown in graphs. The data were given in tables in Ref. [98]

Table 2 (continued)

Reaction	Detected particles	Data obtained	$E_{\rm lab}$ (MeV)	$E_{\rm c.m.}$ (MeV)	σ (mb)	$\delta\sigma$ (mb)	$\sigma^{\rm cal}$ (mb)
			534.507	149.165	717.045	—	887.347
			559.550	156.154	790.293	—	999.470
			584.816	163.204	546.656	—	1096.828
^{132}Sn+^{48}Ca	EvR	authors' graph [88] $E_{\rm c.m.}$	411.362	109.697	0.881	—	2.870
			420.095	112.025	11.055	—	22.493
			427.785	114.076	45.691	—	63.030
			435.475	116.127	108.694	—	119.632
			445.502	118.801	178.293	—	203.454
			465.651	124.174	366.884	—	368.708
			485.788	129.544	437.655	—	516.930
			504.392	134.504	560.527	—	639.758
			505.541	134.811	580.218	—	646.943
			534.537	142.543	758.599	—	814.003
			544.489	145.197	774.479	—	865.547
			564.764	150.604	789.109	—	962.331
^{132}Sn+^{58}Ni	EvRFF	authors' graph [225] $E_{\rm c.m.}$	499.793	152.568	4.758	—	9.078
			506.853	154.723	11.820	—	20.457
			518.242	158.200	34.160	—	53.787
			529.087	161.511	78.130	—	101.772
			545.255	166.446	185.028	—	193.041
			560.462	171.088	285.516	—	287.764
			578.094	176.471	401.354	—	396.026
			618.127	188.691	616.318	—	612.690
			635.552	194.011	680.196	—	693.217
			645.151	196.941	730.429	—	734.014
^{132}Sn+^{64}Ni	EvRFF	authors' graph [226] $E_{\rm c.m.}$	453.156	147.969	0.709	—	0.289
			462.020	150.864	5.811	—	5.302
			471.138	153.841	29.650	—	26.017
			482.928	157.691	67.216	—	77.651
			509.428	166.344	213.858	—	253.961
			524.120	171.141	359.997	—	361.901
			539.753	176.246	505.227	—	472.374
			561.511	183.351	646.504	—	613.275
			597.069	194.961	824.837	—	810.426
^{208}Pb+^{26}Mg	FF	authors' graph [227] $E_{\rm c.m.}$	989.075	109.897	60.786	—	106.723
			1041.804	115.756	232.951	—	289.036
			1090.598	121.178	359.142	—	475.953
			1145.534	127.281	524.813	—	673.715
			1227.936	136.437	715.158	—	930.665
			1353.964	150.440	965.425	—	1244.737
			1677.110	186.345	1324.966	—	1746.812